MAGNETIC AND THERMAL CONDUCTIVITY STUDIES ON IRON OXIDE BASED NANOFLUIDS

Thesis Submitted to AcSIR for the Award of the Degree of

DOCTOR OF PHILOSOPHY

In **Chemical Sciences**

By

R. Lenin

Registration Number: 10CC11J26009

Under the guidance of

Dr. P. A. Joy

CSIR-National Chemical Laboratory
Pune 411008, India

July 2016

.....Dedicated to my Mother…...

सीएसआयआर–राष्ट्रीय रासायनिक प्रयोगशाला
(वैज्ञानिक तथा औद्योगिक अनुसंधान परिषद)
डॉ. होमी भाभा मार्ग, पुणे – 411 008. भारत
CSIR-NATIONAL CHEMICAL LABORATORY
(Council of Scientific & Industrial Research)
Dr. Homi Bhabha Road, Pune - 411008. India

Certificate

This is to certify that the work incorporated in this Ph.D. thesis entitled **Magnetic and Thermal conductivity Studies on Iron Oxide based Nanofluids** submitted by **Mr. R. Lenin** to Academy of Scientific and Innovative Research (AcSIR) in fulfillment of the requirements for the award of the Degree of **Doctor of Philosophy in Chemical Sciences** embodies original research work under my supervision. I further certify that this work has not been submitted to any other University or Institution in part or full for the award of any degree or diploma. Research material obtained from other sources has been duly acknowledged in the thesis. Any text, illustration, table etc., used in the thesis from other sources, have been duly cited and acknowledged.

Research Guide

(Dr. P. A. Joy)

Date: 29-07-'16

Place: Pune

Communications Channels
NCL Level DID : 2590
NCL Board No. : +91-20-25902000
Four PRI Lines : +91-20-25902000
FAX
Director's Office : +91-20-25902601
COA's Office : +91-20-25902660
SPO's Office : +91 20 25902664
WEBSITE
www.ncl-india.org

DECLARATION

I, hereby declare that all the experiments in this thesis entitled, "**Magnetic and Thermal conductivity Studies on Iron Oxide based Nanofluids**" submitted for the degree of **Doctor of Philosophy in Chemical Sciences** to Academy of Scientific and Innovative Research (AcSIR), has been carried out by me at the Physical and Materials Chemistry Division of CSIR-National Chemical Laboratory, Pune, India under the guidance of **Dr. P. A. Joy**. Research material obtained from other sources has been duly cited and acknowledged in the thesis. This work is original and has not been submitted in part or full by me for any degree or diploma to this or any other University.

R. Lenin

(R. Lenin)

Date: 29-07-2016

CSIR-NCL

Pune, India

Acknowledgements

It is a great pleasure to express my gratitude and sincere thanks to all those who helped me directly and indirectly to complete this work. This thesis would not have been possible without all these people and their constant encouragement.

First of all, I would like to express my immense and sincere gratitude to my research supervisor ***Dr. P.A. Joy*** *for his constant support, encouragement and guidance throughout my Ph. D. I really admire the way he teaches many complicated things in a simple manner and giving freedom to work in different aspects without any pressure. I am deeply indebted to him for his immense help, suggestions and the inspiring discussions during writing and completion of this thesis.*

I express my sincere thanks to the former directors Dr. Sivaram and Dr. S. Pal, and the present director, Dr. Ashwini Kumar Nangia, for allowing me to work in the prestigious Laboratory and making all the facilities available for my research work. I would like to acknowledge UGC for the financial assistance in the form of a research fellowship. I wish to thank Dr. Anilkumar, former Head of the Physical Chemistry Division, for allowing me to use all the divisional facilities. My sincere thanks to all the DAC members, Dr. Guruswamy kumaraswamy, Dr. B. L. V. Prasad, and Dr. C. S. Gopinath. They were kind enough to spend their valuable time for my evaluation presentations. The valuable suggestions given by them helped me to shape the thesis more perfectly.

I thank all my seniors, Vijay, Sreeja, Khaja, Mangesh, Pankaj for their help and support in the initial stages of my work, and my lab mates, Bindhu, Ramsundar, Govindraj, Jayaprabha, Anjali, Manjunath, Mohan, Anantharamaiah, and Arun, for providing the nice working environment in the lab. My special thanks to Sandeep (appu) who has supported me in my work and I really enjoyed working with him. I also thank all the projects students for their companionship.

I would like to thank all my friends who made my life at NCL more cheerful. Nagaraj, Edwin, Palani, Dhanalakshmi, Venki, Mohanraj, Kannan, Pandiraj, Dharma, Lalitha,

Ramanujam, Mallikarjuna, Marimuthu, Suresh, Sridhar, Murugeshan, Senthil, Sivaranjini, Senthil, Rajambal, Roopa, Suman, Devaraj, Prabhu D, Venkat, Vasu, Naren, Anuj, Ashok, Preiyaswamy, Mani, Prabhu K, Prabhu M, Ananthan, Kubendiran, Punith, Rajaperumal, Kumar, Arulkashmir, Sudhakar, Chitravel, Manikandan, Loganathan, Subramani, Suresh, Jumbu, Kuyil, Jijil, Beena, Leena, Rajesh, Unni, Joby, Aneesh, Soumya, Manu, Prajitha, Nisha, Rashid, Chaithanya, Rami, Himadri, and Susantha.

I would like to express the deepest gratitude to my lovable mother, who is behind every success in my life and I am really missing her at this memorable moment. I must express my very profound gratitude to my brother Dr. Marx Nirmal and sister-in-law Suganya for providing me with unfailing support and continuous encouragement throughout my years of study and through the process of thesis work. This accomplishment would not have been possible without them.

Lenin

Contents

List of tables

List of figures

List of abbreviations

ARES: Advanced Rheometric Expansion System

CCD: Charge Coupled Device

CNT: Carbon Nanotube

DA: Decanoic Acid

DC: Direct Current

DDP: Dodecayl Phosphonic acid

DHDP: Dihexadecayl Phosphate

DTG: Derivative Thermogravimetric analysis

EG: Ethylene Glycol

EMA: Effective Medium Approximation

EMT: Effective Medium Theory

EO: Engine Oil

FC: Field Cooled

FCC: Face Centered Cube

FWHM: Full Width at Half Maximum

HDP: Hexadecayl Phosphonic acid

HS: Hashin-Shtrikman

IR: Infrared Spectroscopy

JCPDS: Joint Committee on Powder Diffraction Standards

K-D: Krieger- Dougherty

LA: Lauric Acid

MD: Magnetite coated with Decanoic acid

MDE: Magnetite coated with Decanoic acid

MEG: Mono Ethylene Glycol

M-G: Maxwell-Garnett

MKR: Magnetite dispersed in Kerosene

ML: Magnetite coated with Lauric acid

MLd: Delayed washed Lauric acid coated Magnetite

MLE: Magnetite coated with Linoleic acid

MLN: Magnetite coated with Linolenic acid

MMC: Magnetite dispersed in Methylcyclohexane

MME: Magnetite dispersed in Mesitylene

MOD: Magnetite dispersed in Octadecene

MOL: Magnetite coated with Oleic acid

MPL: Magnetite dispersed in Paraffin

MPMS: Magnetic Property Measurement Systems

MRI: Magnetic Resonance Imaging

MST: Magnetite coated with Stearic acid

MTO: Magnetite dispersed in Toluene

MXY: Magnetite dispersed in Xylene

PCW: Powder Cell for Windows

PG: Propylene Glycol

RKKY: Ruderman-Kittel-Kasuya-Yosida

SDBS: Sodium Dodecyl Benzene Sulphonate

SFB: Surface Force Balance

SMF: Standard Measuring Flask

SQUID: Superconducting Quantum Inference Device

ST: Stearic acid

TCNT: Treated Carbon Nanotubes

TEM: Transmission Electron Microscopy

TGA: Thermogravimetric Analysis

TG-DTA: Thermogravimetric analysis- Differential Thermal Analysis

THW: Transient Hot Wire

TIM: Thermal Interface Materials

VSM: Vibrating Sample Magnetometer

XRD: X-ray Diffraction

ZFC: Zero Field Cooled

Abstract

Nanofluids are considered to be future coolants due to their enhanced thermal conductivity over that of the conventional heat transfer fluids. Many experimental results reported in the literature showed that the observed enhancement in the thermal conductivity is beyond the effective medium theory predictions. The anomalous enhancement in the thermal conductivity of nanofluids is due to the contribution of various factors such as particulate material, particle size, particle morphology, surfactant, pH, temperature, viscosity, etc. Many theoretical models are developed to account for the anomalous enhancement in the thermal conductivity of nanofluids by including the contribution from different factors. Although there are numerous experimental studies on various factors affecting the thermal conductivity of nanofluids, the exact mechanism of thermal conductivity enhancement of nanofluids is still unclear. Different mechanisms have been proposed for the thermal conductivity enhancement and among them, Brownian motion of the nanoparticles, aggregation/clustering of the nanoparticles in a fluid, and liquid layering at the particle-fluid interface are considered to be the important. The solvent-surfactant interaction at the interface is one of the important factors for dispersion and stability of nanofluids and which may directly affect the thermophysical properties of nanofluids. In this thesis we have studied some of the interfacial related issues on the thermal conductivity of iron oxide (magnetite) based nanofluids.

Chapter 1 is a general introduction to nanofluids, synthesis and stabilization methods of nanofluids, different theoretical models and mechanisms for thermal conductivity of nanofluids and review of some of the experimental results reported in the literature on the factors affecting the thermal conductivity of nanofluids. Since the work reported in this thesis is on the thermal conductivity studies on magnetite based nanifluids, this chapter also discusses about magnetic properties of nanoparticles, magnetic fluids, dipole-dipole interaction in magnetic fluids, relaxation mechanisms of magnetic nanoparticles in magnetic fluids and heat transfer in magnetic fluids.

Chapter 2 discusses about the synthesis of fatty acid coated magnetite nanoparticles, preparation of nanofluids, details of various characterization techniques used in the present study, fabrication of a setup for thermal conductivity measurement of fluids based on the transient hot wire method (THW), calibration of the setup using standard fluids and method

of calculation of thermal conductivity. This chapter also discusses about the thermal conductivity measurements in the presence of a magnetic field.

Chapter 3 reports studies on short-chain and long-chain saturated fatty acids as surfactants on the thermal conductivity of magnetite based nanofuids. Short-chain capric acid ($C_9H_{19}COOH$) and long-chain stearic acid ($C_{17}H_{35}COOH$) coated magnetite nanoparticles are prepared under identical conditions, with comparable particle sizes, and characterized using different techniques. The coated magnetite nanoparticles are dispersed in toluene and thermal conductivity studies have been carried out to understand the role of the long-chain and short-chain surfactants on the thermal conductivity of the nanofluids. The critical concentration of the nanoparticles dispersed in the fluids is found to be lower for the stearic acid coated fluid. However, the rate of increase of thermal conductivity above the critical concentration is found to be comparable for both fluids. The results are discussed in terms of the difference in the aggregation of the nanoparticles in the fluids.

In **Chapter 4**, thermal conductivity studies on capric (decanoic) acid coated magnetite nanoparticles of comparable average size (5–7 nm) but with different particle size distributions are described. Thermal conductivity measurements have been carried out on the magnetite nanofluids prepared by dispersing the nanoparticles in toluene. Enhancement in the thermal conductivity is found to be correlated with the average size and distribution of the nanoparticles, where the thermal conductivity is found to be relatively lower for the fluids with wider particle size distribution. For narrow particle size distribution, the experimental thermal conductivity enhancement is found to be comparable to that predicted by the Brownian motion caused convection whereas for wider particle size distribution, large deviation is observed.

In **chapter 5**, thermal conductivity studies on fluids of lauric (dodecanoic) acid coated magnetite nanoparticles, with different amounts of primary and secondary surfactant layers on the surface of the nanoparticles, dispersed on toluene, are reported. Two sets of the surfactant coated nanoparticles are prepared; one with comparable amount of primary surfactant and the other with comparable amount of secondary surfactant. Stability of the nanofluids is found to decrease with increasing amount of the secondary surfactant on the surface of the nanoparticles. Thermal conductivity and viscosity of the nanofluids are found to increase with increasing amount of the secondary surfactant layer on the surface of the nanoparticles, whereas only a small increase in the thermal conductivity is observed for fluids

with relatively larger amount of the primary surfactant. Larger enhancement in the thermal conductivity is observed in the presence of a small magnetic field for the fluids containing particles with lower amount of the secondary surfactant.

C**hapter 6** reports studies on fluids of magnetite nanoparticles coated with long-chain fatty acids containing the same number of carbon atoms but with differing degree of unsaturation in the alkyl chain (stearic acid $C_{18}H_{36}O_2$, oleic acid $C_{18}H_{34}O_2$, linoleic acid $C_{18}H_{32}O_2$ and linolenic acid $C_{18}H_{30}O_2$). The coated nanoparticles are dispersed in toluene for thermal conductivity and viscosity measurements. Viscosity studies on the fluids showed larger variation in the viscosity for saturated fatty acid coated fluid and less variation for unsaturated fatty acid coated fluids. The difference in the thermal conductivity and viscosity of the fluids with different surfactants is attributed to the conformation of the surfactant molecules. Due to the bend and hook structures of linoleic and linolenic acid, these fatty acids coated nanoparticles form less aggregation in the fluid, whereas due to the straight and kink structures of the stearic and oleic acids on the coated nanoparticles, they form clusters/aggregated/self-assembled particles due to the large hydrophobic interaction between the alkyl chains. The aggregated nanoparticles in the nanofluids give rise to relatively larger enhancement in the thermal conductivity and viscosity compared to the fluids with highly dispersed particles.

In **chapter 7**, the effect of the base fluid (solvent) on the thermal conductivity of oleic acid coated magnetite nanofluids is discussed. The oleic acid coated nanoparticles showed good dispersion in the base fluids toluene, xylene, mesitylene, kerosene, and methylcyclohexane, whereas the nanoparticles in the fluids octadecene and paraffin showed poor dispersion. The difference in the enhancement in the thermal conductivity is examined based on the thermophysical properties of the corresponding base fluids. From the studies, it is concluded that the compatibility of the solvent with the surface of the nanoparticles is crucial for the thermal conductivity enhancement since it affects the dispersion stability and interfacial resistance at the particle-fluid interface.

Chapter 8 summarizes the work reported in different chapters in this thesis and based on the findings, discusses the role of some of the important interface related factors which affect and need to be considered while analyzing the thermal conductivity of nanofluids.

Chapter 1

Introduction

1.1. Nanofluids

Nanofluids are a class of fluids which consist of solid-liquid composite materials. These are suspensions of solid nanostructures, in the size range 1 to 100 nm, in liquid carriers (base fluid). The solid-liquid composite material can be a dispersion of solid nanoparticles, nanotubes, nanorods, nanowires, nanofibers, nanosheets etc in base fluids. In other words, nanofluids are colloidal suspensions of nanostructured materials in suitable liquids. The solid nanomaterials include nanosized metals, metal oxides, metal nitrides, metal carbides, non-metals etc. and the liquid carriers can be water, organic solvents, ethylene glycol and oils.[1] Nanofluids have attracted the attention of researchers worldwide in the recent past due to the large number of potential applications. In 1995, U. S. Choi, from Argonne National Laboratory, USA, observed large enhancement in the thermal conductivity of conventional fluids by introducing solid nanoparticles in to these liquids, and the term 'nanofluid' was first coined by Choi.[2] Since then, there is an exponential growth in the number of publications in the field of nanofluids, as shown in Figure 1.1.[3]

Nanosized particles dispersed in conventional heat transfer fluids give stable fluids with large enhancement in the thermal conductivity, and sometimes anomalous enhancement in the thermal conductivity with respect to that of the base fluid is observed even at very low volume concentrations.[4-5] Due to these interesting features, nanofluids are considered to be future coolants for various heat transfer applications. Nanofluids show excellent thermophysical properties from the application point of view over the micro or macrofluids.[6] The surface area of the nanoparticles is more compared to that of the micro particles due to the exposure of the large number of surface atoms on the surface of the nanoparticles. The high surface area of the nanoparticles gives rise to enhanced thermal interaction between the base fluid and the surface of the particles when dispersed in a base fluid to form a colloidal suspension which allows more heat to transfer. Moreover, the smaller sized nanoparticles moves fast in the dispersed fluid due to Brownian motion and the particles carry the solvent molecules with it. The micro-convection of the solvent molecules leads to increase in the thermal conductivity of the fluid due to dissipation of heat in to the bulk through micro-convection.[6]

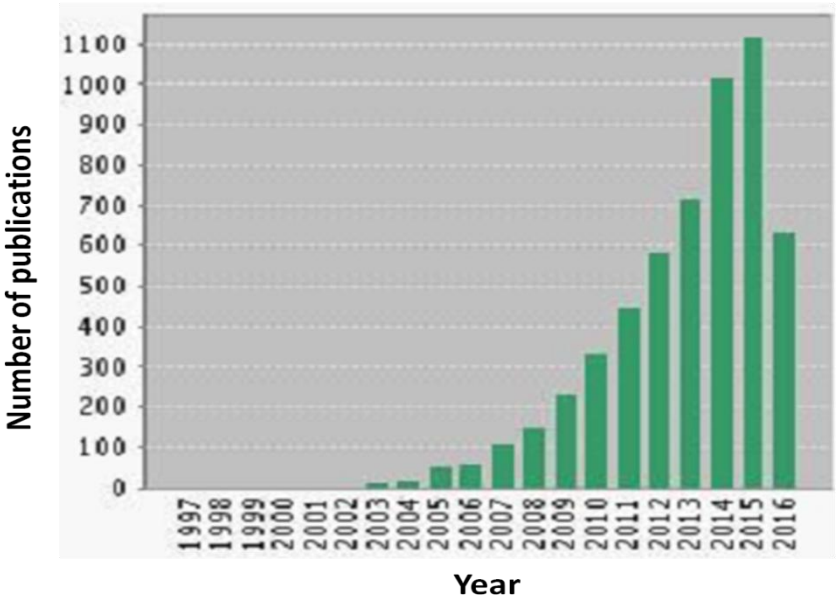

Figure 1.1. Growth of publications by the nanofluid community[3]

1.2. Synthesis and stability of nanofluids

Nanofluids are generally prepared by two methods, one is single-step method and the other is two-step method. In the two-step method, bare nanoparticles are synthesized initially and then the synthesized nanoparticles are dispersed in a liquid carrier. This step by step process isolates synthesis of nanoparticles and preparation of nanofluids, which leads to the possibility of agglomeration of the nanoparticles during both the steps. Agglomeration of the nanoparticles is also possible during the process of drying, storage and transportation of the nanoparticles. Agglomeration of the nanoparticles not only causes sedimentation, but also affects the heat transfer and viscosity properties of the nanofluids. Nanoparticles synthesized from different synthesis methods under different conditions may give rise to different particle size and distribution as well as morphology which will affect the quality and dispersion characteristics of the nanofluids. The degree of agglomeration can be different for the nanoparticles and fluids prepared under different manufacturing and processing conditions.[7] Stabilization methods such as electrostatic and steric stabilizations are required to stabilize the nanoparticles prepared in the two-step method. The main advantage of this method is that it is very simple and attractive towards industrial scaling and the main disadvantage is the formation of agglomerates. Synthesis of nanoparticles and preparation of homogenized nanofluids using the two-step method are still a challenging task in the area of nanofluid research.[8]

In the single step process of preparation of nanofluids, synthesis of nanoparticles and preparation of nanofluids are combined together. This method of nanofluid preparation avoids the processes such as drying, storing and transportation. Therefore, agglomeration of the nanoparticles in the nanofluids is minimized and the stability of the nanoparticles in the fluid is increased. In this method, nanoparticles are prepared by physical vapor deposition technique or by liquid chemical method. There are variations in this technique, but the direct evaporation method is one of the common methods which involve the solidification of gaseous phase inside the base fluids. The main disadvantage of this method is that the process works only for low vapor pressure liquids (like ethylene glycol) and this limits the application of this method.[7-8] The dispersion characteristics of the nanoparticles are better in the case of single-step method compared to the two-step method, without any agglomeration, and this is the main advantage of this method. Unlike the two-step method, the one step method is not suitable for industrial scale production of nanofluids. This is one of the main disadvantages of this method and also this method is not cost effective compared to the two-step method and this limits its commercialization.[9]

Stability of a nanofluid is one of the great challenges, especially by the widely used two-step process where the possibility of aggregation of nanoparticles is more. The aggregation of the nanoparticles is due the sum of the attractive and repulsive forces between the particles and aggregation occurs when the attractive forces are dominated over the repulsive forces between the particles. Due to the strong van der Waals attraction and the difference in the densities between the solid particles and base fluids, there is a possibility of sedimentation of the nanoparticles in fluid. According to Stokes law, reducing the density difference between the particles and a base fluid, by increasing the viscosity of the base fluid and decreasing the particle size leads to stable nanofluids. The process of aggregation, sedimentation and clogging of the nanoparticles in a fluid alter the dispersion and thermophysical characteristics such as thermal conductivity, viscosity and specific heat of a nanofluid. Physical and chemical treatments are generally employed to obtain stable nanofluids, such as addition of surfactants, surface coating of the nanoparticles before dispersing in base fluids or applying powerful forces to the aggregated structures. The aggregation of the nanoparticles can be prevented by increasing the repulsive forces between the particles.

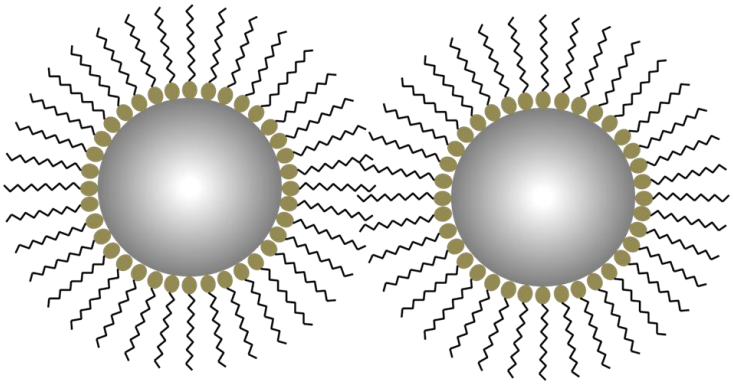

Figure 1.2. Schematic representation of steric stabilization of nanoparticles in a fluid

The increase in the repulsive force between the particles is achieved mainly by two mechanisms: steric stabilization and electrostatic stabilization. Macromolecules are used in the steric stabilization of nanoparticles in a fluid, in which a macromolecule containing a functional group is attached to the surface of the nanoparticle. Mostly polymer molecules containing carboxylic acid groups are easily attracted to the charged surface of the nanoparticles and the attached polymer molecules provide stability to the nanoparticle in a fluid. The steric effect of the polymer molecules depends on the concentration of the dispersant in the fluid.[5] Long chain fatty acid molecules are also used for steric stabilization of the nanoparticles in aqueous and non-aqueous medium.[10-11] The carboxylic group of the fatty acids is attached to the surface of the nanoparticles through chemical bonding. The long aliphatic chain exposed on the surface of the nanoparticles provides steric stabilization in a fluid (as shown in Figure 1.2).[11] Fatty acid bilayer over the surface of the nanoparticles also provides stability to the nanoparticles in the aqueous medium through steric and electrostatic stabilization.[10, 12]

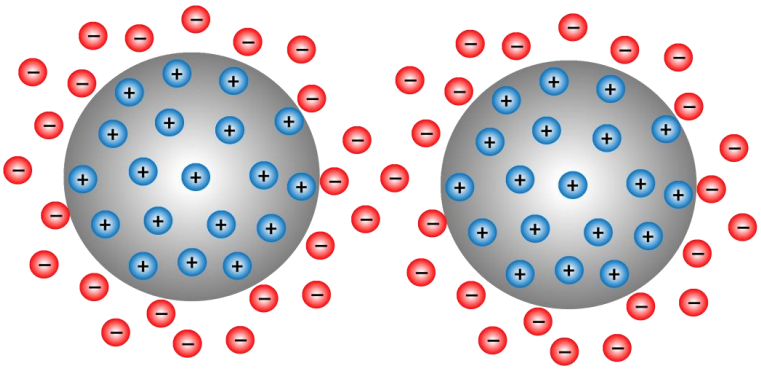

Figure 1.3. Schematic representation of electrostatic stabilization of nanoparticles in a fluid

When nanoparticles are dispersed in a polar medium, charges can be formed on the surface of the colloidal nanoparticles and formation of the charge can happen in different ways. Due to the surface charge on the surface of the nanoparticles, opposite charge could form around the charged nanoparticles in order to maintain electrical neutrality. The double layer of the surface charge provides stability to the nanoparticles due to the electrostatic repulsion between the charged particles (as shown in Figure 1.3). In electrostatic stabilization, the charge on the surface of a nanoparticle is formed through mechanisms such as i) preferential adsorption of ions, ii) dissociation of the surface charged species, iii) isomeric substitution of ions, iv) accumulation or depletion of the electrons at the surface, and v) physical adsorption of the charged species on the surface.[7]

1.3. Nanofluids for heat transport

The growth of technologies and miniaturization of technological devices along with increase in the rate of operation and data storage are brought about serious problems in the thermal management.[6] Cooling is one of the major technical challenges faced by many industries such as in microelectronics, transportation, and manufacturing.[13] The heat transfer ability of conventional heat transfer fluids is much low to meet the requirements of various industries for heat transfer applications. Therefore, researchers are looking for innovative coolants with improved heat transfer properties. Generally, solids are having much higher thermal conductivity (few orders of magnitude) than the conventional liquid coolants (water, ethylene glycol and oils) as shown in Figure 1.4.[14-16]

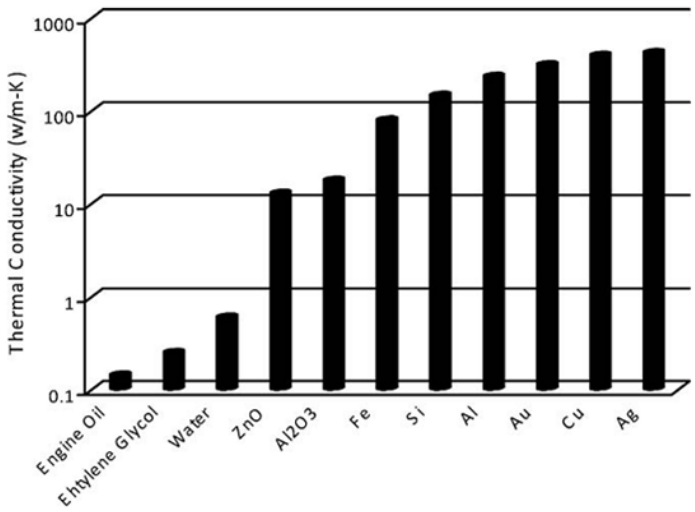

Figure 1.4. Comparison of the thermal conductivity of liquids and solids[16]

By introducing solid particles in to the conventional heat transfer fluids, it is expected to enhance the thermal conductivity of the heat transfer fluids. The idea of enhancement of thermal conductivity by introducing solid particles in to liquids is not new and it came to mind more than a century ago. Maxwell introduced a model for effective thermal conductivity of solid suspensions by his theoretical work in 1881.[17] Followed by Maxwell's predictions, there are many theoretical and experimental studies carried out to predict and enhance the thermal conductivity of solid suspensions.[18-22]

Most of the studies conducted initially on the thermal conductivity of suspensions used micro- and macro-sized particles. These larger sized particles settle rapidly in the suspensions, due to the gravitational force which reduces the heat transfer ability of the fluid. Moreover, the larger particles in a fluid tend to clog the channels in flow channel applications, especially in the case of narrow flow channels, and this will increase the pressure drop in the fluid. Therefore, researchers are looking for stable fluids with enhanced heat transfer properties in order to overcome the above limitations of the micro or macro fluids.

Sedimentation of the particles in a fluid is one of the major drawbacks in the case of microfluids. The chance for sedimentation is comparatively less in the case of nanofluids due to the smaller size of the particles in the fluid. The reduced possibility of sedimentation of nanoparticles makes a nanofluid more stable.[6] Nanofluids are more ideal for micro-channel applications where high heat loads are encountered. A highly conducting fluid, along with large heat transfer area, can be achieved in the microchannel-nanofluid combination and this is not possible in the case of meso or microfluids. This is because the micro and macro particles in a fluid clog the flow channels in the microchannel applications. The erosion of the components such as the exchangers, pumps and pipeline is less is the case of nanofluids due to the reduced momentum of impact to the solid wall. Also, the required pumping power for the nanofluids will be low due to the lesser enhancement in the viscosity with respect to the viscosity of the base fluid. The larger enhancement in the thermal conductivity, even with small volume fraction of the particles, and lesser enhancement in the viscosity are suitable for heat transfer applications. These significant factors make nanofluids as potential candidates for heat transfer applications.[6]

1.4. Models and mechanisms for thermal conductivity of nanofluids

1.4.1. Maxwell model

Maxwell, in 1881,[17] derived an expression for the thermal conductivity of a dilute and stationary suspension of spherical solid particles (micro/mini size) in liquid matrix based on the effective medium theory (EMT). The suspended particles are considered to be motionless and there is no interparticle interaction between the particles. The effective thermal conductivity of a solid-liquid mixture is given by,

$$k = \frac{k_p + 2k_f + 2(k_p - k_f)\varphi}{k_p + 2k_f - (k_p - k_f)\varphi} k_f \tag{1.1}$$

where, k is the effective thermal conductivity of the mixture, k_p and k_f are the thermal conductivities of the solid particle and liquid matrix, respectively, and φ is the volume fraction of the particles. The effective thermal conductivity of the solid-liquid mixture thus depends on the thermal conductivity of the solid particles and liquid matrix and the volume fraction of the particles present in the suspension.

Series and parallel modes of thermal conductivities are the mean field models for thermal conductivity.[15] In the parallel mode, the conducting phase, base fluid and the particles, are in parallel to the direction of heat flux whereas in the series mode, the conducting phases are in series. The effective thermal conductivities by these two modes are given by equation 1.2 and 1.3,

$$\frac{1}{k^{=}} = \frac{(1-\varphi)}{k_f} + \frac{\varphi}{k_p} \tag{1.2}$$

$$k^{\parallel} = (1-\varphi)k_f + \varphi k_p \tag{1.3}$$

where $k^{=}$ and $k^{\parallel}$ are series and parallel thermal conductivities, respectively. The parallel mode allows efficient way to transfer heat compared to the series mode.

The series and parallel mode are not the narrowest that can be estimated through the mean field approach. Hashin and Shtrikman (HS) [23-25] derived the set of bounds based on the volume fraction of the particles in the binary system. The HS model for thermal conductivity of a nanofluid is given by,

$$k_f\left(1+\frac{3\varphi[k]}{3k_f+(1-\varphi)[k]}\right)\leq k\geq\left(1-\frac{3(1-\varphi)[k]}{3k_p-\varphi[k]}\right)k_p \tag{1.4}$$

where $[k] = k_p - k_f$ and k is the thermal conductivity of the nanofluid. The terms on the left and right sides in the equation are the upper and lower limits of thermal conductivity. It is assumed that $k_p > k_f$, otherwise the lower and upper limits are simply reverse. In the lower HS limit, the nanoparticles are assumed to be well dispersed and the effective thermal conductivity is biased towards the conduction path in the fluid. In the upper HS limit, the conductivity is biased towards the conduction path along the dispersed nanoparticles. The lower HS limit lies closer to the series mode of conduction and the upper HS limit lies closer to the parallel mode of conduction.

1.4.2. Brownian motion

Particles in a suspension undergo collision with the nearby particles due their random motion leading to solid-solid heat transfer and this possibly enhances the thermal conductivity of a suspension. The random movement of the solid nanoparticles in a fluid carries the surrounding solvent molecules along with them leading to local convection effect and enhances the thermal conductivity of the nanofluids. Jang and Choi[26] found that the Brownian motion of the nanoparticles at the molecular scale and nanoscale level is the key mechanism for the thermal conductivity enhancement of nanofluids. The authors proposed a model based on the contribution from the base fluid, suspended particles and Brownian motion of the particles.

$$k = k_f(1-\varphi) + k_p\varphi + 3C\frac{d_f}{d_p}k_f Re_{d_f}^2 Pr\varphi \tag{1.5}$$

where C is a proportionality constant, d_f and d_p are the diameters of the base fluid molecule and the nanoparticle, respectively, Re is the Reynolds number $\left[Re = \frac{1}{\upsilon}\sqrt{\left(\frac{18k_BT}{\pi\rho d}\right)}\right]$ and Pr is the Prandtl number ($Pr = \frac{C_P\mu}{k_f}$). k_B is the Boltzmann constant, T is the temperature, ρ is the density of the particle, d diameter of the particle, C_P is the specific heat and μ is the dynamic viscosity. The proposed model is able to predict the particle size and temperature dependant thermal conductivity of many nanofluids.[27]

Xuan *et al*[28] modified the Maxwell model by introducing the Brownian contribution of the nanoparticles in a nanofluid. The effective thermal conductivity of the nanofluid is expressed as,

$$\frac{k}{k_f} = \frac{k_p + 2k_f - 2(k_f - k_p)\varphi}{k_p + 2k_f + (k_f - k_p)\varphi} + \frac{\rho_p \varphi C_p}{2k_f}\sqrt{\frac{k_B T}{3\pi r_C \eta}} \tag{1.6}$$

where r_c is the apparent radius of the clusters which depends on the fractal dimension of the clusters and η is the viscosity. This equation reduces to Maxwell equation for larger particles.

Prashar *et al*[29-30] modified the Maxwell model for larger enhancement in the thermal conductivity of nanofluids by including the convection of solvent molecules along with the nanoparticles due to Brownian motion. The modified Maxwell model by including the convection contribution is given as,

$$\frac{k}{k_f} = (1 + A\, Re^m Pr^{0.333}\phi)\left[\frac{(1+2\alpha) + 2\phi(1-\alpha)}{(1+2\alpha) - \phi(1-\alpha)}\right] \tag{1.7}$$

where, $\alpha = \frac{2R_b k_f}{d}$, R_b is the interfacial thermal resistance, d is the diameter of a particle, A is a constant (A = 40000) and m is a constant which depends on the base fluid.

1.4.3 Liquid layering at particle-fluid interface

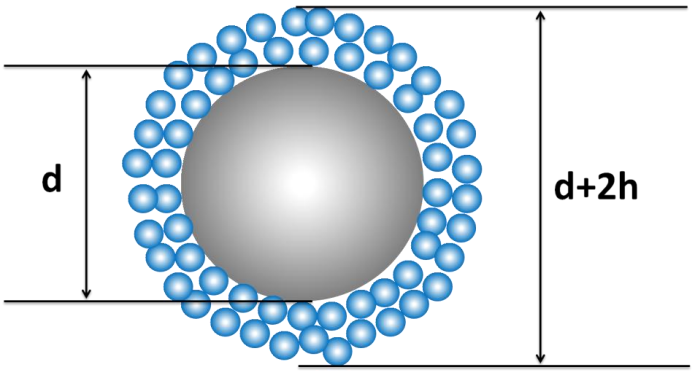

Figure 1.5. Ordered liquid layer at solid-liquid interface. 'd' is diameter of the particle and 'h' is the thickness of the interfacial layer

The solvent molecules near the surface of a particle are highly ordered compared to the solvent molecules in the bulk liquid (as shown in Figure 1.5). The ordered liquid layer at the interface of a particle and fluid behaves like a solid. Thermal conductivity of this ordered liquid layer is larger than that of the bulk liquid. Although the thickness of the liquid layer at the interface is of the order of nanometers, larger heat transfer capacity of this layer has considerable impact on the heat transport properties of nanofluids. The effect of the interfacial layer is negligible in the case of micron sized particles due to the less surface area. However, in the case of nanoparticles with larger surface area, the interfacial layer becomes more important due to its larger thermal conductivity.

Yu and Choi[31] proposed a modified Maxwell model by incorporating the effect of the interfacial layer on the effective thermal conductivity of a nanofluid. The thermal conductivity of the nanoparticle (k_p) is changed to k_{pe} in the modified model.

$$k_{pe} = \frac{[2(1-\gamma) + (1+\beta)^3(1+2\gamma)\gamma]}{-(1-\gamma) + (1+\beta)^3(1+2\gamma)} k_p \tag{1.8}$$

where, $\gamma = \frac{k_{layer}}{k_p}$ is the ratio between the nanolayer thermal conductivity (k_{layer}), and the thermal conductivity of the particle (k_p) and $\beta = \frac{h}{r}$ is the ratio between the thickness of the nanolayer (h) and the radius of the particle (r). The Maxwell model is modified as,

$$\frac{k}{k_f} = \frac{k_{pe} + 2k_f + 2(k_{pe} - k_f)(1-\beta)^3\varphi}{k_{pe} + 2k_f - (k_{pe} - k_f)(1+\beta)^3\varphi} \tag{1.9}$$

1.4.4. Interfacial thermal resistance

The interfacial thermal resistance is the phenomenon which reduces the conductivity of the interfacial layer at the particle-fluid interface. This is in contrast with the earlier discussed conductive layer at the particle-fluid interface which enhances the thermal conductivity at the interface and in turn enhances the overall heat transfer of the nanofluid. The discontinuity of the thermal conductance at the interface is also called as the Kapitza resistance. Nan *et al*[32] proposed a general methodology for effective thermal conductivity of composite materials of arbitrary shape by including interfacial thermal resistance using the effective medium approximation (EMA). The interfacial resistance at the interface has pronounced effect on the thermal conductivity of composite materials.

The effective medium approximation by including the interfacial thermal resistance for spherical particles is given by,

$$\frac{k}{k_f} = \frac{k_p(1+2\alpha) + 2k_h + 2\varphi\left[k_p(1-\alpha) - k_h\right]}{k_p(1+2\alpha) + 2k_h - \varphi\left[k_p(1-\alpha) - k_h\right]} \tag{1.10}$$

where, k_h is the thermal conductivity of the host material, $\alpha = \frac{2R_b k_f}{d}$, R_b is the interfacial thermal resistance and d is the diameter of the particles.

In the case of nanofluids, thermal conductivity of the host material (base fluid) is much lower than the thermal conductivity of the solid inclusions (nanoparticles), i.e. $k_h = k_f << k_p$, and the above equation is modified by Prasher *et al*[29-30] as,

$$\frac{k}{k_f} = \frac{(1+2\alpha) + 2\phi(1-\alpha)}{(1+2\alpha) - \phi(1-\alpha)} \tag{1.11}$$

1.4.5. Aggregation / clustering

Formation of aggregation/clustering of the particles in fluids are more common especially in the case of nanoparticles with larger surface area. The formation of percolating patterns of nanoparticle clusters has more impact on the effective thermal conductivity of nanofluids which reduces the thermal resistance. Formation of larger clusters could lead to settling of nanoparticles in a fluid and creates more particle-free space in the fluid leading to reduction in the thermal conductivity of a nanofluid. Although formation of percolating structures in a fluid requires larger volume fraction of the particles, anomalous enhancement in the thermal conductivity is observed even at lower concentrations, which is much lower than the threshold concentration for the formation of percolating structures. Even though percolating structures are not possible at lower concentrations, formation of local clusters is possible even at these concentrations.[33-34] The effective volume of the clusters is much larger than the volume of a particle and the heat transfer within these clusters is more. The volume fraction of these highly conductive clusters is larger than the volume of the solids. The larger volume fraction of these highly conductive clusters significantly enhances the thermal conductivity of the nanofluids.

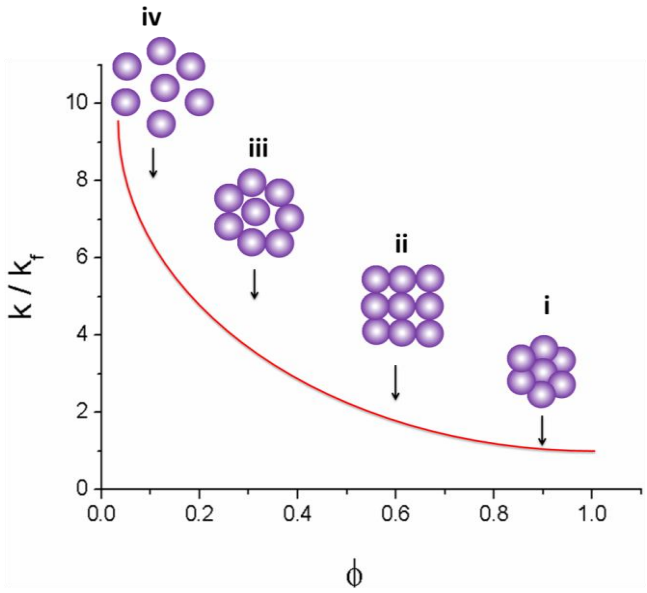

Figure 1.6. Enhancement in the thermal conductivity with increasing the effective volume fraction of clusters. (i) close packed FCC arrangement of particles, (ii) simple cubic arrangement, (iii) loosely packed irregular arrangement of particles which are in physical contact, and (iv) cluster of particles separated by liquid layer.[14]

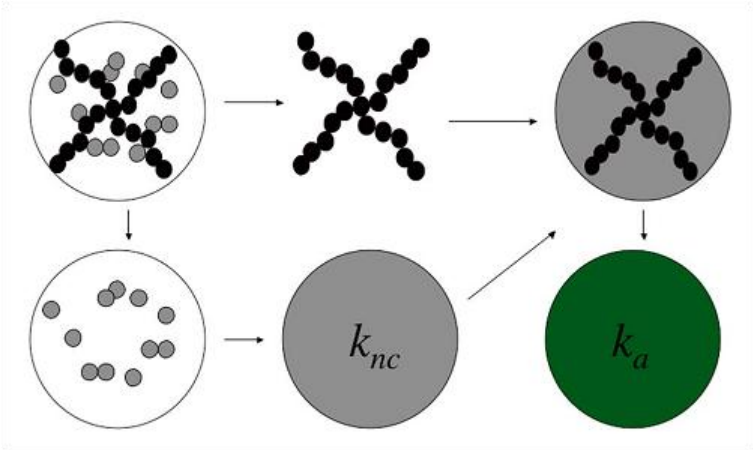

Figure 1.7. Schematic diagram of an aggregate consisting of backbones (black circles) and dead ends (gray circles). k_{nc} is the thermal conductivity of the aggregate only with particles belonging to the dead ends and k_a is the thermal conductivity of aggregates including the back bone with the effective conductivity of k_{nc}[35]

The effective volume of the clusters decreases with increasing packing fraction of the nanoparticles in the clusters and thermal conductivity enhancement decreases with increasing the packing fraction of the particles. Figure 1.6 shows the variation of the thermal conductivity ratio with the packing fraction of the particles in the clusters. For larger thermal

conductivity enhancement of the nanofluids, the particles need not to be in physical contact and separated by a specific distance which provides rapid increase in heat transfer. The clusters with very low packing fraction and high effective volume could be one of the reasons for the observed anomalous enhancement in the thermal conductivity of nanofluids.

Prashar *et al*[36] extended the Maxwell model by incorporating the effect of aggregation in the effective thermal conductivity of nanofluids. In the model, the authors considered that each aggregate consists of nanoparticles of a conductive phase (back bone) and nanoparticles of dead ends inside the aggregates. The effective thermal conductivity is calculated from the thermal conductivity of the base fluid and the dead ends of the nanoparticles inside the aggregates (k_{nc}) and then the thermal conductivity of the aggregates including the back bones (k_a) as shown in Figure 1.7. For calculating the thermal conductivity of the aggregates using this method, one need to know the size of the aggregates and the proportion of nanoparticles in the conductive path, which makes the method more difficult. The modified equation for the effective thermal conductivity is,

$$\frac{k}{k_f} = \frac{(k_a + 2k_f) + 2\varphi_a(k_a - k_f)}{(k_a + 2k_f) - \varphi_a(k_a - k_f)} \tag{1.12}$$

where k_a is the thermal conductivity of the aggregate sphere which includes the dead ends and back bones, φ_a is the volume fraction of the aggregates.

Different theoretical models have been proposed for the thermal conductivity of nanofluids by including various factors in the classical Maxwell model and some of these models are listed in Table 1.1.

Table 1.1. Different theoretical models proposed for thermal conductivity of nanofluids[37-38]

Investigator	Relative thermal conductivity (k_{eff}/k_b)	Remarks
Maxwell[17]	$\frac{k_p + 2k_f + 2(k_p - k_f)\varphi}{k_p + 2k_f - (k_p - k_f)\varphi}$	This model accounts for the thermal conductivity of the particles, base fluid and volume fraction
Hashin-Shtrikman (HS)[23]	$k_f\left(1 + \frac{3\varphi[k]}{3k_f + (1-\varphi)[k]}\right) \leq k \geq \left(1 - \frac{3(1-\varphi)[k]}{3k_p - \varphi[k]}\right)k_p$	Upper and lower limit of thermal conductivity
Hamilton and Crosser[18]	$\frac{k_p + (n-1)k_f - (n-1)(k_f - k_p)\varphi}{k_p + (n-1)k_f + (k_f - k_p)\varphi}$	For non-spherical particles, $k_p/k_f > 100$, n is an empirical shape and n=3/ψ, where ψ is the sphericity
Wasp *et al*[19]	$\frac{k_p + 2k_f - 2(k_f - k_p)\varphi}{k_p + 2k_f + (k_f - k_p)\varphi}$	Special case of Hamilton-Crosser model with ψ=1
Bruggeman[20]	$\frac{1}{4}\left[(3\varphi - 1)\frac{k_p}{k_f} + (2 - 3\varphi) + \frac{1}{4}\sqrt{\Delta}\right]$ $\Delta = \left[(3\varphi-1)^2\left(\frac{k_p}{k_f}\right)^2 + (2-3\varphi)^2 + 2(2 + 9\varphi - 9\varphi^2)\left(\frac{k_p}{k_f}\right)\right]$	Include the interactions between the particles
Jeffrey[21]	$1 + 3\left(\frac{k_p/k_f - 1}{k_p/k_f + 2}\right)\varphi + \left(3\left(\frac{k_p/k_f - 1}{k_p/k_f + 2}\right)^2 + \frac{3}{4}\left(\frac{k_p/k_f - 1}{k_p/k_f + 2}\right)^2 + \cdots\right)\varphi^2$	Spherical particles
Davis[22]	$1 + \frac{3(k_p/k_f - 1)\varphi}{(k_p/k_f + 2) - (k_p/k_f - 1)\varphi}\left(\varphi + f(k_p/k_f)\varphi^2 + O(\varphi^3)\right)$	Higher order terms represents pair interaction of randomly dispersed spheres
Yu and Choi[31,39]	$\frac{k_{pe} + 2k_f + 2(k_{pe} - k_f)(1+\beta)^3\varphi}{k_{pe} + 2k_f - (k_{pe} - k_f)(1+\beta)^3\varphi}$, $1 + \frac{n\varphi_{eff}A}{1 - n\varphi_{eff}A}$	Modified Maxwell and Hamilton-Crosser model by including the effect of interfacial layer
Xue[40]	$9\left(1 - \frac{\varphi}{\lambda}\right)\frac{k - k_f}{2k + k_f} + \frac{\varphi}{\lambda}\left[\frac{k - k_{C,x}}{k + B_{2,x}(k_{C,x} - k)}\right] + 4\frac{k - k_{C,x}}{2k + (1 - B_{2,x})(k_{C,y} - k)} = 0$	This includes the effect of interface between the solid and liquid
Xue and Xu[41]	$\left(1 - \frac{\varphi}{\alpha}\right)\frac{k - k_f}{2k + k_f} + \frac{\varphi}{2}\frac{(k-k_2)(2k_2 + k_1) - \alpha(k_1 - k_2)(2k_2 + k)}{(2k + k_2)(2k_2 + k_1) + 2\alpha(k_1 - k_2)(k_2 - k)} = 0$	Modified Bruggeman model including interfacial shells
Xie et al[42]	$1 + 3\Theta\varphi_T + \frac{2\Theta^2\varphi_T^2}{1 - \Theta\varphi_T}$	This includes the effect of nanolayer on the nanoparticle surface
Xuan *et al*[28]	$\frac{k_p + 2k_f - 2(k_f - k_p)\varphi}{k_p + 2k_f + (k_f - k_p)\varphi} + \frac{\rho_p\varphi C_p}{2k_f}\sqrt{\frac{k_B T}{3\pi r_C \eta}}$	This includes the effect of random motion, interfacial interactions
Kumar *et al*[43]	$1 + C\frac{2k_B T}{(\pi\nu d_p^2)}\frac{\varphi r_b}{k_f(1-\varphi)r_p}$	This includes the effect of particle size, concentration and temperature
Prashar *et al*[29]	$(1 + A\,Re^m Pr^{0.333}\phi)\left[\frac{(1+2\alpha) + 2\phi(1-\alpha)}{(1+2\alpha) - \phi(1-\alpha)}\right]$	Convection of the liquid around the particle surface
Koo and Kleinstreuer[44]	$\frac{k_{\ Maxwell}}{k_f} + 5\times10^4\beta\varphi\rho_p C_p\sqrt{\frac{kT}{\rho_p D}}\frac{f(T,\varphi)}{k_f}$	Surrounding liquid motion along with the nanoparticle motion
Nan *et al*[32]	$\frac{k_p(1+2\alpha) + 2k_f + 2\varphi[k_p(1-\alpha) - k_f]}{k_p(1+2\alpha) + 2k_f - \varphi[k_p(1-\alpha) - k_f]}$	model includes interfacial thermal resistance
Prashar *et al*[35-36]	$\frac{(k_a + 2k_f) + 2\varphi_a(k_a - k_f)}{(k_a + 2k_f) - \varphi_a(k_a - k_f)}$	model includes the effect of aggregation

1.5. Experimental studies on thermal conductivity of nanofluids

In the recent years, research work has been focused on heat transport using nanofluids due to the anomalous enhancement in the thermal conductivity beyond the Maxwell's predictions based on the effective medium theory even at very low volume fractions of the particles.[33, 45] There are various factors which contribute to the enhancement of thermal conductivity of nanofluids such as particle volume concentration, particle size, particle shape, particulate material, base fluid, temperature etc, and some of these factors are discussed below.

1.5.1. Effect of concentration

The effect of volume fraction of the nanoparticles on thermal conductivity of nanofluids has been studied by different research groups using different nanoparticle materials of various sizes dispersed in different base fluids. It is generally observed that thermal conductivity increases with increasing concentration of the nanoparticles. However, the percentage enhancement of the thermal conductivity is found to be quantitatively different for different materials dispersed in the same base fluid. Some experimental results showed no enhancement in the thermal conductivity of the nanofluids up to certain volume fraction of the particles and enhancement in the thermal conductivity beyond a certain concentration.[46] Table 1.2 compares some of the experimental results on the variation of thermal conductivity of nanofluids with volume fraction of the particles.

1.5.2. Effect of particle size

The size of the nanoparticles in nanofluids is one of the important factors that determine the thermal conductivity. The smaller size of the particles with larger surface area allows more heat transfer due to the presence of large number of surface atoms responsible for more thermal interaction. Moreover, the smaller particles in a fluid moves randomly due to the thermal energy and this also induces convection of the fluid molecules which leads to enhancement in the thermal conductivity. However, some of the experimental results show increase in the thermal conductivity of nanofluids with decreasing particle size,[47-49] whereas other experimental results show increasing thermal conductivity of nanofluids with increasing particle size.[50-55] Table 1.3 lists variation of thermal conductivity with particle size studied by different research groups using different particulate materials and base fluids.

Table 1.2. Experimental results on the variation of thermal conductivity enhancement of nanofluids with volume percentage of particles

Nanoparticle/ base fluid (Nanofluid)	**Volume% range**	k/k_f	**Reference**
Ag/ H_2O	0 – 0.4	1.11	56
Al/ EG	1 - 5	1.45	57
Al/ EO		1.31	
AlN/ EG	0 - 10	1.387	58
AlN/ PG		1.402	
Al_2O_3/ EG	1 - 5	1.18	57
Al_2O_3/ EG	0 - 8	1.32	59
Al_2O_3/H_2O	0 - 5	1.3	60
Al_2O_3/ H_2O	0 - 9.3	1.17	59
Al_2O_3/ NH_3-H_2O	0 - 4	1.18	61
Au/ EG	0 - 5	1.45	62
CNT/ Oil	0 - 1	2.6	45
Cu/ EG (acid)	0 - 0.3	1.4	33
Cu/ EG (fresh)	0 - 0.55	1.15	
Cu/ EG (old)	0 - 0.55	1.10	
Cu (30 nm)/ Paraffin	0-5	1.519	63
Cu (40 nm)/ Paraffin		1.481	
CuO (30 nm)/ MEG		1.479	
CuO (40 nm)/ MEG		1.397	
CuO/ H_2O	0-5	1.6	60
Fe/ EG	0.1 – 0.55	1.18	64
Fe_3O_4/ H_2O	0 - 3	1.114	65
Fe_3O_4/ H_2O	0 - 5	1.41	66
Fe_3O_4/ Kerosene	0 -7.8	1.23	46
Fe_3O_4/ Kerosene	0 - 1	1.35	67
SiC (26 nm)/ H_2O	0 – 4.2	1.158	68
SiC (600 nm)/ H_2O	0 - 4	1.229	
SiC/ H_2O	0 - 7.4	1.30	69
SiC/ NH_3-H_2O	0 - 4	1.08	61
SiO_2/ H_2O	0 – 0.4	1.05	56
TCNT/ H_2O	0.2 - 1	1.196	70
TCNT/ EG		1.127	
TiN/ NH_3H_2O	0 - 4	1.03	61
TiO_2 (10 nm)/ H_2O	0 - 5	1.33	71
TiO_2 (15 nm)/ H_2O		1.30	
TiO_2/ NH_3 H_2O	0 - 4	1.125	61
TiO_2/ EG	0 - 5	1.18	62
TiO_2/ EG	1 - 5	1.17	57
ZnO/ EG	0 - 3	1.175	72

Table 1.3. Experimental results on the variation of thermal conductivity enhancement of nanofluids with size of nanoparticles

Nanoparticle/ fluid (Nanofluid)	Particle size (nm)	Volume%	k/k_f	Reference
Ag_2Al/ H_2O	33	2	2.07	48
	80		1.9	
	120		1.75	
Ag_2Al/ EG	33	2	1.96	
	80		1.76	
	120		1.63	
Al_2Cu/ H_2O	32	2	1.97	
	68		1.77	
	100		1.62	
Al_2Cu/ EG	32	2	1.84	
	68		1.67	
	100		1.56	
Al_2O_3/ H_2O	36	4	1.093	73
	47		1.097	
Al_2O_3/ H_2O	11	1	1.08	49
	47		1.03	
	150		1.01	
Al_2O_3/ H_2O	12	2	1.088	53
	16		1.092	
	245		1.12	
	282		1.132	
CeO_2/ H_2O	12	4	1.122	54
	74		1.217	
Fe_3O_4/ Oil	4	4	1.264	47
	6		1.226	
	10		1.21	
	24		1.17	
	44		1.16	
Fe_3O_4/ Kerosene	2.8	5.5	1.05	55
	3.6		1.08	
	4.5		1.12	
	6.1		1.17	
	8.5		1.21	
	9.5		1.25	
α- SiC/ H_2O	16	4.1	1.07	51
	29		1.097	
	66		1.12	
	90		1.125	
SiO_2/ H_2O	10.7	16	1.058	74
	16.7		1.079	
	28.6		1.165	
TiO_2/ H_2O	5	5	1.215	50
	20		1.3	
	50		1.325	
	100		1.37	

1.5.3. Effect of particle shape

Table 1.4. Experimental results on the variation of thermal conductivity enhancement of nanofluids with shape of particles

Nanoparticle/ base fluid (Nanofluid)	Volume%	Shape	k/k_f	Reference
Al_2O_3/ H_2O: EG (50:50)	7	Bricks	1.245	75
		Blades	1.18	
		Cylinders	1.27	
		Platelets	1.18	
CuO/ H_2O	0.1	Sphere	1.15	76
		Rod	1.17	
CuO/ EG	0.1	Sphere	1.19	
		Rod	1.21	
CuO/ EO	2 Wt %	Nanosphere	1.045	77
		Nanorhombic	1.053	
		Nanorod	1.0606	
SiC/ H_2O	4	Sphere	1.15	68
		Cylinder	1.23	
TiO_2/ EG	5	Sphere	1.175	57
		Cylindrical	1.2	

It has been observed that nanostructures with high aspect ratio dispersed in base fluids showed larger enhancement in the thermal conductivity compared to that of the nanofluids containing spherical particles of the same material and at same volume concentrations (as shown in Table 1.4). Pal *et al*[76] observed 15% enhancement for CuO spherical nanoparticles dispersed in water at 0.1 volume% whereas at the same concentration CuO nanorods showed 17% enhancement in the thermal conductivity. Murshed *et al*[57] observed 17.5% enhancement in the thermal conductivity for TiO_2 spherical nanoparticles dispersed in ethylene glycol at 5 volume%, but at the same concentration, TiO_2 cylindrical particles showed 20% enhancement in the thermal conductivity. Similarly, spherical SiC nanoparticles dispersed in water showed 15% enhancement at 4 volume% and cylindrical SiC nanoparticles showed 23% enhancement at the same concentration.[68]

1.5.4. Effect of particulate material

The intrinsic thermal conductivity of the nanoparticle material is important in the thermal conductivity enhancement of nanofluids. In most of the reports, nanoparticles having larger intrinsic thermal conductivity showed relatively larger enhancement in the thermal

conductivity for the fluids. However, it is also reported that nanoparticles with lower intrinsic thermal conductivity enhances the thermal conductivity of the fluid than with the material with higher intrinsic thermal conductivity at same concentration. Zhu *et al*[78] observed higher thermal conductivity for Fe_3O_4 (38%) nanofluids compared to other metal oxide based nanofluids such as TiO_2, CuO and Al_2O_3 (30%), although the intrinsic thermal conductivity of the Fe_3O_4 (7 W/mK) is lower than that of TiO_2 (11.7 W/mK), CuO (20 W/mK) and Al_2O_3 (36 W/mK). The authors claimed that the observed enhancement for Fe_3O_4 based nanofluid is due to the alignment of the nanoparticles as close clusters and the thermal conductivity increases with increasing concentration because of the length of the aligned particles increased. Similarly, Hong *et al*[64] observed that Fe based nanofluids have higher thermal conductivity enhancement than Cu based nanofluids, even though bulk Fe (80 W/mK) is less thermal conducting than bulk Cu (384 W/mK). Fe nanofluids showed 18% enhancement at 0.55 volume percentage of the particles whereas the Cu nanofluid showed 14% enhancement at the same volume percentage of the particles. The authors concluded that highly thermal conducting material is not always the best candidate for improving the thermal property of the fluids.

1.5.5. Effect of base fluid

The dynamic properties of the nanoparticles in a fluid are strongly influenced by the viscosity of the base fluid. For the nanoparticles dispersed in highly viscous base fluid, the particles experience more dragging force due to the surrounding solvent molecules, reducing the Brownian velocity and eventually reducing the Brownian motion dependent thermal conductivity of the nanofluid.[79-80] Aggregation/clustering of nanoparticles in nanofluids are common due to the van der Waals interaction between the high surface energy nanoparticles. It was observed that slight aggregation/clustering of the nanoparticles could form highly conductive heat transfer path in the nanofluid leading to larger enhancement in thermal conductivity of nanofluids.[36] The viscosity of the base fluid also influences the interaction between the particles. Highly viscous nanofluid reduces the van der Waals interaction and reduces the aggregation of nanoparticles eventually changing the heat transport properties.[81-82] The thermophysical properties of the base fluid at the interface also influence the heat transport at the interface and in turn that of the nanofluid.[81, 83-85]

1.5.6. Effect of temperature

Table 1.5. Experimental results on the variation of thermal conductivity of nanofluids with temperature.

Nanoparticle/ base fluid (Nanofluid)	Volume%	Temperature (°C)	k/k_f	Reference
Al_2O_3/ H_2O	4	21	1.094	27
		31	1.13	
		41	1.195	
		51	1.243	
Al_2O_3/ H_2O	4	21	1.08	49
		31	1.12	
		41	1.165	
		51	1.19	
		61	1.24	
		71	1.29	
Al_2O_3/ H_2O	4	27.5	1.077	73
		35	1.181	
Cu/ EG	0.5	10	1.08	86
		20	1.125	
		30	1.18	
		40	1.29	
		50	1.46	
Graphene/ H_2O	0.2	30	1.108	87
		40	1.164	
		50	1.27	
Fe_3O_4/ Kerosene	9.5	25	1.25	88
		35		
		45		
Fe_3O_4/ Kerosene	4.7	25	1.195	89
		35		
		45		
Fe_3O_4/ EG:H_2O (60:40)	0.2	20	1.05	90
		30	1.08	
		40	1.095	
		50	1.105	
SiC/ H_2O	4	23	1.21	69
		49		
		70		

The Brownian motion of the nanoparticles in a fluid increases with increasing temperature leading to increase in the thermal conductivity enhancement with increasing temperature. Most of the experimental studies have reported increased thermal conductivity with increasing temperature.[27, 49, 73, 86-87, 90-91] However, few experimental results showed decreased thermal conductivity with increasing temperature.[92-93] Some experimental results showed no

significant change in the thermal conductivity with the temperature.[69, 88-89] Table 1.5 compares variation of the thermal conductivity with temperature for different nanofluids.

1.5.7. Other factors

The dispersion and stability are important characteristics of nanofluids which mainly influence the thermophysical properties of nanofluids. Apart from the various factors discussed in the previous sections 1.5.1 to 1.5.6, the interfacial related factors such as surface chemistry, surfactants, nature of surfactants, surface charge and pH are also important factors which affects the thermal conductivity of nanofluids since these factors are directly related to the dispersion and stability of nanofluids.[94-96] Xie *et al*[70] observed that entangled CNTs show poor dispersion in water whereas the CNTs disentangled with nitric acid shows good dispersion due to the oxygen containing functional groups, and larger enhancement in the thermal conductivity. Patel *et al*[97] observed that thiolate molecules on the surface of Au nanoparticles are less effective compared to citric acid for thermal conductivity enhancement. Lee *et al*[98] demonstrated that the surface charge present on the surface of nanoparticles is primarily responsible for thermal conductivity enhancement.

1.6. Viscosity of nanofluids

Table 1.6. Classical models for the effective viscosity of solid-liquid mixtures

Model name	Effective viscosity	Remarks
Einstein[99]	$\frac{\eta}{\eta_f} = 1 + 25\varphi$	Spherical particles of low volume concentrations $\varphi \leq 0.02$
Krieger and Dougherty (K-D model)[100]	$\frac{\eta}{\eta_f} = \left[1 - \frac{\varphi_p}{\varphi_m}\right]^{-\eta_0 \varphi_m}$	Based on randomly monodispersed hard spheres. Valid for maximum close packed particles
Nielson[101]	$\frac{\eta}{\eta_f} = (1 + 1.5\varphi_p) e^{\frac{\varphi_p}{(1-\varphi_m)}}$	Power law based model and is more appropriate for particle concentration $\varphi > 0.02$
Batchelor[102]	$\frac{\eta}{\eta_f} = 1 + 25\varphi + 6.5\varphi^2$	Extension of Einstein model considering the Brownian motion

Addition of solid nanoparticles in a liquid (base fluid) not only increases the thermal conductivity of the fluid but also increases the viscosity. Viscosity of a nanofluid is

considered to be an important parameter for many practical applications because viscosity of the nanofluids directly affects the pressure drop in forced convection. The increase in viscosity leads to increase in the power required for pumping the nanofluids. Highly thermal conducting and less viscous nanofluid can be pumped at higher velocity leading to larger heat transfer.[103] Viscosity of the nanofluids can be affected by the particle size, shape, distribution, surfactants, liquid layering, interparticle interaction, dispersion characteristics and compatibility of the solvent with the surface of the nanoparticles. There are various models proposed for the viscosity of a nanofluid originating from the classical models for simple solid suspensions in a liquid carrier by including various other factors.[104] Table 1.6 lists some of the classical models for viscosity of solid-liquid mixtures.

Many of the experimental results report non-Newtonian behaviour (change in viscosity with shear rate) for a nanofluid.[105-113] However, there are experimental results showing Newtonian behaviour (constant viscosity with shear rate) of the nanofluids which are most useful for practical applications, because it requires less pumping power.[108, 114-117] Nguyen *et al*[118-119] measured the viscosity of Al_2O_3 based nanofluids of different particle sizes and found increase in the viscosity with increasing particle size. Tao *et al*[117] and Fei *et al*[120] reported decrease in the viscosity of SiO_2 nanofluids with increasing particle size. Timofeeva *et al*[121] measured the viscosity of nanofluids containing Al_2O_3 nanoparticles of different sizes and did not observe any variation in the viscosity with particle size. However, in another study the authors observed increase in the viscosity with decreasing particle size of SiC nanoparticles in water.[51] Some of the reports show that aggregation of nanoparticles in a fluid leads to increase in the viscosity.[108-109] It is also reported that the nature of the surfactants also affects the viscosity of the nanofluids.[11]

1.7. Magnetic nanofluids

Magnetic (nano) fluids or ferrofluids are the suspension of surfactant coated single domain magnetic nanoparticles dispersed in non-magnetic liquid carriers. Magnetic nanoparticles in a fluid behave like tiny magnets with permanent magnetic dipoles. In addition to the weak van der Waals interaction, magnetic dipole-dipole interaction between the magnetic nanoparticles leads to aggregation or sedimentation of the particles in a fluid. Coating the nanoparticles with a surfactant stabilizes the particles against dipole-dipole and van der Waals interactions by steric and/or electrostatic stabilization of the particles. This results in stable magnetic suspensions even in the presence of an applied magnetic field.[122, 123]

1.7.1. Magnetic nanomaterials

Nanosized magnetic materials exhibit interesting and anomalous magnetic properties compared to that of the bulk counterpart due to their smaller size.[124]Therefore, magnetic nanomaterials are useful for a variety of applications such as in magnetic recording industry, magneto-optical devices, ferrofluid based applications, and biomedical applications such as drug delivery, drug targeting, magnetic resonance imaging (MRI), cell separation, hyperthermia etc.[125-127] Finite size and surface effects are the major contributions toward the anomalous magnetic properties of magnetic nanoparticles.

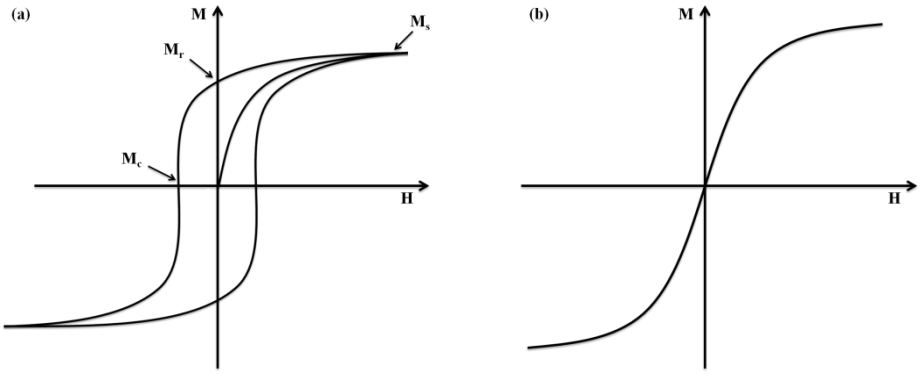

Figure 1.8. Magnetization behaviour of a typical (a) ferromagnetic material and (b) superparamagnetic material, as a function of applied magnetic field.

Magnetization of bulk ferromagnetic/ferrimagnetic materials shows irreversibility in the magnetization with the applied magnetic field. With increasing magnetic field, the magnetization of the material increases non-linearly and reaches a maximum value, called the saturation magnetization (M_s). The reversal of magnetic field leads to decrease in the magnetization with a finite magnetization at zero field, called the remanent magnetization (M_r). The negative magnetic field applied to bring the magnetization to zero is called the coercive field (H_c). A plot of magnetization with applied magnetic field for a ferromagnetic material shows hysteresis loop (as shown in Figure 1.8 (a)). The hysteresis loop represents the energy loss during the magnetization and demagnetization processes. The energy loss or hysteresis loss is directly proportional to the area of the loop.[128-129]

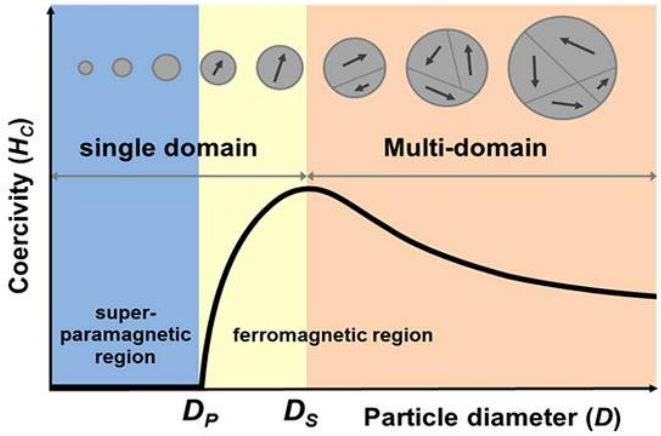

Figure 1.9. Schematic diagram showing variation of coercivity (H_C) as a function of particle diameter (D).[130]

Finite size effect in magnetic nanoparticles arises from the quantum confinement of electrons and it dominates the magnetic properties of the individual magnetic nanoparticles. Single domain limit and superparamagnetic limit are the most studied finite size effects in small magnetic nanoparticles. In bulk magnetic particles, the magnetization vectors in each magnetic domain are uniformly magnetized in the same direction and are separated from other domains, magnetized in different directions by domain walls in order to minimize the magnetostatic energy. Domain wall formation is the process driven by the balance between the domain wall energy (ΔE_{dw}) and the magnetostatic (ΔE_{MS}) energy. The magnetostatic energy depends on the size of the magnetic particles and the domain wall energy depends on the interfacial region between the domains. When the size of a particle is reduced to smaller dimensions, particularly in the nanoscale level, it requires more energy to create a domain wall than to support the magnetostatic energy. Thus, the particles exist as single domain below the critical diameter (D_S), below which it costs more energy to create a domain wall.[131-132] The critical diameter (D_S) is different for different materials and it is in the rage of few tens of nanometers.[133]

At the critical diameter, the magnetostatic energy and the domain wall energy become equal ($E_{MS} = E_{dw}$) and the particles exist as single domain particles. The critical diameter (D_S) for a particular material is expressed as,[132]

$$D_S \approx 18\frac{\sqrt{AK}}{\mu_0 M^2} \tag{1.13}$$

where A is the exchange constant, K is the anisotropy constant, μ_0 is the vacuum permeability, and M is the saturation magnetization. The magnetization vector in a single domain particle is spontaneously magnetized in a particular direction. The single domain particle in a magnetic field reverses the direction of magnetization by spin rotation and there is no domain wall motion due to the absence of domain walls. The general trend in the variation of the coercivity of a magnetic material with particle diameter is shown in Figure 1.9. The coercivity of a single domain particle is initially high due to larger anisotropy of the particles, and it is difficult to reverse the direction of magnetization which requires larger magnetic field. The decrease in the coercivity below the critical diameter (D_S) is due to the increase in the randomization due to thermal energy. Finally the coercivity reaches zero at the particle diameter, D_P, where the flipping of the magnetization with thermal energy is more and is called the superparamagnetic state (as shown in Figure 18(b)).[130]

Superparamagnetism in magnetic nanoparticles is an important finite size effect. In single domain particles, the anisotropy energy of the particle holds the magnetization in a particular direction. Anisotropy energy of the magnetic nanoparticle depends on the volume of the nanoparticle.

$$E(\theta) = KVsin^2\theta \tag{1.14}$$

where, K is the anisotropy constant, V is the volume of a particle and θ is the angle between the easy axis and magnetization. The anisotropy energy barrier (KV) separates the two energetically equivalent easy directions of magnetization. The anisotropy energy of the bulk materials is much larger than the thermal energy (k_BT) and the anisotropy energy (KV) decreases with decreasing the particle size of the magnetic nanoparticle. Thermal energy (k_BT) dominates over the anisotropy energy (KV) for smaller particles and the magnetization flips from the easy direction as shown in Figure 1.10.[134] When the thermal energy is larger than the anisotropy energy ($k_BT>>KV$) the material behaves like a paramagnet with a huge moment inside the nanoparticles which is called superparamagnetism. Due to the flipping of the magnetization by thermal energy, superparamagnetic systems show zero remanence and coercivity.

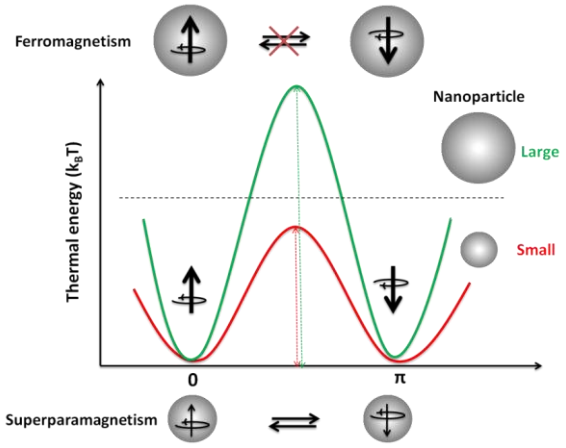

Figure 1.10. Energy diagram of magnetic nanoparticles with different spin alignments. Larger particles show ferromagnetism (top) and smaller particles show superparamagnetism (bottom).[134]

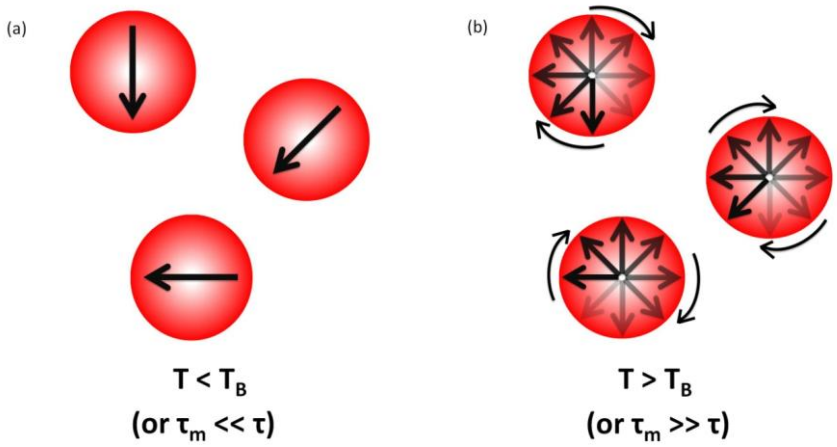

Figure 1.11. Schematic diagram indicating the concept of superparamagnetism. The red circles indicate the particles and arrow indicates the net magnetic moment of the particles. (a) at temperature (T) lower than the blocking temperature (T_B), the relaxation time (τ) of the particle is larger than the measurement time (τ_m). At temperature larger than the blocking temperature, the relaxation time (τ) is lower than the measurement time (τ_m).[125]

Magnetic nanoparticles with uniaxial anisotropy randomly flip their magnetization due to the thermal energy. The average relaxation time to flip the magnetization is given by the Neel-Brown expression.

$$\tau = \tau_0 \, exp\left(\frac{KV}{k_B T}\right) \tag{1.15}$$

where, τ is the relaxation time, τ_0 is the pre-exponential factor and it is in the order of 10^{-10} to 10^{-12} s and weakly dependent on temperature, k_B is the Boltzmann constant and T is the temperature. Superparamagnetism of a particle not only depends on the temperature but also on the measurement time (τ_m). If the measurement time (τ_m) is much larger than the relaxation time (τ), $\tau_m >> \tau$, magnetic moment of a nanoparticle flips randomly many times and the particle is seen in the superparamagnetic state. If the measurement time (τ_m) is much smaller than the relaxation time (τ), $\tau_m << \tau$, then magnetic moment of the nanoparticle is in the blocked state. The temperature which separates the two regimes, superparamagnetic and blocked sate, is called the superparamagnetic blocking temperature (T_B).[125, 135] The blocking temperature (T_B) can be calculated by considering the time window of the measurement ($\tau \approx$ 10–100 s),

$$T_B \approx \frac{KV}{25k_B} \tag{1.16}$$

At temperatures below the blocking temperature ($T < T_B$), the magnetic moment is blocked and above the blocking temperature ($T > T_B$) direction of magnetization flips its direction randomly as shown in Figure 1.11. The blocking temperature can be obtained from filed cooled (FC) and zero field cooled (ZFC) DC magnetization measurements, as shown in Figure 1.12. The temperature corresponding to the maximum in the ZFC magnetization curve and below which the FC and ZFC magnetizations bifurcate is the superparamagnetic blocking temperature. Magnetic hysteresis loop will be observed below the blocked state and superparamagnetic state is characterized by absence of magnetic hysteresis.

The blocking temperature depends on the anisotropy constant, particle size, applied magnetic field and measurement time. The anisotropy energy of the particle increases with the size of the nanoparticles and the thermal energy (k_BT) required to overcome the anisotropy energy of a particle will be higher for larger particles.[136-140] Nanoparticles of the same size show different blocking temperatures in different applied magnetic field, where the blocking temperature decreases with increasing applied magnetic field.[137-139]

The magnetic properties of a nanoparticle system are often influenced by the interactions between the particles. These interactions can have significant influence on the superparamagnetic relaxation of the nanoparticles. There are four major types of interactions possible in a nanoparticle system; (i) dipole-dipole interactions, (ii) direct exchange interactions between particles which are in close contact, (iii) super-exchange interactions for

metal particles in an insulating matrix, and (4) RKKY (Ruderman-Kittel-Kasuya-Yosida) interactions for metallic particles embedded in a metallic matrix.[131] Out of these interactions, the magnetic dipole-dipole interaction is one of the most important in the case of magnetic nanoparticles. The effect of dipole-dipole interaction on the magnetic properties of magnetite nanoparticles is studied by dispersing magnetite nanoparticles in non-magnetic paraffin liquid matrix at different concentrations (Figure 1.12).[141] The observed decrease in the blocking temperature with decreasing concentration of the particles is attributed to the reduced anisotropy contribution from dipole-dipole interaction due to the increased separation between the particles in paraffin liquid. Due to the reduced anisotropy, less thermal energy is required to overcome the anisotropy energy. The nature of the field cooled curves below the blocking temperature also changes with decreasing concentration; a continuous increase in magnetization with decreasing temperature for the less concentrated sample (C005) and saturating trend for the highly concentrated (C45) as well solid (powder) samples. The increasing magnetization below T_B is again due to the decreased anisotropy from interparticle interactions because the small applied field is sufficient to overcome the anisotropy energy and the temperature effect.

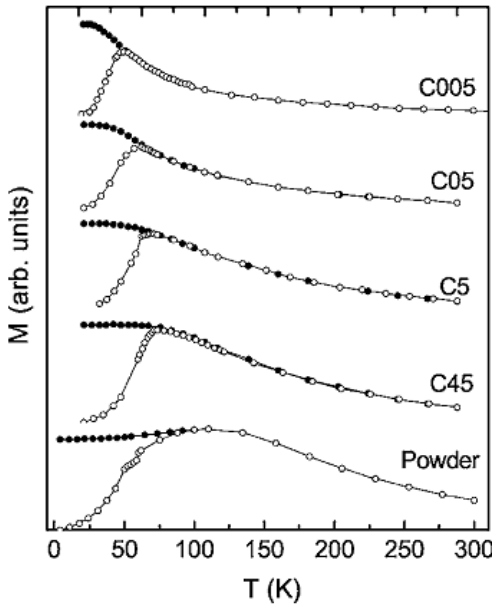

Figure 1.12. ZFC (open circles) and FC (closed circles) magnetization curves of solid magnetite nanoparticles and particles dispersed in paraffin liquid at different concentrations (C005, C05, C5, and C45 correspond to 0.005, 0.05, 0.5 and 45% mass of Fe_3O_4 in paraffin liquid). The maximum in the ZFC curve (at the blocking temperature) moves to lower temperatures, with decreasing the concentration of the particles. The irreversibility (difference between ZFC and FC magnetization) increases with decreasing concentration indicating reduction in the interparticle interaction.[141]

When particle size is reduced to nanoscale, large number of atoms is exposed on the surface of the nanoparticles. This larger number of surface atoms, compared to that in the bulk, contributed more to the magnetic properties of the nanoparticles. In the case of magnetic nanoparticles, the magnetization is reduced when the particle size is decreased. The reduction in the magnetization could be attributed to the loss of magnetic ordering due to the formation of an amorphous layer because of the changes in the bond length, bond angle and coordination environment on the surface of the nanoparticles, magnetically dead layer, canted spin structure, or spin-glass behavior of the spins on the surface of the nanoparticles.[142]

The enhancement in the anisotropy with decreasing particle size is another surface effect, contributed by surface anisotropy.[143-144] Increase in the magnetization is reported for antiferromagnetic nanoparticles, due to the enhanced contribution from the canted spins on the surface.[145] It has been reported that gold coated cobalt nanoparticles show less anisotropy than uncoated cobalt whereas gold coated iron nanoparticles exhibit enhanced anisotropy than the uncoated iron nanoparticles.[146] Organic ligands, used as surfactants to stabilize magnetic nanoparticles, also influence the magnetic properties of the nanoparticles after coating. It has been shown that carboxylate layer, which is attached to the iron atom on the surface of magnetite nanoparticles, decreases magnetization whereas phosphonate group attached to the iron atom on the surface of the magnetite nanoparticle does not affect the magnetic properties of the nanoparticles.[147] Thus, magnetic properties of nanoparticles are highly sensitive to the particular surface coating.

1.7.2. Dipole-dipole interaction in the presence of a magnetic field

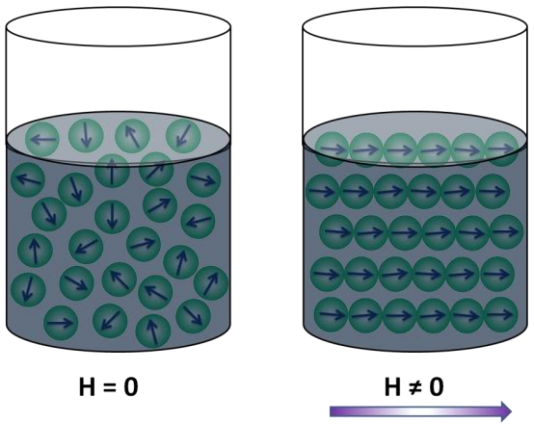

Figure 1.13. Magnetic nanoparticles in a magnetic fluid in the absence and presence of an external magnetic field.

For single domain nanoparticles of ferro- or ferrimagnetic substances dispersed in magnetic fluids, each and every particle will have its own magnetic moment *m*, and the magnetic moment depends on the core volume of the particle. Every particle in a fluid undergoes Brownian motion due the temperature effect and interacts with other particles and could form different kind of aggregation. In the presence of a magnetic field, magnetic nanofluids show optical anisotropic behavior and viscosity of magnetic fluids also increases with applied magnetic field.[148-152] The changes in the physical properties of a magnetic fluid are due to the formation of high strength dipolar systems through chain like aggregation of particles.[46, 153] In the absence of a magnetic field, the nanoparticles are randomly oriented due to the thermal energy which fluctuates the magnetization energy (anisotropy energy) of the particles and leads to less interparticle interaction between the particles. In the presence of a magnetic field, the magnetic dipoles in the magnetic nanoparticles are oriented in the direction of the applied magnetic field (as shown in Figure 1.13). The formation of the dipolar chain in a magnetic fluid in the presence of a magnetic field is due to the interparticle magnetic dipole-dipole interaction ($U_d(ij)$) between the particles in a fluid.[154]

$$U_d(ij) = -\left[3\frac{(m_i.r_{ij})(m_j.r_{ij})}{r_{ij}^5} - \frac{(m_i.m_j)}{r_{ij}^3}\right] \tag{1.17}$$

$$r_{ij} = r_i - r_j \tag{1.18}$$

where, m_i and m_j are the magnetic moments of i^{th} and j^{th} particles, respectively, and r_{ij} is the separation between the i^{th} and j^{th} particles. The length of the dipolar chain formed in a magnetic fluid depends on the concentration of the magnetic nanoparticles in the fluid and the strength of the applied magnetic field. Drastic changes in the physical and thermophysical properties of magnetic fluids are observed in the presence of a magnetic field.[153] The tunable thermophysical properties of a magnetic fluid in the presence of a magnetic field are useful for various applications.[125-127]

1.7.3. Neel and Brownian relaxation in magnetic fluids

Magnetization vectors (dipole) of magnetic nanoparticles in a fluid align in the direction of the applied magnetic field. When the magnetic field is removed, relaxation of magnetization occurs in two different ways such as Neel relaxation (τ_N) and Brownian relaxation (τ_B).[155] The Neel's relaxation is caused by the thermal fluctuations of the magneto-crystalline anisotropy

between the easy directions of magnetization (shown in Figure 1.14), by which the magnetization vector in the nanoparticles reorient against the anisotropy energy barrier. The time constant for the Neel's relaxation strongly depends on the particle diameter and in turn to the magnetocrystalline anisotropy of the particle. The Neel's relaxation time (τ_N) can be determined from the ratio between the anisotropy energy and the thermal energy, as given by equation 1.15.

Another type of relaxation is the Brownian relaxation (τ_B). The Brownian relaxation of a particle is due to the rotational diffusion of the whole particles in the fluid (shown in Figure 1.14). The Brownian relaxation mainly depends on the hydrodynamic diameter of the particles and the viscosity of the fluid. The Brownian relaxation time is given by,[156]

$$\tau_B = \frac{3\eta V_{hyd}}{k_B T} \tag{1.19}$$

where η is the viscosity of the fluid, and V_{hyd} is the hydrodynamic volume of the particles. The effective relaxation time (τ) is given by,[155]

$$\tau = \frac{\tau_N \tau_B}{\tau_N + \tau_B} \tag{1.20}$$

The effective relaxation time is dominated by the fastest relaxation.

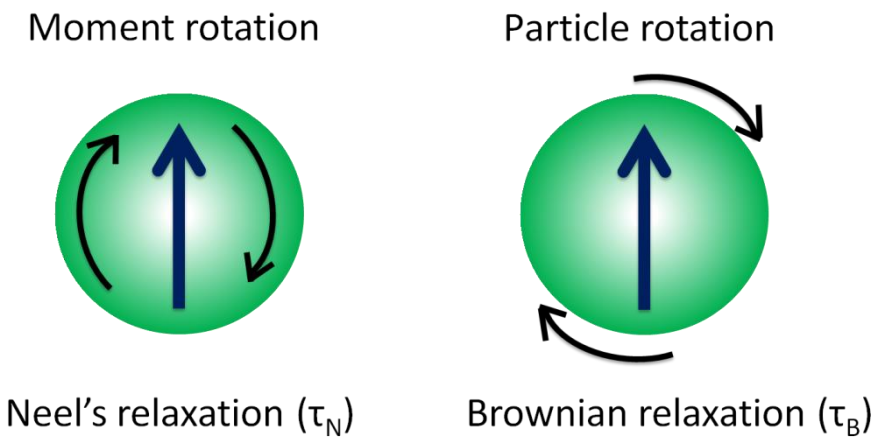

Figure 1.14. Illustration of Neel's (moment rotation) and Brownian (particle rotation) relaxations of magnetic nanoparticles

1.8. Magnetic nanofluids for heat transfer

Nanoparticles of the ferrimagnetic iron oxides, magnetite (Fe_3O_4) and maghemite (γ-Fe_2O_3) show superparamagnetism when their size is reduced to nanodimensions (<30 nm).[136] The superparamagnetic behavior of these ultra-small nanoparticles is useful for various applications including biomedical applications.[125-127] Superparamagnetic magnetite nanoparticles can be synthesized by different methods such as co-precipitation, thermal decomposition, hydrothermal, polyol and microemulsion techniques.[132] Many applications using magnetite nanoparticles, especially for biomedical applications, require monodispersed and stable nanoparticles. Various surfactants such as fatty acids, polymers, inorganic materials etc. are used to stabilize the nanoparticles against agglomeration and also the non-magnetic surfactant layer reduces the magnetic interaction between the nanoparticles.[157-158] Fatty acids with acid head group and long hydrophobic alkyl chain are mostly studied as surfactants for stabilization of the nanoparticles in aqueous and non-aqueous medium.[159-161]

Surfactant coated superparamagnetic magnetite based stable nanofluids can be made and these nanofluids are highly stable even in the presence of a strong applied magnetic field. Formation of reversible aggregation of these magnetic nanoparticles in a fluid in the presence of a magnetic field is useful for tuning the various thermophysical properties of the fluid. Thus, magnetite based fluids are useful for many applications such as ferrofluid seal,[162] fluid bearings,[163] dampers in loud speakers,[164] biomedical applications such as hyperthermia,[165] MRI imaging,[166] drug targeting and delivery,[167] cell separation,[168] and in optical devices such as optical switches, optical limiter, optical grating, optical fiber filter etc.[169-174]

The addition of highly thermal conductive solid nanoparticles to the less thermal conductive base fluid enhances the thermal conductivity of the base fluid. Experimental studies on concentration dependent thermal conductivity of nanofluids show thermal conductivity enhancement even at very low particle loading (as shown in Table 1.2). In the most widely used two-step method, the synthesized nanoparticles are dispersed in a base fluid either by ultrasonication, by adding dispersants or surfactants and changing the pH of the suspension in order to stabilize the nanoparticle suspensions.[59, 61, 64-67, 70,] Philip *et al*[175] used chemically modified magnetite nanoparticles (6.7 nm) using oleic acid to prepare nanofluids in kerosene as base fluid and the thermal conductivity studies showed no enhancement up to 1.71 volume percentage of the particles. Further increasing volume fraction of the particles showed linear enhancement in the thermal conductivity and the authors observed 23%

enhancement in the thermal conductivity for 7.8 volume percentage of the particles (shown in Figure 1.15). The unchanged thermal conductivity at lower concentrations is due to the highly dispersing nature of the chemically modified nanoparticles. The enhancement at higher concentration is due to the formation of dimers and trimers of the nanoparticles in kerosene. Wei *et al*[67] observed enhancement of thermal conductivity even at lower concentrations (0.1 vol%) of oleic acid coated magnetite nanoparticles (15 nm) dispersed in kerosene.

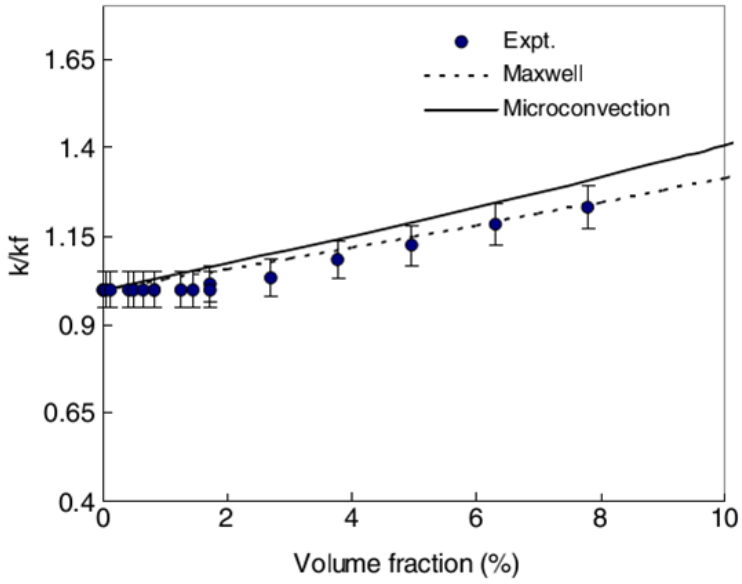

Figure 1.15. Variation of thermal conductivity with the volume percentage for oleic acid coated magnetite nanoparticles dispersed in kerosene (filled circles). The experimental data compared with the Maxwell (dashed line) and microconvection (solid line) models[175]

Heat transfer using magnetic nanofluids is a recent research area due to the large enhancement in the thermal conductivity in the presence of an applied magnetic field and the possible potential applications.[55, 176] Philip *et al*[46] observed almost 300% enhancement in the thermal conductivity for oleic acid coated magnetite nanoparticles dispersed in kerosene at a magnetic field of 0.08 T applied in the direction parallel to the temperature gradient (shown in Figure 1.16). Magnetic field applied in the direction perpendicular to the temperature gradient showed no appreciable enhancement in the thermal conductivity.[153] The very large enhancement in the thermal conductivity in the presence of an applied magnetic field is due to the formation of nanoparticle chain and the heat energy transferred through the back bone of the chain. The aspect ratio of the chain increases with increasing the magnetic field which leads to increase in the thermal conductivity. Maximum thermal conductivity is observed at a

particular field and then thermal conductivity decreases with increasing strength of the applied magnetic field.[177] The decrease in the thermal conductivity at higher magnetic fields is ascribed to the zippering effect of the nanoparticle chains.[175]

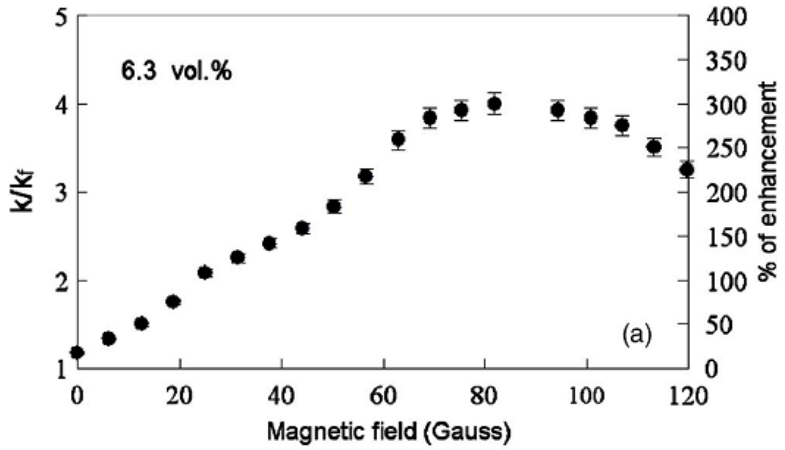

Figure 1.16. Variation of the thermal conductivity of magnetite nanofluid in kerosene as a function of applied magnetic field in the direction parallel to the temperature gradient.[46]

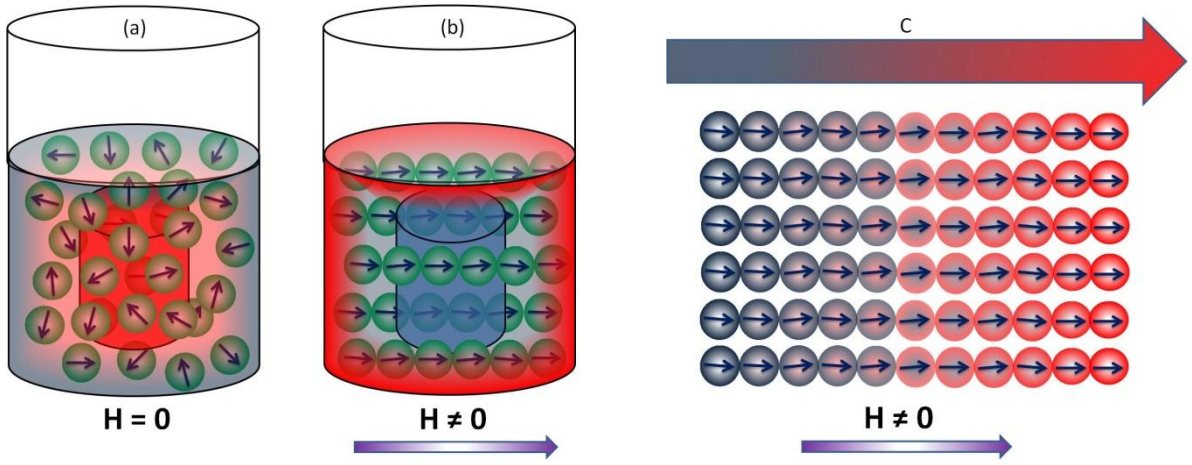

Figure 1.17. (a) Randomly oriented nanoparticles in the absence of a magnetic field in a fluid and the object placed inside the nanofluid remains hot, (b) chain like aggregation of the nanoparticles in the presence of a magnetic field and heat is removed from the hot object, and (c) heat flow through the chain-like aggregated nanoparticles.[178]

Figure 1.17 illustrates how heat is removed from a hot object through nanoparticle chain structure by applying a magnetic field in the direction parallel to the temperature

gradient. The nanoparticle chain acts as an effective heat transfer medium inside the magnetic fluid. Magnetic nanofluids are considered to be potential coolants for heat transfer applications due to the tremendous enhancement in the thermal conductivity in the presence of a magnetic field.[46]

1.9. Scope of the present work

Numerous experimental and theoretical studies are reported on the thermal conductivity of nanofluids, and the exact mechanism for the enhancement in the thermal conductivity is still not understood properly. Most of the experimental studies are focused on the factors such as volume fraction of the particles in the fluid, particle size, particle shape, particulate material, base fluid, temperature and pH. There are contradicting reports on the changes in the thermal conductivity enhancement using the same particulate material of comparable particle size dispersed in different base fluids. One of the major factors, which is not addressed so far, is the surfactant-solvent interface related issue. It is possible that the reported experimental results differ much due to the different dispersion characteristics and stability of the nanoparticles in base fluids. There are various surfactant related problems which may affect the heat transfer characteristics of the nanofluids which need to be studied to understand the thermal conductivity of nanofluids. Factors such as amount of surfactant on the surface of the nanoparticles, monolayer/bilayer nature of the coated surfactants, thickness (or physical length) of the surfactant molecules, conformation of the surfactant molecules, compatibility of the surfactant molecules in different solvents, interaction between the free end of the surfactant molecule and the solvent, effect of surfactants on self-assembly of the nanoparticles to form clusters, etc. These are some of the major factors which may affect the dispersion and stability properties of the nanoparticles in a fluid which in turn may affect the heat transfer characteristics of nanofluids.

The objective of the present study is to address some of the surfactant and solvent related factors on the thermal conductivity of magnetite based nanofuids. The surfactant molecules coated on the surface of nanoparticles separate the particles away from one another and reduce the van der Waals interaction between the particles. The surfactant molecules play an important role in the dispersion and stability of the nanoparticles in a fluid. There are only limited number of studies reported on focusing on the effect of surfactant on heat transfer characteristics of nanofluids. The present work is an attempt to investigate the effect of the amount of surfactant molecules on the surface of the nanoparticle on dispersion, stability,

thermal conductivity and viscosity of magnetite fluids. Superparamagnetic magnetite nanoparticles (< 10 nm) are coated with different fatty acid surfactants of varying chain length and conformation and the role of these parameters on the stability, dispersion, self-assembly of the nanoparticles and finally the thermal conductivity of the dispersion of these coated nanoparticles are studied. Studies are also performed on the effect of the amount of primary and secondary surfactants coated on the nanoparticles on the thermal conductivity of the nanofluids.

The properties of base fluids, in which the coated nanoparticles are dispersed, especially thermal conductivity and viscosity, are also important parameters determining the thermal conductivity of the nanofluids. There are few experimental studies reported on the thermophysical properties of the base fluids on the thermal conductivity of nanofluids. Apart from the thermophysical properties of the base fluids, the compatibility of the nanoparticle surfaces with the base fluid, which in turn may affect the viscosity of the nanofluid, is another important factor which may affect the thermophysical properties of the nanofluids. The present study attempts to address this issue by dispersing the fatty acid coated magnetite nanoparticles in different base fluids of different thermophysical properties. Attempts have been made to correlate the thermal conductivity of the nanofluids with the thermophysical properties of the base fluids.

Different fatty acid surfactant coated magnetite nanoparticles are used for the preparation of magnetite nanofluids. The magnetic properties, thermal conductivity and viscosity of the magnetite nanofluids are studied in detail to understand the correlation between different surfactant-solvent related issues. Thermal conductivity of the magnetite fluids is also studied in the absence and presence of a magnetic field. The size of the nanoparticles is one of the important factors for the heat transfer applications, where nanoparticles of smaller size with larger surface area allow more heat to transfer. However, in most of the studies, the particle size dependent thermal conductivity focuses on the average particle size. It is known that most of the synthesis methods produce particles with wide range of distribution and this may affect the effective thermal conductivity of the nanofluids. The present study also attempts to investigate the effect of particle size distribution of magnetite nanoparticles of comparable average size on the thermal conductivity of nanofluids.

References

1. Rashmi, W.; Khalid, M.; Ong, S.; Saidur, R., *Materials Research Express* **2014**, *1*, 032001.
2. Choi, S., Developments and Applications of Non-Newtonian Flows. *ASME FED* **1995**, *66*, 99-105.
3. The total number of publications in the field of nanofluids from year 1997-2016 by searching the word "*Nanofluids*" in Web of science.
4. Chol, S., Enhancing Thermal Conductivity of Fluids with Nanoparticles. ASME FED **1995**, *231*, 99-106.
5. Yu, W.; Xie, H. Q., *J. Nanomater.* **2012**, *2012*, 1-17.
6. Sarit Kumar, D.; Stephen, U. S. C.; Hrishikesh, E. P., *Heat Transfer Eng.* **2006**, *27*, 1-19.
7. Li, Y. J.; Zhou, J. E.; Tung, S.; Schneider, E.; Xi, S. Q., *Powder Technol.* **2009**, *196*, 89-101.
8. Ghadimi, A.; Saidur, R.; Metselaar, H. S. C., *Int. J. Heat Mass Transfer* **2011**, *54*, 4051-4068.
9. Rao, N.; Gahane, L.; Ranganayakulu, S., Synthesis, *IOSR Journal of Applied Physics* **2014**, 21-28.
10. Doina, B.; Ladislau, V.; Mikhail, V. A.; Oana, M.; Vlad, S.; Maria, B.; Vasil, M. G., *J. Magn. Magn. Mater.* **2007**, *311*, 17-21.
11. Vékás, L.; Bica, D.; Marinica, O., *Rom. Rep. Phys.* **2006**, *58*, 257.
12. Tombácz, E.; Bica, D.; Hajdú, A.; Illés, E.; Majzik, A.; Vékás, L., *J. Phys.: Condens. Matter* **2008**, *20*, 204103.
13 Manca, O.; Jaluria, Y.; Poulikakos, D., *Adv. Mech. Eng.* **2015**, *2*, 380826-380826.
14. Eastman, J. A.; Phillpot, S. R.; Choi, S. U. S.; Keblinski, P., *Annu. Rev. Mater. Res.* **2004**, *34*, 219-246.
15. Eapen, J.; Rusconi, R.; Piazza, R.; Yip, S., *J.Heat Transfer* **2010**, *132*, 102402.
16. Paul, G.; Chopkar, M.; Manna, I.; Das, P. K., *Renewable Sustainable Energy Rev.* **2010**, *14*, 1913-1924.
17. Maxwell, J. C., A Treatise on Electricity and Magnetism. *Clarendon press* **1881**, *1*.
18. Hamilton, R. L.; Crosser, O. K., *Ind. Eng. Chem. Fund.* **1962**, *1*, 187-191.

19. Wasp, E. J.; Kenny, J. P.; Gandhi, R. L., Solid--Liquid Flow: Slurry Pipeline Transportation.[Pumps, Valves, Mechanical Equipment, Economics]. *Ser. Bulk Mater. Handl.;(United States)* **1977**, *1*.
20 Bruggeman, V. D., *Ann. Phys.* **1935**, *416*, 636-664.
21. Jeffrey, D. J., *Proc. R. Soc. London, Ser. A* **1973**, *335*, 355-367.
22. Davis, R. H., *Int. J. Thermophys.* **1986**, *7*, 609-620.
23. Hashin, Z.; Shtrikman, S., *J. Appl. Phys.* **1962**, *33*, 3125.
24. Eapen, J.; Williams, W. C.; Buongiorno, J.; Hu, L. W.; Yip, S.; Rusconi, R.; Piazza, R., *Phys. Rev. Lett.* **2007**, *99*, 095901.
25. Eapen, J.; Li, J.; Yip, S., *Phys. Rev. E* **2007**, *76*, 062501.
26. Jang, S. P.; Choi, S. U. S., *Appl. Phys. Lett.* **2004**, *84*, 4316-4318.
27. Das, S. K.; Putra, N.; Thiesen, P.; Roetzel, W., *J. Heat Transfer* **2003**, *125*, 567-574.
28 Xuan, Y.; Li, Q.; Hu, W., *AlChE J.* **2003**, *49*, 1038-1043.
29. Prasher, R.; Bhattacharya, P.; Phelan, P. E., *Phys. Rev. Lett.* **2005**, *94*, 025901.
30. Prasher, R.; Bhattacharya, P.; Phelan, P. E., *J. Heat Transfer* **2006**, *128*, 588.
31. Yu, W.; Choi, S. U. S., *J. Nanopart. Res.* **2003**, *5*, 167-171.
32. Nan, C.-W.; Birringer, R.; Clarke, D. R.; Gleiter, H., *J. Appl. Phys.* **1997**, *81*, 6692.
33. Eastman, J.; Choi, S.; Li, S.; Yu, W.; Thompson, L., *Appl. Phys. Lett.* **2001**, *78*, 718-720.
34. Eastman, J.; Choi, U.; Li, S.; Soyez, G.; Thompson, L.; DiMelfi, R. *Mater. Sci. Forum* **1999,** *312-314* 629-634.
35. Prasher, R.; Evans, W.; Meakin, P.; Fish, J.; Phelan, P.; Keblinski, P., *Appl. Phys. Lett.* **2006**, *89*, 143119.
36. Prasher, R.; Phelan, P. E.; Bhattacharya, P., *Nano Lett.* **2006**, *6*, 1529-1534.
37. Xiang-Qi, W.; Arun, S. M., Heat Transfer Characteristics of Nanofluids: A Review. *Int. J. Therm. Sci.* **2007**, *46*, 1-19.
38. Kleinstreuer, C.; Feng, Y., *Nanoscale Res. Lett.* **2011**, *6*, 229.
39. Yu, W.; Choi, S., *J. Nanopart. Res.* **2004**, *6*, 355-361.
40. Xue, Q.-Z., *Phys. Lett. A* **2003**, *307*, 313-317.
41. Xue, Q.; Xu, W.-M., *Mater. Chem. Phys.* **2005**, *90*, 298-301.
42. Xie, H.; Fujii, M.; Zhang, X., *Int. J. Heat Mass Transfer* **2005,** *48***,** 2926-2932.
43. Kumar, D.; Patel, H.; Kumar, V. R.; Sundararajan, T.; Pradeep, T.; Das, S., *Phys. Rev. Lett.* **2004**, *93*, 144301.
44. Koo, J.; Kleinstreuer, C., *J. Nanopart. Res.* **2005**, *6*, 577-588.

45. Choi, S.; Zhang, Z.; Yu, W.; Lockwood, F.; Grulke, E., *Appl. Phys. Lett.* **2001**, *79*, 2252-2254.
46. Philip, J.; Shima, P. D.; Raj, B., *Appl. Phys. Lett.* **2007**, *91*, 203108.
47. Wang, B.; Wang, B.; Wei, P.; Wang, X.; Lou, W., *Dalton Trans.* **2012**, *41*, 896-899.
48. Chopkar, M.; Kumar, S.; Bhandari, D.; Das, P. K.; Manna, I., *Mater. Sci. Eng., B* **2007**, *139*, 141-148.
49. Chon, C. H.; Kihm, K. D.; Lee, S. P.; Choi, S. U. S., *Appl. Phys. Lett.* **2005**, *87*, 153107.
50. Nisha, M. R.; Philip, J., *Heat Mass Transfer.* **2012**, *48*, 1783-1790.
51. Timofeeva, E. V.; Smith, D. S.; Yu, W.; France, D. M.; Singh, D.; Routbort, J. L., *Nanotechnology* **2010**, *21*, 215703.
52. Warrier, P.; Teja, A., *Nanoscale Res. Lett.* **2011**, *6*, 247.
53. Beck, M. P.; Yuan, Y.; Warrier, P.; Teja, A. S., *J. Nanopart. Res.* **2008**, *11*, 1129-1136.
54. Beck, M. P.; Yuan, Y.; Warrier, P.; Teja, A. S., *J. Appl. Phys.* **2010**, *107*, 066101.
55. Philip, J.; Shima, P. D., *Adv. Colloid Interface Sci.* **2012**, *183-184*, 30-45.
56. Kang, H. U.; Kim, S. H.; Oh, J. M., *Exp. Heat Transfer* **2006**, **19**, 181-191.
57. Murshed, S. M. S., *Heat Transfer Eng.* **2012**, *33*, 722-731.
58. Yu, W.; Xie, H.; Li, Y.; Chen, L., *Particuology* **2011**, *9*, 187-191.
59. Barbés, B.; Páramo, R.; Blanco, E.; Pastoriza-Gallego, M. J.; Piñeiro, M. M.; Legido, J. L.; Casanova, C., *J. Therm. Anal. Calorim.* **2013**, *111*, 1615-1625.
60. Eastman, J.; Choi, U.; Li, S.; Thompson, L.; Lee, S. *MRS proceedings*, Cambridge Univ Press: 1996; p 3.
61. Yang, L.; Du, K.; Zhang, X.-s., *J. Cent. South Univ.* **2012**, *19*, 1622-1628.
62. Murshed, S. M. S.; Leong, K. C.; Yang, C., *Int. J. Therm. Sci.* **2008**, *47*, 560-568.
63. Moghadassi, A.; Hosseini, S. M.; Henneke, D. E., *Ind. Eng. Chem. Res.* **2010**, *49*, 1900-1904.
64. Hong, T. K.; Yang, H. S.; Choi, C. J., *J. Appl. Phys.* **2005**, *97*, 064311.
65. Abareshi, M.; Sajjadi, S. H.; Zebarjad, S. M.; Goharshadi, E. K., *J. Mol. Liq.* **2011**, *163*, 27-32.
66. Zhu, H.; Zhang, C.; Liu, S.; Tang, Y.; Yin, Y., *Appl. Phys. Lett.* **2006**, *89*, 23123-23123.
67. Yu, W.; Xie, H.; Chen, L.; Li, Y., *Colloids Surf., A* **2010**, *355*, 109-113.
68. Xie, H.; Wang, J.; Xi, T.; Liu, Y., *Int. J. Thermophys.* **2002**, *23*, 571-580.

69. Singh, D.; Timofeeva, E.; Yu, W.; Routbort, J.; France, D.; Smith, D.; Lopez-Cepero, J. M., *J. Appl. Phys.* **2009**, *105*, 064306.
70. Xie, H.; Lee, H.; Youn, W.; Choi, M., *J. Appl. Phys.* **2003**, *94*, 4967.
71. Murshed, S.; Leong, K.; Yang, C., *Int. J. Therm. Sci.* **2005**, *44*, 367-373.
72. Yu, W.; Xie, H.; Chen, L.; Li, Y., *Thermochim. Acta* **2009**, *491*, 92-96.
73. Li, C. H.; Peterson, G. P., *J. Appl. Phys.* **2007**, *101*, 044312.
74. Chen, G.; Yu, W. H.; Singh, D.; Cookson, D.; Routbort, J., *J. Nanopart. Res.* **2008**, *10*, 1109-1114.
75. Timofeeva, E. V.; Routbort, J. L.; Singh, D., *J. Appl. Phys.* **2009**, *106*, 014304.
76. Pal, B.; Pal, B., *Part. Sci. Technol.* **2014**, *33*, 224-228.
77. Farbod, M.; Kouhpeymani asl, R.; Noghreh abadi, A. R., *Colloids Surf., A* **2015**, *474*, 71-75.
78. Zhu, H.; Zhang, C.; Liu, S.; Tang, Y.; Yin, Y., *Appl. Phys. Lett.* **2006**, *89*, 023123.
79. Tsai, T. H.; Kuo, L. S.; Chen, P. H.; Yang, C. T., *Appl. Phys. Lett.* **2008**, *93*, 233121.
80. Nara, S.; Bhattacharya, P.; Vijayan, P.; Lai, W.; Rosenthal, W.; Phelan, P.; Prasher, R.; Song, D.; Wang, J. ASME 2005 International Mechanical Engineering Congress and Exposition, American Society of Mechanical Engineers: **2005**; pp 755-758.
81 Hosseini, S. M.; Moghadassi, A. R.; Henneke, D.; Elkamel, A., *J. Therm. Anal. Calorim.* **2009**, *101*, 113-118.
82 Younes, H.; Christensen, G.; Luan, X. N.; Hong, H. P.; Smith, P., *J. Appl. Phys.* **2012**, *111*, 064308.
83 Timofeeva, E. V.; Yu, W.; France, D. M.; Singh, D.; Routbort, J. L., *J. Appl. Phys.* **2011**, *109*, 014914.
84 Altan, C. L.; Bucak, S., *Nanotechnology* **2011**, *22*, 285713.
85 Lopez-Lopez, M. T.; Duran, J. D.; Delgado, A. V.; Gonzalez-Caballero, F., *J. Colloid Interface Sci.* **2005**, *291*, 144-1451.
86. Yu, W.; Xie, H.; Chen, L.; Li, Y., *Powder Technol.* **2010**, *197*, 218-221.
87. Gupta, S. S.; Siva, V. M.; Krishnan, S.; Sreeprasad, T.; Singh, P. K.; Pradeep, T.; Das, S. K., *J. Appl. Phys.* **2011**, *110*, 084302.
88. Shima, P. D.; Philip, J.; Raj, B., *J. Phys. Chem. C* **2010**, *114*, 18825-18833.
89. Parekh, K.; Lee, H. S., *J. Appl. Phys.* **2010**, *107*, 09A310.
90. Sundar, L. S.; Singh, M. K.; Sousa, A. C. M., *Int. Commun. Heat Mass Transfer* **2013**, *49*, 17-24.
91 Lee, J.-H.; Lee, S.-H.; Jang, S. P., *Appl. Phys. Lett.* **2014**, *104*, 161908.

92. Yang, B.; Han, Z. H., *Appl. Phys. Lett.* **2006**, *89*, 3111.
93. Duangthongsuk, W.; Wongwises, S., *Exp. Therm Fluid Sci.* **2009**, *33*, 706-714.
94. Wang, X.-j.; Li, X.; Yang, S., *Energy & Fuels* **2009**, *23*, 2684-2689.
95. Raghu, G.; Hongwei, S.; Pengtao, W.; Majid, C.; Fan, G.; Zhiyong, G.; Bridgette, B., *Adv. Mech. Eng.* **2010**, *2010*, 1-10.
96. Zhu, D.; Li, X.; Wang, N.; Wang, X.; Gao, J.; Li, H., *Curr. Appl Phys.* **2009**, *9*, 131-139.
97. Patel, H. E.; Das, S. K.; Sundararajan, T.; Sreekumaran Nair, A.; George, B.; Pradeep, T., Appl. *Phys. Lett.* **2003**, *83*, 2931-2933.
98. Lee, D.; Kim, J.-W.; Kim, B. G., *J. Phys. Chem. B.* **2006**, *110*, 4323-4328.
99. Einstein, A., *Ann. Phys.* **1906**, *19*, 289-306.
100. Krieger, I. M.; Dougherty, T. J., *Trans. Soc. Rheol.* **1959**, *3*, 137-152.
101. Nielsen, L. E., *J. Appl. Phys.* **1970**, *41*, 4626-4627.
102. Batchelor, G., *J. Fluid Mech.* **1977**, *83*, 97-117.
103. Routbort, J. L.; Singh, D.; Timofeeva, E. V.; Yu, W.; France, D. M., *J. Nanopart. Res.* **2011**, *13*, 931-937.
104. Kumar, P. M.; Kumar, J.; Suresh, S., *IJEIR* **2012**, *1*, 182-188.
105. Ko, G. H.; Heo, K.; Lee, K.; Kim, D. S.; Kim, C.; Sohn, Y.; Choi, M., *Int. J. Heat Mass Transfer* **2007**, *50*, 4749-4753.
106. Żyła, G.; Cholewa, M.; Witek, A., *Nanoscale Res. Lett.* **2012**, *7*, 1-10.
107. Kole, M.; Dey, T., *Exp. Therm Fluid Sci.* **2010**, *34*, 677-683.
108. Kole, M.; Dey, T., *Int. J. Therm. Sci.* **2011**, *50*, 1741-1747.
109. Hong, J.; Kim, D., *Thermochim. Acta* **2012**, *542*, 28-32.
110. Yang, Y.; Oztekin, A.; Neti, S.; Mohapatra, S., *J. Nanopart. Res.* **2012,** *14*, 1-10.
111. Cabaleiro, D.; Pastoriza-Gallego, M. J.; Gracia-Fernández, C.; Piñeiro, M. M.; Lugo, L., *Nanoscale Res. Lett.* **2013**, *8*, 1-13.
112. Li, F.-C.; Yang, J.-C.; Zhou, W.-W.; He, Y.-R.; Huang, Y.-M.; Jiang, B.-C., *Thermochim. Acta* **2013**, *556*, 47-53.
113. Phuoc, T. X.; Massoudi, M.; Chen, R.-H., *Int. J. Therm. Sci.* **2011**, *50*, 12-18.
114. Vasheghani, M.; Marzbanrad, E.; Zamani, C.; Aminy, M.; Raissi, B.; Ebadzadeh, T.; Barzegar-Bafrooei, H., *Heat Mass Transfer.* **2011**, *47*, 1401-1405.
115. Chen, L.; Xie, H.; Yu, W.; Li, Y., *J. Dispersion Sci. Technol.* **2011**, *32*, 550-554.
116. Colla, L.; Fedele, L.; Scattolini, M.; Bobbo, S., *Adv. Mech. Eng.* **2012**, *4*, 674947.
117. Wang, T.; Ni, M.; Luo, Z.; Shou, C.; Cen, K., *Chin. Sci. Bull.* **2012**, *57*, 3644-3651.

118. Nguyen, C.; Desgranges, F.; Galanis, N.; Roy, G.; Maré, T.; Boucher, S.; Mintsa, H. A., *Int. J. Therm. Sci.* **2008**, *47*, 103-111.
119. Nguyen, C.; Desgranges, F.; Roy, G.; Galanis, N.; Maré, T.; Boucher, S.; Mintsa, H. A., *Int. J. Heat Fluid Flow* **2007**, *28*, 1492-1506.
120. Jia-Fei, Z.; Zhong-Yang, L.; Ming-Jiang, N.; Ke-Fa, C., *Chin. Phys. Lett.* **2009**, *26*, 066202.
121. Timofeeva, E. V.; Gavrilov, A. N.; McCloskey, J. M.; Tolmachev, Y. V.; Sprunt, S.; Lopatina, L. M.; Selinger, J. V., *Phys. Rev. E* **2007**, *76*, 061203.
122. Berkovsky, B.; Medvedev, V. F.; Krakov, M. S., Magnetic Fluids; Oxford Univ. Press, **1993**.
123. Odenbach, S., *Colloids Surf., A* **2003**, *217*, 171-178.
124. Gubin, S. P., Magnetic Nanoparticles; John Wiley & Sons, **2009**.
125. Pankhurst, Q. A.; Connolly, J.; Jones, S. K.; Dobson, J., *J. Phys. D: Appl. Phys.* **2003**, *36*, R167-R181.
126. Philip, J.; Laskar, J. M., *J. Nanofluids* **2012**, *1*, 3-20.
127. Popplewell, J., *Phys. Technol.* **1984**, *15*, 150-156.
128. Bertotti, G., Hysteresis in Magnetism: For Physicists, Materials Scientists, and Engineers; Academic press, **1998**.
129. Dattagupta, S.; Scientific, W., A Paradigm Called Magnetism; World Scientific, **2008**.
130. Sung Lee, J.; Myung Cha, J.; Young Yoon, H.; Lee, J.-K.; Keun Kim, Y., *Sci. Rep.* **2015**, *5*, 12135.
131. Batlle, X.; Labarta, A., *J. Phys. D: Appl. Phys.* **2002**, *35*, R15.
132. Lu, A. H.; Salabas, E. e. L.; Schüth, F., *Angew. Chem. Int. Ed.* **2007**, *46*, 1222-1244.
133. Krishnan, K. M., *IEEE Trans. Magn.* **2010**, *46*, 2523-2558.
134. Jun, Y. W.; Seo, J. W.; Cheon, A., *Acc. Chem. Res.* **2008**, *41*, 179-189.
135. Papaefthymiou, G. C., *Nano Today* **2009**, *4*, 438-447.
136. Liu, C.; Zou, B.; Rondinone, A. J.; Zhang, Z. J., *J. Am. Chem. Soc.* **2000**, *122*, 6263-6267.
137 Liu, C.; Rondinone, A. J.; Zhang, Z. J., *Pure Appl. Chem.* **2000**, *72*, 37-45.
138. Liu, C.; Zhang, Z. J., *Chem. Mater.* **2001**, *13*, 2092-2096.
139. Chesnel, K.; Trevino, M.; Cai, Y.; Hancock, J. M.; Smith, S. J.; Harrison, R. G., *J. Phys. Conf. Ser.* **2014**, *521*, 12004.
140. Mukadam, M.; Yusuf, S.; Sharma, P.; Kulshreshtha, S., *J. Magn. Magn. Mater.* **2004**, *272*, 1401-1403.

141 Vargas, J.; Nunes, W.; Socolovsky, L.; Knobel, M.; Zanchet, D., *Phys. Rev. B.* **2005**, *72*, 184428.

142. Kodama, R., *J. Magn. Magn. Mater.* **1999**, *200*, 359-372.

143. Respaud, M.; Broto, J.; Rakoto, H.; Fert, A.; Thomas, L.; Barbara, B.; Verelst, M.; Snoeck, E.; Lecante, P.; Mosset, A., *Phys. Rev. B.* **1998**, *57*, 2925.

144. Bodker, F.; Morup, S.; Linderoth, S., *Phys. Rev. Lett.* **1994**, *72*, 282-285.

145. Makhlouf, S. A., *J. Magn. Magn. Mater.* **2002**, *246*, 184-190.

146. Paulus, P. M.; Bonnemann, H.; van der Kraan, A. M.; Luis, F.; Sinzig, J.; de Jongh, L. J., *EPJ Data Sci.* **1999**, *9*, 501-504.

147. Daou, T. J.; Greneche, J. M.; Pourroy, G.; Buathong, S.; Derory, A.; Ulhaq-Bouillet, C.; Donnio, B.; Guillon, D.; Begin-Colin, S., *Chem. Mater.* **2008**, *20*, 5869-5875.

148. Odenbach, S.; Gilly, H., *J. Magn. Magn. Mater.* **1996**, *152*, 123-128.

149. Odenbach, S.; Störk, H., *J. Magn. Magn. Mater.* **1998**, *183*, 188-194.

150. Scholten, P., *IEEE Trans. Magn.* **1980**, *16*, 221-225.

151. Skibin, Y. N.; Chekanov, V. V.; Raikher, Y. L., *Zh Eksp Teor Fiz* **1977**, *72*, 949-955.

152. Taketomi, S., *Jpn. J. Appl. Phys., Part 1* **1983**, *22*, 1137.

153. Shima, P. D.; Philip, J., *J. Phys. Chem. C* **2011**, *115*, 20097-20104.

154. Mendelev, V. S.; Ivanov, A. O., *Phys. Rev. E* **2004**, *70*, 051502.

155. L. Raikher, Y.; Stepanov, V. I., *J. Magn. Magn. Mater.* **2014**, *368*, 421-427.

156. Fischer, B.; Huke, B.; Lücke, M.; Hempelmann, R., *J. Magn. Magn. Mater.* **2005**, *289*, 74-77.

157. Laurent, S.; Forge, D.; Port, M.; Roch, A.; Robic, C.; Vander Elst, L.; Muller, R. N., *Chem. Rev.* **2008**, *108*, 2064-2110.

158. Wu, W.; He, Q.; Jiang, C., *Nanoscale Res Lett* **2008**, *3*, 397-415.

159. Zhang, L.; He, R.; Gu, H.-C., *Appl. Surf. Sci.* **2006**, *253*, 2611-2617.

160. Sun, S.; Zeng, H., *J. Am. Chem. Soc.* **2002**, *124*, 8204-8205.

161. Park, J.; An, K.; Hwang, Y.; Park, J. G.; Noh, H. J.; Kim, J. Y.; Park, J. H.; Hwang, N. M.; Hyeon, T., *Nat. Mater.* **2004**, *3*, 891-5.

162. Rosensweig, R. E., Magnetic Fluid Seals. Google Patents: 1971.

163. Hoffman, G. J., Ferro-Fluid Bearing. Google Patents: 1987.

164. Raj, K.; Moskowitz, R., *IEEE Trans. Magn.* **1980**, *16*, 358-363.

165. Thiesen, B.; Jordan, A., *Int J Hyperthermia* **2008**, *24*, 467-74.

166. Na, H. B.; Song, I. C.; Hyeon, T., *Adv. Mater.* **2009**, *21*, 2133-2148.

167. Arruebo, M.; Fernandez-Pacheco, R.; Ibarra, M. R.; Santamaria, J., *Nano Today* **2007**, *2*, 22-32.
168. McCloskey, K. E.; Chalmers, J. J.; Zborowski, M., *Anal. Chem.* **2003**, *75*, 6868-74.
169. Chieh, J. J.; Yang, S. Y.; Horng, H. E.; Hong, C. Y.; Yang, H. C., *Appl. Phys. Lett.* **2007**, *90*, 133505.
170. Horng, H. E.; Chen, C. S.; Fang, K. L.; Yang, S. Y.; Chieh, J. J.; Hong, C. Y.; Yang, H. C., *Appl. Phys. Lett.* **2004**, *85*, 5592-5594.
171. Liao, W. J.; Chen, X. F.; Chen, Y. P.; Pu, S. K.; Xia, Y. X.; Li, Q., *Appl. Phys. Lett.* **2005**, *87*, 151122.
172. Martinez, L.; Cecelja, F.; Rakowski, R., *Sens. Actuators, A* **2005**, *123-24*, 438-443.
173. Nair, S. S.; Thomas, J.; Sandeep, C. S. S.; Anantharaman, M. R.; Philip, R., *Appl. Phys. Lett.* **2008**, *92*, 171908.
174. Pu, S. L.; Chen, X. F.; Chen, L. J.; Liao, W. J.; Chen, Y. P.; Xia, Y. X., *Appl. Phys. Lett.* **2005**, *87*, 021901.
175. Philip, J.; Shima, P. D.; Raj, B., *Nanotechnology* **2008**, *19*, 305706.
176. Younes, H.; Christensen, G.; Li, D.; Hong, H.; Ghaferi, A. A., *J. Nanofluids* **2015**, *4*, 107-132.
177. Shima, P. D.; Philip, J.; Raj, B., *Appl. Phys. Lett.* **2009**, *94*, 223101.
178. Philip, J.; Shima, P. D.; Raj, B., *Appl. Phys. Lett.* **2008**, *92*, 043108.

Chapter 2

Experimental methods

2.1 Introduction

This chapter explains the method of synthesis of magnetite nanoparticles, surface coating of the nanoparticles with various fatty acid molecules and different techniques used for the characterization of the coated nanoparticles as well as nanofluids. Details of the different characterization techniques used such as powder X-ray diffraction (XRD), Transmission Electron Microscopy (TEM), Infrared spectroscopy (IR), Thermogravimetric analysis (TGA), and magnetic measurements using a SQUID magnetometer are provided in this chapter. Fabrication, principle, calibration and method of measurement of the thermal conductivity of nanofluids using a homemade thermal conductivity set up based on the principle of transient hot wire (THW) method are also described.

2.2 Materials and methods

2.2.1 Materials used

The following chemicals are used for the synthesis of surfactant coated magnetites nanoparticles.

Ferric chloride, $FeCl_3.6H_2O$ (97%) – Sigma-Aldrich

Ferrous chloride, $FeCl_2.4H_2O$ (99%) – Sigma-Aldrich

Capric acid (decanoic acid, 98%) – Sigma-Aldrich

Lauric acid (dodecanoic acid, 99%) – Sigma-Aldrich

Stearic acid (octadecanoic acid, 95%) – Sigma-Aldrich

Oleic acid (cis-9-octadecenoic acid, 90%) – Sigma-Aldrich

Linoleic acid (cis,cis-9,12-octadecadienoic acid, 74%) – Sigma-Aldrich

Linolenic acid (cis,cis,cis-9,12,15-octadecatrienoic acid, 70%) – Sigma-Aldrich

Octadecene (90%) – Sigma-Aldrich

Methylcyclohexane (99%) – Sigma-Aldrich

Aqueous ammonia (25%) – Merck India

Hydrochloric acid (37%) – Merck India

Acetone (99.5%) – Merck India

Hexane (95%) – Merck India

Iso-propanol (99.5%) – Merck India

Toluene (99.5%) – Merck India

Mesitylene (98%) – Merck India

Xylene – Merck India

Paraffin liquid, light – Merck India

Kerosene - commercially available for domestic use in India

All the chemicals were used without any further purification and double distilled water was used throughout the synthesis and washing of the prepared samples.

2.2.2 Synthesis of fatty acid coated magnetite nanoparticles

There are different synthesis methods generally used for the preparation of magnetite (Fe_3O_4) nanoparticles such as co-precipitation,[1] thermal decomposition,[2] microemulsion,[3] sol-gel,[4] hydrothermal/solvothermal,[5] polyol,[6] sonochemical,[7] elecrochemical[8] etc. Out these various synthesis methods, coprecipitation is the simplest and economical method to synthesize magnetite nanoparticles in large scale.

In a co-precipitation method, water soluble metal salts such as chlorides, nitrates or sulphates are precipitated as a sparingly soluble species such as hydroxides, carbonates, oxalates and oxides under supersaturation condition using suitable precipitating agents.[9] There are two stages in the coprecipitation process; short burst nucleation at supersaturation condition followed by growth process by diffusion of solute species towards the surface of the formed nucleus. In order to synthesize monodispersed particles, these two steps in the co-precipitation process need to be separated and nucleation should be avoided during the growth process. If nucleation and growth are happened simultaneously, the growth histories would be different for different nucleus and lead to polydispersity of the nanoparticles. The size control of monodispersed particles is normally performed by short time period nucleation and the number of particles is determined by the end of nucleation and does not affect by the growth process.[10-11] Various factors such as concentration of the metal salt solution, rate of

addition of the precipitant (base), temperature, pH and digestion time affect the size, distribution and shape of the nanoparticles.[11-14]

In a typical synthesis, 0.4 M $FeCl_3.6H_2O$ and 0.2 M $FeCl_2.4H_2O$ solutions were prepared by dissolving corresponding iron chloride salt in double distilled water and made up to 100 ml in a standard measuring flask. 100 ml of the mixture of $FeCl_3.6H_2O$ and $FeCl_2.4H_2O$ solution (corresponding to Fe^{2+}:Fe^{3+} = 1:2) was taken in a three necked 500 ml round bottom flask and heated to 50 °C under flowing argon atmosphere with constant stirring using a laboratory magnetic stirrer. Fatty acid (2 to 4 g) dissolved in 20 ml of acetone (isopropanol in some cases) was added to the preheated (50 °C) solution. Then, 50 ml NH_4OH solution was added to the reaction mixture through a burette. A black precipitate was formed immediately after the addition and pH of the reaction mixture was 11 after the precipitation reaction. Then the temperature was increased to 80 °C and maintained for 45 minutes to complete the surface coating process. After the completion of the reaction, the reaction mixture was cooled to room temperature. The precipitate formed was then filtered, and washed with acetone-hexane mixture (or isopropanol-hexane mixture in some cases) to remove the excess fatty acid present on the surface of the nanoparticles and in the reaction mixture. The fatty acid coated nanoparticles were transferred from the aqueous to the non-aqueous layer during the washing process. The non-aqueous layer was separated from the aqueous layer using a separating funnel, washed three times with water and then dried at room temperature. The dried samples are used for the characterization studies as well as for the preparation of nanofluids.

2.2.3 Preparation of magnetic nanofluids

For thermal conductivity and viscosity measurements, the dried nanoparticles were dispersed in a non-aqueous solvent (base fluid) at different volume concentrations by ultrasonication. Volume% of the particles are calculated from the mass and density of the magnetite nanoparticles as well as mass and density of the base fluid, as shown in equation 2.1.

$$\varphi = \frac{m_p/\rho_p}{m_f/\rho_f + m_p/\rho_p} \times 100 \qquad (2.1)$$

where, φ is the volume% of the particles, m_p is the mass of Fe_3O_4 nanoparticles after subtracting the mass contribution of the surfactants (obtained from TGA studies), m_f is mass

of the base fluid, ρ_p and ρ_f are the densities of the dispersed particles and the base fluid, respectively. The typical volume of fluid used for thermal conductivity studies is 25 ml.

2.3. Characterization and measurement techniques

2.3.1 Powder X-ray diffraction

Powder X-ray diffraction (XRD) is one of the fundamental characterization techniques used for the identification of solid materials in the bulk and nanocrystalline forms.[15] Powder X-ray diffraction pattern of a crystalline material is the finger print of that material and gives information about the crystal structure and phase purity of the material.[16] Peaks in the powder XRD pattern becomes broader with decreasing crystallite size for nanomaterials compared to that of the bulk counterpart and therefore, the width of a peak in the powder XRD pattern can give information on the average crystallite size of nanomaterials.[15] The average crystallite size (t) of the nanomaterials can be determined from the broadening of the XRD peak using the Scherrer equation,[17]

$$t = \frac{K\lambda}{\beta \cos\theta} \tag{2.2}$$

where K is the constant which depends on the shape of the nanomaterials and it is 0.9 for spherical particles,[17] λ is the wavelength of the X-rays, θ is the Bragg's angle and β is the full width at half maximum (FWHM) of a peak after correcting for the instrumental contribution to the peak broadening,

$$\beta^2 = \beta_M^2 - \beta_S^2 \tag{2.3}$$

where β_M is the measured full width of a peak at half maximum, β_S is the instrumental contribution to peak broadening, and β is the peak broadening due to crystallite size. Silicon is used as a reference sample and the instrumental contribution to the peak broadening is 0.15 degrees.

In the present study, powder X-ray diffraction patterns were recorded on a PANalytical XPERT PRO model X-ray diffractometer, Cu Kα radiation with the wavelength 1.5418 Å was used as source and Ni is used as filter. XRD patterns of the synthesized

samples were recorded in the 2θ range 10-80 degrees with the scan rate of 2 degree/minute. Powder XRD pattern of Fe_3O_4 was simulated using the crystallographic parameters such as space group, unit cell lattice parameters, atomic positions and occupancy parameter of the different atoms in the unit cell of the material, using the computer program, 'Powder Cell for Windows (PCW)' version 2.4, developed by W. Krauz and G. Nolze.[18] The experimental pattern was compared with the simulated pattern. The XRD patterns of the synthesized samples were also compared with the standard Joint Committee on Powder Diffraction Standards (JCPDS) data, international center for diffraction, with the card number 19-0629. Lattice parameter was obtained by least squares fitting of the experimental pattern using the PCW software.

2.3.2 Transmission electron microscopy

Transmission electron microscopy (TEM) is an imaging technique in which a beam of electrons is focused on to a specimen causing enlarged version to appear on a fluorescent screen or photographic film or CCD camera. TEM is a useful technique to determine the particle size, distribution, shape and arrangement of particles in a specimen.[19-20] TEM analysis of the synthesized samples in the present work was carried out on a FEI model TECNAI G2 F30 transmission electron microscope operated at an accelerating voltage of 300 kV (C_S = 0.6 mm, resolution = 1.7 Å). Bright-field TEM imaging mode was used to obtain microstructure, particle size and its size distribution. For TEM analysis, samples were prepared by dispersing the dried nanoparticles in a small amount of toluene by ultrasonication and dropped on to a carbon coated copper grid (200 mesh). The average particle size and particle size distribution were analysed by the digital micrograph software provided with the instrument.

2.3.3 Infrared spectroscopy

Infrared (IR) spectroscopy is an important tool to identify functional groups and nature of bonding in molecules.[21-22] IR spectroscopy is used to identify the site of attachment of the fatty acid molecules used as surfactants on to the surface of the magnetite nanoparticles as well as to obtain information on the nature of attachment. In the present work, IR spectra of the synthesized fatty acid coated magnetite nanoparticles were recorded on a Perkin Elmer Spectrum-One FTIR spectrometer, in the frequency range from 4000 cm^{-1} to 400 cm^{-1}. The powder sample was made in to the form of a circular pellet after mixing with KBr and spectra were recorded. Background spectra were recorded on a KBr pellet without the sample.

2.3.4 Thermogravimetric analysis

Thermogravimetric analysis (TGA) is the one of the thermal analysis techniques which measures change in the weight of a sample with temperature. In thermogravimetric analysis, a sample is heated in a particular environment and measures the change in the weight of a sample as a function of temperature. The change in the weight of a sample is plotted against temperature and is called thermogravimetric (TGA) curve. The rate of change in the mass can also be plotted against temperature and is called differential thermogravimetric (DTG) curve. Thermogravimetric analysis provides information on the thermal stability of materials under different environments. In thermogravimetric analysis, materials show weight loss when it undergoes desorption, decomposition, vaporization, oxidation, reduction, sublimation, etc.[23-24] In the present study, thermogravimetric analysis of the fatty acid coated powder samples was carried out on a SDT Q600 TG-DTA analyser in the temperature range 25–500 °C, at a heating rate 10 °C per minute, under nitrogen atmosphere.

2.3.5 Magnetic measurements

Magnetization measurements of the samples as a function of magnetic field, at room temperature, and as a function of temperature, have been carried out to obtain information on the magnetic nature of the samples. Magnetization measurements of the fatty acid coated powder and fluid samples were performed on a super conducting quantum inference device (SQUID) using the principle of a vibrating sample magnetometer (VSM).[25-27] In the present work, a Quantum Design MPMS 7T SQUID-VSM was used for the measurement. Field dependant magnetization measurements were carried out up to a magnetic field of 3 T, at room temperature. The magnetization of a sample was measured by increasing or decreasing the magnetic field in five quadrants. Temperature dependent magnetization measurements were carried out under zero field cooled (ZFC) and field cooled (FC) conditions. In the zero field cooled measurement, samples were cooled from room temperature to 5 K in the absence of a magnetic field and magnetization was measured while heating the sample to 300 K in the presence of a small magnetic field (50 Oe = 0.05 mT). In the field cooled measurement, samples were cooled in the presence of a small magnetic field (0.05 mT) and magnetization was measured while heating the sample in the presence of the same field.

When increasing the temperature, thermal energy relaxes the magnetic moment of the particles and it helps to align the magnetic moments in the field direction. On increasing the temperature, thermal energy overcomes the anisotropy energy of the particles, leading to

randomizing the direction of the magnetic moment of the particles. The temperature at which thermal energy overcomes the anisotropy energy is called blocking temperature (T_B).[28] Each and every magnetic nanoparticles will have its own anisotropy energy which is directly proportional to the diameter of the magnetic nanoparticle and hence different blocking temperatures for different particles. The distribution in the blocking temperature can be calculated from the zero field cooled magnetization curve using the equation,[29]

$$f(T_B) = \frac{d[T\chi_{ZFC}(T)]}{dT} \tag{2.4}$$

where T_B is the blocking temperature, χ_{ZFC} is the magnetic susceptibility from the zero field cooled magnetization curve (M_{ZFC}/H) , and T is the temperature.

2.3.6 Thermal conductivity measurements

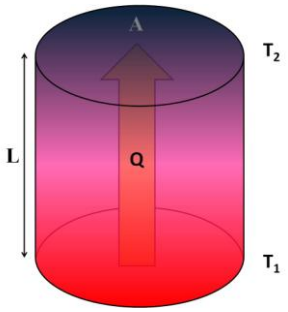

Figure 2.1. Heat flow in a material when there is a heat flux inside the material

Thermal conductivity of materials can be explained based on the Fourier's law.[30] For the simplest case, the steady one dimensional heat flow through a material can be established by the application of a known heat flux. By measuring the temperature at two known locations in the direction of the heat flow, one can calculate the thermal conductivity of that particular material (shown in Figure 2.1). Thermal conductivity based on Fourier's law, given by,

$$k = \frac{q/A}{\Delta T/L} \tag{2.5}$$

where q is the amount of heat flow, A is the cross sectional area, ΔT is the temperature gradient and L is the length of the material.

In the case of liquids, the convection current due to the gravitational effect would lead to wrong estimation of the thermal conductivity. For accurate measurement of thermal conductivity, the convectional current has to be minimized as much as possible. This is more complicated in the case of nanofluids, where nanoparticles dispersed in a fluid experience more convection current due to the gravitational force leading to inaccurate measurement of thermal conductivity. The convection current in the thermal conductivity measurement can be minimized by reducing the measurement time. There are various techniques that have been proposed to measure the thermal conductivity of fluids by considering the above mentioned factors. The different methods to measure the thermal conductivity of fluids are transient hot wire method, steady state method, cylindrical method, temperature oscillation method, 3-ω method etc.[30] Out of the various techniques, transient hot wire method is widely used method to measure thermal conductivity of nanofluids.[31]

2.3.6.1 Transient hot wire method

Principle

Transient hot wire (THW) method is based on the principle of measurement of the temperature of a wire, with time, when it is subjected to an abrupt electrical pulse. A long and thin platinum wire is used as the heater as well as the temperature sensor. The wire is placed inside a fluid and is heated by applying a constant current. The heat from the wire is removed by the surrounding fluid which leads to change in the resistance of the wire with time.[31-32] The temperature response of the wire when constant heat is applied to the wire is given by Fourier's equation,[30]

$$\Delta T = \frac{q}{4\pi k} Ei\left(\frac{-r^2}{4Dt}\right) \quad 0 < t < t_1 \tag{2.6}$$

where q is the heat applied, k is the thermal conductivity, r is the distance from the line at which the temperature is measured, D is the thermal diffusion of the medium, t is the time, T is the temperature and Ei is the exponential integral, which is given by

$$Ei(\alpha) = \int_{\alpha}^{\infty} \frac{1}{u} exp(-u)\, du = -\beta - \ln \alpha - \frac{\alpha^2}{4} + \cdots \tag{2.7}$$

where β is Euler's constant and equal to 0.5772 and $\alpha = r^2/4Dt$. In equation 2.7, the terms beyond $ln\ \alpha$ are negligibly small for longer time duration when r is small and D is larger. The equation 2.6 can be modified as,

$$\Delta T = \frac{q}{4\pi k}\left[-\beta - \ln\left(\frac{r^2}{4Dt}\right)\right] = \frac{q}{4\pi k}\left[\ln t - \ln\left(\frac{r^2}{4DC_E}\right)\right] \tag{2.8}$$

where $C_E = exp(\beta)$. After an initial time delay, the graph of ΔT versus $ln\ t$ shows a straight line with the slope $q/4\pi k$. Then k can be calculated from the slope using the equation,

$$k = \left[\frac{q}{4\pi(\Delta T_2 - \Delta T_1)}\right]\ln\left(\frac{t_2}{t_1}\right) \tag{2.9}$$

Transient hot wire method has advantage over other methods such that the method is simple, fast and accurate than the other methods. The conduction and radiation losses in this method are lowest and the effect of convection is almost ruled out due to the very low measurement time for the thermal conductivity measurements. Due to these interesting features, this method is widely used for measurement of the thermal conductivity of nanofluids.

Homemade cell for thermal conductivity measurements

The homemade experimental set up in the present work consists of a thin platinum wire of diameter of 50 μm and length of 9.8 cm. The wire was tightly fixed between two copper wires (two potential leads) as shown in Figure 2.2 and the whole measurement setup is shown in Figure 2.3. A KEITHLEY 220 programmable current source was used to apply a constant current to the platinum wire. The voltage across the wire was measured using a programmable KEITHLEY 2010 multimeter. The experimental set up was interfaced with a computer to acquire data. The wire was heated by applying a constant current (100 mA) and the change of resistance of the wire due to heating was monitored as a function of time, by measuring the voltage across the wire. The resistance of the wire was measured for 10 seconds and data points were collected at intervals of every 20 milliseconds. The temperature increase of the wire was calculated from the change in the resistance of the wire. Thermal conductivity was calculated from the heating power and slope of the temperature change in logarithmic time.

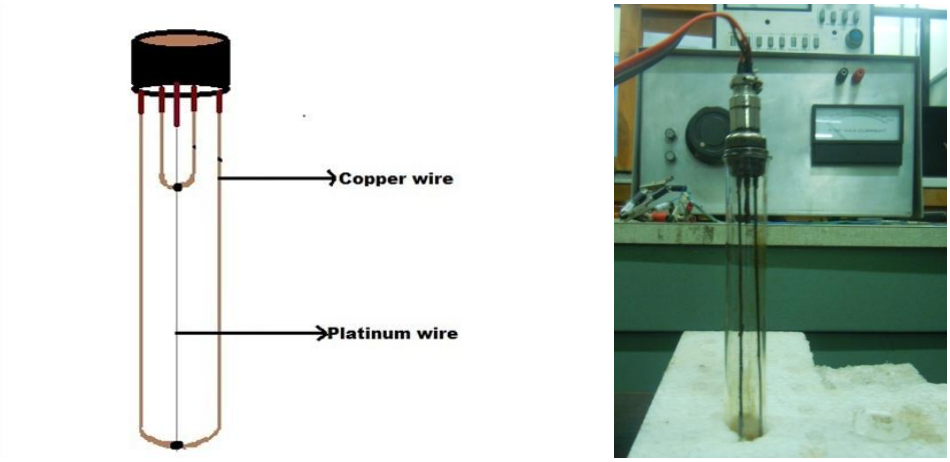

Figure 2.2. Schematic diagram of the homemade cell (left) and the photograph of the cell set up (right) for thermal conductivity measurements of fluids

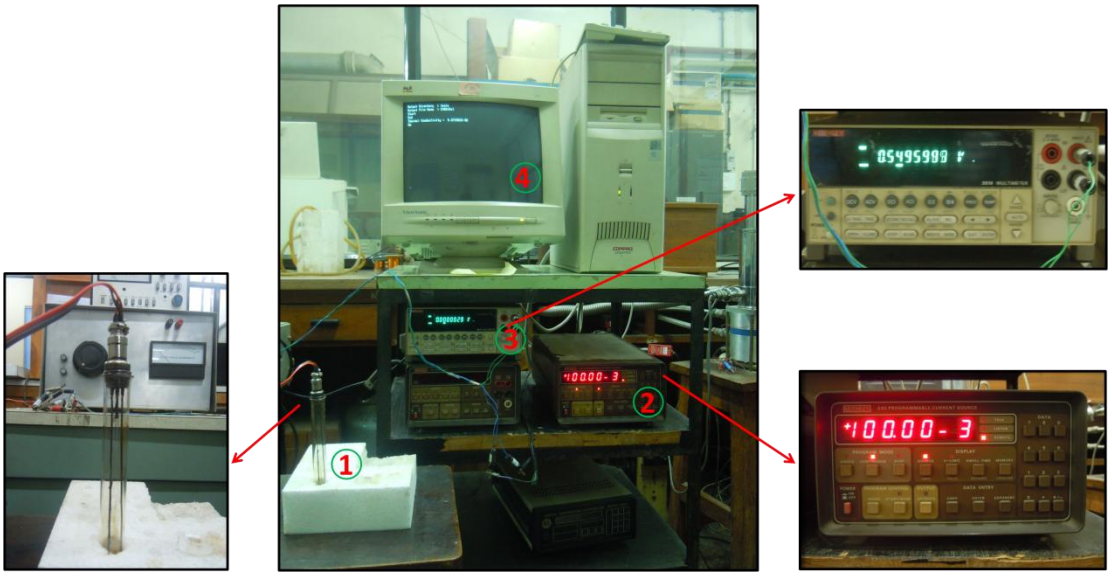

Figure 2.3. Image of the measurement setup, (1) homemade cell, (2) current source, (3) multimeter, and (4) computer.

For the measurement of fluid samples, a 25 ml test tube was used. The experimental set up was initially calibrated with the standard fluids water, ethylene glycol (EG) and toluene. The experimental results are plotted as change in voltage with logarithmic time and thermal conductivity was calculated from the slope of the linear portion of the graph and the heating power. The change in voltage with *ln t* for the standard fluids is shown in Figure 2.4.

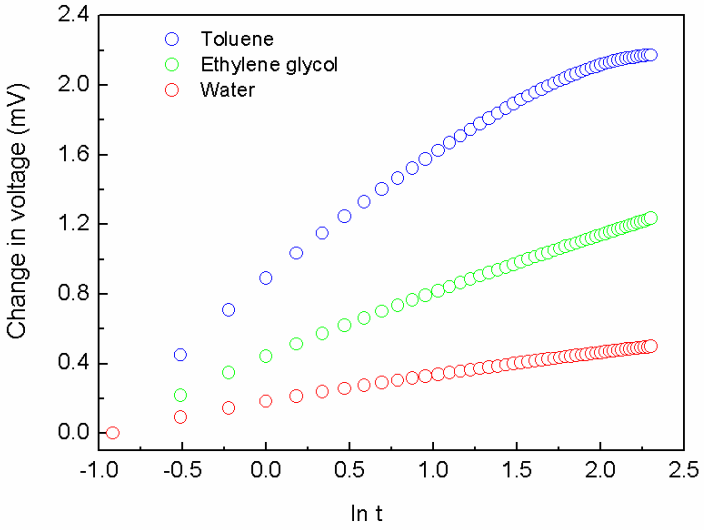

Figure 2.4. The change in voltage with logarithmic time for standard fluids

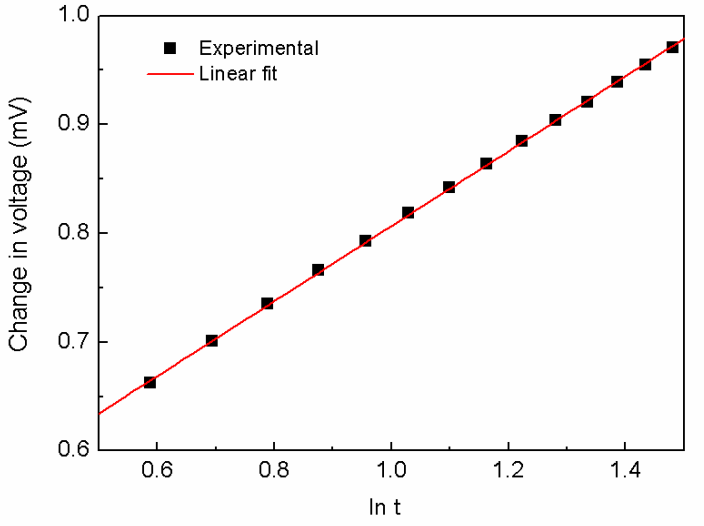

Figure 2.5. The linear fitted region for voltage *vs ln t* curve for ethylene glycol

The slope of the linear portion of the curve is obtained by least squares fitting where the linear region is selected from 0.5 to 1.5 on the *ln t* axis for all fluids. The linear fitting of the data points in this region for ethylene glycol is shown in Figure 2.5. Thermal conductivity was calculated from the slope of the linear region and the heating power of the wire using the following equation,

$$k = \frac{I^3 R_0}{4\pi l} \frac{dR/dT}{d(\Delta V)/d(\ln t)} \tag{2.10}$$

where, I is the current applied to the platinum wire (100 mA), R_0 is the initial resistance of the wire, dR/dT is the temperature coefficient of resistance of the wire (0.0189), ΔV is the change in voltage, t is the time, and l is the length of the wire (9.8 cm). Equation 2.13 can be written as,

$$k = \frac{15.35 \times R_0}{slope} \tag{2.11}$$

The thermal conductivity of the standard fluids calculated from the slope is shown in Table 2.1, and compared with the values reported in the literature. The experimental values match with the reported values within ±1% uncertainty.

Table 2.1. Comparison of the measured values of thermal conductivity of standard fluids with the literature reported values[33-34]

Fluid	***k* reference (W/m-K)**	***k* measured (W/m-K)**
Water	0.60	0.59
Ethylene glycol	0.254	0.252
Toluene	0.131	0.130

Measurements were repeated several times for each standard fluid. After each measurement, 20 minutes time gap was given to cool down the wire before the next measurement. Results of four repeated measurements using ethylene glycol is shown in Figure 2.6 showing almost same slope in the linear region with 0.1% error in the calculated values of the thermal conductivity.

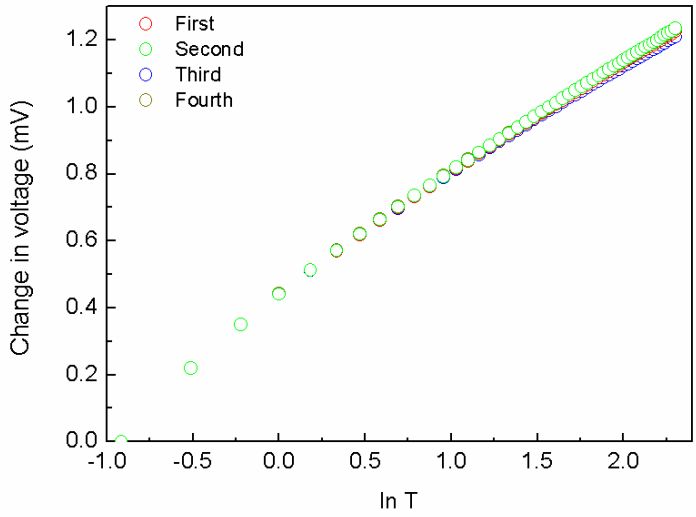

Figure 2.6. Voltage vs *ln t* curves for repeated measurements using ethylene glycol

Figure 2.7 shows photographs of oleic acid coated magnetite nanofluid in the absence and presence of magnetic field. The highly concentrated fluid shows spikes in the presence of a magnetic field (Figure 2.7(b)). The magnetic fluid responds to the magnetic field at very low concentrations (shown in Figure 2.7(d)).

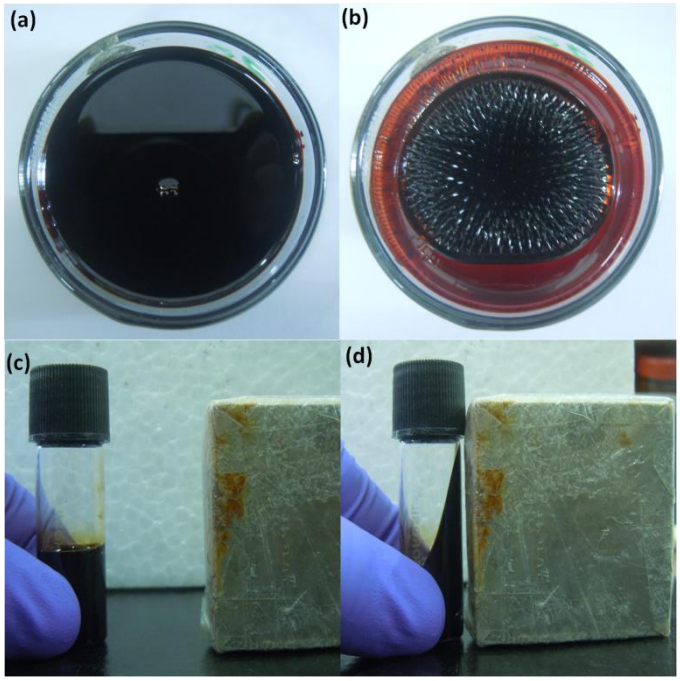

Figure 2.7. Images of magnetic fluids in the absence of a magnetic field (a,c) and in the presence of a magnetic field (b,d). Images (a) and (b) are for a concentrated fluid, and (c) and (d) for diluted fluids used for measurements.

Figure 2.8. The experimental setup used for thermal conductivity measurements in the presence of a DC magnetic field, (1) Electromagnet, (2) DC power source, (3) gauss meter, (4) the fluid sample in a test tube located between the pole pieces of the electromagnet.

Thermal conductivity measurements of different magnetic fluids were also measured in the presence of a magnetic field. DC magnetic field, up to 1 T was used for thermal conductivity measurements, produced by an electromagnet. The magnetic field strength of the electromagnet was measured using a Walker Magnemetrics Gauss meter Model MG-3A by maintaining a gap of 3 cm between the poles of the electromagnet. The transient hot wire set up was placed in a test tube containing the magnetic fluid and the tube was placed between the magnetic poles of the electromagnet (as shown in Figure 2.8). Magnetic field was applied parallel to the temperature gradient and thermal conductivity of the fluid was measured by varying the magnetic field. For each measurement, magnetic field was switched on for two minutes before the thermal conductivity measurement in order to form microstructures inside the fluid and measurements were taken after two minutes without switching off the field. After thermal conductivity measurement, the field was switched off for 10 minutes to bring the magnetic particles in normal position (well dispersed condition) and to cool down the wire.

2.3.7 Viscosity measurements

Viscosity of a fluid is the measure of the resistance to flow or it is the measure of the fluid's willingness to flow. In the presence of an external force, two layers of a fluid move past one another with a relative velocity, and both layers experience a force which opposes relative motions. The magnitude of this force is directly related to the plane area of contact between the two layers and the velocity gradients normal to it.

$$F \propto A\frac{du}{dx} \tag{2.12}$$

where A is the area of contact, u is the velocity in the direction of flow and x is the position. This force per unit area is called shear stress (R), and equation 2.12 becomes,

$$\frac{F}{A} \propto \frac{du}{dx}, \qquad \frac{F}{A} = R = \mu\frac{du}{dx} \tag{2.13}$$

where R is the shear stress and μ is the dynamic viscosity.[35-36]

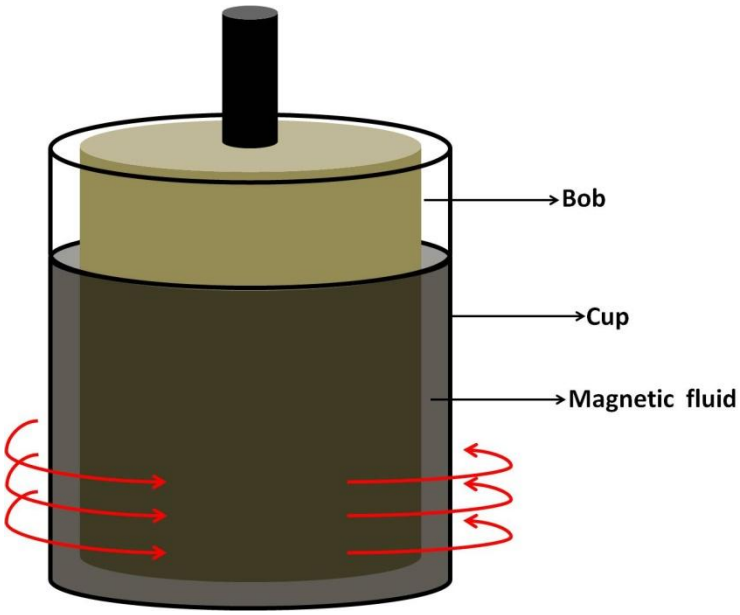

Figure 2.9. Cup and bob geometry for measuring viscosity of nanofluids

In the present study, viscosity measurements of the fluids were made on an Advanced Rheometric Expansion System (ARES). This is a mechanical spectrometer which can subject

a sample to either a dynamic or steady shear strain deformation. The resultant torque extended by the sample is measured in response to the shear strain. A motor is used to apply shear strain and a transducer is used for measuring the torque. Viscosity measurements of the fluid samples were carried out on an ARES strain controlled Rheometer using the steady motor mode. For viscosity measurement, a couette geometry (cup and bob geometry), with cup diameter as 27 mm and diameter of the bob as 25 mm, was used as shown in Figure 2.9. 8 ml of a fluid was filled in the cup and the bob was inserted in to the cup by maintaining a small gap between the cup and the bob. Single point viscosity measurements for all fatty acid coated samples dispersed in different solvents were done at a shear rate of 50 s^{-1}. Viscosity as a function of shear rate was measured in the shear rate range of 10 s^{-1}–1000 s^{-1}. All viscosity measurements were carried out at 28 °C using a temperature controlled furnace. The TA orchestrator software was used to analyze the data collected from the instrument.

References

1. Massart, R. *IEEE Trans. Magn.* **1981**, *17*, 1247-1248.
2. Sun, S.; Zeng, H. *J. Am. Chem. Soc.* **2002**, *124*, 8204-8205.
3. Lee, Y.; Lee, J.; Bae, C. J.; Park, J. G.; Noh, H. J.; Park, J. H.; Hyeon, T. *Adv. Funct. Mater.* **2005**, *15*, 503-509.
4. Xu, J.; Yang, H. B.; Fu, W. Y.; Du, K.; Sui, Y. M.; Chen, J. J.; Zeng, Y.; Li, M. H.; Zou, G. *J. Magn. Magn. Mater.* **2007**, *309*, 307-311.
5. Ge, S.; Shi, X.; Sun, K.; Li, C.; Baker, J. R.; Banaszak Holl, M. M.; Orr, B. G. A *J Phys Chem C, Nanomater interfaces* **2009**, *113*, 13593-13599.
6. Gunay, M.; Kavas, H.; Baykal, A. *Mater. Res. Bull.* **2013**, *48*, 1296-1303.
7. Marchegiani, G.; Imperatori, P.; Mari, A.; Pilloni, L.; Chiolerio, A.; Allia, P.; Tiberto, P.; Suber, L. *Ultrason. Sonochem.* **2012**, *19*, 877-882.
8. Fajaroh, F.; Setyawan, H.; Widiyastuti, W.; Winardi, S. *Adv. Powder Technol.* **2012**, *23*, 328-333.
9. Paike, V. V.; Niphadkar, P. S.; Bokade, V. V.; Joshiw, P. N. *J. Am. Ceram. Soc.* **2007**, *90*, 3009-3012.
10. Schwertmann, U.; Friedl, J.; Stanjek, H. *J. Colloid Interface Sci.* **1999**, *209*, 215-223.
11. Schwertmann, U.; Cornell, R. M. *Iron Oxides in the Laboratory*; John Wiley & Sons, **2008**.
12. Kazemzadeh, H.; Ataie, A.; Rashchi, F. *Int. J. Mod. Phys: Conference Series*, World Scientific: **2012**; pp 160-167.
13. Gnanaprakash, G.; Mahadevan, S.; Jayakumar, T.; Kalyanasundaram, P.; Philip, J.; Raj, B. *Mater. Chem. Phys.* **2007**, *103*, 168-175.
14. Aono, H.; Hirazawa, H.; Naohara, T.; Maehara, T.; Kikkawa, H.; Watanabe, Y. *Mater. Res. Bull.* **2005**, *40*, 1126-1135.
15. Cullity, B. D.; Weymouth, J. W. Elements of X-Ray Diffraction. *AmJPh* **1957**, *25*, 394-395.
16. West, A. R. *Solid State Chemistry and Its Applications*; John Wiley & Sons, **2007**.
17. Patterson, A. L. *Phys. Rev.* **1939**, *56*, 978-982.
18. Kraus, W.; Nolze, G. *J. Appl. Crystallogr.* **1996**, *29*, 301-303.
19. Thomas, G. *Transmission Electron Microscopy of Metals*; John Wiley & Sons Inc, **1962**.

20. Williams, D. B.; Carter, B. *Transmission Electron Microscopy Iv: Spectrometry*; Plenum Press, **1996**.
21. Banwell, C.; McCash, E. M. Fundamentals of Molecular Spectroscopy, **1994**. McGraw Hill, England, ISBN 0-07-707976-0.
22. Silverstein, R. M.; Webster, F. X.; Kiemle, D. J.; Bryce, D. L. *Spectrometric Identification of Organic Compounds*; John Wiley & Sons, **2014**.
23. Scoog, D.; Holler, F.; Crouch, S. Principles of Instrumental Analysis (Thomson Brooks/Cole, Bellmont, Ca). **2007**.
24. Menczel, J. D.; Prime, R. B. *Thermal Analysis of Polymers: Fundamentals and Applications*; John Wiley & Sons, **2014**.
25. Foner, S. *Rev. Sci. Instrum.* **1959**, *30*, 548-557.
26. Buschow, K. H. J.; Boer, F. R. *Physics of Magnetism and Magnetic Materials*; Springer, **2003**; Vol. 92.
27. Anderson, P. W.; Rowell, J. M. *Phys. Rev. Lett.* **1963**, *10*, 230.
28. Joy, P. A.; Date, S. K. *J. Magn. Magn. Mater.* **2000**, *218*, 229-237.
29. Zheng, R. K.; Gu, H. W.; Zhang, B.; Liu, H.; Zhang, X. X.; Ringer, S. P. *J. Magn. Magn. Mater.* **2009**, *321*, L21-L27.
30. Paul, G.; Chopkar, M.; Manna, I.; Das, P. K. *Renewable Sustainable Energy Rev.* **2010**, *14*, 1913-1924.
31. Nagasaka, Y.; Nagashima, *J Phys E Sci Instrum* **1981**, *14*, 1435-1440.
32. Nagasaka, Y.; Nagashima, A. *Rev. Sci. Instrum.* **1981**, *52*, 229-232.
33. de Castro, C. N.; Li, S.; Nagashima, A.; Trengove, R.; Wakeham, W. Standard *J. Phys. Chem. Ref. Data* **1986**, *15*, 1073-1086.
34. Lide, D. R. *CRC Handbook of Chemistry and Physics*; CRC press, **2004**.
35. Brujan, E. *Cavitation in Non-Newtonian Fluids: With Biomedical and Bioengineering Applications*; Springer Science & Business Media, **2010**.
36. Dutt, N.; Ghosh, T.; Prasad, D.; Rani, K.; Viswanath, D. *Springer* **2007**, *33*, 444-553.

Chapter 3

Effect of chain length of surfactant on the thermal conductivity of magnetite nanofluids

Abstract

Studies on the thermal conductivity of the long-chain, unsaturated, oleic acid coated magnetite nanofluids are reported in the literature. However, so far there are only few reports on the studies using saturated fatty acids as surfactants. This chapter reports studies on saturated short-chain capric acid (decanoic acid) and saturated long-chain stearic acid (octadecanoic acid) as surfactants on the thermal conductivity of magnetite-based nanofuids. Short-chain decanoic acid ($C_9H_{19}COOH$) and long-chain stearic acid ($C_{17}H_{35}COOH$) coated magnetite nanoparticles, dispersed in toluene, are studied for their role as surfactants on the thermal conductivity of the nanofluids. The coated nanoparticles are prepared under identical conditions, with comparable particle sizes, and characterized using different techniques.

3.1. Introduction

The surfactant coated on the surface of nanoparticles is known to play an important role in the dispersion and stability of nanofluids.[1-2] The chemistry of the surface of the surfactant coated nanoparticles (hydrophilic or hydrophobic) is decided by the choice of the surfactants and the nature of stabilization (monolayer or bilayer). Fatty acids are one of the major surfactants studied for the stabilization of magnetite nanoparticles dispersed in aqueous as well as non-aqueous medium.[3-7] The surfactant layer on the surface of the nanoparticles not only stabilizes the nanoparticles in the carrier liquid but also makes changes in the physical, chemical and thermophysical properties of the nanofluids.[1, 8-12] The effective thickness of the surfactant layer determines the interparticle distance between the nanoparticles and the hydrodynamic diameter of the nanoparticles in a fluid.[13] There fore, the amount of surfactant on the surface of a nanoparticle and the thickness of the surfactant (physical length) molecules also influence the thermophysical properties of the nanofluids.

The amount of the non-magnetic surfactant layer on the surface of a magnetic nanoparticle is known to change the magnetic properties of the nanoparticles. Fu *et al*[14] observed a decrease in the magnetization of lauric acid (dodecanoic acid) coated Fe_3O_4 nanoparticles compared to that of uncoated Fe_3O_4 nanoparticles. The authors also observed a further decrease in the magnetization by coating with decanoic acid as a secondary surfactant layer over the lauric acid (primary layer) coated nanoparticles. Barbeta *et al*[15] studied the magnetic properties of Fe_3O_4 nanoparticles coated with dodecanoic acid and oleic acid as surfactants. The authors observed an increase in the superparamagnetic blocking temperature for the nanofluid with increasing the concentration of the nanoparticles in the fluid due to the increased interparticle interactions. However, the authors did not observe any appreciable change in the overall magnetic behavior by changing the surfactant on the surface of the nanoparticles.

The hydrodynamic diameter of the nanoparticles in a fluid depends on the amount and thickness (physical length) of the surfactant on the surface of the nanoparticles. The Brownian relaxation of the particles (particle rotation) mainly depends on the hydrodynamic diameter. Regmi *et al*[16] prepared Fe_3O_4 nanoparticles of comparable size (12 nm) and coated with fatty acid surfactants of different chain lengths (lauric, myristic and oleic acid) and studied the hydrodynamic contribution (Brownian relaxation) for hyperthermia and magneto-optic characteristics by keeping the Neel's contribution as constant. From their studies, it was

found that the magnetohydrodynamic behavior of the magnetic fluids can be controlled by choosing the appropriate surfactant. Vekas *et al* (1999)[17] studied the rheological behavior of oleic acid coated magnetite nanoparticles dispersed in non-polar (transformer oil) and polar (pentanol, heptanol and dioctylsebacate) solvents. The authors found that the rheological behavior of magnetic fluids is highly sensitive to the type of stabilization (monolayer/bilayer or hydrophobic/hydrophilic) and quality of the surfactants.

The thickness of the surfactant also influences the size and distribution of the stabilized nanoparticles. Vekas *et al* (2006)[13] used fatty acid surfactants of different chain lengths to stabilize magnetite nanoparticles and it was found that short chain length surfactants (lauric and myristic acids) stabilize smaller particles and longer chain length surfactant (oleic acid) stabilizes wide range of particle sizes. The short-chain surfactant stabilized nanoparticles showed narrow size distribution whereas longer chain length surfactant gave a broader distribution. The authors also observed different initial susceptibilities and different magnetoviscous effects for the magnetite nanoparticles coated with surfactants of different chain lengths. The initial susceptibility and relative viscosity in the presence of a magnetic field are found to be less for the short-chain (lauric and myristic acids) stabilized nanoparticles than the oleic acid stabilized magnetite nanoparticles dispersed in transformer oil. Avdeev *et al*[18] studied saturated fatty acid surfactants with different chain lengths (lauric, myristic, palmitic and stearic acids) for the stabilization of magnetite nanoparticles in a non-polar solvent (decahydronaphthalene) and compared the results with that for oleic acid coated magnetite nanoparticles. From the results, the authors found that all the saturated fatty acid surfactants showed similar stabilizing properties and similar size distribution, whereas the oleic acid coated nanoparticles showed broader size distribution. Avdeev *et al*[19] also studied short chain fatty acids for stabilization of magnetite nanoparticles and found that the chain length is an important parameter that determines the organization of the surfactant molecules on the surface of the nanoparticles and that the short-chain surfactants stabilize smaller particles with reduced polydispersity. The effect of the surfactant on the heat transfer properties, using thiolate coated Au nanoparticles dispersed in toluene and citrate coated Au nanoparticles dispersed in water, has been reported by Patel *et al*[20]. It is found that the thiolate coated Au nanoparticles are less effective in thermal conductivity enhancement compared to the citrate coated Au nanoparticles. From the results, it has been concluded that the effective heat transfer at the surface of the nanoparticles is decided by the type of surfactant coating.

In the present study, we have compared the properties of the short-chain fatty acid, capric acid (decanoic acid), and the long-chain fatty acid, stearic acid (octadecanoic acid), coated magnetite nanoparticles, synthesized under identical conditions and with comparable particle size. The magnetic and thermophysical properties of the magnetite nanofluids dispersed in toluene are studied. The changes in the thermal conductivity of the magnetite nanofluids containing the fatty acid coated magnetite nanoparticles for different concentrations as well as the variation of the thermal conductivity in the presence of an applied magnetic field are studied.

3.2. Materials and methods

3.2.1. Materials

Figure 3.1 shows structures of the fatty acids used for surface coating on the surface of the magntite nanoparticles. Fatty acids used in the present study are the saturated straight chain 10 carbon capric acid (decanoic acid, $C_9H_{19}COOH$) and 18 carbon stearic acid (octadecanoic acid, $C_{17}H_{35}COOH$). Some of the physical properties of the two fatty acids are compared in Table 3.1. The name decanoic acid is used throughout the chapter instead of the less common name, capric acid.

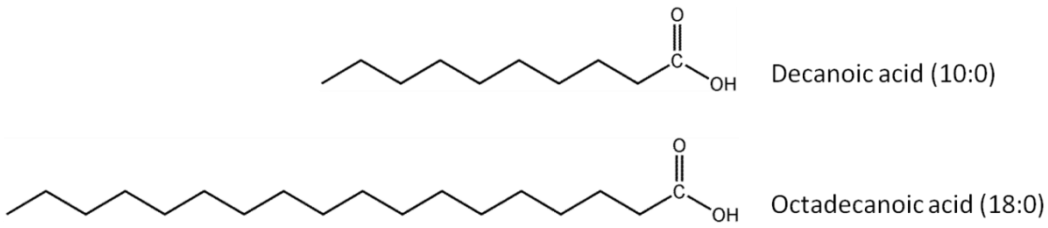

Figure 3.1. Structure of the fatty acids used as surfactants

Table 3.1. Physical properties of the fatty acids

Fatty acid	Formula	Melting point (°C)[21]	Boiling point (°C) (@10mmHg)[22]	Density @80 °C (kg/m^3)[23]	Thermal conductivity (W/mK)[24]
Decanoic acid	$C_{10}H_{20}O_2$	31.4	150	851.8	0.149 (@40 °C)
Stearic acid	$C_{18}H_{36}O_2$	69.6	227	837.4	0.172 (@70 °C)

3.2.2. Synthesis

Decanoic acid and stearic acid coated magnetite nanoparticles were synthesized by the coprecipitation method using the iron chloride precursors ($FeCl_3.6H_2O$ and $FeCl_2.4H_2O$) and ammonium hydroxide (NH_4OH) as the base, in the presence of the corresponding surfactant in the reaction medium. 2 g of decanoic acid dissolved in 20 ml acetone (for decanoic acid coating) and 2 g of stearic acid in 20 ml of 2-propanol (for stearic acid coating) used and remaining procedure is same as discussed in section 2.2.2 in chapter 2. A dispersion obtained was cooled to room temperature and washed with 1:1 acetone-hexane mixture (in decanoic acid case) and 1:1 2-propanol-hexane (in stearic acid case). The nanoparticles in the aqueous layer were transferred to the non-aqueous layer (hexane) during the washing process and the non-aqueous layer containing the nanoparticles was separated using a separating funnel and dried at room temperature to obtain nanoparticles in the powder form. The dried powder samples are labelled as MDE and MST, respectively, for the decanoic acid and stearic acid coated samples, and used for further studies.

3.3. Characterization of surfactant coated magnetite nanoparticles

3.3.1 Powder X-ray diffraction

The dried powder samples are initially characterized for phase formation and purity, by X-ray diffraction studies. The powder XRD patterns of the as-synthesized samples, MDE and MST, are shown in Figure 3.2. In the figure, the experimental XRD patterns are compared with the simulated pattern of Fe_3O_4 (magnetite). The positions and intensities of all the peaks in the XRD patterns of the two samples match very well with the simulated pattern, showing the formation of magnetite. The cubic lattice parameter is calculated by least-squares refinement of the experimental patterns (using PCW software) and the lattice parameter is obtained as 8.39 Å and 8.40 Å for MDE and MST, respectively, which is comparable to that of magnetite (8.40 Å, JCPDS #19-0629). All the peaks in the experimental patterns are very broad, suggesting nanocrystalline nature of the samples. The average crystallite size is calculated from the full width at half maximum (FWHM) of the major peak (311) using the Scherrer equation (equation 2.2, section 2.3.1 in chapter 2). The average crystallite size is calculated as 6±1 nm and 7±1 nm for MDE and MST, respectively.

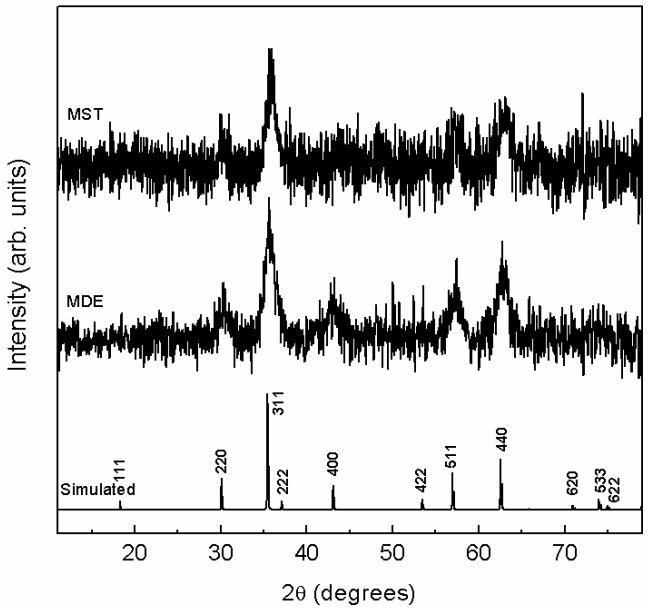

Figure 3.2. Powder XRD patterns of decanoic (MDE) and stearic acid (MST) coated magnetite nanoparticles. The simulated pattern of Fe_3O_4 is shown and indexed at the bottom for comparison.

3.3.2 Transmission electron microscopy

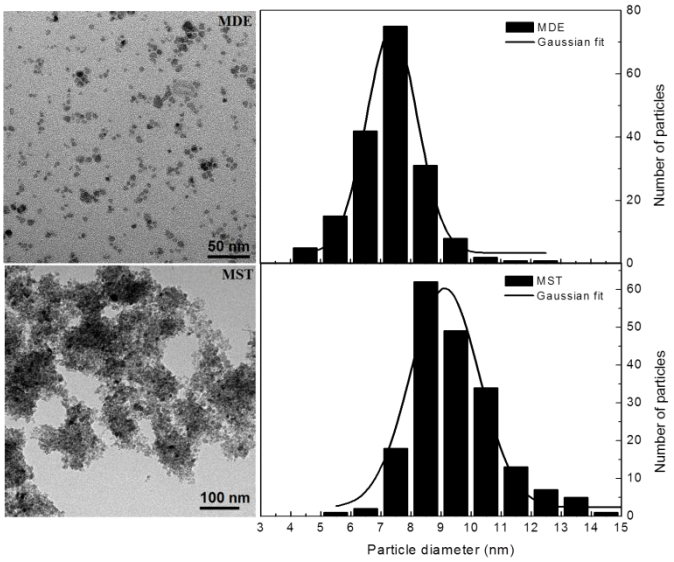

Figure 3.3. TEM images (left) and the corresponding particle size histogram (right) of the decanoic acid (MDE) and stearic acid (MST) coated samples

Table 3.2. Crystallite and particle sizes of the decanoic and stearic acid coated samples

Sample	Crystallite size (±1 nm)	Particle size (±0.5 nm)	Size distribution from TEM histogram, FWHM (nm)
MDE	6	7.4	2.0
MST	7	9.1	2.3

TEM images of the decanoic acid and stearic acid coated samples and their corresponding particle size histogram are shown in Figure 3.3. The decanoic acid coated sample shows well separated nanoparticles, with some of them forming small clusters. The particle size distribution in the histogram is narrow and the FWHM of the Gaussian fitted curve is obtained as 2.0 nm. The Gaussian fitted histogram in Figure 3.3 shows that the average particle size is 7.4 nm for MDE. The TEM image of the stearic acid coated sample shows clusters of nanoparticles. The average particle size distribution is slightly larger for stearic acid coated sample than that for the decanoic acid coated sample and the FWHM of the Gaussian fitted curve is 2.3 nm. The average particle size obtained from the Gaussian fitted particle size histogram is 9.1 nm for MST. The crystallite size calculated from XRD and particle size obtained from TEM images are compared in Table 3.2.

For both samples, the average particle size is slightly larger than the average crystallite size calculated from the XRD patterns using the Scherrer equation. The larger size obtained from the TEM images can be due to the surfactant layer present on the surface of the nanoparticles. The chain length of the fatty acid attached to the surface of the nanoparticles may be contributing towards the observed larger size of the nanoparticles. For example, the chain length of decanoic acid and stearic acid are reported as 1.4 nm and 2.4 nm respectively.[25-28] Larger size distribution is observed for the stearic acid coated sample compared to the decanoic acid coated sample and this could be due to the fact that surfactant with larger carbon chain length stabilizes nanoparticles in a wider size range and short chain fatty acid stabilizes only smaller particles, as reported.[13] The stearic acid coated sample (MST) shows highly aggregated particles in the TEM image but the decanoic acid coated sample (MDE) shows well separated particles with small clusters (Figure 3.3). However, in both cases, the individual particles are separated from one another due to the surface coating with the fatty acid molecules.

3.3.3 Thermogravimetric analysis

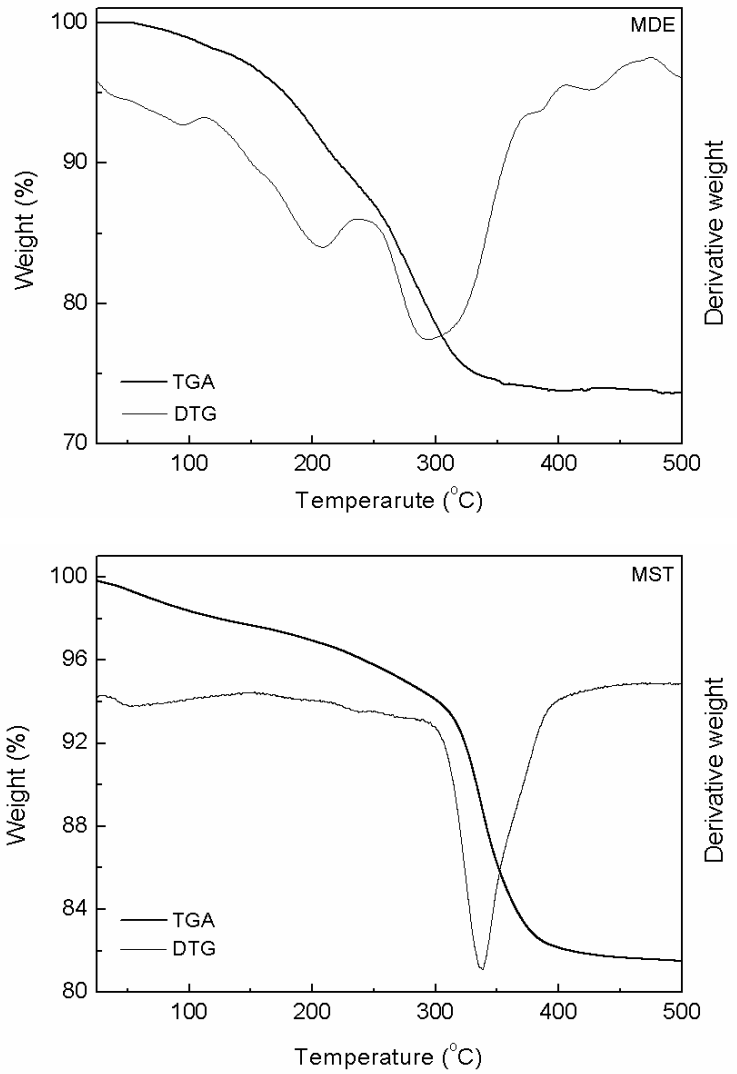

Figure 3.4. Thermogravimetric (thick lines) and the corresponding derivative curves (thin lines) of decanoic acid (MDE) and stearic acid (MST) coated samples.

Thermogravimetric analysis curves (thick lines) and the corresponding derivative curves (thin lines) of decanoic and stearic acid coated samples are shown in Figure 3.4. The total weight losses below 500 °C are obtained as 26% and 18%, respectively, for MDE and MST. Both samples show three-step weight loss below 500 °C. The first weight loss below 150 °C corresponds to the loss of solvent molecules and/or moisture and the second and third weight losses correspond to the removal of the surfactant molecules. For the sample MDE, the second weight loss is observed in the temperature range 150-250 °C and the third weight loss

is observed above 250 °C, as clearly evident from the DTG cure shown in the figure. The second and third weight losses show minimum at 203 °C and 276 °C, respectively in the derivative curve, and could be due to the removal of the surfactant molecules attached to the surface of the nanoparticles. The second weight loss corresponds to desorption, decomposition and evaporation of weakly bound secondary layer of decanoic acid over the primary layer and attached through week van der Waals interaction. The weight loss at higher temperatures (276 °C) corresponds to decomposition of the decanoic acid molecules chemically bounded to the nanoparticle surfaces. Shen *et al*[6] observed a similar two-step weight loss above 200 °C for bilayer coated magnetite nanoparticles using short chain saturated fatty acids (C9-C13) as surfactants, the first weight loss at the lower temperature is ascribed to removal of secondary layer of surfactants and the weight loss at a higher temperature corresponds to the primary layer attached the surface through chemical bond.

In the case of stearic acid coated sample (MST) the second and third weight losses are observed at slightly higher temperatures than that for the decanoic acid coated sample. The second minor weight loss from 160 to 290 °C (shows minimum in the DTG curve at 242 °C) could be due to desorption, decomposition and evaporation of the weakly bound stearic acid to the surface of the nanoparticles, possibly the secondary surfactant layer over the primary layer. The major weight loss from 290 to 500 °C (minimum at 355 °C in DTG) corresponds to decomposition of the strongly bound stearic acid to the nanoparticle surfaces possibly through chemical bond. Zhao *et al*[29] also observed similar kind of weight loss for oleic acid coated magnetite nanoparticles including the solvent weight loss at lower temperatures. From the TGA studies on the stearic acid coated sample, it is clear that mainly a primary layer (monolayer) is coated on the nanoparticles, with small amount of the secondary surfactant layer attached over the primary layer through weak van der Waals interaction. Thus, the thermogravimetric analysis of the samples MDE and MST indicates that there are two groups of surfactants attached to the nanoparticle surfaces.

The decanoic and stearic acid coated samples show almost the same amount of the primary surfactant. However, the amount of the secondary surfactant on the surface of the nanoparticles is more for the decanoic acid coated sample compared to the stearic acid coated sample (Table 3.3).

Table 3.3. Amount of total, primary and secondary surfactants on the decanoic and stearic acid coated magnetite nanoparticles

Sample code	Total surfactant (±1%)	Primary surfactant (±1%)	Secondary surfactant (±1%)
MDE	26	13	13
MST	18	12	6

3.3.4 Infrared spectroscopy

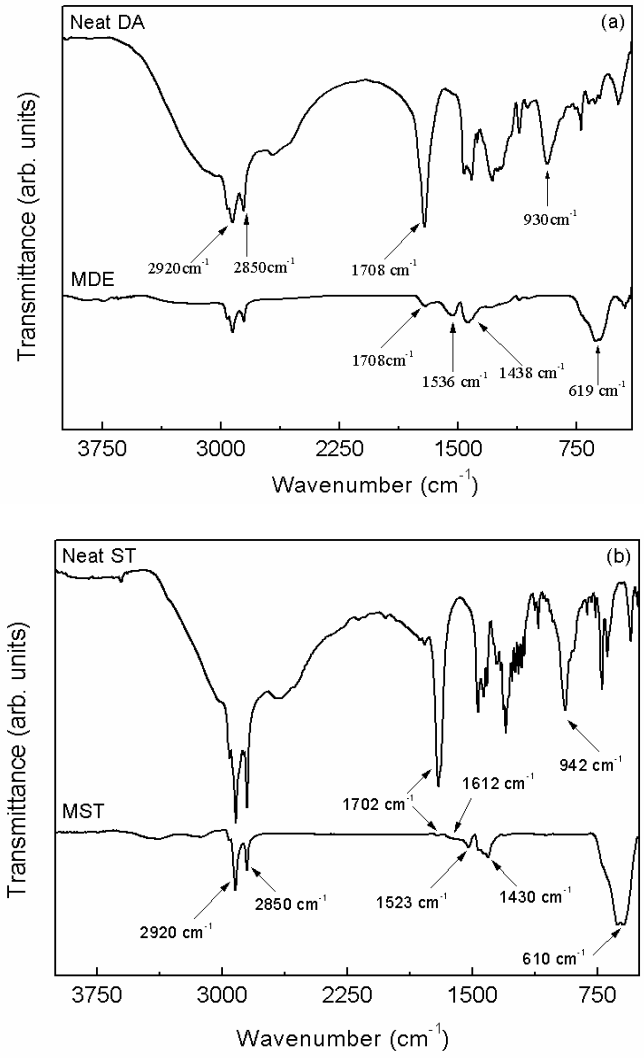

Figure 3.5. Infrared spectra of (a) decanoic acid coated sample (MDE) compared with that of neat decanoic acid (DA), and (b) stearic acid coated sample (MST) compared with that of neat stearic acid (ST).

To obtain information on the nature of bonding of the surfactant molecules with the surface of the nanoparticles, infrared spectroscopy studies have been carried out. Figure 3.5 shows comparison of the IR spectra of the fatty acid coated samples with that of the corresponding neat fatty acids. IR spectra of the decanoic acid coated sample (MDE) and neat decanoic acid (DA) are compared in Figure 3.5(a) and Figure 3.5(b) shows a comparison of the IR spectra of the stearic acid coated sample (MST) and neat stearic acid (ST). The bands at 2850 cm^{-1} and 2920 cm^{-1} in the spectra of neat acids and the coated samples correspond to symmetric and asymmetric C-H stretching vibrations of the methylene ($-CH_2-$) groups. The strong band at 1708 cm^{-1} in the spectra of decanoic acid and at 1702 cm^{-1} for stearic acid corresponds to the carbonyl stretching vibration of the carboxylic group. The intensity of this band is reduced to a large extent in the spectra of coated nanoparticles. The band at 930 cm^{-1} and 942 cm^{-1} in the spectra of DA and ST, respectively, is a characteristic band for dimeric form of fatty acid molecules, which corresponds to O-H bending vibration. This band is completely vanished in the spectra of MDE and MST. The new band at 610-620 cm^{-1} in the spectra of both the coated samples corresponds to Fe-O stretching frequency of Fe_3O_4, including the Fe-O bond due to the attachment of the fatty acid to the Fe atom on the surface of the nanoparticles through the oxygen atoms of the carboxyl group.[30]

A new band appeared in the spectra of the decanoic acid coated sample at 1536 cm^{-1} and at 1523 cm^{-1} in the spectra of the stearic acid coated sample. This band corresponds to the asymmetric stretching vibration of the carboxylate group ($-COO^-_{asym}$).[31]The positions and separation of the bands due to asymmetric carboxyl vibration ($-COO_{asym}$) of the metal-carboxylate group and the symmetric carboxyl vibration ($-COO_{sym}$) at ~1430 cm^{-1}, provide information on the type of coordination of the surfactant molecules on the surface of the nanoparticles. It has been reported that the separation between these two bands, $\Delta\nu$ (= $\nu COO_{asym} - \nu COO_{sym}$), greater than 200 cm^{-1} is due to unidentate, $\Delta\nu$ below 110 cm^{-1} is due to chelating bidentate and $\Delta\nu$ between 140 cm^{-1} to 200 cm^{-1} is due to bridged bidentate ligand.[31] The difference ($\Delta\nu$) between the vibrational frequencies of the asymmetric carboxylate stretching band from the symmetrical carboxylate stretching band can therefore indicate the nature of the bonding of the decanoic acid and stearic acid molecules to the surface of the nanoparticles.

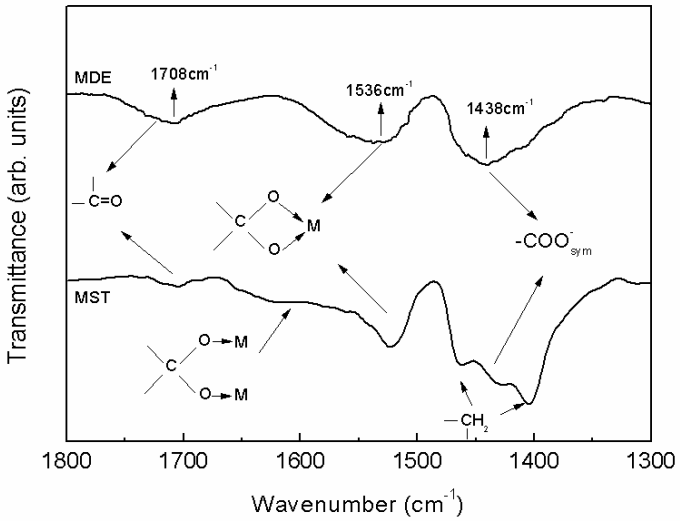

Figure 3.6. The carboxylate region from the IR spectra of decanoic (MDE) and stearic acid (MST) coated samples

Figure 3.6 shows the carboxylate region of the IR spectra of the decanoic acid and stearic acid coated magnetite nanoparticles. For the decanoic acid coated sample, the bands due to asymmetric and symmetric carboxylate stretching vibration are observed at 1536 and 1438 cm^{-1}, respectively, giving $\Delta\nu = 98\ cm^{-1}$. Similarly, for the stearic acid coated sample, the carboxylate bands are observed at 1523 and 1430 cm^{-1} and $\Delta\nu$ is obtained as 93 cm^{-1}. This ($\Delta\nu < 110\ cm^{-1}$) corresponds to the chelating bidentate coordination of the carboxylate group to the iron atom on the surface of the nanoparticles.[31-32] Apart from the strong band at ~1530 cm^{-1}, a shoulder to the band is observed around 1580 cm^{-1} for both the coated samples. This corresponds to $\Delta\nu \approx 150\ cm^{-1}$, suggesting that some fatty acid molecules may be forming bridged bidentate coordination with the $Fe^{2+/3+}$ ions on the surface of the nanoparticles. The weak band at 1700-1710 cm^{-1} in the spectra of both the coated samples suggest the presence of small amounts of the respective free fatty acid molecules that are either free or indirectly attached to the surface of the nanoparticles through weak van der Waals interaction with the primary surfactant that are directly attached to the surface of the nanoparticle.[33] Intensity of this band is relatively larger for MDE than for MST corresponding to relatively larger amount of secondary surfactant in MDE. This concluion is supported by the thermogravimetric analysis data which also provided (weight loss at 203 °C) information for the presence of the secondary surfactant layer on the nanoparticles surfaces and relatively larger amount of the secondary surfactant in MDE. The absence of the characteristic band corresponding to

dimeric carboxylic acids at ~930-940 cm^{-1} indicates that the fatty acid molecules in the coated samples are in their monomeric form.

Thus the IR spectral studies indicate absence of dimeric form of the carboxylic acid molecules and small amounts of free carboxylic acid as a secondary layer over the primary layer attached to the surface of the nanoparticles through chelating bidentate coordination. Based on these observations, the probable mode of attachment of the primary and secondary surfactant molecules on the surface of a nanoparticle is schematically shown in Figure 3.7. As evidenced from the TGA studies, the total amount of the surfactant attached to the surface of the nanoparticle is larger for the decanoic acid coated sample than the stearic acid coated sample (Figure 3.4). However, the amount of the primary layer of the surfactants attached directly to the surface of the nanoparticle is same for both the decanoic and stearic acid coated samples. The amount of the secondary layer of the surfactants is less for the stearic acid coated sample than for the decanoic acid coated sample (see Table 3.3).

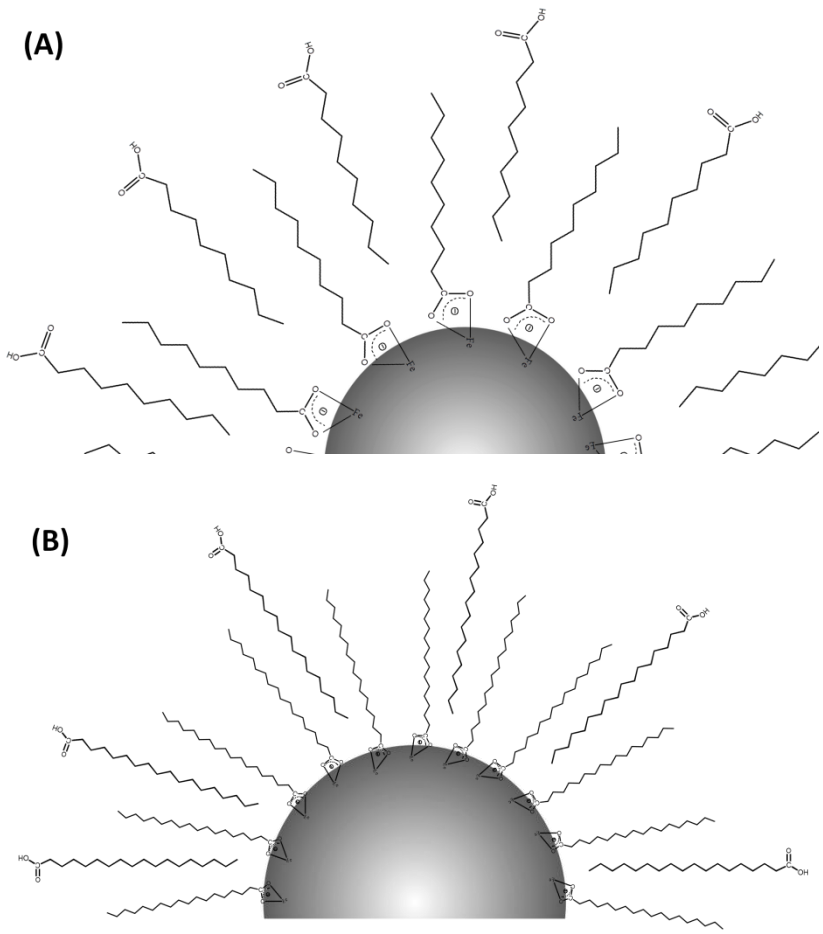

Figure 3.7. Schematic diagrams showing (A) decanoic acid coated magnetite nanoparticle and (B) stearic acid coated magnetite nanoparticle.

3.3.5 Magnetic measurements

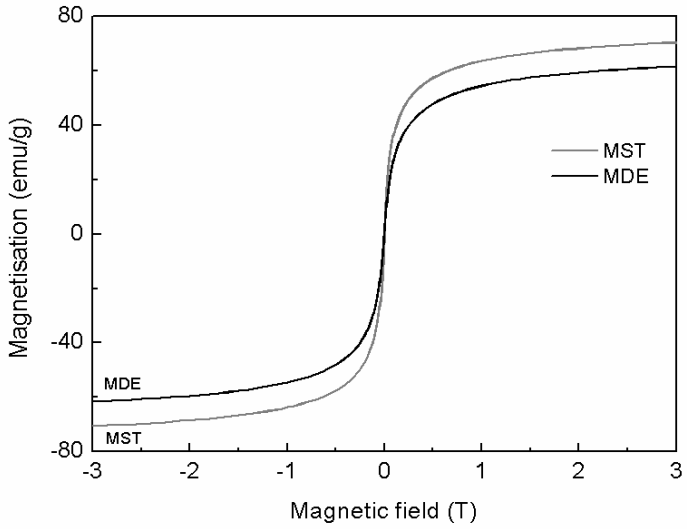

Figure 3.8. Room temperature magnetization curves of the decanoic acid (thick line) and stearic acid (thin line) coated samples

Figure 3.8 shows the results of room temperature magnetization curves (M vs H) of the decanoic and stearic acid coated powder samples. Magnetization increases with increasing magnetic field even at higher applied fields. This observation, along with the absence of magnetic hysteresis (zero remanence and coercivity) indicates the superparamagnetic nature of the nanoparticles.[34] Magnetization is expressed in emu per gram of Fe_3O_4, after correcting for the amount of surfactants obtained from the TGA curves. The magnetization of the decanoic and stearic acid coated samples at the magnetic field of 3 T is obtained as 61.1 emu/g and 70.5 emu/g, respectively. Saturation magnetization is calculated by plotting M vs 1/H and extrapolating to 1/H=0. Saturation magnetization is obtained as 65.5 emu/g and 74.4 emu/g for the samples MDE and MST, respectively, which is much lower than the saturation magnetization (92 emu/g) of bulk magnetite.[35] The reduction in the magnetization is attributed to the finite size and surface effects due to the smaller particle size and the magnetically dead layer on the surface of the nanoparticles.[36] The observed lower magnetization for the decanoic acid coated sample (MDE) is due to the relatively smaller particle size as well as the narrow size distribution compared with that of MST. The average particle size of MDE is relatively smaller (7.4 nm) when compared to that of MST (9.1 nm). Similarly, the stearic acid coated sample contains relatively more number of larger particles (>10 nm) and the particle size distribution is relatively wider (Figure 3.3). The larger particles contribute to the higher magnetization observed for the stearic acid coated sample.

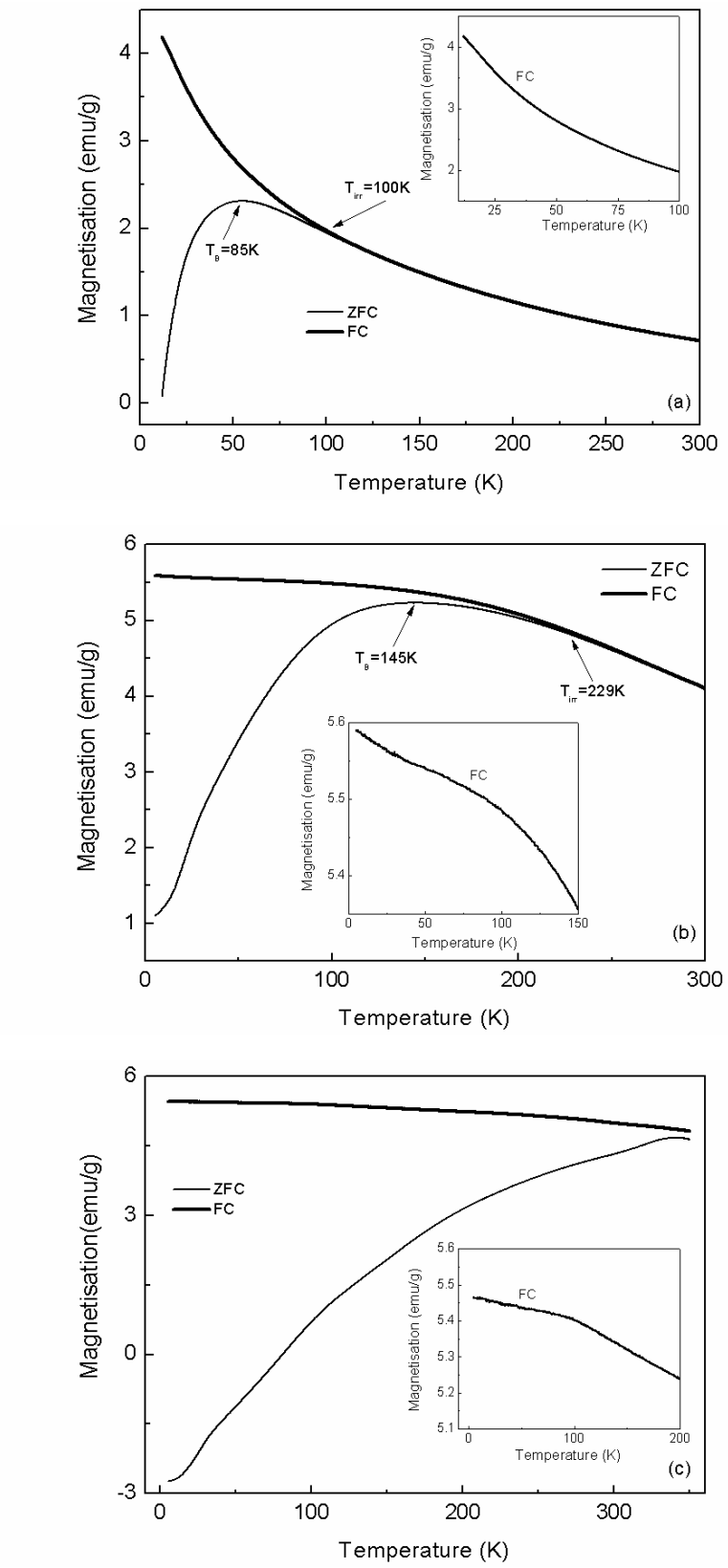

Figure 3.9. Temperature dependant FC (thick line) and ZFC (thin line) magnetization curves of (a) decanoic acid coated, (b) stearic acid coated and (c) uncoated samples. The insets show the zoomed FC curves.

Temperature dependant magnetization studies have been carried out to get more information on the magnetic nature of the particles. The magnetization of the samples measured under zero field cooled (ZFC) and field cooled (FC) conditions are shown in Figure 3.9. For the zero field cooled measurements, the sample was cooled from 300 K to 5 K in the absence of a magnetic field (under zero field) and the magnetization was measured while warming to room temperature in the presence of a field of 5 mT (50 Oe). For the field cooled measurements, the sample was cooled to 5 K in a field of 5 mT and the magnetization was measured while heating the sample in the same field to room temperature. A maximum is observed in the ZFC magnetization curve for both the coated samples and the temperature at which the magnetization of the sample reaches a maximum value is considered as the superparamagnetic blocking temperature (T_B). The blocking temperature is the temperature alone which thermal energy (kT) overcomes magnetic anisotropy (KV) energy. The anisotropy energy of the particles is directly related to the size of the particles, where larger particles require more thermal energy to overcome the anisotropy energy.[37] The anisotropy energy also depends on the inter-particle magnetic interactions (dipolar and exchange), and this contribution depends on the strength and type of the inter-particle interactions. For non-interacting particles, such as those particles which are well separated by effectively coated with the surfactants, this contribution will be less due to the reduced co-operative effect and the thermal energy required to overcome the anisotropy energy will be low.[38] The interparticle interaction is larger in the case of the uncoated sample, due to the larger co-operative effect between the particles and it requires more thermal energy to overcome the anisotropy energy.

The observed blocking temperatures for MDE and MST are 85 K and 145 K, respectively (Figure 3.9(a) & (b)). The observed blocking temperature for the coated samples is much less than that for the uncoated sample (340 K) as shown in Figure 3.9(c). The blocking temperature of the decanoic acid coated sample is much less compared to that for the stearic acid coated sample. This is due to the presence of relatively larger particles in the stearic acid coated sample (9.1 nm) compared to that in the decanoic acid (7.4 nm) coated sample. Similarly, the broad ZFC curve of the stearic acid coated sample is due to the wider particle size distribution.[39]

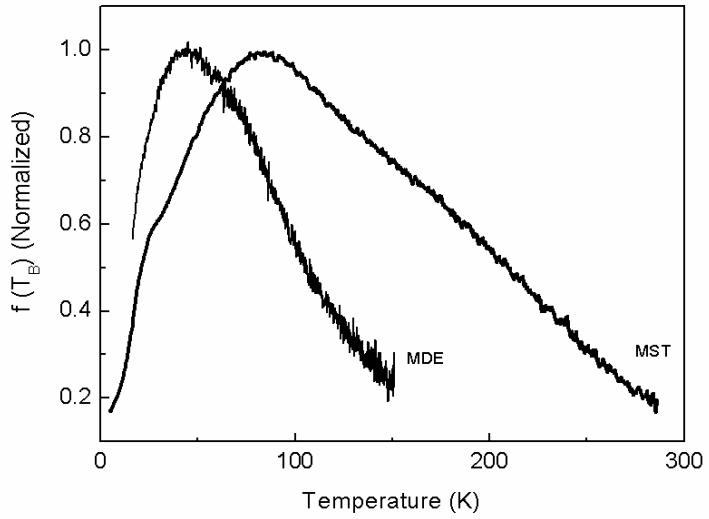

Figure 3.10. Blocking temperature distribution (T_B) of the decanoic acid (MDE) coated and stearic acid (MST) coated samples

For ideal superparamagnetic particles, with uniform and narrow size distribution, the bifurcation between the FC and ZFC magnetization is expected at the blocking temperature.[39] However, for both the coated samples, the bifurcation temperature or the temperature below which the magnetization is irreversible, T_{irr}, is larger than the blocking temperature. For MDE and MST, T_{irr} is obtained as 100 K and 200 K, respectively, compared to the blocking temperatures (T_B) as 85 K and 145 K. The observed maximum in the ZFC magnetization curve is at the average blocking temperature and T_{irr} may considered as the blocking temperature of the largest particles. Thus the larger difference between T_B and T_{irr} for MST is due to the wider particle size distribution compared to the relatively narrow distribution for MDE. Further, the distribution of the blocking temperature of the nanoparticles of different sizes is calculated from the ZFC magnetization curves of the fatty acid coated samples, using equation 2.4 (section 2.3.5, chapter 2), as shown in Figure 3.10.[40] The decanoic acid coated sample shows a relatively narrow distribution of the blocking temperatures, whereas for the stearic acid coated sample, a wider distribution is obtained. The maximum of the distribution of the T_Bs obtained for the decanoic acid and stearic acid coated samples is at 45 K and 83 K, respectively. The difference in the distribution of the blocking temperatures for the two samples is related to the difference in the particle size distribution. This could be due to the fact that the short chain saturated fatty acid could stabilize smaller sized particles and the long chain saturated fatty acid could stabilize even larger particles. Stearic acid stabilizes the magnetite nanoparticles in wide range of sizes, as reported.[13]

The nature of the FC magnetization curve below the blocking temperature can give information on the interparticle interactions. A continuous decrease in the magnetization with increasing temperature indicates that the particles are non-interacting where as a flat curve with a saturation trend in the magnetization indicates large interparticle interactions. The continuous decrease in the magnetization with temperature indicates that the interparticle interaction in the decanoic acid coated sample is suppressed and the particles are well separated from one another (thick line in Figure 3.9(a) and inset in the Figure 3.9(a)).[41] However, the slight flatness in the FC curve of the stearic acid coated sample, at low temperatures, indicates weak interparticle interactions, probably due to the slight aggregation/assembly of the nanoparticles (thick line in Figure 3.9(b) and inset in the Figure 3.9(b)). For the uncoated sample, the FC curve does now show much variation, suggesting strong interparticle interactions. The TEM studies also support the results from temperature dependant magnetization measurements, where the decanoic acid coated sample is found to form well separated particles whereas the stearic acid coated sample shows assembly of particles forming aggregates (Figure 3.3).

3.4. Studies on nanofluids

Magnetic nanofluids are prepared by dispersing the dried decanoic acid and stearic acid coated magnetite nanoparticles in toluene as the base fluid at different concentrations (volume%). Volume% is calculated by considering the magnetite content of the samples based on the results from the TGA studies as discussed in section 3.3.3.

3.4.1 Magnetic measurements

Figure 3.11 shows the temperature variation of magnetization of the decanoic acid and stearic acid coated fluid samples at a concentration of 2.2 volume%. New characteristic features are observed in the FC and ZFC magnetization curves, compared to that observed for the dried particles (Figure 3.9). For both fluid samples, the bifurcation between the FC and ZFC curves is observed at a higher temperature than for the corresponding solid samples. T_{irr} is observed as 261 K for the decanoic acid coated fluid (compared to 100 K for the powder) and at 290 K for the stearic acid coated fluid (compared to 200 K for the powder). The maximum in the ZFC magnetization curve is shifted to lower temperatures compared to that of the powder samples. For MDE, the maximum is obtained at 46 K (85 K for powder sample) and for MST, the maximum is at 110 K (145 K for the powder sample).

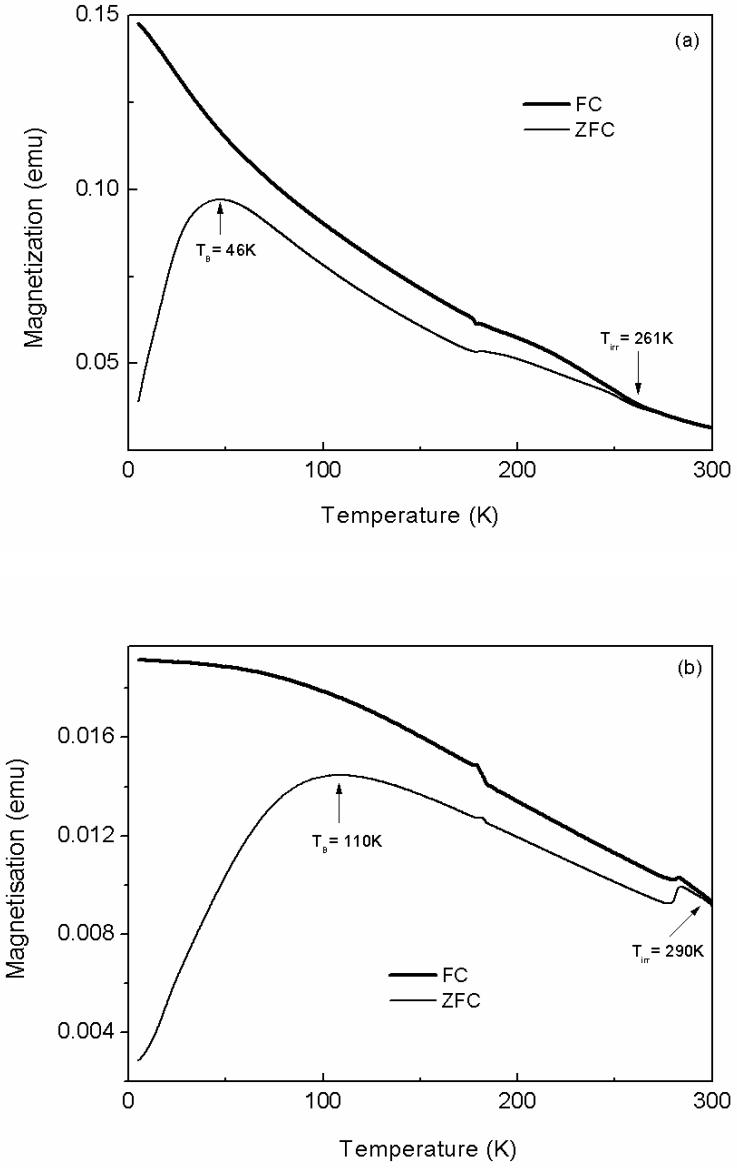

Figure 3.11. Field cooled (thick line) and zero field cooled (thin line) magnetization curves of (a) decanoic and (b) searic acid coated nanoparticles dispersed in toluene at 2.2 volume%.

A small kink is observed in the magnetization curves for both samples, at 178 K, and this temperature corresponds to the freezing point of toluene. As discussed in section 3.3.5 for powder samples, the bifurcation between the FC and ZFC curves corresponds to the blocking temperature of the largest particles or the freezing of the magnetic moments of the larger particles when the thermal energy is lower than the anisotropy energy. Both the Brownian and Neel relaxation are suppressed below this temperature. However, when the nanoparticles are dispersed in a solid matrix, the Brownian relaxation is no longer possible

and the magnetic moments may be frozen at a higher temperature. It is possible that the higher T_{irr} for both fluid samples correspond to the freezing of the surfactant layer over the nanoparticles. However, these temperatures (261 K and 290 K) are relatively lower than the corresponding melting points of bulk decanoic acid (305 K) and stearic acid (343 K).

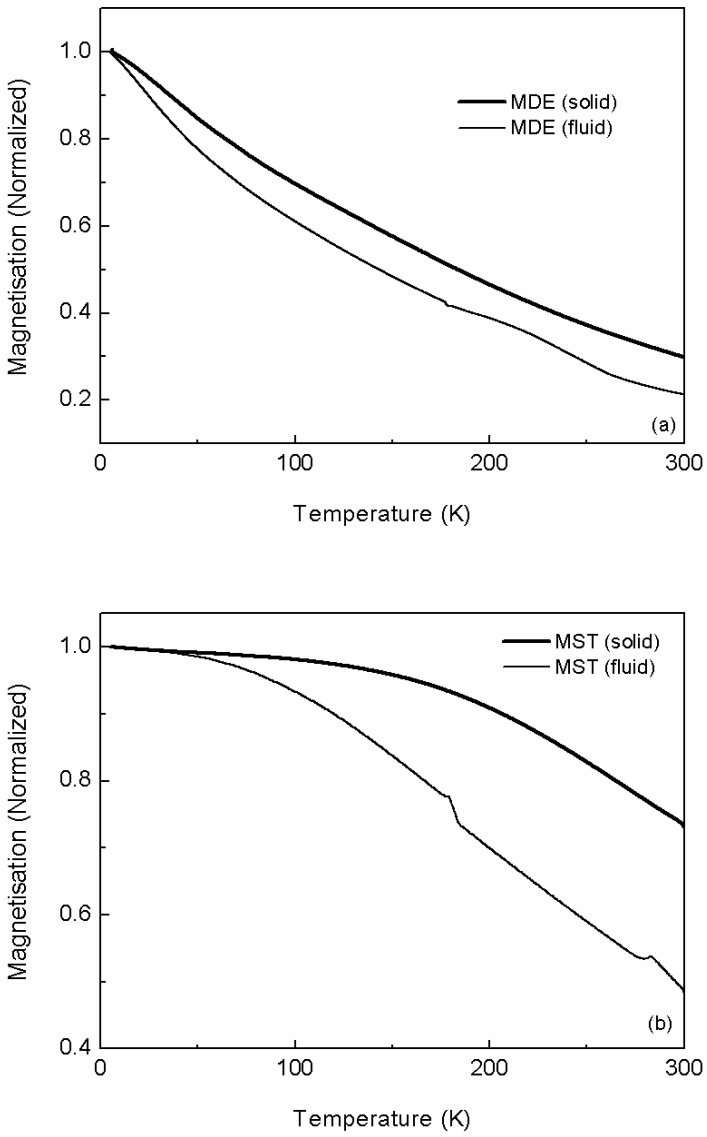

Figure 3.12. Field cooled magnetization curves of solid (thick line) and fluid (thin line) samples of (a) decanoic acid coated and (b) stearic acid coated magnetite nanoparticles.

It is known that the melting point of organic compounds decreases with decreasing size of the particles.[42] Similarly, it has been reported that the melting point of fatty acids

coated on magnetite nanoparticles is less than that of the corresponding bulk acid.[6-7] Thus, it is expected that the melting temperatures of decanoic acid and stearic acid layers coated on the nanoparticles would be much lower than that for the corresponding bulk acids, due to the smaller thickness of the surfactant layers with reduced hydrophobic interactions compared to the free surfactants. Thus, T_{irr} observed for the fluid samples in the present case corresponds to the melting temperature of the surfactant layer. Due to the freezing of the surfactant layer, the magnetic moments of the nanoparticles are blocked below this temperature due to the suppression of the Brownian relaxation.

The decrease in the blocking temperature of the fluid samples with respect to the corresponding powder samples, the temperature at which a maximum is observed in the ZFC magnetization curve, is due to the decreased anisotropy contribution from interparticle magnetic interactions, where the magnetite nanoparticles are well separated from each other due to the solid matrix formed by freezing of the base fluid, toluene. This is obvious from the relatively larger decrease in the FC magnetization with temperature, as shown in Figure 3.12, where the normalized FC magnetization of the powder and the fluid samples is compared for both the decanoic acid and stearic acid coated samples.

3.4.2 Thermal conductivity

Variation of the thermal conductivity with the volume% of the particles of MDE and MST, dispersed in toluene, is shown in Figure 3.13. There is no change in the thermal conductivity from that of the base fluid, up to 1.7 volume% of the nanoparticles of MDE (triangles in Figure 3.13(a)). With further increase in the concentration of the nanoparticles, thermal conductivity is increased almost linearly with the volume% of the particles. For the fluid of stearic acid coated magnetite nanoparticles dispersed in toluene, similar features are observed (triangles in Figure 3.13(b)). Stearic acid coated fluid shows no enhancement up to 1.0 volume% of particles and shows linear enhancement in the thermal conductivity with increasing volume% of particles at higher concentrations. Similar trend in the thermal conductivity enhancement with the volume% of nanoparticles has been reported for oleic acid coated magnetite nanoparticles (6.7 nm) dispersed in kerosene as the base fluid.[43]

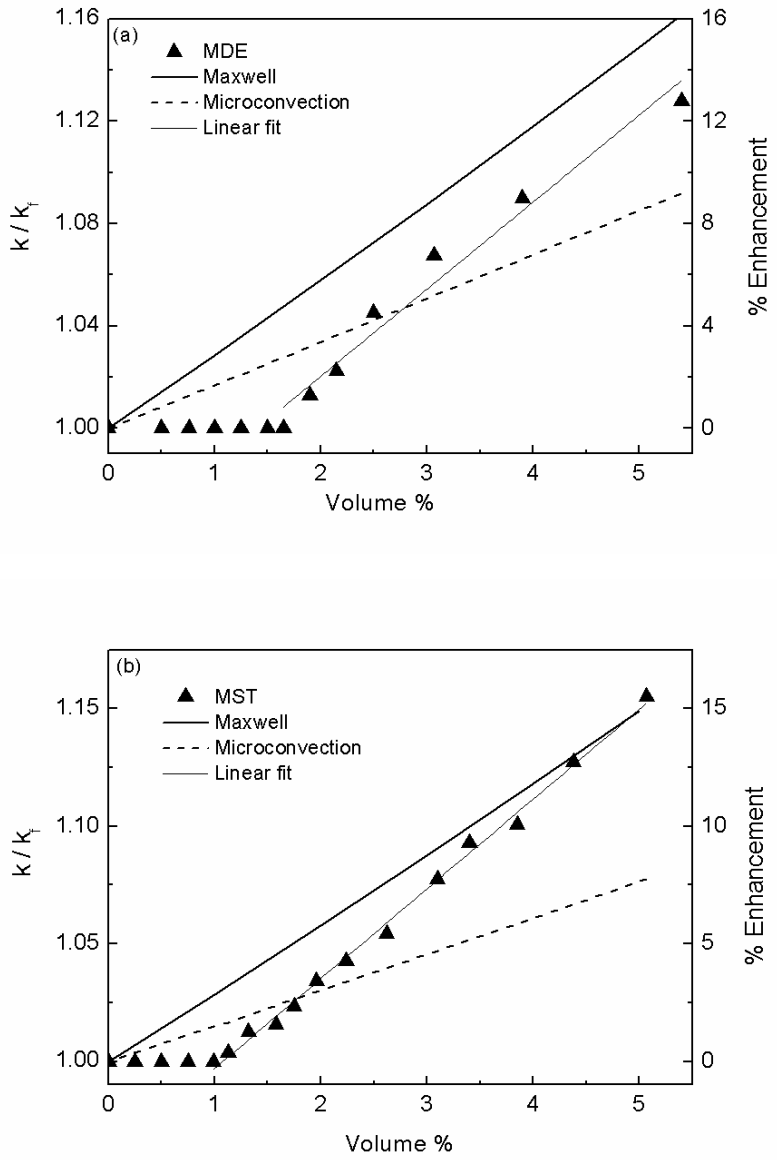

Figure 3.13. The experimental relative thermal conductivity (k/k_f) with concentration of particles is compared with the Maxwell model for (a) decanoic acid and (b) stearic acid coated magnetite fluids

The concentration above which the thermal conductivity of the magnetite nanofluid starts to increase over that of the base fluid is the critical concentration of that fluid for the thermal conductivity enhancement. The critical concentration is observed as 1.7% for MDE and 1.0% for MST and the critical concentration is lower in the case of the stearic acid coated fluid compared to the decanoic acid coated fluid for thermal conductivity enhancement. The unchanged thermal conductivity with the volume fraction of the nanoparticles, at lower concentrations, is probably due to the fact that the particles are well separated from each

other and therefore, the thermal conductivity is only due to the conduction through the base fluid. However, with increasing the concentration above the critical concentration (1.7 volume% for MDE and 1.0 volume% for MST), the particles come closer to each other and could form small clusters in the fluid through weak van der Waals and magnetic interactions. The formation of these small clusters enhances the thermal conductivity over that of the base fluid (as shown in the Figure 3.14). The number of these clusters increases by increasing the concentration of the particles in the nanofluid and leads to increase in the thermal conductivity. The deviation from linearity in the enhancement in the thermal conductivity at higher concentration for the decanoic acid coated sample could be due to the formation of larger clusters which could create less concentrated liquid matrix in the nanofluid, because of the larger separation between the clusters. Even though the clusters are highly thermally conductive, the less concentrated and thermally low conductive liquid matrix slightly reduces the thermal conductivity at higher concentrations. Moreover, there is a possibility for sedimentation of the larger clusters in the fluid due to the gravitational force. The stabilization ability of the 10-carbon decanoic acid is less effective compared to the 18-carbon stearic acid to suspend the larger clusters, as reported.[13] It is reported that short-chain fatty acids could stabilize only smaller particles, whereas long-chain stearic acid stabilizes particles in a wider range of diameters.[13]

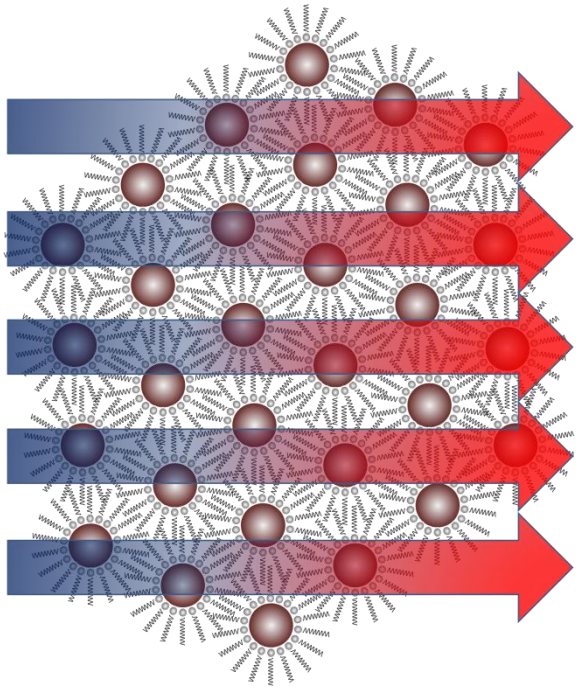

Figure 3.14. Heat transfer through clusters of stearic acid coated magnetite nanoparticles

The enhancement in the thermal conductivity at a lower concentration for the fluid of the stearic acid coated sample could be due to the formation of clusters at low concentrations. The cluster formation at lower concentrations for the stearic acid coated sample is due to the larger hydrophobic interaction between the long chain (18-carbon) fatty acid compared to the short chain (10-carbon) fatty acid. Unlike the fluid of the decanoic acid coated sample, the fluid of MST shows linear enhancement in the thermal conductivity even at higher concentrations. This indicates that the saturated long chain fatty acid stabilizes the clusters even at higher concentrations and linear enhancement in the thermal conductivity is observed with increasing concentration of the nanoparticles in the fluid. Least-squares linear fit to the experimental data, above the critical concentration, for the fluids of both MDE and MST (thin solid lines in the Figures 3.13(a) and 3.13(b)), gave comparable slope of 0.034 and 0.038, respectively, suggesting almost similar performance of the fluids irrespective of the chain length of the fatty acid surfactant. The critical concentration, slope and thermal conductivity at a particular concentration of the samples MDE and MST are compared in Table 3.4.

Table 3.4: Comparison of different parameters of decanoic and stearic acid coated samples

Sample name	Particle size (nm)	Size distribution (nm)	Critical concentration (vol %)	Slope (linear region)	k/k_f @ 3.85 vol %
MDE	7.4	2.0	1.7	0.034	1.09
MST	9.1	2.7	1.0	0.038	1.10

The experimental results are compared with the Maxwell model[44] by considering only the thermal conductivity of the solid particle (k_p), liquid matrix (k_f) and volume fraction (φ) of the particles as discussed in section 1.4.1 in chapter 1. The calculated thermal conductivity values using the Maxwell model based on equation 1.1 shows linear variation of the relative thermal conductivity with increasing concentration of the particles (thick solid lines in Figure 3.13(a) and 3.13(b)). The experimental value of the thermal conductivity for the fluid of the decanoic acid coated sample (MDE) is lower than the calculated value using the Maxwell

model at all the studied concentrations. Although the experimental data of the stearic acid coated sample (MST) shows deviation from the Maxwell model at lower concentration, the experimental results almost match at higher concentrations. The large deviation in the experimental thermal conductivity enhancement from that predicted by the Maxwell model could be due to the increase in the interfacial thermal resistance due to the surface coating or less compatibility of the surface of the particles with the solvent molecules.

Brownian motion of the nanoparticles dispersed in the fluids is also an important mechanism for the enhancement in the thermal conductivity of nanofluids.[45] Experimental data of the variation of the thermal conductivity of decanoic and stearic acid coated magnetite nanofluids are compared with the Brownian motion induced micro-convection model (based on the equation 1.7 as discussed in chapter 1) by considering the particle size (d), thermal conductivity of particle (for Fe_3O_4, k_p = 7 W/mK) and base fluid (for toluene, k_f = 0.13 W/mK), concentration of the particles (φ) and the Prandtl number for toluene at 25 °C as 7, m = 3.375 for toluene.[46] The interfacial thermal resistance, R_b, is calculated for toluene-nanoparticle interface from the acoustics character of water and toluene and their volumetric heat capacities.[47] The calculated R_b value for toluene is 2.16 x 10^{-8} m^2K/W which is almost comparable to the reported conductance at the interface (50 MW/m^2K) for particles of size >10 nm dispersed in toluene.[48] The calculated thermal conductivity ratio based on the Brownian motion induced microconvection model shows larger deviation from the experimental results for all the studied concentrations (dashed line in Figure 3.13a and 3.13b). At lower concentrations, the experimental results show lesser enhancement than that predicted by the microconvection model whereas at higher concentrations larger enhancement is observed than that predicted. Thus, the Brownian motion could not be a possible mechanism for the thermal conductivity enhancement in magnetite nanofluids. It is possible that the observed enhancement in the thermal conductivity at higher concentrations could be due to the formation of clusters in the nanofluid, apart from other contributions.

3.4.3. Thermal conductivity in a magnetic field

Since the nanoparticles are magnetic, thermal conductivity of the two fluids in the presence of a DC magnetic field has been measured. The variation of the thermal conductivity as a function of magnetic field for different concentrations of the decanoic acid coated nanoparticles dispersed in toluene is shown in Figure 3.15. The thermal conductivity is found to increase with increasing strength of the magnetic field for all concentrations.

The thermal conductivity enhancement in the presence of a magnetic field is quantitatively different for different concentrations of the fluid. Fluids near to the critical concentration (1.7 volume%) show lesser enhancement in the thermal conductivity in the magnetic field and up to 50% enhancement is observed in a field of 1 T. However, concentrations above 2 volume% show much larger enhancement in a magnetic field. Up to 150% enhancement is observed at 1 T at these concentrations. At lower concentrations (below 2 volume%) the thermal conductivity continuously increases with the applied magnetic field, whereas at higher concentrations, thermal conductivity reaches maximum and then decreases with increasing magnetic field. Thermal conductivity reaches maximum value for the highly concentrated samples (larger than the critical concentration) at a magnetic field of ~0.7 T, and above this field the thermal conductivity decreases with increasing applied magnetic field. The large enhancement in the thermal conductivity for the highly concentrated (above the critical concentration) fluids could be due to the availability of large number of nanoparticles to form more number of nanoparticle chains along the field lines produced by the magnet. The decrease in the thermal conductivity above 0.7 T for the concentrated samples could be due to the zippering of the nanoparticle chains.[49] The continuous increase in the thermal conductivity in the less concentrated fluids is due to the non-availability of sufficient number of particles to form chains at lower fields and requires higher field to bring the particles closer in order to form the chains.

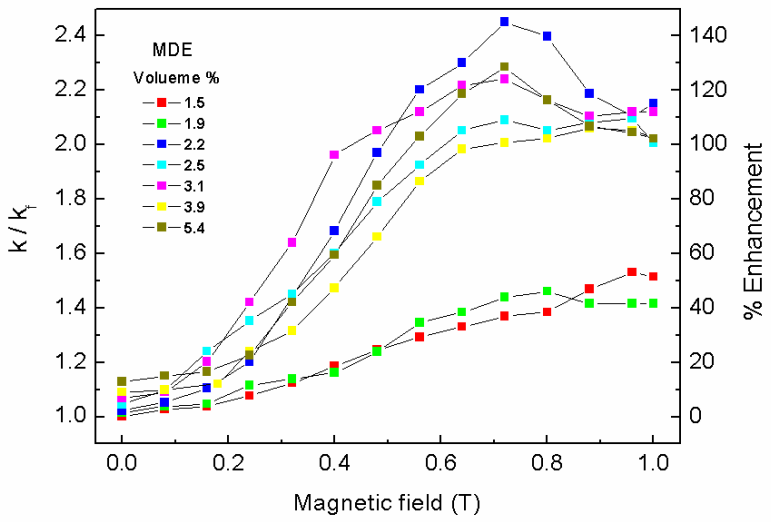

Figure 3.15. Variation of the relative thermal conductivity of the fluid of MDE with applied magnetic field at different concentrations

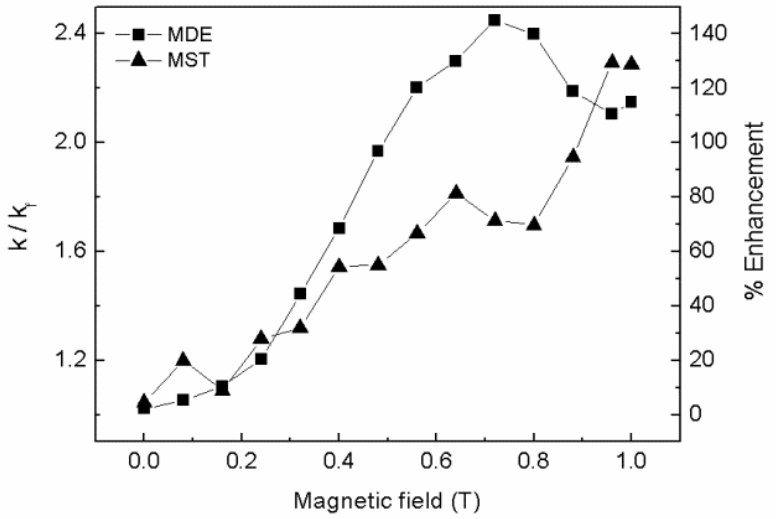

Figure 3.16. Comparison of the thermal conductivity enhancement of decanoic acid (squares) and stearic acid (triangles) coated samples in presence of applied magnetic field, at 2.2 volume%

Figure 3.16 shows a comparison of the thermal conductivity enhancement for the decanoic acid and stearic acid coated magnetite fluids in presence of an applied magnetic field. Comparative studies are made at a concentration of 2.2 volume%, which is larger than the critical concentration of the stearic acid (1.0 volume%) and decanoic acid (1.7 volume%) coated fluids. The thermal conductivity enhancement is initially low in the low field region (up to 0.24T), starts to increase drastically at higher fields, reaches a maximum at ~0.7 T and then decreases with further increasing the magnetic field (squares in the Figure 3.16). However, in the case of the stearic acid coated fluid sample, the thermal conductivity increases almost linearly with increasing magnetic field (triangles in the Figure 3.16). The observed enhancement is almost comparable for the fluids of MDE and MST up to a field of 0.4 T. At higher fields (above 0.4 T), the stearic acid coated fluid shows lesser enhancement in the thermal conductivity than that for the decanoic acid coated fluid. It is possible that the short chain fatty acid (decanoic acid) coated nanoparticles in the fluid show easy response to the applied magnetic field, due to the lower interparticle magnetic interactions and therefore shows larger enhancement in the thermal conductivity. In the case of the long chain fatty acid (stearic acid) coated nanoparticles, slow response to the applied magnetic field leads to quantitatively less enhancement in the thermal conductivity. Moreover, the stearic acid coated nanoparticles could form loose clusters through interdigitation of the surfactant

molecules due to the larger hydrophobic interaction between the surfactants. The co-operative effect of the nanoparticles present in the loose clusters affects the response of nanoparticles to the applied magnetic field.

Thermogravimetric studies showed that the amount of the surfactant present on the surface of the nanoparticles is less for the stearic acid coated magnetite nanoparticles (18%) compared to the decanoic acid coated magnetite nanoparticles (26%). The different amount of the surfactant on the surface of the nanoparticles could also affect the response to the applied magnetic field. The nature of attachment and the amount of the primary and secondary surfactant molecules on the surface of the nanoparticles also can affect the dispersibility and compatibility of the nanoparticles with solvent and affects the response in the presence of a magnetic field. These could be the major reasons for the observed difference in the thermal conductivity for the two different fatty acid coated samples in the presence of a magnetic field.

Philip *et al*[43] showed that the increase in the thermal conductivity in the presence of a magnetic field is due to the increase in the dipolar interaction between the particles. The dipolar interaction energy (U_{dij}) between the particles overcomes the thermal energy (kT) and the dipolar energy increases with increasing the magnetic field.[50] The dipolar interaction energy aligns the nanoparticles in the direction of the applied field and forms chains of nanoparticles or dipolar chains in the fluid.[43] It is also reported that the aspect ratio of the chain increases with increasing the strength of the magnetic field and the heat energy is transferred through the back bone of the nanoparticle chains.[49, 51]

The observed enhancement in the thermal conductivity in the presence of a magnetic field is less than that reported in the literature. For example, Philip *et al*[43] reported 125% enhancement in the thermal conductivity for 1.71 volume% of 6.7 nm magnetite nanoparticles coated with oleic acid and dispersed in kerosene in a magnetic field of 0.038 T. Although the size of the magnetite nanoparticles used in the present study is comparable with the literature report, the observed large difference in the experimental thermal conductivity in the presence of a magnetic field could be due to various factors such as the difference in the particle size distribution, thickness of the surfactant molecules (decanoic vs oleic acid), nature of the surfactant molecules (saturated vs unsaturated), the solvent used (toluene vs kerosene), the interaction between the surfactant and the solvent, the difference in the dispersibility of the coated nanoparticles, difference in the amount of primary/secondary

surfactant layers and compatibility of the solvent with the primary/secondary surfactant on the surface of the nanoparticles, etc.

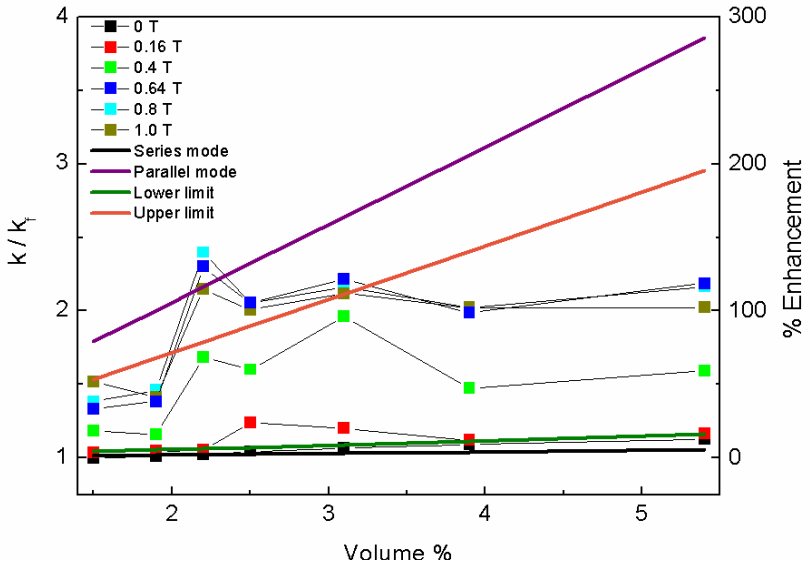

Figure 3.17. Comparison of the experimental thermal conductivity of the fluid of MDE in different applied magnetic fields for different volume concentrations (squares) with the calculated values based on series and parallel modes as well as the Hashin-Shtrikman upper and lower limits (solid lines)

Series and parallel modes of thermal conductivity are the simplest mean field models for the thermal conductivity of nanofluids (equations 1.2 and 1.3 in chapter 1).[52-53] The series mode corresponds to well-dispersed particles and the parallel mode corresponds to the geometric configuration that allows maximum heat transfer. Neither the series mode nor the parallel mode is strictly applicable for the thermal conductivity of the nanofluids. Hashin and Shtrikman (HS) derived the set of limits (upper and lower) based on the volume fraction (φ) of the nanoparticles in the fluid (see equation 1.4 in chapter 1).[54] In the lower HS limit, nanoparticles are assumed to be well-dispersed and the effective conductivity is biased towards the conduction path along the surrounding fluid. In upper HS limit, the effective conductivity is biased towards the conduction path along the dispersed particles.

Figure 3.17 shows a comparison of the experimental results (filled squares) at different magnetic fields for different volume concentrations with the values calculated based on the models of series, parallel, upper HS and lower HS bounds (solid lines). In the absence of a magnetic field, nanoparticles are well dispersed and the experimental thermal

conductivity values almost follow the series mode of thermal conductivity. Also, in the absence of magnetic field, the experimental thermal conductivity variation is observed with in the lower HS limit. However, the experimental data in the presence of a magnetic field show variation within the parallel mode of conduction (Figure 3.17). In the presence of a magnetic field, most of the experimental data points fall within the values calculated based on the upper and lower HS limits. Similar results have been reported by Shima *et al*[55] for oleic acid coated magnetite nanoparticles (9.5 nm) dispersed in kerosene at different volume percentages under different applied magnetic fields. From the experimental results, the authors observed that variation of the thermal conductivity is within the Maxwell's lower limit and follows the series mode of conduction. In the presence of a magnetic field the experimental results varied within the parallel mode.

3.4.4. Viscosity

Information for the formation of clusters by increasing the concentration of the nanoparticles in the fluid is obtained from viscosity measurements. Figure 3.18 shows variation of the relative viscosity with volume% of the particles in the fluid. In the case of small magnetic nanoparticles, the magnetic moments of the nanoparticles are randomly flipped by thermal energy and the van der Waals interaction contributes more to the cluster/aggregation formation.[56, 57] The observed large increase in the viscosity with increase in the volume% of the fatty acid coated fluids could be due to the formation of clusters/aggregates in the fluids.

The temperature dependant magnetic measurements of the decanoic acid coated fluid sample showed non-interacting nature of the particles. The van der Waals interaction between the nanoparticles or between the surfactants could form clusters in the fluid at higher concentrations. The decanoic acid coated fluid shows very large enhancement in the viscosity (Figure 3.18(a)) than that for the stearic acid coated fluid (Figure 3.18(b)). The short chain decanoic acid (10-carbon) is less efficient to stabilize the nanoparticle clusters in the nanofluid at higher concentrations. The formation of less stable clusters/aggregates in the decanoic acid coated fluid leads to increase in the viscosity of the nanofluid.

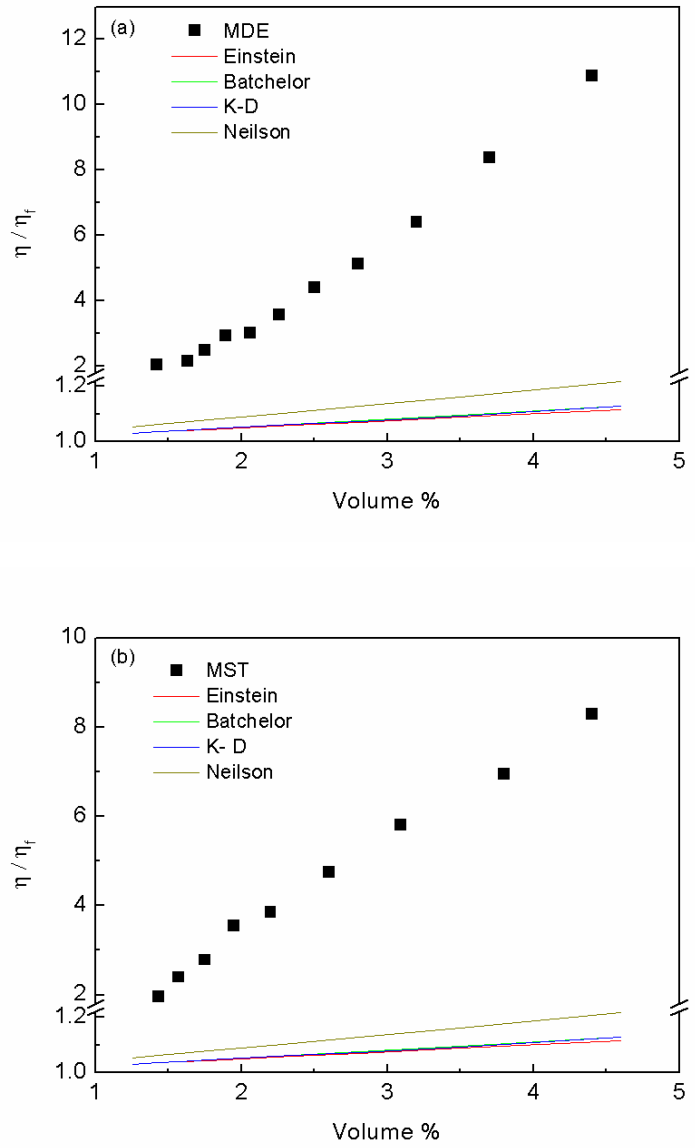

Figure 3.18. Variation of the relative viscosity (η/η_f) with the volume% for (a) decanoic acid and (b) stearic acid coated fluid samples

Thermal conductivity measurements indicated that clusters are formed in the stearic acid coated fluid at a lower concentration (1.0 volume%) than the decanoic acid coated fluid (1.7 volume%). The long hydrophobic chain (18-carbon) in stearic acid stabilizes larger clusters in the fluid even at higher concentrations. The relatively lower viscosity is particularly due to well suspended or stabilized clusters in the nanofluid of the stearic acid coated fluid (Figure 3.18b). The difference in the viscosity of the two nanofluids could also be due to the compatibility of the surfactant with the solvent molecules (toluene).

The enhancement in the viscosity with volume% of the particles is compared with that calculated using different theoretical models (solid lines in the Figure 3.18), as discussed in chapter 1, using equations in Table 1.6. In the Einstein model, the variation of viscosity with volume% of the particles is given by,[58] $\eta/\eta_f = 1 + 2.5\phi$, where, η, η_f and ϕ are viscosity of the nanofluid, viscosity of the base fluid and the volume fraction of the nanoparticles in the fluid, respectively. The Batchelor model[59] considers Brownian motion and hydrodynamic interactions between the particles, $\eta/\eta_f = 1 + 2.5\phi + 6.5\phi^2$. The above models are applicable only for lower concentrations (<0.01volume fraction). Since the concentration used in the present work is much larger (volume fraction up to 0.046), the results are compared with the power law based models. The relative viscosity for the simple hard sphere systems is given by the K-D model,[60] $\eta/\eta_f = (1 - \phi/\phi_m)^{-[\eta o]\phi_m}$, where, η_o is the intrinsic viscosity of hard spheres (η_0=*2.5*) and ϕ_m is the packing fraction of particles (ϕ_m=*0.64* for monodispersed particles). Neilson[61] equation for relative viscosity is given by $\eta/\eta_f = (1 + 1.5\phi)e^{\phi/(1-\phi_m)}$. The calculated relative viscosity (η/η_f) using the above theoretical models show much lower enhancement in the viscosity than the experimentally observed values. The experimental values are much larger than the viscosity calculated from the theoretical models, because, most of the theoretical models consider only the viscosity of the base fluid (η_f) and the volume% (φ) of the nanoparticles. The larger values of the viscosity of the nanofluids could be due to the contribution from various factors, in addition to the volume% effect. These contributions come from the particle size, size distribution, amount of the surfactant on the surface of the nanoparticles, primary and secondary surfactant layers and the interaction between the surfactant and the solvent, thickness of the surfactant layer, hydrodynamic diameter (which is different for different fatty acid coated nanoparticles), formation of cluster/aggregation due to the van der Waals interaction between the particles and between the surfactant molecules**,** magnetic dipole-dipole interaction between the nanoparticles, interdigitation of the surfactant molecules at higher concentrations, compatibility of the solvent molecules with the surfactant on the nanoparticle surfaces, and dispersibility of the nanoparticles in the base fluid. More studies are required to understand the role of each factor towards the enhancement in the viscosity of the fluids, by keeping all factors constant except one at a time, which is beyond the scope of the present work.

3.5. Conclusions

Magnetite nanoparticles coated with 10-carbon short chain (decanoic acid) and 18-carbon long chain (stearic acid) fatty acids are synthesized and characterized using various techniques. Thermogravimetric analysis showed the presence of two groups of surfactants on the nanoparticle surfaces, chemically bound primary layer and physically adsorbed secondary surfactant layer on the nanoparticle surfaces. IR spectra of the coated powder samples also showed the presence of small amount of secondary layer apart from the primary layer attached to the nanoparticle surfaces through chelating bi-dentate co-ordination. Magnetic measurements showed the formation of superparamagnetic nanoparticles. The zero field cooled (ZFC) and field cooled (FC) magnetization curves indicated non-interacting nature of the particles in the case of the decanoic acid coated sample and formation of clusters in the stearic acid coated sample.

Thermal conductivity measurements of the nanofluids obtained by the fatty acid coated nanoparticles dispersed in toluene showed a critical concentration below which there is no change in the thermal conductivity from that of the base fluid. The critical concentration is obtained as 1.7 volume% and 1.0 volume%, for the fluids of decanoic acid coated and stearic acid coated nanoparticles, respectively. The lower critical concentration for the stearic acid coated fluid could be due to the formation of loose clusters at lower concentrations. The superparamagnetic nanoparticles formed clusters in the fluid through van der Waals interaction between the nanoparticles and between the surfactants attached on the neighboring nanoparticles leading to enhancement in the thermal conductivity beyond the critical concentration. Large enhancement in the thermal conductivity is obtained in a magnetic field for both fluids. The relatively larger enhancement in the thermal conductivity for the decanoic acid coated fluid than for the stearic acid coated fluid at higher magnetic fields could be due to easy response of the short chain decanoic acid coated nanoparticles to the applied magnetic field. The thickness of the surfactant molecules and the nature of the attachment of the surfactant molecules to the nanoparticle surfaces could be the reason for the different response with the magnetic field which in turn leads to difference in the enhancement in the thermal conductivity in a magnetic fluid.

References

1. Saterlie, M. S.; Sahin, H.; Kavlicoglu, B.; Liu, Y. M.; Graeve, O. A. *Chem. Mater.* **2012**, *24*, 3299-3306.
2. Murshed, S. M. S.; de Castro, C. A. N.; Lourenço, M. J. V. *J. Nanofluids* **2012**, *1*, 175-179.
3. Sun, S.; Zeng, H. *J. Am. Chem. Soc.* **2002**, *124*, 8204-8205.
4. Park, J.; An, K.; Hwang, Y.; Park, J. G.; Noh, H. J.; Kim, J. Y.; Park, J. H.; Hwang, N. M.; Hyeon, T. *Nat. Mater.* **2004**, *3*, 891-895.
5. Tombácz, E.; Bica, D.; Hajdú, A.; Illés, E.; Majzik, A.; Vékás, L. *J. Phys.: Condens. Matter* **2008**, *20*, 204103.
6. Shen, L. F.; Laibinis, P. E.; Hatton, T. A. *Langmuir* **1999**, *15*, 447-453.
7. Shen, L. F.; Laibinis, P. E.; Hatton, T. A. *J. Magn. Magn. Mater.* **1999**, *194*, 37-44.
8. Guardia, P.; Batlle-Brugal, B.; Roca, A. G.; Iglesias, O.; Morales, M. P.; Serna, C. J.; Labarta, A.; Batlle, X. *J. Magn. Magn. Mater.* **2007**, *316*, E756-E759.
9. Filippousi, M.; Angelakeris, M.; Katsikini, M.; Paloura, E.; Efthimiopoulos, I.; Wang, Y. J.; Zambouis, D.; Van Tendeloo, G. *J. Phys. Chem. C* **2014**, *118*, 16209-16217.
10. Felicia, L. J.; Johnson, J. C.; Philip, J. *J. Nanofluids* **2014**, *3*, 328-335.
11. Yuan, Y.; Rende, D.; Altan, C. L.; Bucak, S.; Ozisik, R.; Borca-Tasciuc, D. A. *Langmuir* **2012**, *28*, 13051-13059.
12. Younes, H.; Christensen, G.; Luan, X. N.; Hong, H. P.; Smith, P. *J. Appl. Phys.* **2012**, *111*, 64308.
13. Vékás, L.; Bica, D.; Marinica, O. *Rom. Rep. Phys.* **2006**, *58*, 257-267.
14. Fu, L.; Dravid, V. P.; Johnson, D. L. *Appl. Surf. Sci.* **2001**, *181*, 173-178.
15. Barbeta, V. B.; Jardim, R. F.; Kiyohara, P. K.; Effenberger, F. B.; Rossi, L. M. *J. Appl. Phys.* **2010**, *107*,1-8.
16. Regmi, R.; Black, C.; Sudakar, C.; Keyes, P. H.; Naik, R.; Lawes, G.; Vaishnava, P.; Rablau, C.; Kahn, D.; Lavoie, M.; Garg, V. K.; Oliveira, A. C. *J. Appl. Phys.* **2009**, *106*, 113902.
17. Vekas, L.; Bica, D.; Gheorghe, D.; Potencz, I.; Rasa, M. *J. Magn. Magn. Mater.* **1999**, *201*, 159-162.
18. Avdeev, M. V.; Bica, D.; Vekas, L.; Aksenov, V. L.; Feoktystov, A. V.; Marinica, O.; Rosta, L.; Garamus, V. M.; Willumeit, R. *J. Colloid Interface Sci.* **2009**, *334*, 37-41.

19. Avdeev, M. V.; Bica, D.; Vekas, L.; Marinica, O.; Balasoiu, M.; Aksenov, V. L.; Rosta, L.; Garamus, V. M.; Schreyer, A. *J. Magn. Magn. Mater.* **2007**, *311*, 6-9.
20. Patel, H. E.; Das, S. K.; Sundararajan, T.; Sreekumaran Nair, A.; George, B.; Pradeep, T. *Appl. Phys. Lett.* **2003**, *83*, 2931-2933.
21. Lide, D. R. *CRC Handbook of Chemistry and Physics*; CRC press, **2004**.
22. Cermak, S. C.; Kenar, J. A.; Evangelista, R. L. *Distillation of Natural Fatty Acids and Their Chemical Derivatives*; INTECH Open Access Publisher, **2012**.
23. Anneken, D. J.; Both, S.; Christoph, R.; Fieg, G.; Steinberner, U.; Westfechtel, A. Fatty Acids. In *Ullmann's Encyclopedia of Industrial Chemistry*, Wiley-VCH Verlag GmbH & Co. KGaA: **2000**.
24. Abhat, A. *Solar Energy* **1983**, *30*, 313-332.
25. Kuwahara, Y.; Zhang, G.; Wu, J.; Akai-Kasaya, M.; Saito, A.; Aono, M. *molecules* **2002**, *2*, 4.
26. Somiya, S. *Handbook of Advanced Ceramics: Materials, Applications, Processing, and Properties*; Academic Press, **2013**.
27. Muramatsu, A.; Miyashita, T., *Nano-Hybridization of Organic-Inorganic Materials*; Springer, **2009**.
28. Lane, C. A.; Burton, D. E.; Crabb, C. C. *J. Chem. Educ.* **1984**, *61*, 815.
29. Zhao, S. Y.; Lee, D. K.; Kim, C. W.; Cha, R. G.; Kim, Y. H.; Kang, Y. S. *Bull. Korean Chem. Soc.* **2006**, *27*, 237-242.
30. Waldron, R. D. *Phys. Rev.* **1955**, *99*, 1727-1735.
31. Bronstein, L. M.; Huang, X. L.; Retrum, J.; Schmucker, A.; Pink, M.; Stein, B. D.; Dragnea, B. *Chem. Mater.* **2007**, *19*, 3624-3632.
32. Ding, X.; Bao, L.; Jiang, J.; Gu, H. *RSC adv.* **2014**, *4*, 9314-9320.
33. Yang, K.; Peng, H.; Wen, Y.; Li, N. *Appl. Surf. Sci.* **2010**, *256*, 3093-3097.
34. Bean, C.; Livingston, J. *J. Appl. Phys.* **1959**, *30*, S120-S129.
35. Cao, S.-W.; Zhu, Y.-J.; Chang, J. *New J. Chem.* **2008**, *32*, 1526-1530.
36. Lu, A. H.; Salabas, E. e. L.; Schüth, F. *Angew. Chem. Int. Ed.* **2007**, *46*, 1222-1244.
37. Liu, C.; Zhang, Z. J. *Chem. Mater.* **2001**, *13*, 2092-2096.
38. Sreeja, V.; Joy, P. *Int. J. Nanotechnol.* **2011**, *8*, 907-915.
39. Chesnel, K.; Trevino, M.; Cai, Y.; Hancock, J. M.; Smith, S. J.; Harrison, R. G. *J Phys. Conf. Ser.* **2014**, 521, 12004.
40. Zheng, R. K.; Gu, H. W.; Zhang, B.; Liu, H.; Zhang, X. X.; Ringer, S. P. *J. Magn. Magn. Mater.* **2009**, *321*, L21-L27.

41. Vargas, J.; Nunes, W.; Socolovsky, L.; Knobel, M.; Zanchet, D. *Phys. Rev. B.* **2005**, *72*, 184428.
42. Rosa, F.; Corvis, Y.; Lai-Kuen, R.; Charrueau, C.; Espeau, P. *J. Therm. Anal. Calorim.* **2015**, *120*, 783-787.
43. Philip, J.; Shima, P. D.; Raj, B. *Appl. Phys. Lett.* **2007**, *91*, 203108.
44. Maxwell, J. C. A Treatise on Electricity and Magnetism. *Clarendon press* **1881**, *1*.
45. Prasher, R.; Bhattacharya, P.; Phelan, P. E. *Phys. Rev. Lett*. **2005**, *94*, 025901.
46. Lenin, R.; Joy, P. A. *J. Nanofluids* **2015**, *4*, 310-317.
47. Wilson, O. M.; Hu, X. Y.; Cahill, D. G.; Braun, P. V. *Phys. Rev. B.* **2002**, *66*, 224301.
48. Prasher, R.; Bhattacharya, P.; Phelan, P. E. *J. Heat Transfer* **2006**, *128*, 588-595.
49. Philip, J.; Shima, P. D.; Raj, B. *Nanotechnology* **2008**, *19*, 305706.
50. Mendelev, V. S.; Ivanov, A. O. *Phys. Rev. E* **2004**, *70*, 051502.
51. Shima, P. D.; Philip, J.; Raj, B. *Appl. Phys. Lett.* **2009**, *94*, 223101.
52. Eapen, J.; Li, J.; Yip, S. *Phys. Rev. E* **2007**, *76*, 062501.
53. Eapen, J.; Williams, W. C.; Buongiorno, J.; Hu, L. W.; Yip, S.; Rusconi, R.; Piazza, R. *Phys. Rev. Lett.* **2007**, *99*, 095901.
54. Hashin, Z.; Shtrikman, S. *J. Appl. Phys.* **1962**, *33*, 3125.
55. Shima, P. D.; Philip, J. *J. Phys. Chem. C* **2011**, *115*, 20097-20104.
56. Jiang, W.; Wang, L. Q. *J. Appl. Phys.* **2010**, *108*, 114311.
57. Lalatonne, Y.; Richardi, J.; Pileni, M. P. *Nat. Mater.* **2004**, *3*, 121-125.
58. Einstein, A. *Ann. Phys.* **1906**, 19, 289-306.
59. Batchelor, G. *J. Fluid Mech.* **1977**, *83*, 97-117.
60. Krieger, I. M.; Dougherty, T. J. *Trans. Soc. Rheol.* **1959**, *3*, 137-152.
61. Nielsen, L. E. *J. Appl. Phys.* **1970**, *41*, 4626-4627.

Chapter 4

Effect of particle size distribution on the thermal conductivity of capric acid coated magnetite nanofluids

Abstract

Capric acid (Decanoic acid) coated magnetite nanoparticles of comparable average size (5–7 nm) but with different particle size distributions are synthesized by varying the rate of addition of ammonium hydroxide in the coprecipitation method. The particle size distribution is obtained from TEM measurements which showed that faster rate of base addition gives narrow size distribution and very slow rate of addition gives particles with wider distribution. Magnetic measurements confirmed the different particle size distributions in the studied samples. Thermal conductivity measurements have been carried out on the magnetic nanofluids prepared by dispersing the nanoparticles in toluene as the base fluid. Enhancement in the thermal conductivity is found to be correlated with the average size and distribution of the nanoparticles, where the thermal conductivity is found to be relatively lower for the fluids with wider particle size distribution.

4.1. Introduction

The observation of anomalous enhancement in the thermal conductivity of nanofluids, even at low volume fractions, has attracted the attention of the scientific community world-wide.[1] Many experimental results showed enhancement in the thermal conductivity of a nanofluid beyond the Maxwell's predictions of stationary solid suspension.[2,3] However, there are also reports on the thermal conductivity of nanofluids showing enhancement within the predictions of Maxwell's effective medium theory.[4,5] The deviation of the experimental results from the classical predictions of solid suspension shows that there are various factors which contribute to the enhancement of the thermal conductivity of nanofluids, such as particle size, size distribution, particle morphology, surfactants,[6-9] etc. Various mechanisms have also been proposed for the anomalous enhancement in the thermal conductivity of nanofluids based on the nanoscale effects such as Brownian motion, interfacial thermal layer, and aggregation/clustering.[10-15] Numerous theoretical work have been carried out based on the effective medium approximation for thermal conductivity of solid suspensions by including the different factors.[16-21] However, the exact cause of the anomalous enhancement in the thermal conductivity still remains unclear.

Out of the various factors, the size of the nanoparticles is one of the most important factors on the enhancement in the thermal conductivity, due to the large surface area of the particles. Nanoparticles of large surface area allow more heat to transfer because the thermal interaction mainly takes place on the surface of the nanoparticles. More number of such interactions on the surface of the nanoparticles is important for microconvection of nanoparticles with solvent molecules due to Brownian motion.[22] The theoretical models for the size dependant thermal conductivity, however, consider that the nanoparticles in a nanofluid are monodisperse. Similarly, many experimental studies on thermal conductivity of nanofluids consider the average size of the nanoparticles for size dependant thermal conductivity.[23] Average diameter of the nanoparticles is an inconsistent parameter for prediction of thermal conductivity of composite materials.[24] In real case, most of the synthesis methods produce nanoparticles with varying size distribution. Dan *et al*[25] made theoretical studies on the effect of polydispersity on the thermal conductivity of thermal interface materials (TIM). From the simulated results, based on the finite element method, it is found that the optimum value of polydispersity shows larger enhancement in the thermal conductivity. Xu *et al*[26] proposed a theoretical model for heat conduction based on fractal

distribution of nanoparticles in nanofluids, considering the heat convection between the fluid and particles due to Brownian motion. In the model, a large enhancement of the thermal conductivity of nanofluids is observed for particles of size smaller than 15 nm. The authors claimed that the large enhancement in the thermal conductivity for smaller particles is due to the contribution from convection to the conductivity of nanofluids. The thermal conductivity model based on the particle size distribution has predicted that nanofluids with large volume fraction of clusters show larger enhancement in the thermal conductivity.[27] This model is found to match well with the experimental results of stable oleic acid coated magnetite fluids.[28] The observed different trends in the theoretical models based on the particle size distribution analysis and the lack of experimental results on thermal conductivity make researchers more to focus on the effect of particle size distribution.

In the present work, we have studied the effect of particle size distribution on the thermal conductivity of nanofluids using capric acid (decanoic acid) coated magnetite (Fe_3O_4) nanoparticles of average size 5–7 nm. Decanoic acid coated magnetite nanoparticles of comparable average size but with different size distributions are synthesized by varying the base addition rate in the coprecipitation method. Magnetite nanofluids with different particle size distributions are prepared by dispersing the decanoic acid coated magnetite nanoparticles in toluene at 2.2 volume%. Thermal conductivity measurements have been carried out and the results are compared with different theoretical models.

4.2. Synthesis

Materials used in the present study and their purities are same as that mentioned in the chapter 2 (section 2.2.1). Decanoic coated magnetite nanoparticles were synthesized by the co-precipitation method. The detailed synthesis procedure and washing of as-synthesized nanoparticles using the solvent mixture are discussed in chapter 2 (section 2.2.2). The name decanoic acid is used throughout the chapter instead of the less common name capric acid.

Decanoic acid coated magnetite nanoparticles of different size distribution were synthesized by varying the base (NH_4OH) addition rate to the precursor and surfactant mixture. Five different samples MD1, MD2, MD3, MD4 and MD5 were prepared by using the base addition rate as 10 ml/s, 4 ml/s, 1 ml/s, 0.2 ml/s and 0.1 ml/s, respectively (Table 4.1). Similar procedure is reported for the synthesis of magnetite nanoparticles of different sizes.[29] The temperature, stirring speed, concentration of iron chlorides and the amount of

surfactant were maintained constant for all the syntheses. Magnetite nanofluids of the different samples were prepared by dispersing the dried nanoparticles in toluene at 2.2 volume% and these fluids were used for the thermal conductivity and viscosity studies.

Table 4.1. Sample codes, crystallite size from XRD and particle sizes

S. No	Sample code	Rate of base addition (ml/s)	Particle size from TEM (±0.5 nm)	Size distribution from TEM histogram, FWHM (nm)
1	MD1	10	4.5	1.4
2	MD2	4	5.0	1.5
3	MD3	1	6.3	1.9
4	MD4	0.2	5.5	3.9
5	MD5	0.1	6.0	5.1

4.3. Characterization of surfactant coated magnetite nanoparticles

4.3.1. Powder X-ray diffraction

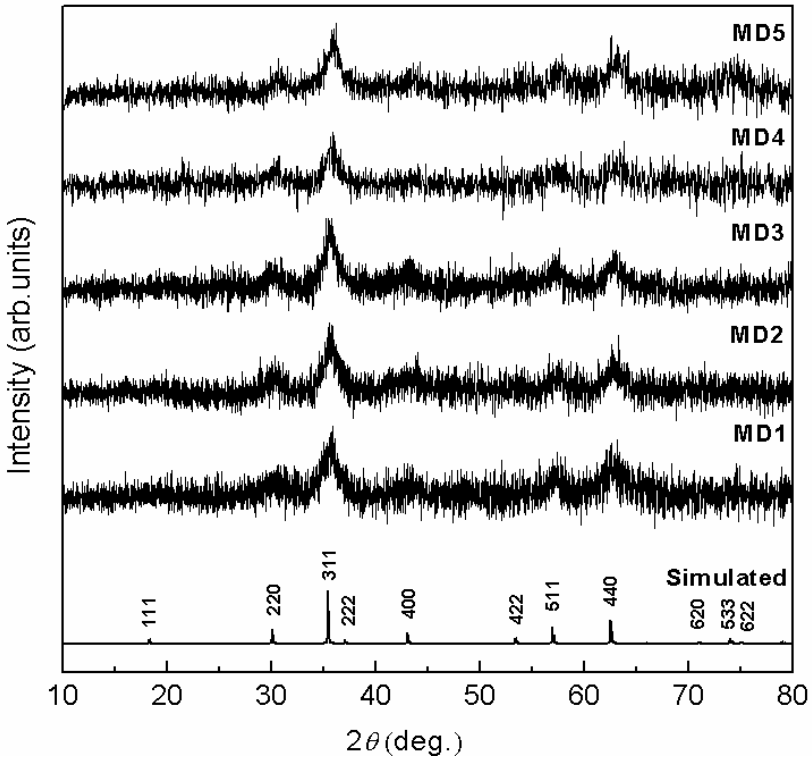

Figure 4.1. Powder XRD patterns of different decanoic acid coated samples compared with the simulated pattern of Fe_3O_4

All the dried powder samples were initially characterized using powder XRD studies to verify formation of the magnetite nanoparticles. Powder XRD patterns of MD1 to MD5 are shown in Figure 4.1 and compared with the simulated pattern of Fe_3O_4. No additional peaks are observed in the experimental patterns other than that of Fe_3O_4, indicating single phase nature of the samples. Very broad peaks in the experimental XRD patterns indicate formation of nanoparticles. The cubic lattice parameter is calculated by least-squares refinement of the XRD patterns using the PCW software and the lattice parameter is obtained as 8.39 Å, which is comparable to that reported in the literature for magnetite (8.40 Å, JCPDS 19-0629). Average crystallite sizes of the as-synthesized samples are calculated from the width of the most intense (311) peak, using the Scherrer equation (equation 2.2, chapter 2). The average crystallite size is calculated as 4±1 nm for all the five samples.

4.3.2. Thermogravimetric analysis

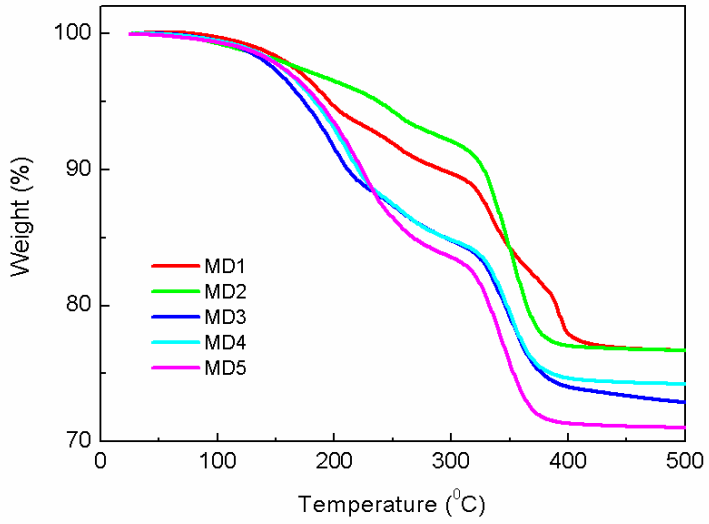

Figure 4.2. Thermogravimetric analysis curves of the different decanoic acid coated samples.

Thermogravimetric analysis curves of the synthesized samples, recorded from room temperature to 500 °C, are shown in Figure 4.2. The TGA curves show two-step weight loss, one in the temperature range 100–300 °C and another weight loss above 300 °C. The first weight loss above 100 °C could be due to the evaporation of free solvent and/or due to the

desorption and decomposition of weakly attached (secondary) surfactants to the surface of the nanoparticles through weak van der Waals forces. The second weight loss at a higher temperature corresponds to the decomposition of the surfactant molecules strongly bound to the surface of the nanoparticles, through chemical bond between the surfactants and the iron atoms on the nanoparticle surfaces. Thus, thermogravimetric analysis clearly shows the presence of two groups of surfactants attached to surface of the nanoparticles in addition to the solvent molecules trapped on the surface.[30] The amount of the total, primary and secondary surfactants are shown in Table 4.2. Although the same synthesis and washing procedures are followed for all the five studied samples, the different amounts of the surfactant on the surface of the nanoparticles could be possibly due to the time delay during the addition of the base in the coprecipitation process and/or the time difference in the washing process and/or the different size and distribution of the particles in the samples.

Table 4.2: Amounts of total, primary and secondary surfactants on the decanoic and coated magnetite nanoparticles

Sample name	Total surfactant (±1%)	Primary surfactant (±1%)	Secondary surfactant (±1%)
MD1	23	12	11
MD2	23	14	9
MD3	26	10	16
MD4	27	11	16
MD5	29	12	17

4.3.3. Transmission electron microscopy

Figure 4.3 shows the TEM images and the corresponding particle size distribution histograms of the different samples. From the histograms, the average particle sizes for the samples MD1, MD2, MD3, MD4 and MD5 are obtained as 4.5 nm, 5.0 nm, 6.3 nm, 5.5 nm, and 6.0 nm, respectively. Average particle sizes obtained from the TEM images show slight increase

with decreasing the rate of base addition. The FWHM of the Gaussian fitted histograms for the samples MD1, MD2, MD3, MD4 and MD5 are obtained as 1.4, 1.5, 1.9, 3.9 and 5.1 nm**,** respectively. Although there is only a very small variation in the average particle size with the base addition rate, there is an appreciable difference in the size distribution in the case of MD4 and MD5. The very slow rate of addition of base increases the pH of the reaction medium slowly and forms particles with widely differing sizes rather than the case of fast addition of base which increases the pH immediately and therefore a narrow size distribution. This shows that the base addition rate mainly affects the size distribution.

Different samples of the decanoic acid coated magnetite nanoparticles are prepared by changing the rate of base addition. In the case of fast addition, higher concentration of the growth species can be generated in the reaction medium to attain supersaturation. The nucleation occurs in a very short time period with the possibility of formation of small particles in large numbers. Due to the fast addition of the base, the pH of the reaction medium increases immediately to 11 and faster the formation of magnetite nanoparticles. At higher pH (=11), there is a possibility for the formation of large amount of ammonium decanoate (NH_4^+ $^-OOC(-CH_2-)_8CH_3$) in the reaction medium at 50 °C.[31] The decanoate ion replaces the surface OH^- ions and forms decanoic acid coated magnetite nanoparticles immediately after the nucleation. The attachment of the decanoic acid molecule to the surface iron atoms makes the sites unavailable for the further growth of the nanoparticles. The short-time nucleation and the subsequent surface coating could result in the formation of small particles with narrow size distribution. Slower addition of the base to the iron precursor solution leads to slow increase of the pH and forms the highly crystalline iron oxyhydroxide (akaganeite) by hydrolysis of iron (III) chloride with high crystallinity.[32] At higher pH, these grown oxyhydroxides becomes spinel structure by the absorption of Fe (II) ions in the solution. Thus, the slow base addition rate leads to the formation of larger particles along with the possibility of formation of smaller particles at higher pH resulting in a broad distribution of the particles.

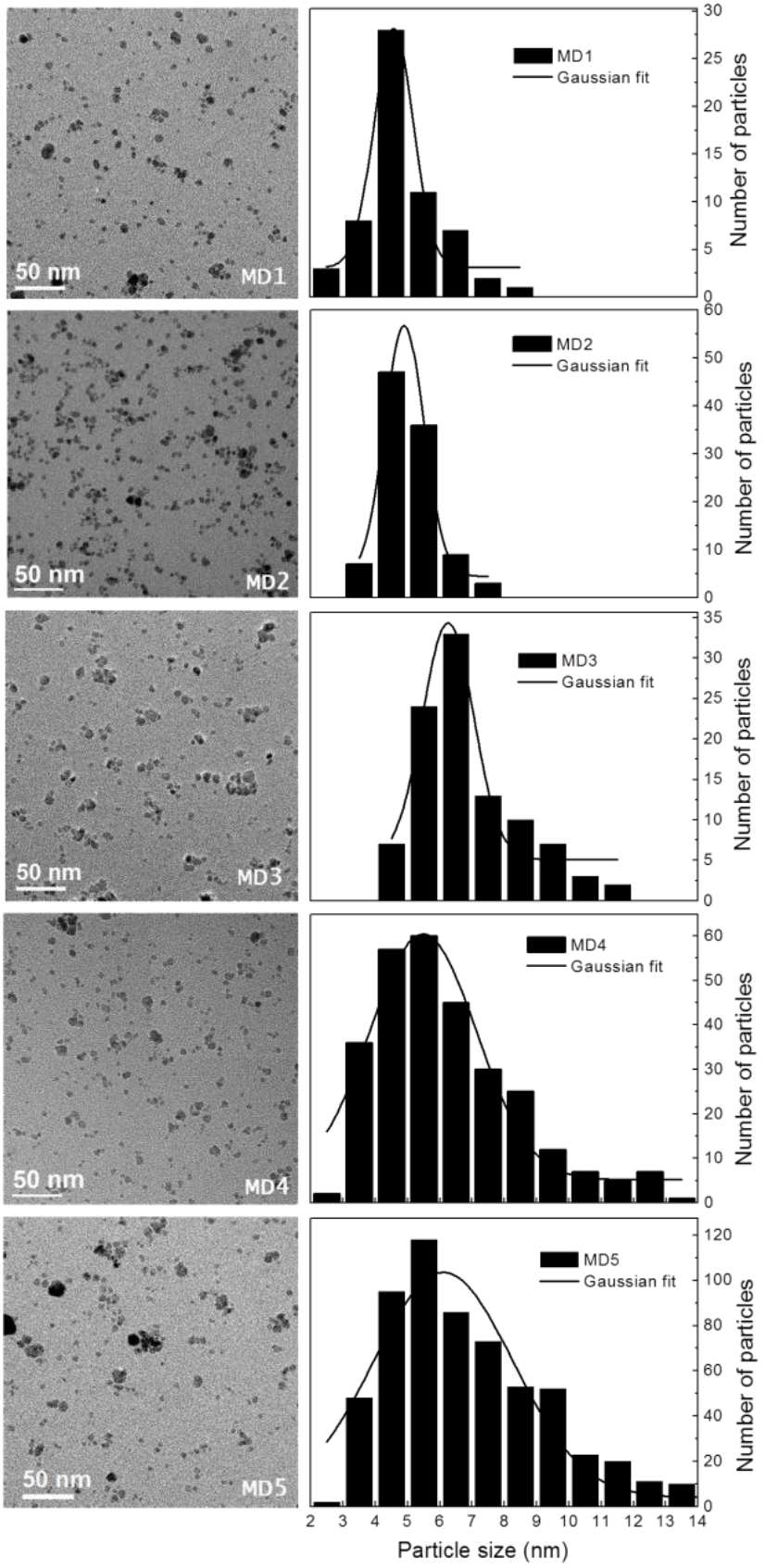

Figure 4.3. TEM images (left) and the corresponding particle size distribution histograms (right).

4.3.4. Infrared spectroscopy

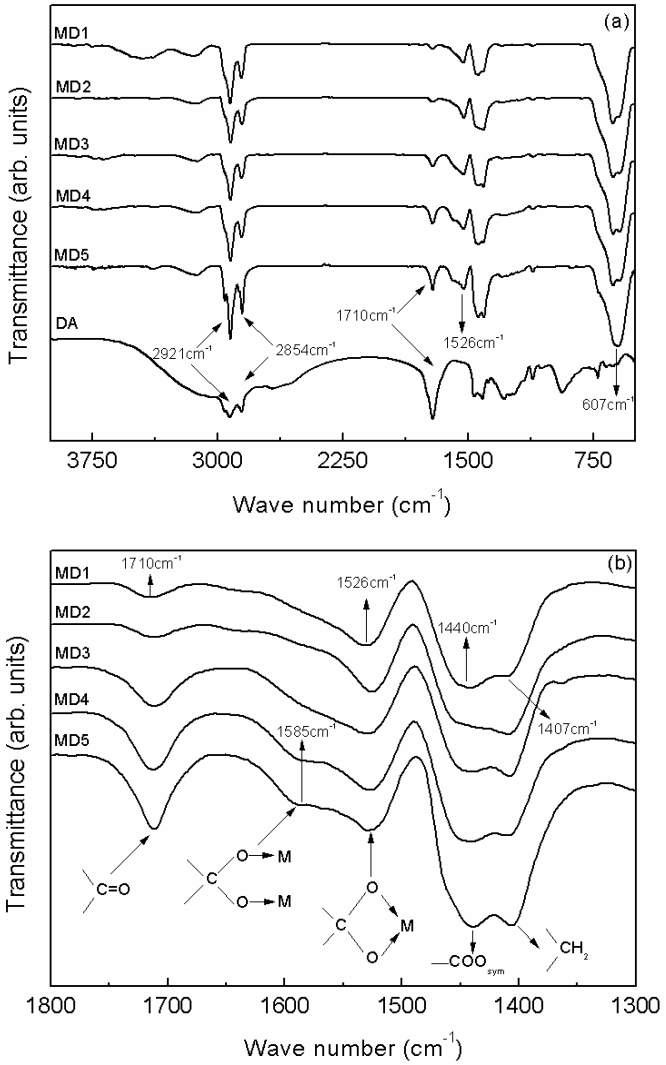

Figure 4.4. (a) Infrared spectra of neat decanoic acid (DA) and decanoic acid coated magnetite nanoparticles (MD) and (b) zoomed curves showing the bands in the C=O vibrational region.

The effectiveness of the surface functionalization of the decanoic acid coated magnetite nanoparticle samples is studied by infrared spectroscopy, by comparing with the IR spectrum of neat decanoic acid (Figure 4.4(a)). In the IR spectrum of decanoic acid (DA), a strong C=O stretching band is observed at 1710 cm^{-1}. The intensity of this C=O band is reduced and a new band at 1526 cm^{-1} is observed in the spectra of the decanoic acid coated magnetite (MD) nanoparticles. The weak band at 1710 cm^{-1} in the coated nanoparticles is likely to be

due to the secondary surfactant molecules present on the surface of the nanoparticles. Thermogravimetric analysis showed increasing amount the secondary surfactant in samples MD1 to MD5 (Table 4.2). IR studies also shows that the intensity of the band due to C=O stretching decreases with decreasing amount of the secondary surfactant, as shown in Figure 4.4(b). The band at 1526 cm^{-1} is due to asymmetric stretching of the carboxylate ($-COO^-$) group.[33] The decanoic acid coated samples show additional bands at 1440 cm^{-1} and 1407 cm^{-1} corresponding to the symmetric stretching of carboxylate group and deformation of the $-CH_2$ respectively. As discussed in section 3.3.4, the difference between the values of these two carboxylic group (symmetry and asymmetry) stretching frequencies ($\Delta\nu$) is 86 cm^{-1}, indicating that the carboxylic acid is attached to the surface of the nanoparticles through the two oxygen atoms by chelating bidentate coordination.[34] The bands at 2854 cm^{-1} and 2921 cm^{-1}, which are not affected after coating, correspond to the symmetric and asymmetric stretching of the $–CH_2$ groups in the coated as well as the free decanoic acid. The decanoic acid coated samples show additional strong bands at 607 cm^{-1} which correspond to the stretching vibration of the Fe-O bonds in Fe_3O_4.[35]

4.3.5. Magnetic measurements

Field dependant magnetization studies measured at room temperature (Figure 4.5), show formation of superparamagnetic nanoparticles with negligible remanence and coercivity. The magnetization measured at 3 T is relatively lower for MD1 (~60 emu/g) and the values for MD2, MD3, MD4 and MD5 are comparable at high fields (~67 emu/g). The distribution in the particle size, as evidenced from TEM studies, is also evident from the magnetization measurements. The magnetization is relatively larger for MD3 at low magnetic fields, compared to that of MD4 and MD5, indicating the presence of large number of relatively smaller particles in the latter two samples (Table 4.3). Even though the magnetization at 3 T is comparable for MD2, MD3, MD4 and MD5, samples MD4 and MD5 show higher magnetization than that for MD2, at low fields, due to the presence of more number of larger particles.

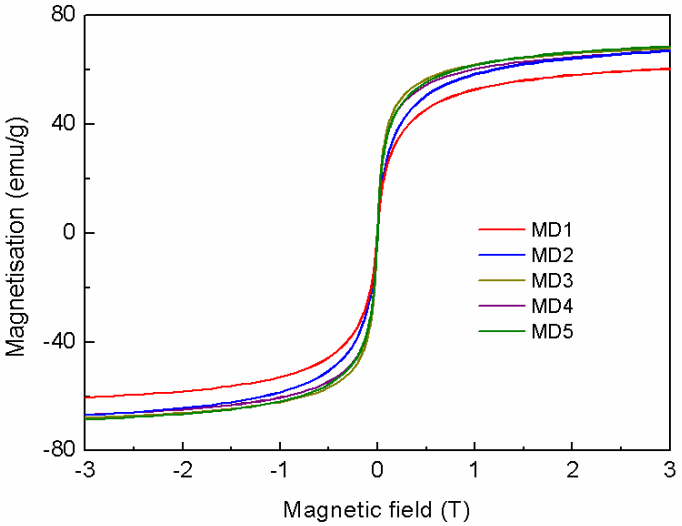

Figure 4.5. Magnetization curves of different decanoic acid coated samples measured at room temperature

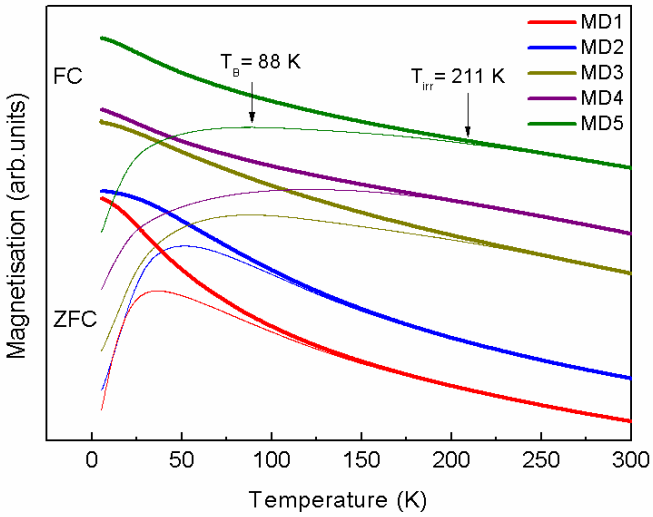

Figure 4.6. Zero field cooled (thin lines) and field cooled (thick lines) magnetization curves of the decanoic acid coated magnetite nanoparticles. The curves are shifted along the *y*-axis.

Temperature dependant magnetization measurements were carried out after cooling the samples to 5 K under zero field cooled (ZFC) and field cooled (FC) conditions, in a magnetic field of 5 mT. The ZFC curves of the decanoic acid coated magnetite nanoparticles show increase in the superparamagnetic blocking temperature, T_B (temperature at which a maximum is observed in the ZFC magnetization curve), with increasing average particle size

(Figure 4.6). The observed T_Bs for the samples MD1, MD2, MD3, MD4 and MD5 are 45 K, 50 K, 88 K, 123 K and 88 K, respectively. The increase in the T_B for larger particles is attributed to the increase in the anisotropy energy barrier which requires more thermal energy to overcome the anisotropy energy barrier (see section 1.7.1, Chapter 1).[36] Although the observed T_Bs for the samples MD3 and MD5 are identical, the sample MD5 showed wider particle size distribution with large number of small particles (Figure 4.3). Since the observed blocking temperature is the average of the blocking temperatures of particles of different sizes, the width of the ZFC magnetization curve is an indication for the particle size distribution. Wide particle size distribution gives rise to broader ZFC magnetization curve.[37,38] Considering this, it can be seen that the width of the magnetization curve increases from MD1 to MD5, indicating increasing particle size distribution. These observations agree very well with the particle size distribution obtained from the TEM analysis. The nature of FC curve is generally an indication for the interaction between the particles. For non-interacting particles, the FC magnetization increases continuously with decreasing temperature below the blocking temperature, whereas for interacting particles (due to clustering, aggregation and/or inefficient coating by the surfactant) FC magnetization remains a constant or decreases below T_B.[39-41] In the present case, FC magnetization of all five samples increase continuously below T_B indicating the non-interacting nature and suggesting effective capping of the particles by the surfactant. The individual particles are well separated due to the decanoic acid molecules attached to the surface of the magnetite nanoparticles which suppress the inter-particle interactions.

Table 4.3. Comparison of T_B and T_{irr} for the different samples

Sample name	Magnetization @ 3T (emu/g)	Bifurcation temperature T_{irr} (K)	Blocking temperature T_B (K)
MD1	60.4	117	45
MD2	66.9	105	50
MD3	67.8	215	88
MD4	66.7	175	123
MD5	68.5	211	88

The difference in the size distribution is further confirmed from the distribution of blocking temperature (T_B) calculated by differentiating the magnetic susceptibility from zero field cooled measurements with respect to temperature. The distribution of the blocking temperature is calculated using equation 2.4 (chpter 2). [42] Figure 4.7 shows that the blocking temperature (T_B) distribution of the decanoic acid coated samples increases from MD1 to MD5, with a much broader distribution in the case of MD4 and MD5. The particle size histograms (Figure 4.3) of MD4 and MD5 showed wider particle size distribution and this is also clearly evidenced from the T_B distribution curves (Figure 4.7) of these two samples. This clearly indicates the presence of smaller and larger particles in the samples MD4 and MD5 with wider particle size distribution.

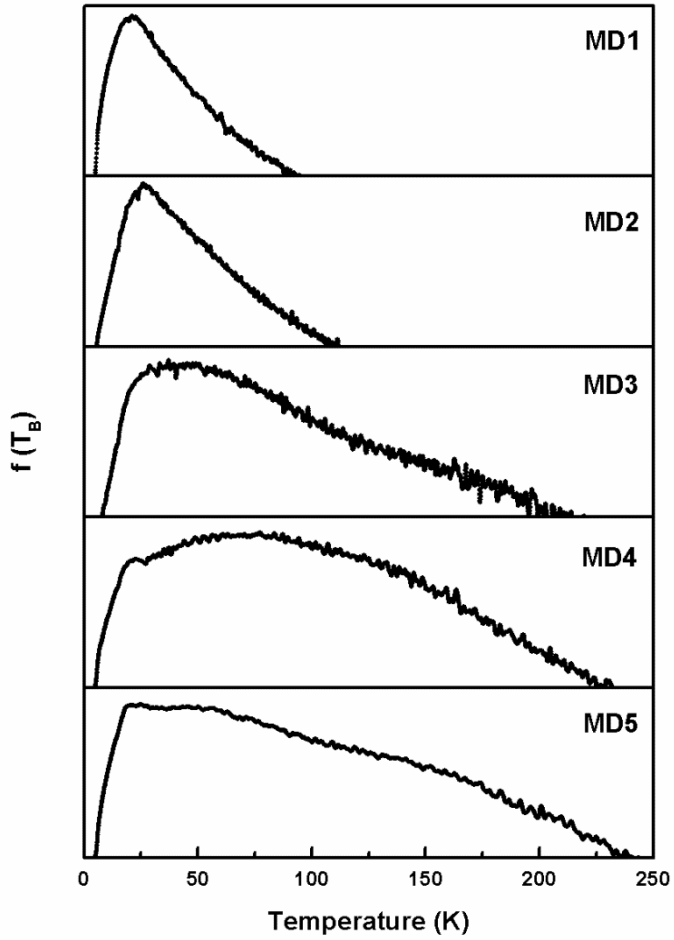

Figure 4.7. Distribution of the blocking temperatures of the different decanoic acid coated samples

4.4 Studies on nanofluids

4.4.1 Thermal conductivity

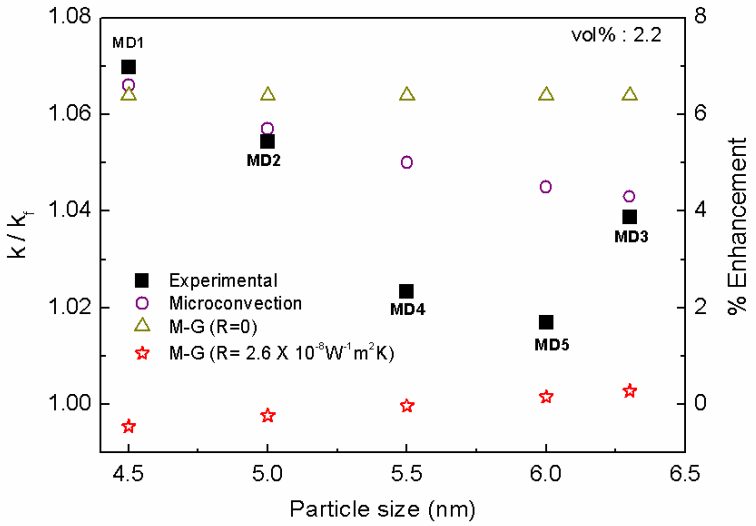

Figure 4.8. Experimental thermal conductivity (filled squares) of the nanofluids of different average particle sizes is compared with the theoretical models; the Maxwell-Garnett (M-G) model with the interfacial thermal resistance $R_b = 0$ (open triangles) and $R_b \neq 0$ (open stars) and the Brownian motion induced microconvection model (open circles).

The different coated magnetite nanoparticles are dispersed in toluene and thermal conductivity of the resulting nanofluids is measured to compare the effect of particle size distribution on thermal conductivity. Studies are made on fluids with 2.2 volume% of particles dispersed in toluene. Figure 4.8 shows the thermal conductivity ratio of the five fluids plotted against the average particle size obtained from the TEM images. All the decanoic acid coated magnetite nanofluids show enhancement in the thermal conductivity compared to that of the base fluid. The fluid samples MD1, MD2, MD3, MD4 and MD5 show enhancement in the thermal conductivity as 6.9%, 5.4%, 3.9%, 2.2% and 1.7%, respectively. The experimental results show that the thermal conductivity of the nanofluid decreases with increasing the average particle size. There are reports in the literature on the decreasing and increasing trends in the thermal conductivity of magnetite nanofluids with increasing particle size. Shima *et al*[43] reported an increase in the thermal conductivity of oleic acid coated magnetite nanofluids (particle size in the range 3–10 nm), whereas Wang *et al*[44] reported decrease in the thermal conductivity with increasing particle size in the range 16–44

nm. In the present case, there is only a minor variation of the average size of the particles (5–7 nm) compared to the previous reports.[43,44] Therefore, the present observed changes can be due to the difference in the size distributions of particles in the fluid which was not considered in the previous particle size dependant thermal conductivity studies.

In order to get information on the mechanism of thermal conductivity enhancement, the experimental results are compared with different theoretical models. The open triangles in Figure 4.8 correspond to the Maxwell-Garnett (M-G)[22] model of effective medium approximation for the thermal conductivity of dilute solid suspension based on Maxwell's idea of binary mixtures (equation 1.1, chapter 1). The effective thermal conductivity (k) based on Maxwell's equation accounts only the thermal conductivity of the nanoparticle (k_p) and the base fluid (k_f) along with the volume fraction (ϕ) of the dispersed particles. The model does not consider the particle size, size distribution, interfacial thermal resistance, and interparticle interactions between the nanoparticles. The calculated thermal conductivity enhancement based on the M-G model is 6.4% for the all the five samples. The present experimental results show value of thermal conductivity comparable to that predicted by the M-G model for MD1 and to some extent for MD2. Both MD1 and MD2 have relatively smaller particle size and narrow size distribution. The difference between the calculated value and the experimental result increases with increasing particle size distribution and the difference is larger than the error in the measured value of the thermal conductivity (within 1%). However, error in the measurement of the particle size and hence the measured size distribution may also be factors contributing to the difference between the calculated and measured values, apart from the fact that the values are shown against the average particle size. For the samples MD3, MD4 and MD5, with wide particle size distributions, the experimental values are much lower than the calculated value because the simple model of solid-liquid suspension ignores factors such as particle size and distribution.

The open star symbols in Figure 4.8 shows thermal conductivity enhancement by including interfacial thermal resistance factor in the Maxwell-Garnett equation (equation 1.11, chapter 1),[22] The thermal conductivity, by including the interfacial resistance effect, shows much less value compared to the experimental results (Figure 4.8). The experimental results are also compared with the semi-empirical model based on the convection caused by Brownian motion. This includes the effect of conduction, interfacial thermal resistance (R_b) and contribution from convection to the effective thermal conductivity of nanofluids.[45] In this

model, the thermal conductivity is given by equation 1.7, chapter 1. The value of '*A*' in the equation is generally taken as 40,000 for all base fluids and the value of '*m*' depends on the base fluid. Prashar *et al*[45] studied the effective thermal conductivity of water and ethylene glycol based nanofluids using the above model. They considered m = 2.5 for water and m = 1.6 for ethylene glycol based fluids which gave best fit to their experimental data. We have considered the interfacial resistance as 2.16 x 10^{-8} $W^{-1}m^2K$ for the toluene-nanoparticle interface for all the samples (as discussed in section 3.4.2 in chapter 3) and the Prandtl number for toluene at 25 °C as 7. The open circles in Figure 4.8 is the calculated values using m = 3.375 for toluene based fluid in the above equation.

A comparison of the experimental data with the theoretical model shows that the particles with narrow size distribution show good agreement with the Brownian model. Since the theoretical model does not consider the distribution of the particles in the fluid, the experimental result largely deviated from the theoretically predicted value for the samples MD4 and MD5. The large deviation of the experimental results for MD4 and MD5, thus, could be due to the wide size distribution of the particles. Moreover, the Reynolds number (*Re*) is inversely proportional to the square root of the particle diameter. *Re* reduces with increase in the particle size and it reaches zero for larger particle sizes.[46] The measured thermal conductivities of MD4 and MD5 are relatively low and is closer to the value calculated by including the interfacial thermal resistance (Figure 4.8) due to the presence of larger sized particles.

Zhou *et al*[27] predicted the thermal conductivity of fluids based on particle size distribution analysis and compared their results with that for stable long chain oleic acid coated magnetic fluid by considering that cluster formation in the fluid enhances the thermal conductivity. However, in the case of short-chain decanoic acid coated nanoparticles, the cluster formation is expected to lead to aggregation and sedimentation. Moreover, the nature of the FC magnetization curves (Fig. 4.6) shows non-interacting nature of the magnetic particles. Similarly, the TEM images also (Fig. 4.3) show completely isolated particles. Therefore, cluster formation and aggregation cannot be the possible mechanism for thermal conductivity enhancement in the present case. The Brownian motion caused convection could be a possible mechanism for the observed thermal conductivity enhancement.

Thermogravimetric analysis showed that the amount of the surfactant coated on the nanoparticles is different for different samples. The amount of the primary surfactant is varied randomly in the range 10-14%, and the amount of the secondary surfactant is varied in the range 9-17%. Thus, apart from the variation in the particle size distribution, there is a difference in the amount of the primary and secondary surfactants coated on the nanoparticles. There is no systematic variation of thermal conductivity with the amount of the surfactants present on the surface of the nanoparticles. The stability of the nanofluid is decided by the interaction between the solvent and the surfactant molecules exposed to the solvent. More hydrophilic groups are exposed when the amount of the secondary surfactant is more, leading to less interaction between the surfactant and the solvent. Hence increasing the amount of the secondary surfactant may decrease the stability of the fluid. Thus, the interface between the nanoparticles and the solvent may be an additional factor deciding thermal conductivity, apart from the particle size and distribution. This issue is addressed in chapter 5, by keeping the particle size and distribution the same, using the same surfactant.

4.4.2 Viscosity

Viscosities of the different fluid samples are measured to obtain information on the changes in the thermal conductivity with particle size distribution. The Brownian motion induced convection is known to decrease with increasing the particle size due to reduction of Brownian velocity with size.[47] Viscosity measurements of the fluids have been carried out to verify the Brownian motion caused convection mechanism. For fluids with narrower distribution of the particles (MD1, MD2, MD3), the viscosity increases almost linearly with increasing average size, as shown in Figure 4.9. The viscosity increases with increasing the particles size which decreases the Brownian motion. However, a large enhancement in the viscosity is observed for the fluids of MD4 and MD5 having wider particle size distribution and these two fluids showed large difference between the experimental thermal conductivity and that calculated based on the Brownian model (Figure 4.8). The larger interfacial resistance due to the presence of large number of smaller particles (information obtained from TEM image and magnetic measurements) in the fluids samples with wider particle size distribution (fluids of MD4 and MD5) also reduces the thermal conductivity enhancement. The higher viscosities of MD4 and MD5 suppress Brownian motion and therefore, reduced thermal conductivity is obtained for these two samples. The reduction in the Brownian velocity due to the larger particles in combination with the interfacial thermal resistance due

to smaller particles reduces the thermal conductivity of the nanofluid containing widely distributed particles (MD4 and MD5). This result supports the conclusion that convection due to Brownian motion may be a possible mechanism for thermal conductivity enhancement in nanofluids.

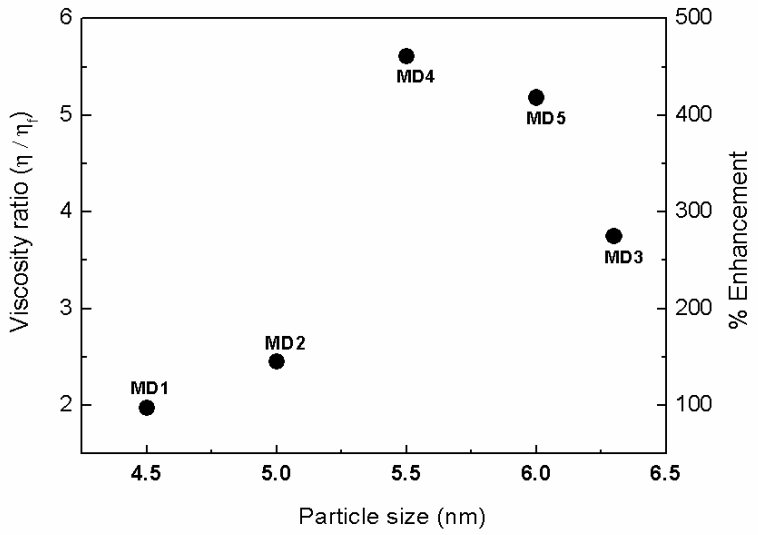

Figure 4.9. Viscosity of the different nanofluids as a function of the average particle size

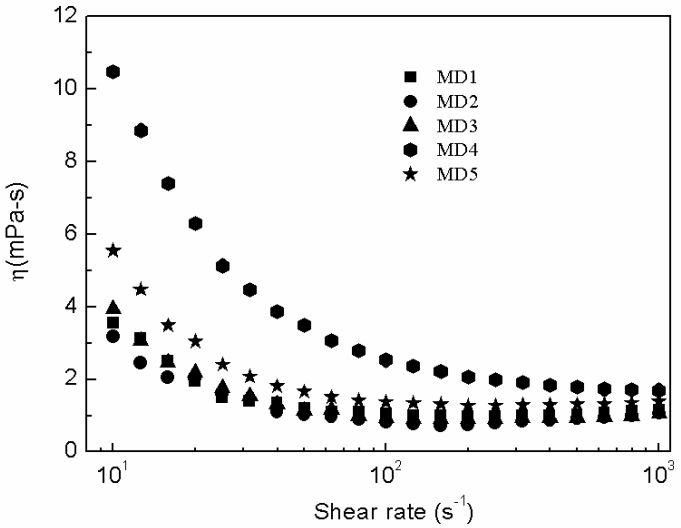

Figure 4.10. Variation of viscosity of the nanofluids with shear rate.

Figure 4.10 shows variation of viscosity with shear rate for all the decanoic acid coated fluid samples. The variation of viscosity with shear rate indicates the shear thinning

behaviour of the fluids, where viscosity is decreased with increasing the shear rate for all the fluids (see section 1.6 in chapter 1). All the fluid samples show non-Newtonian behaviour at lower shear rate (<40 s^{-1}) and Newtonian behaviour at higher shear rate (>40 s^{-1}).

4.5. Conclusions

The effect of particle size distribution on the thermal conductivity enhancement of decanoic acid coated magnetite nanofluids is studied. Magnetite nanoparticles with comparable average size and different size distribution are prepared by varying the rate of addition of ammonium hydroxide in the coprecipitation reaction. Particle size distribution obtained from TEM analysis and further confirmed from magnetic measurements. Experimental results show decrease in the thermal conductivity enhancement with increasing average particle size. However, nanofluids containing particles with very wide distribution show much lower enhancement in the thermal conductivity. For narrow particle size distribution, the experimental thermal conductivity enhancement is comparable to that predicted by the Brownian motion caused convection whereas for wider particle size distribution, large deviation is observed. From the results, it is concluded that the Brownian motion caused convection could be a possible mechanism for enhancement in the thermal conductivity of the studied nanofluids. However, since the amount of the surfactant is found to be different for the different decanoic coated samples, the role of the surfactant and the interface cannot be ruled out.

References

1. Taylor, R.; Coulombe, S.; Otanicar, T.; Phelan, P.; Gunawan, A.; Lv, W.; Rosengarten, G.; Prasher, R.; Tyagi, H. *J. Appl. Phys.* **2013**, *113*, 011301.
2. Eastman, J.; Choi, S.; Li, S.; Yu, W.; Thompson, L. *Appl. Phys. Lett.* **2001**, *78*, 718-720.
3. Choi, S.; Zhang, Z.; Yu, W.; Lockwood, F.; Grulke, E. *Appl. Phys. Lett.* **2001**, *79*, 2252-2254.
4. J. Buongiorno, D. C. Venerus, N. Prabhat, T. McKrell, J. Townsend, R. Christianson, Y. V. Tolmachev, P. Keblinski, L.-w. Hu, J. L. Alvarado, I. C. Bang, S. W. Bishnoi, M. Bonetti, F. Botz, A. Cecere, Y. Chang, G. Chen, H. Chen, S. J. Chung, M. K. Chyu, S. K. Das, R. Di Paola, Y. Ding, F. Dubois, G. Dzido, J. Eapen, W. Escher, D. Funfschilling, Q. Galand, J. Gao, P. E. Gharagozloo, K. E. Goodson, J. G. Gutierrez, H. Hong, M. Horton, K. S. Hwang, C. S. Iorio, S. P. Jang, A. B. Jarzebski, Y. Jiang, L. Jin, S. Kabelac, A. Kamath, M. A. Kedzierski, L. G. Kieng, C. Kim, J.-H. Kim, S. Kim, S. H. Lee, K. C. Leong, I. Manna, B. Michel, R. Ni, H. E. Patel, J. Philip, D. Poulikakos, C. Reynaud, R. Savino, P. K. Singh, P. Song, T. Sundararajan, E. Timofeeva, T. Tritcak, A. N. Turanov, S. Van Vaerenbergh, D. Wen, S. Witharana, C. Yang, W.-H. Yeh, X.-Z. Zhao, and S.-Q. Zhou, *J. Appl. Phys.* **2009**, *106*, 094312.
5. Timofeeva, E. V.; Gavrilov, A. N.; McCloskey, J. M.; Tolmachev, Y. V.; Sprunt, S.; Lopatina, L. M.; Selinger, J. V. *Phys. Rev. E: Stat. Phys. Plasmas Fluids Relat.* **2007**, *76*, 061203.
6. Warrier, P.; Teja, A. *Nanoscale Res. Lett.* **2011**, *6*, 247.
7. Hadjov, K. B.; Dontchev, D. P. *J. Nanopart. Res.* **2008**, *11*, 1713-1718.
8. Timofeeva, E. V.; Routbort, J. L.; Singh, D. *J. Appl. Phys.* **2009**, *106*, 014304.
9. Vékás, L.; Bica, D.; Marinica, O. *Rom. Rep. Phys.* **2006**, *58*, 257.
10. Jang, S. P.; Choi, S. U. S. *Appl. Phys. Lett.* **2004**, *84*, 4316-4318.
11. Xue, L.; Keblinski, P.; Phillpot, S. R.; Choi, S. U. S.; Eastman, J. A. *Int. J. Heat Mass Transfer* **2004**, *47*, 4277-4284.
12. Ravi, P.; William, E.; Paul, M.; Jacob, F.; Patrick, P.; Pawel, K. *Appl. Phys. Lett.* **2006**, *89*, 143119.
13. Angayarkanni, S. A.; Philip, J. *J. Nanofluids* **2014**, *3*, 17-25.
14. Chauhan, D.; Singhvi, N. *J. Nanofluids* **2014**, *3*, 361-367.

15. Murshed, S. M. S.; de Castro, C. A. N. *J. Nanofluids* **2012**, *1*, 180-185.
16. Nan, C.-W.; Birringer, R.; Clarke, D. R.; Gleiter, H. *J. Appl. Phys.* **1997**, *81*, 6692.
17. Jeffrey, D. J. *Proc. R. Soc. London, Ser. A* **1973**, *335*, 355-367.
18. Bruggeman, V. D. *Ann. Phys.* **1935**, *416*, 636-664.
19. Hamilton, R. L.; Crosser, O. K. *Ind. Eng. Chem. Fund.* **1962**, *1*, 187-191.
20. Hashin, Z.; Shtrikman, S. *J. Appl. Phys.* **1962**, *33*, 3125.
21. Davis, R. H. *Int. J. Thermophys.* **1986**, *7*, 609-620.
22. Das, S. K.; Choi, S. U. S.; Patel, H. E. *Heat Transfer Eng.* **2006**, *27*, 3-19.
23. Beck, M. P.; Yuan, Y.; Warrier, P.; Teja, A. S. *J. Nanopart. Res.* **2008**, *11*, 1129-1136.
24. Holotescu, S.; Stoian, F. D. *Mater. Sci. Eng. Technol.* **2011**, *42*, 379-385.
25. Dan, B.; Sammakia, B. G.; Subbarayan, G.; Kanuparthi, S.; Mallampati, S. *IEEE Trans. Compon. Packag. Manuf. Technol.* **2013**, *3*, 2068-2074.
26. Xu, J.; Yu, B. M. *J. Phys. D: Appl. Phys.* **2006**, *39*, 4486-4490.
27. Zhou, D.; Wu, H. *Appl. Phys. Lett.* **2014**, *105*, 083117.
28. Philip, J.; Shima, P. D. *Adv. Colloid Interface Sci.* **2012**, *183-184*, 30-45.
29. Gnanaprakash, G.; Philip, J.; Jayakumar, T.; Raj, B. *J. Phys. Chem. B* **2007**, *111*, 7978-7986.
30. Zhao, S. Y.; Lee, D. K.; Kim, C. W.; Cha, R. G.; Kim, Y. H.; Kang, Y. S. *Bull. Korean Chem. Soc.* **2006**, *27*, 237-242.
31. Pérez, N.; López-Calahorra, F.; Labarta, A.; Batlle, X. *Phys. Chem. Chem. Phys.* **2011**, *13*, 19485-19489.
32. Schwertmann, U.; Friedl, J.; Stanjek, H. *J. Colloid Interface Sci.* **1999**, *209*, 215-223.
33. Arita, T.; Yoo, J.; Adschiri, T. *J. Phys. Chem. C* **2011**, *115*, 3899-3909.
34. Dong, T. Y.; Chen, W. T.; Wang, C. W.; Chen, C. P.; Chen, C. N.; Lin, M. C.; Song, J. M.; Chen, I. G.; Kao, T. H. *Phys. Chem. Chem. Phys.* **2009**, *11*, 6269-6275.
35. Waldron, R. D. *Phys. Rev.* **1955**, *99*, 1727-1735.
36. Liu, C.; Zhang, Z. J. *Chem. Mater.* **2001**, *13*, 2092-2096.
37. Tournus, F.; Tamion, A. *J. Magn. Magn. Mater.* **2011**, *323*, 1118-1127.
38. Chesnel, K.; Trevino, M.; Cai, Y.; Hancock, J. M.; Smith, S. J.; Harrison, R. G. *J. Phys. Conf. Ser.* **2014**, *521*, 12004.

39. Vargas, J.; Nunes, W.; Socolovsky, L.; Knobel, M.; Zanchet, D. *Phys. Rev. B.* **2005**, *72*, 184428.
40. Sreeja, V.; Joy, P. *Int. J. Nanotechnol.* **2011**, *8*, 907-915.
41. Jayaprabha, K.; Joy, P. *J. Nanofluids* **2014**, *3*, 1-7.
42. Zheng, R. K.; Gu, H. W.; Zhang, B.; Liu, H.; Zhang, X. X.; Ringer, S. P. *J. Magn. Magn. Mater.* **2009**, *321*, L21-L27.
43. Shima, P. D.; Philip, J.; Raj, B. *Appl. Phys. Lett.* **2009**, *94*, 223101.
44. Wang, B.; Wang, B.; Wei, P.; Wang, X.; Lou, W. *Dalton Trans.* **2012**, *41*, 896-899.
45. Prasher, R.; Bhattacharya, P.; Phelan, P. *Phys. Rev. Lett.* **2005**, *94*, 25901.
46. Azizian, R.; Doroodchi, E.; Moghtaderi, B. *Ind. Eng. Chem. Res.* **2012**, *51*, 1782-1789.
47. Prasher, R.; Bhattacharya, P.; Phelan, P. E. *J. Heat Transfer* **2006**, *128*, 588-595.

Chapter 5

Role of primary and secondary surfactant layers on the thermal conductivity of lauric acid coated magnetite nanofluids

Abstract

Lauric (dodecanoic) acid coated magnetite nanoparticles with different amounts of primary and secondary surfactant layers on the surface of the nanoparticles have been synthesized. Two sets of the surfactant coated nanoparticles are prepared; one with comparable amount of primary surfactant and the other with comparable amount of secondary surfactant. Nanofluids are prepared by dispersing the surfactant coated nanoparticles in toluene. Stability of the nanofluids is found to decrease with increasing amount of the secondary surfactant on the surface of the nanoparticles. Thermal conductivity and viscosity of the nanofluids are found to increase with increasing the amount of the secondary surfactant layer on the surface of the nanoparticles, whereas only a small increase in the thermal conductivity is observed for fluids with larger amount of the primary surfactant. Larger enhancement in the thermal conductivity is observed in the presence of a small magnetic field for the fluids containing particles with lower amount of the secondary surfactant. The overall results suggest that the thermal conductivity of the nanofluids depends on the amount and nature of the primary and secondary surfactants on the dispersed particles which in turn determine the interaction between the base fluid and the surfactant and therefore the dispersibility and stability of the nanofluids.

5.1. Introduction

There are many reports in the literature on the enhanced thermal conductivity of nanofluids, where reproducibility is a major concern. Agglomeration and sedimentation are the most common problems encountered, due to the high surface energy of the dispersed nanoparticles. This is more complicated in the case of fluids containing magnetic nanoparticles due to dipolar interaction between the particles in addition to van der Waals attraction.[1] Stability of a fluid is a key factor in the thermal conductivity studies and applications of magnetic nanofluids, where the surfactant plays an important role in the dispersion and stability.[2, 3] Use of various surfactants for stabilizing and dispersing magnetite nanoparticles in suitable solvents has been reported, such as long chain fatty acids,[4, 5] sulphonic and phosponic acids,[6] polymers,[7-10] and other organic acids,[11, 12]. Out of these, oleic acid (unsaturated fatty acid with 18 carbons and a double bond in the 9th carbon atom), containing a carboxylic acid head group and a hydrophobic tail end, is extensively studied as a surfactant for magnetite nanofluids.[13-15] The fatty acid surfactants separate the nanoparticles away from one another by steric repulsion due to the long aliphatic hydrophobic chain on the surface of the nanoparticles. The steric repulsion suppresses the van der Waals force of attraction between the particles and dipole-dipole interaction between the magnetic nanoparticles.

Stabilization of magnetite nanoparticles in fluids can also be achieved by charge stabilization, in which the charge on the surface of the nanoparticles stabilizes the nanoparticles in a fluid by electrostatic repulsion.[16-18] Long chain saturated and unsaturated fatty acids (anionic stabilizers) such as capric, lauric, myristic, stearic and oleic acids are also used to stabilize magnetite nanoparticles in water. The surface of the nanoparticles is coated with primary fatty acid surfactant through chemical bond between the oxygen atom in the carboxylic group and the iron atom in the magnetite nanoparticles. Then a secondary fatty acid layer over the primary layer is formed through weak hydrophobic interaction between the carbon chains of the primary and secondary surfactants. The carboxylic group of the secondary surfactant makes the particles hydrophilic and allow to disperse in water.[19-21] Wang *et al*[22] synthesized bilayer surfactant coated magnetic nanofluid using sodium oleate as the primary layer and sodium dodezyl benzene sulphonate (SDBS) as the secondary layer. From their studies, it is observed that the strength of the interaction between the inner (primary) and the outer (secondary) layers is weaker than the interaction between the inner layer and the surface. Thermogravimetric analysis showed weight loss at lower temperatures corresponding to the breakage of the weak van der Waals force and the weight loss at higher

temperatures corresponds to breakage of the chemical bond between the primary layer and the surface of the nanoparticles.

Surfactants on the nanoparticle surfaces not only provide stability to the nanofluids but also has great influence on the physical, chemical, and thermophysical properties of the magnetic nanofluids.[2, 4, 23-32] For the preparation of magnetic fluids in non-aqueous liquid carriers, for many applications, the as-synthesized surface coated magnetic nanoparticles in aqueous phase are transferred to the non-aqueous phase by washing with a highly polar solvent to remove the excess surfactant (bilayer) on the surface of the nanoparticle. However, complete removal of excess surfactant (to obtain completely monolayer coated) is impossible because it may remove the primary surfactant which is directly attached to the surface of the magnetic nanoparticles[33]. Sahoo *et al*[34] reported that small amount of secondary surfactants is always associated with the primary surfactants by weak van der Waals interaction. This excess surfactant (secondary layer/ bilayer) affects the dispersion of the particles in the non-aqueous carrier liquid. Eventually, the amount of excess surfactant may affect the physical, chemical and thermophysical properties of magnetic fluids.

To study the effect of particle size distribution on the thermal conductivity of decanoic acid coated magnetite nanoparticles, as reported in the previous chapter (chapter 4), samples were made in different batches to control the size distribution. Thermogravimetric studies showed that the amount of total, primary and secondary surfactants are different on the different samples. Since the size distribution of the particles was also varied, it was not possible to conclude the role of excess surfactant on the thermal conductivity of the nanofluids. Moreover, so far there are no studies reported in the literature on the effect of excess surfactant on the thermophysical properties of magnetic nanofluids. Attempts to control the amount of surfactant on the decanoic acid coated nanoparticles was not feasible due to the removal of large amount of the primary surfactant on washing the nanoparticles using a solvent mixture of varying polarity. Hence, in the present work, we have studied the effect of the amount of the primary and secondary surfactants on the physical, chemical and thermophysical properties of the dodecanoic acid (lauric acid) coated magnetite nanoparticles, synthesized under identical conditions to obtain similar particle size and distribution, and dispersed in toluene as the base fluid. Studies are made on lauric acid coated magnetite nanoparticles where samples with different amounts of surfactant on the surface of the nanoparticles are obtained by controlled washing of the nanoparticles in the reaction medium.

5.2. Synthesis

Lauric acid coated magnetite nanoparticles were synthesized by the coprecipitation of acidic solution of iron precursors ($FeCl_3.6H_2O$ and $FeCl_2.4H_2O$) taken in the stoichiometric ratio (Fe^{3+} to Fe^{2+} ratio of 2:1) using ammonium hydroxide (NH_4OH) as the base. The synthesis procedure is similar to that reported for decanoic acid coated magnetite nanoparticles (see section 2.2.2 in chapter 2). After completion of the coating process, the dispersion was cooled to room temperature, and part of the dispersion was dried to obtain the nanoparticles in powder form for characterization (sample code: ML0).

Table 5.1. Sample codes of lauric acid coated samples washed under different solvent mixtures

S. No	Acetone: hexane ratio	Sample code
1	As-synthesized	ML0
2	1:1	ML1
3	2:1	ML2
4	3:1	ML3
5	1:1	ML1d
6	2:1	ML2d

Acetone mixed with hexane was used for controlled washing of the nanoparticles dispersed in the reaction medium.[35] The dispersion obtained was washed with acetone-hexane mixture to remove the excess surfactant present on the surface of the nanoparticles as well as the free surfactant present in the reaction medium. The water-based fluid obtained in the reaction medium was taken in a 500 ml beaker and acetone-hexane mixture was added from a burette with constant stirring. The coated nanoparticles were transferred from the aqueous to the non-aqueous medium during the washing process. After the washing process, the organic layer containing the nanoparticles was separated using a separating funnel. The separated non-aqueous layer was washed three times with water to remove any unreacted metal ions. Different samples were obtained by repeating the synthesis procedure under identical conditions but washing under different conditions, as shown in Table 5.1, by changing the

acetone to hexane ratio in the solvent mixture used for washing. Finally the nanoparticles dispersed in the non-aqueous layer were dried at room temperature and the dried magnetite nanoparticles were used for further studies (sample codes ML1, ML2 and ML3 for acetone:hexane ratios of 1:1, 2:1 and 3:1, respectively). Another set of samples was obtained by washing with the less polar 1:1 and 2:1 solvent mixtures, and in these cases, the dispersion was stirred well for five minutes after complete addition of the solvent. These samples are labeled as ML1d and ML2d, respectively, where 'd' stands for delayed washing.

5.3. Characterization of surfactant coated magnetite nanoparticles

5.3.1 Powder X-ray diffraction

The dried powder samples obtained after washing with the solvent mixtures are characterized by powder X-ray diffraction for phase purity of the samples. XRD patterns of all five samples, shown in Figure 5.1, confirmed the formation of magnetite phase, without any other impurities. The average crystallite size is calculated for all the samples from the width of the major peak (311) in the XRD pattern using the Scherrer equation (equation 2.2 in chapter 2). The average crystallite size for all the samples is calculated as 6±1 nm.

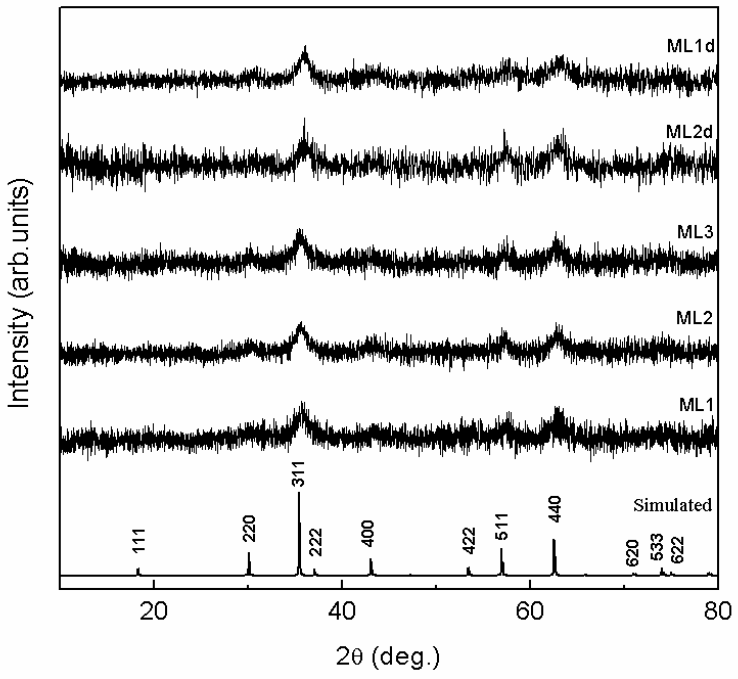

Figure 5.1. Powder X-ray diffraction patterns of the dried lauric acid coated samples, compared with the simulated pattern of Fe_3O_4

5.3.2. Transmission electron microscopy

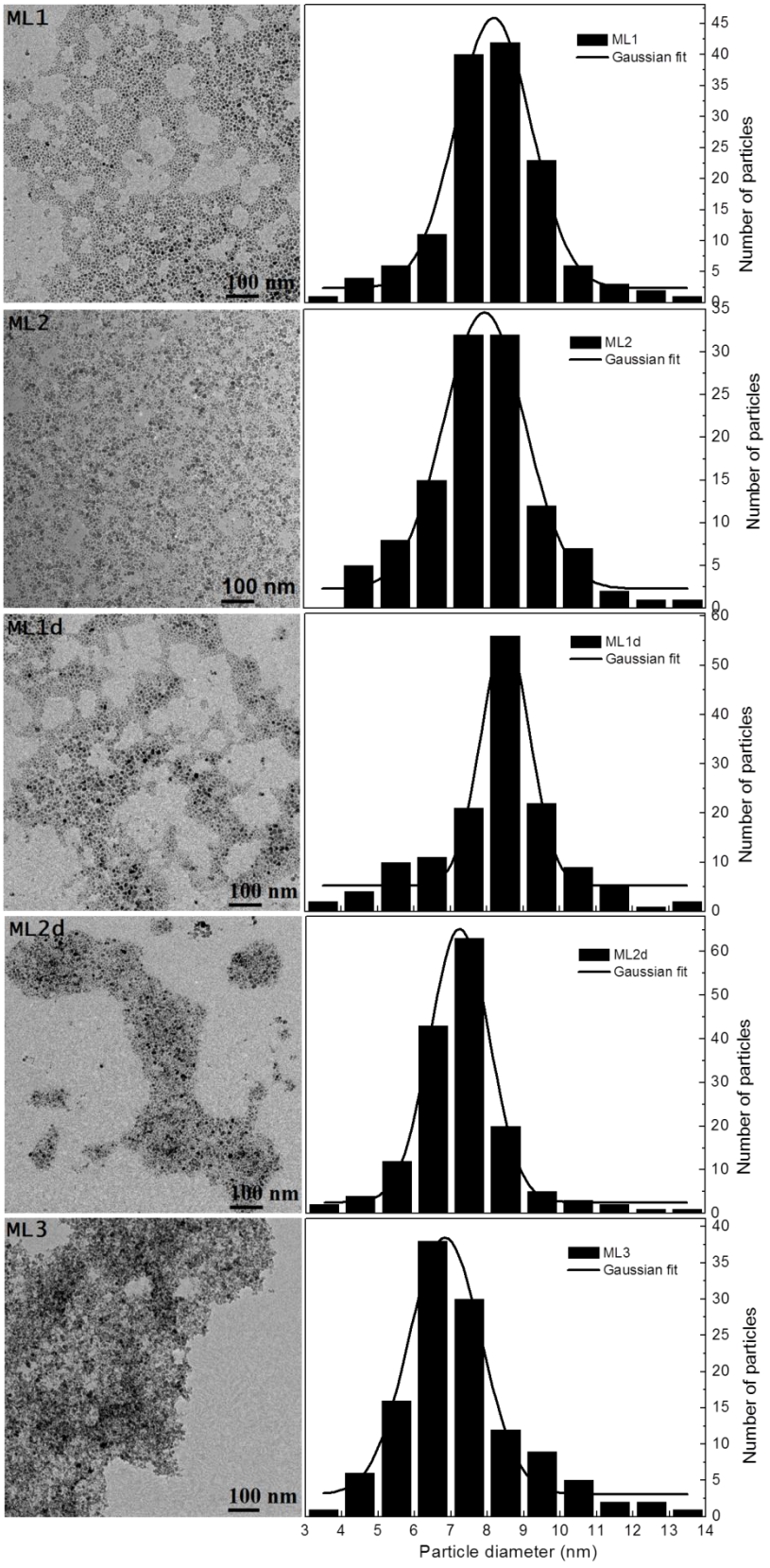

Figure 5.2. Transmission electron microscope images of the lauric acid coated samples (left) and the corresponding particle size distribution histogram (right)

Figure 5.2 shows the TEM images and the corresponding particle size distribution histogram of the samples ML1, ML2, ML1d, ML2d and ML3. The calculated particle sizes from the histograms of the samples ML1, ML2, ML1d, ML2d and ML3 are 8.2, 8.0, 8.5, 7.2 and 6.8 nm, respectively. The particle size obtained from the TEM image is slightly larger than the crystallite size calculated from the XRD patterns (6±1 nm) as shown in the Table 5.2. The larger size in the TEM images can be attributed to the thickness of the amorphous or surfactant layer on the surface of the nanoparticles. The thickness of the amorphous or surfactant layer on the nanoparticle surface for the samples ML1, ML2, ML1d, ML2d and ML3 are 2.3, 2.2, 2.8, 1.7, and 1.3 nm respectively (difference between the average particle and crystallite sizes). The observed difference between the particle size from the crystallite size could be due to the primary and secondary layer of surfactants in addition to the amorphous layer on the nanoparticle surfaces. The smaller size for ML2d and ML3 indicates that the amount of surfactant on the surface of the nanoparticles decreases with increasing the polarity of the solvent used for washing, due to the removal of larger amount of the secondary surfactant when washed with solvent of larger polarity. The larger sizes of ML1 and ML2 and ML1d indicate larger amount of the surfactant on the nanoparticle surfaces due to washing the samples with the less polar solvents (1:1 and 2:1 acetone-hexane mixtures). Although the TEM samples are prepared at the same concentrations, particles having less surfactant on their surface are assembled very closely (ML2d and ML3 in Figure 5.2) and particles having larger amount of the surfactant on their surface are well separated (ML1, ML2 and ML1d in Figure 5.2).

Table 5.2. Lattice parameter, particle size and size distribution of the nanoparticles in the lauric acid coated samples

S. No	Sample name	Lattice parameter (Å)	Particle size (±0.5nm)	Size distribution from TEM histogram, FWHM (nm)
1	ML1	8.38	8.2	2.1
2	ML2	8.38	8.0	2.5
3	ML1d	8.39	8.5	1.4
4	ML2d	8.38	7.2	1.6
5	ML3	8.39	6.8	2.0

5.3.3. Thermogravimetric analysis

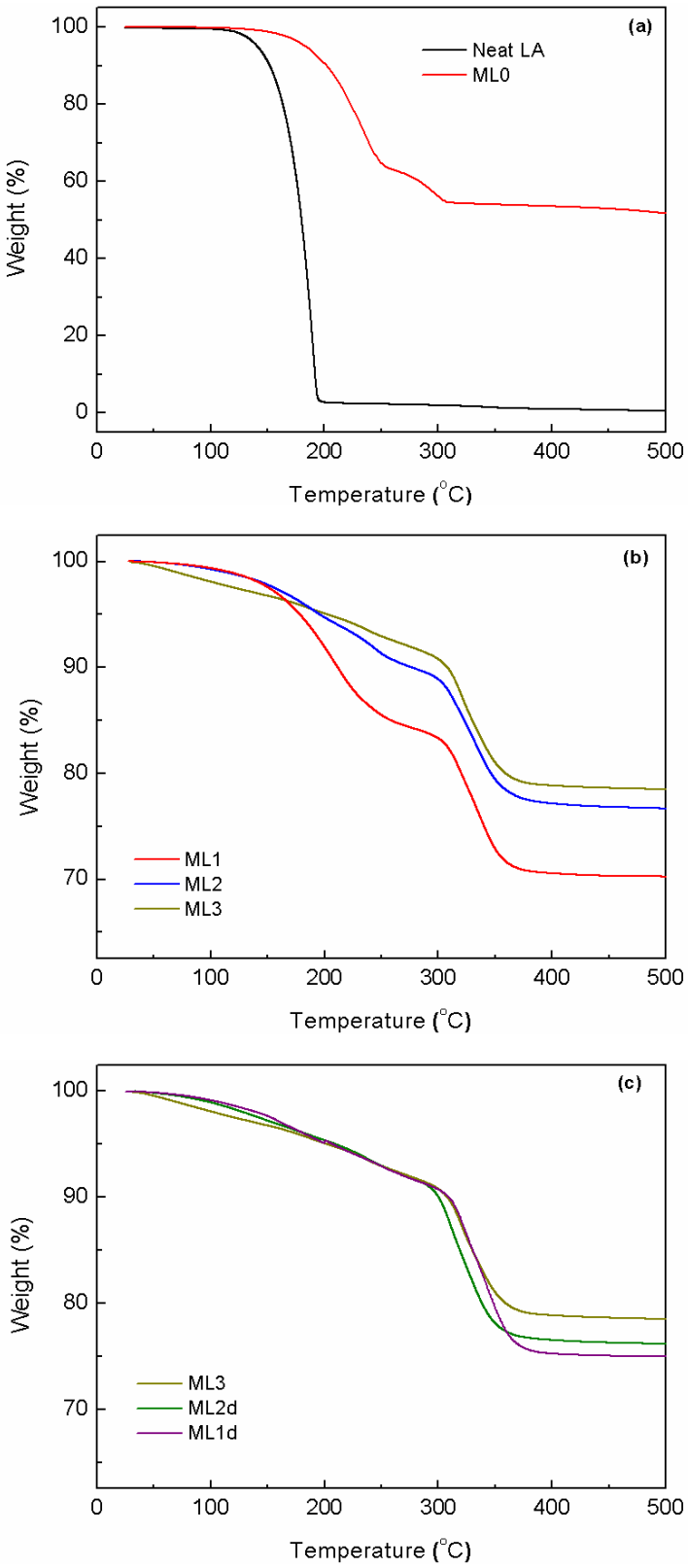

Figure 5.3. Thermogravimetric curves of (a) neat lauric acid (LA) and the lauric acid coated sample (ML0) recovered directly from the reaction medium (unwashed), (b) lauric acid coated samples, washed with different polar solvent mixtures (ML1, ML2, ML3), (c) samples washed after a delay of five minutes (ML1d & ML2d) compared with that of ML3.

Figure 5.3 shows the thermogravimetric analysis (TGA) curves of free lauric acid (LA) and the different coated nanoparticle samples. The TGA curves of neat LA and the as-synthesized sample recovered by evaporation of the solvent after coating (ML0) are shown in Figure 5.3(a). TGA curve of LA shows a sharp single step weight loss at ~180 °C, due to its decomposition. In the case of the coated sample, two major weight losses are observed below 400 °C and these correspond to desorption, decomposition and evaporation of the surfactant molecules from the surface of the nanoparticles.[34] The first broad weight loss at the lower temperature for the coated nanoparticles starts at the decomposition temperature of lauric acid and is extended up to 260 ^{o}C, suggesting that the weight loss is not due to free lauric acid and hence corresponds to loosely bound or physically adsorbed surfactant molecules on the surface of the nanoparticles. The second weight loss at a higher temperature (>260 °C) is due to chemically bound surfactant on the surface of the nanoparticles, possibly through oxygen atoms of the acid group of the carboxylic acid.

TGA curves of all the washed lauric acid coated samples also show two major weight losses below 400 °C (Figure 5.3(b,c)), similar to that observed for the unwashed sample. The first weight loss below 260 °C is due to the desorption of loosely bound (physically adsorbed) lauric acid and the second weight loss at higher temperatures (260-390 °C) is due to decomposition of the chemically bound lauric acid to the surface of the nanoparticles. The small weight loss below 150 °C, especially in the case of ML3, can be due to the evaporation of the solvent molecule or moisture. Zhao *et al*[36] observed similar kind of major weight losses in addition to solvent weight loss (at a lower temperature) for bilayer oleic acid coated magnetite nanoparticles. Thus the TGA studies indicate the possibility of primary and secondary layers of lauric acid on the surface of the nanoparticles.

Table 5.3: Sample codes, amount of total, primary and secondary surfactants present in the different lauric acid coated samples

Sample set	**Sample code**	**Acetone : hexane ratio**	**Total surfactant (±1%)**	**Primary surfactant (±1%)**	**Secondary surfactant (±1%)**
Unwashed	ML0	0	46	11	35
Set 1	ML1	1:1	29	13	16
	ML2	2:1	23	13	10
	ML3	3:1	21	13	8
Set 2	ML3	3:1	21	13	8
	ML2d	2:1	24	16	8
	ML1d	1:1	25	17	8

Table 5.3 shows the total weight loss due to surfactants below 400 °C and the individual weight losses due to primary (chemically bound) and secondary (loosely bound) surfactant layers for all samples, obtained from the TGA curves. The washed samples are divided into two sets, based on the amount of the primary and secondary surfactant molecules on the surface of the nanoparticles, as shown in the Table 5.3. In the first set, the amount of the primary surfactant is comparable whereas the amount of the secondary surfactant decreases with increasing the polarity of the solvent used for washing (Set 1 in Table 5.3). In the second set (Set 2 in Table 5.3) the samples washed after a time delay (ML1d and ML2d) are compared with the sample obtained after a quick wash using highly polar solvent mixture (ML3). In the case of the samples obtained after delayed washing (ML1d and ML2d), the amount of the secondary surfactant is comparable to that obtained after a quick wash using the highly polar 3:1 solvent mixture, whereas the amount of the primary surfactant is slightly larger (Set 2 in Table 5.3), indicating that more amount of the secondary surfactant is removed if kept in the solvent mixture and this is converted to primary surfactant. Thus, there are two sets of samples, one with comparable amount of the primary surfactant (ML1, ML2, ML3 in Set 1) and the other set with comparable amount of the secondary surfactant (ML3, ML2d, ML1d in Set 2).

5.3.4. Infrared spectroscopy

The nature of bonding of the surfactant molecules on the surface of the nanoparticles is studied by IR spectroscopy. The IR spectra of neat lauric acid and the different lauric acid coated magnetite nanoparticles (ML0, ML1, ML2, ML3, ML2d, ML1d) are compared in Figure 5.4. IR spectrum of neat lauric acid shows a strong band at 1711 cm^{-1} which corresponds to carbonyl stretching (-C=O) and the bands at 2851 cm^{-1} and 2927 cm^{-1} are due to symmetric and asymmetric stretching of the $-CH_2$ group. The bands at 1407 cm^{-1} and 1460 cm^{-1} in the spectra of the free acid and the coated particles correspond to $-CH_2$ deformation. The medium intensity band observed at 937 cm^{-1} corresponds to O-H out of plane bending vibration which is characteristic band for dimeric carboxylic acids. The absence of this band in the spectra of all lauric acid coated samples indicates that the fatty acid molecules exist as monomers.[37] The broad intense band at 603 cm^{-1} in all the lauric acid coated samples corresponds to the stretching frequency of the Fe-O bond of Fe_3O_4.[38] The unwashed sample ML0 shows a strong band at 1400 cm^{-1}, which could be due to the symmetric stretching

frequency of the ammonium complexed carboxylate group ($C_{11}H_{23}$-COO^- $NH4^+$) of the secondary layer of lauric acid and/or free lauric acid in the reaction mixture.[39] The broad band near 3100 cm^{-1} in the unwashed sample corresponds to the O-H stretching frequency due to the solvent (water).

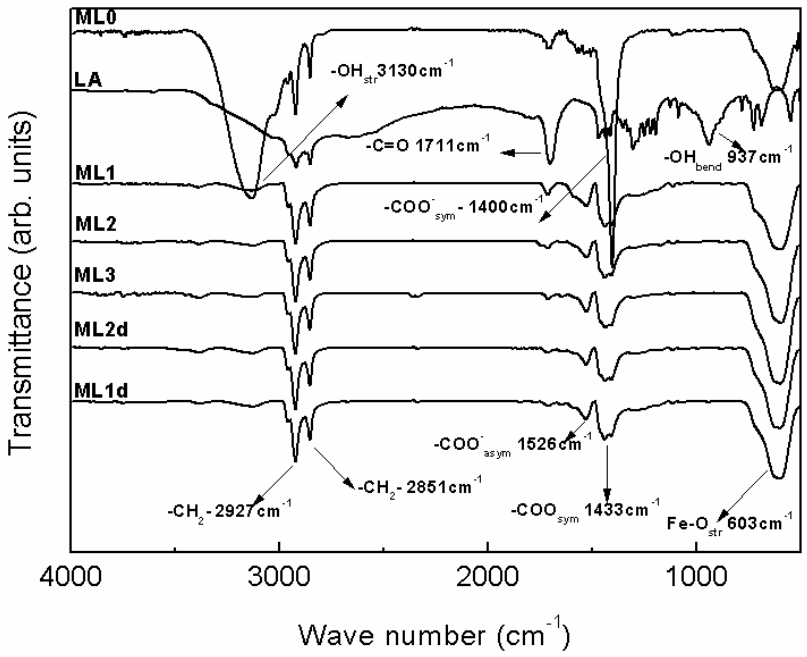

Figure 5.4. Infrared spectra of neat lauric acid (LA) compared with the spectra of different lauric acid coated samples.

The intensity of the carbonyl band at 1711 cm^{-1} is reduced considerably after coating. All the coated samples show only a weak band at 1711 cm^{-1}, indicating the presence of only small amount of free acid group on the surface of the nanoparticles. A close view of the free carbonyl band, as shown in Figure 5.5, suggests decreasing intensity of this band with increasing polarity of the solvent and the intensity of this band decreases in the order ML3 < ML2 < ML1 (Figure 5.5(a)). On the other hand, intensity of this band is comparable for the samples ML3, ML2d and ML1d (Figure 5.5(b)). These observations are in line with the results from the thermogravimetric analysis, where the amount of the secondary surfactant is found to decrease with increasing polarity of the solvent used for washing for the first set of samples whereas the amount of the secondary surfactant layer remains the same in the second set of samples (Figure 5.3(b, c), Table 5.3).

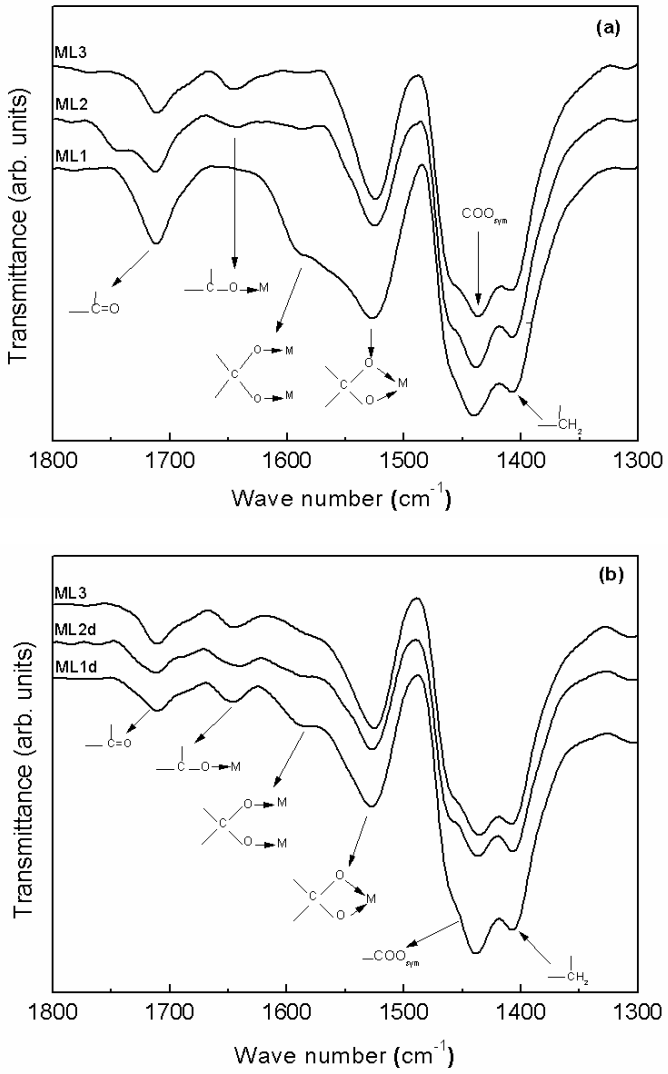

Figure 5.5. Close view of the IR spectra in the carboxylate region of the lauric acid coated samples. (a) Comparison of samples prepared by varying the polarity of the solvent used for washing, (b) comparison of the delayed washed samples (ML1d and ML2d) with that of ML3

All the coated nanoparticles show new bands at 1526 cm^{-1}, 1582 cm^{-1} and 1645 cm^{-1}, as shown in Figure 5.5, in the carboxylate region which corresponds to the vibration of metal-carboxylate bonds, suggesting the attachment of the COO^- group of lauric acid on the surface of the nanoparticles. Values for $\Delta\nu$ (see section 3.3.4 in chapter 3) for the three new asymmetric stretching vibrational bands at 1526 cm^{-1}, 1582 cm^{-1} and 1645 cm^{-1} in the carbonyl region are obtained as 93 cm^{-1}, 149 cm^{-1} and 212 cm^{-1} respectively. These values correspond to chelating bidentate, bridged bidentate and monodentate, respectively, suggesting different modes of coordination of lauric acid on the surface of the nanoparticles. Out of these new bands, the band at 1526 cm^{-1} is more intense than the other two, indicating that chelating bidentate coordination ($\Delta < 110$ cm^{-1}) with the surface of the nanoparticle is the

prominent one. Also, the intensity of this band is comparable for all three samples (ML1, ML2 and ML3) whereas intensities of the other bands change with the polarity of the solvent. The intensity of the band due to bridged bidentate ligand (1582 cm^{-1}) is highest for ML1 and lowest for ML3 and the intensity of the band varies in the reverse order for the monodentate ligand, indicating that washing with increasing polarity of the solvent converts the bridged bidentate ligand to monodentate ligand, apart from removing part of the secondary layer, as suggested by the corresponding decrease in the intensity of the carbonyl band at 1711 cm^{-1}. On the other hand, for the second set of samples (ML3, ML2d and ML1d), the intensity of the band due to monodentate ligand is almost comparable and the intensity of the band due to bridging bidentate ligand increases in the order ML1d > ML2d > ML3, corresponding to the increase in the amount of the primary layer as observed from the TG analysis (Table 5.3). Ding *et al*[40] reported chelating bidentate and bridged bidentate bonding of oleate molecule in Fe- oleate complex. The intensity of the carbonyl band increases with decreasing the solvent polarity, suggesting increasing amount of secondary surfactant on the nanoparticles.[41]

5.3.5. Mode of attachment

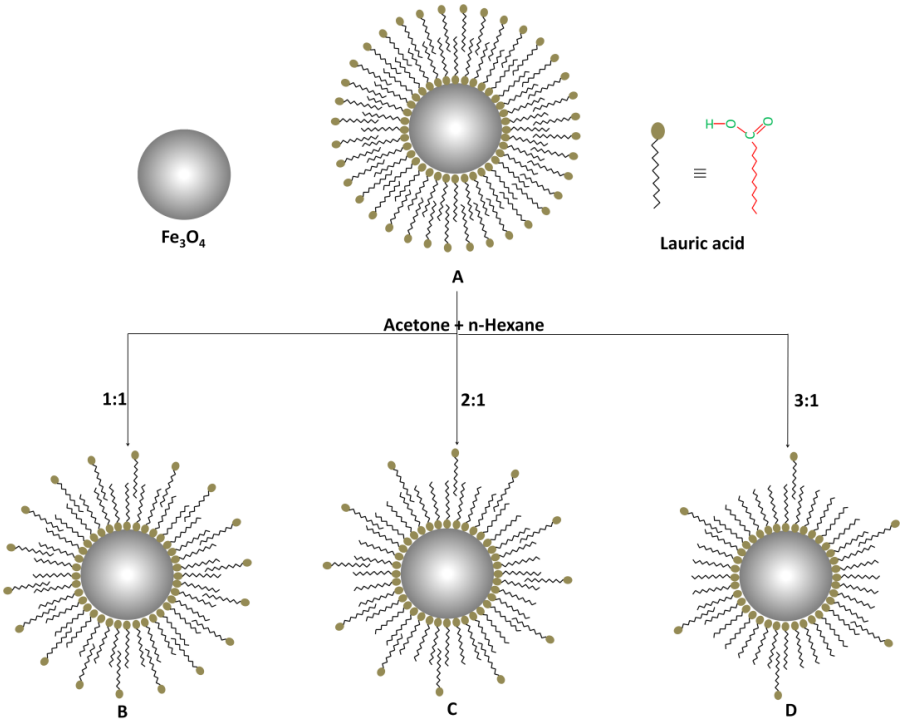

Figure 5.6. Schematic diagram showing the mode of attachment of primary and secondary surfactant layers in the different washed samples. (A) Nanoparticles dispersed in water (in the reaction medium, unwashed), (B) after washing with 1:1 solvent mixture (ML1), (C) after washing with 2:1 solvent mixture (ML2), (D) after washing with 3:1solvent mixture (ML3).

Figure 5.6 shows a schematic diagram of the mode of coating of the surfactant on the surface of the nanoparticles, based on the results obtained from the thermogravimetric and IR spectroscopic studies. It is found that the relative amounts of the primary and secondary surfactants are different in the different samples, after washing with different polarities of the solvent mixture by varying the acetone to hexane ratio. The amount of the secondary surfactant decreases with increasing the polarity of the solvent, by increasing the amount of acetone in the acetone-hexane ratio, used for washing.

5.3.6. Magnetic measurements

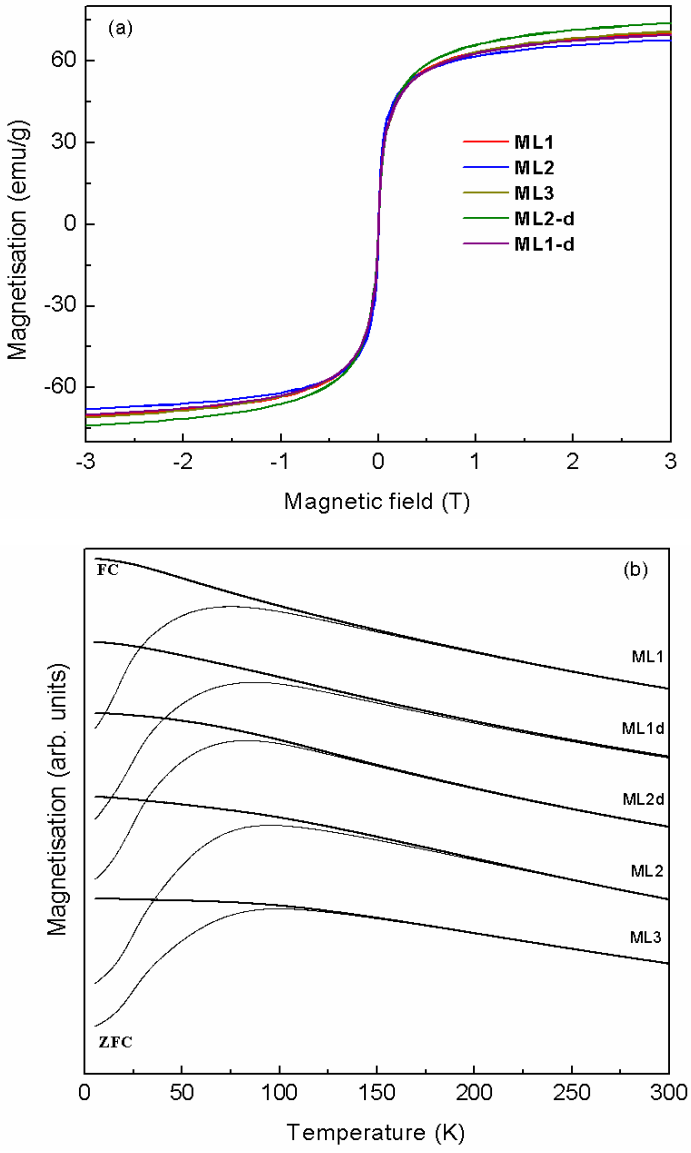

Figure 5.7. Magnetic measurements on the lauric acid coated powder samples. (a) magnetization measurements as a function of field at room temperature (b) zero field cooled (ZFC) and field cooled (FC) measurements

Magnetization measurements as a function of magnetic field at room temperature (Figure 5.7(a)) show absence of magnetic hysteresis loop (zero coercivity) and continuous increase in the magnetization at higher fields suggesting superparamagnetic nature of the nanoparticles. This is further confirmed by temperature dependent field cooled (FC) and zero field cooled (ZFC) magnetization measurements, which also give additional information on the magnetic interaction between the nanoparticles and hence the effectiveness of the surfactant coating (Figure 5.7(b)). The FC/ZFC magnetization measurements are carried out for all the lauric acid coated samples after cooling the samples from room temperature to 5 K, under zero field cooled and field cooled conditions, in a magnetic field of 5 mT. All the data show characteristics of superparamagnetic particles, where the temperature at which a maximum is observed in the ZFC magnetization curve at the superparamagnetic blocking temperature (T_B).

The blocking temperatures of ML1, ML2, and ML3 are obtained as 75 K, 96 K, and 100 K, respectively. Even though the particle sizes of the magnetite core is comparable for all the three samples, T_B decreases with increasing amount of the total surfactant. The differences in the blocking temperature for the three samples indicate difference in the separation between individual coated particles. For magnetic nanoparticles of comparable size, blocking temperature gives information on the strength of the interparticle interactions. If the nanoparticles are effectively capped by the surfactants and well separated, there will not be any exchange interactions between the particles and the interparticle dipolar interactions will decrease with increasing separation between the particles.[42,43] Since the core particle sizes of ML1 to ML3 are comparable, the decreasing blocking temperature with increasing amount of the secondary surfactant indicates reduced anisotropy contribution originating from interparticle interactions, due to the increasing amount of the coated surfactant on the nanoparticles. Interparticle magnetic interaction is reduced due to the increasing thickness of the non-magnetic layer (surfactant) on the magnetic nanoparticles. Due to reduced interparticle interactions, the magnetic anisotropy is reduced and the thermal energy required to overcome the anisotropy energy is less for the samples with larger amount of secondary surfactant on the nanoparticles.[12, 44]

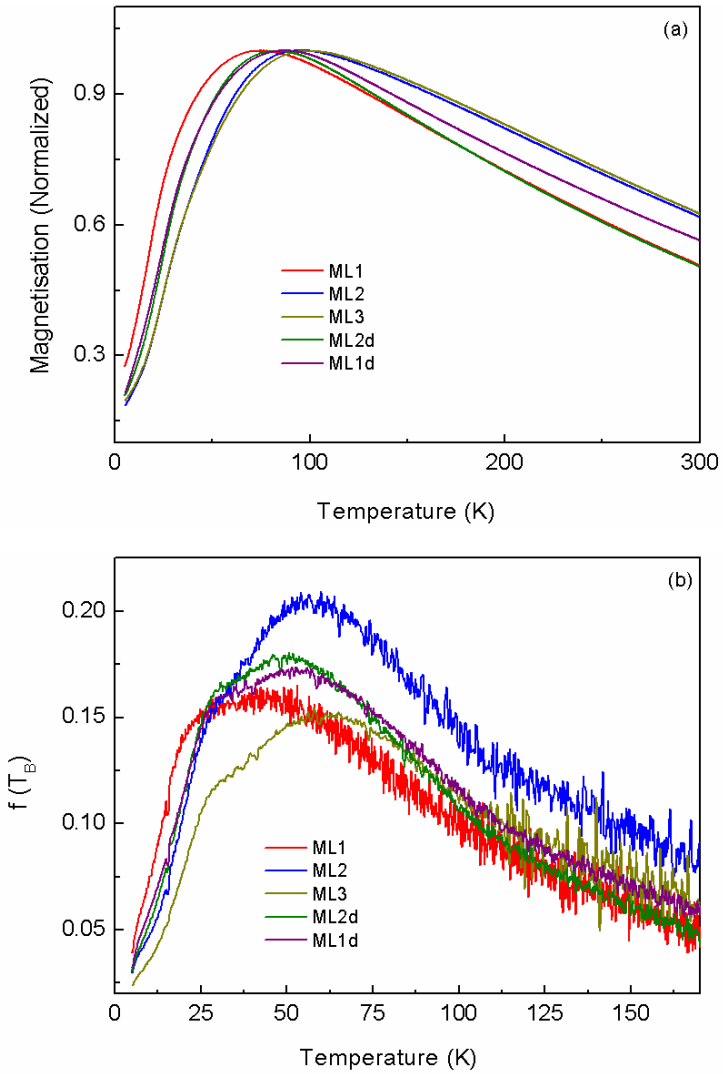

Figure 5.8. (a) Normalized zero field curves of lauric acid coated samples, (b) blocking temperature distribution calculated from the zero field cooled curves

The shape of zero field magnetization curves also indicates the particles size distribution in the sample. The normalized ZFC cures for all the five samples shown in the Figure 5.8(a) indicates that the distribution is almost same for all the samples. Moreover the calculated blocking temperature distribution from the zero field cooled magnetization curve (using equation 2.4 in chapter 2) also shows almost similar distribution for all the samples (Figure 5.8(b)).[45]

The shape of the FC magnetization curve can also give information on the interparticle interactions. Continuously increasing FC magnetization below T_B is an indication for the absence of interparticle interactions whereas a flat FC curve suggests strong interactions. The shape of the FC magnetization curve below T_B is different for the three

samples ML1, ML2, and ML3 (Figure 5.9(a)). For ML1 with larger amount of the secondary surfactant, the FC magnetization curve increases continuously below T_B whereas a saturating trend is observed at lower temperatures for ML3. This suggests reduced interparticle interactions in the order ML1 < ML2 < ML3 where the continuously increasing FC magnetization with decreasing temperature, below T_B, is an indication for the strength of the interparticle interactions, which gives information on the effectiveness of coating and the separation between the nanoparticles.[42, 43] Due to the lower amount of the secondary surfactant layer in ML3, the interparticle interactions are relatively larger in this sample. Similar differences in the ZFC and FC magnetization curves are observed for the samples washed after a delay of 5 minutes. For ML2d and ML1d, the blocking temperatures are obtained as 84 K and 87 K, respectively (Figure 5.7(b)) and corresponding changes in the nature of the FC magnetization curves is also observed (Figure 5.9(b)), suggesting the role of the surfactant layers in determining the interparticle magnetic interactions.

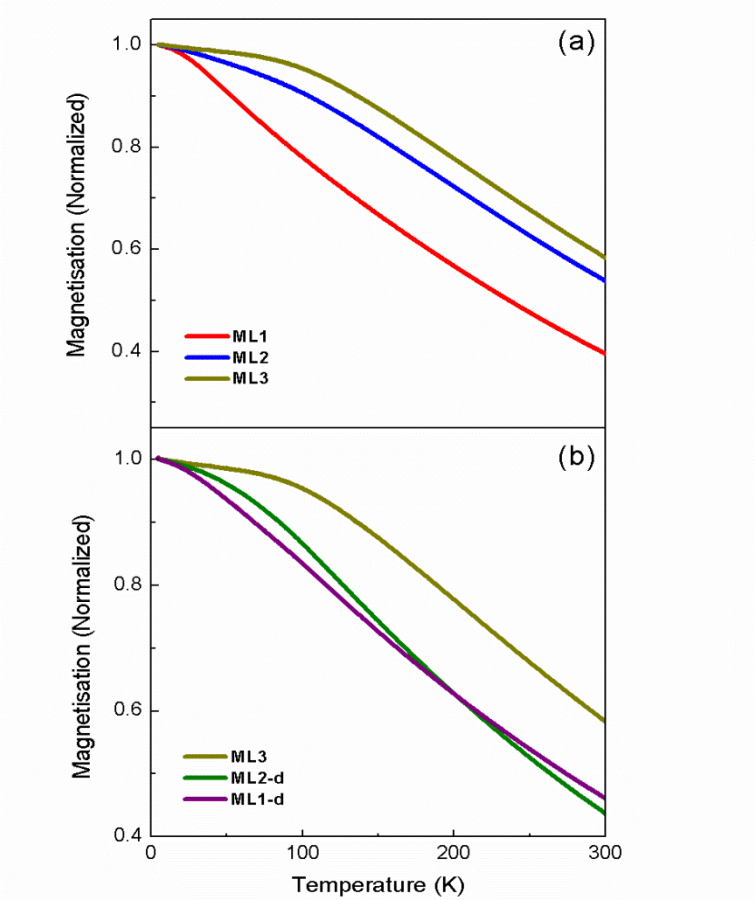

Figure 5.9. (a) Normalized field cooled magnetisation curves of (a) first set of samples and (b) second set of samples

5.4. Studies on nanofluids

5.4.1. Stability

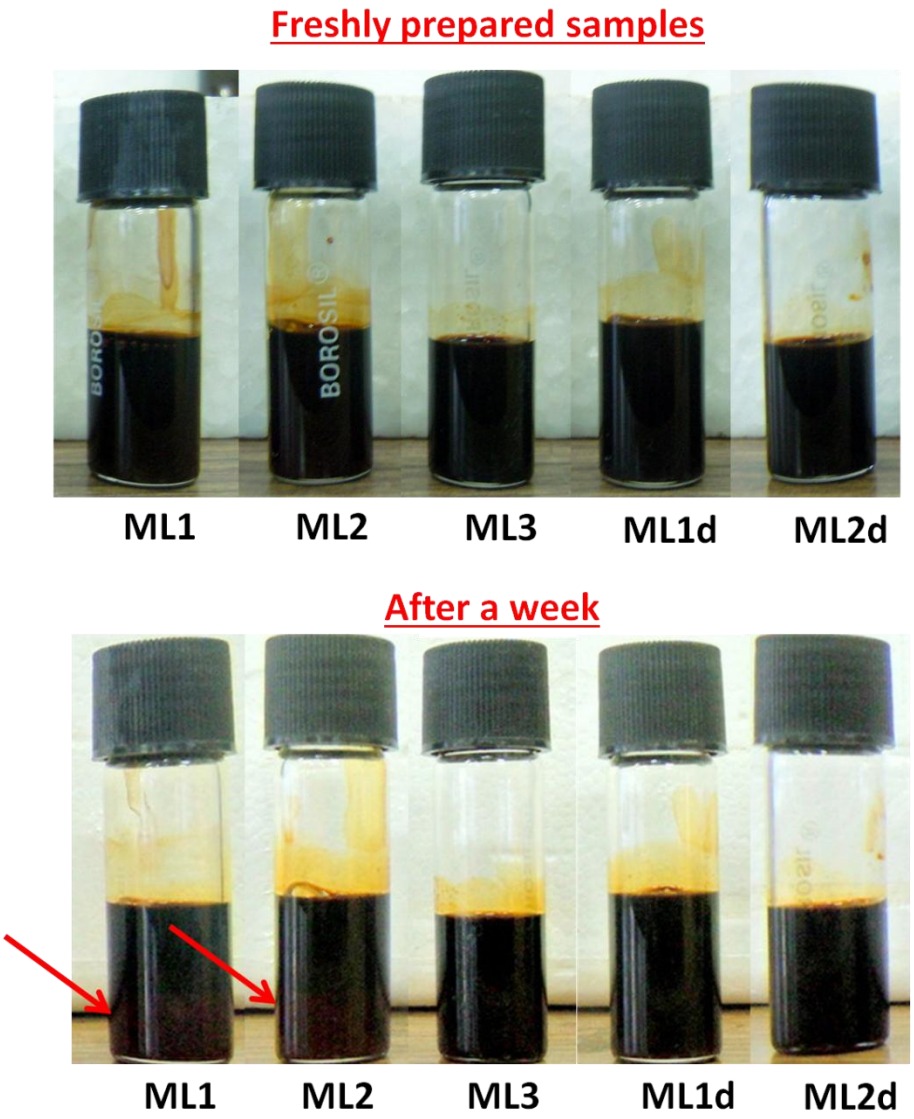

Figure 5.10. Photographs of the freshly prepared fluids (top) and taken a week after the preparation (bottom) of the fluid samples. The arrows indicated in the sample ML1 and ML2 (bottom image) show slight sedimentation of the nanoparticles in the fluid.

For thermal conductivity measurements, nanofluids are prepared by dispersing the different lauric acid coated magnetite nanoparticles in toluene as the base fluid. The samples ML1 and ML2 obtained by washing with the acetone-hexane mixture 1:1 and 2:1, respectively, gave less stable dispersion in toluene and is found to form sedimentation after a week. The sample ML3 obtained after washing with a large amount of acetone in the acetone-hexane (3:1) mixture gave a stable dispersion in toluene, even in the presence of a magnetic field.

Similarly, stable dispersions are also obtained for the delayed washed samples (ML1d and ML2d) like sample ML3. Thus, the stability of the fluids depends on the amount of the secondary surfactants and the nanoparticles with lower amounts of the secondary surfactants (fluids of ML3, ML2d, ML1d) form the most stable fluids. Figure 5.10 shows photographs of the freshly prepared fluids and a week after the preparation of the fluid samples. The freshly prepared fluids are well-dispersed without any sedimentation, whereas the fluids ML1 and ML2 form sedimentation after a week. The fluids of ML3, ML2d and ML1d show stable dispersion even after a week. The lower stability of the fluids of ML1 and ML2 is due to the more number of carboxylic acid groups from the secondary layer exposed to the non-polar solvent, toluene. The large number of carboxylic groups on the surface makes the particles more hydrophilic and reduces the dispersity in the non-polar solvent.

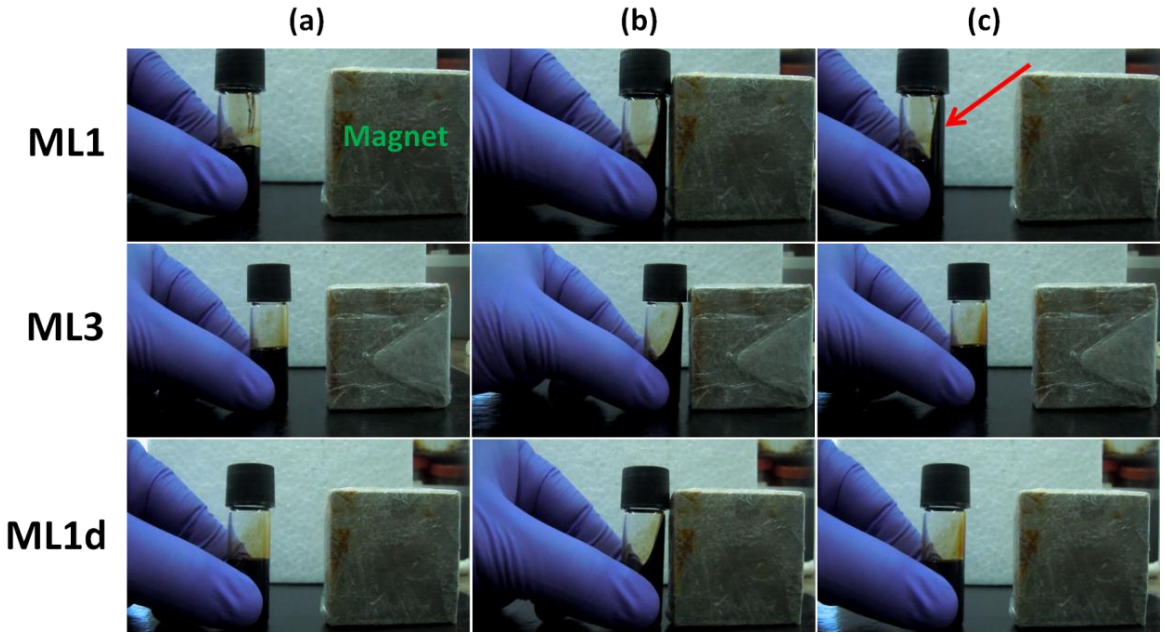

Figure 5.11. Photographs showing the fluid samples ML1, ML3 and ML1d (a) kept away from a magnet, (b) kept closer to the magnet, and (c) after moved away from the magnet. The arrow in the image of ML1 (c) indicates slightly adhered fluid sample on the container wall.

Figure 5.11 shows the photographs of the fluids of ML1, ML3 and ML1d when they are kept away, brought closer to and then removed from a laboratory magnet. Photographs of ML1d and ML3 show that the fluids are stable after moving away from the field whereas photograph of ML1 shows that part of the fluid is not flown back after moving away from the magnet due to the less dispersibility and/or less solvent surface interaction.

5.4.2. Thermal conductivity

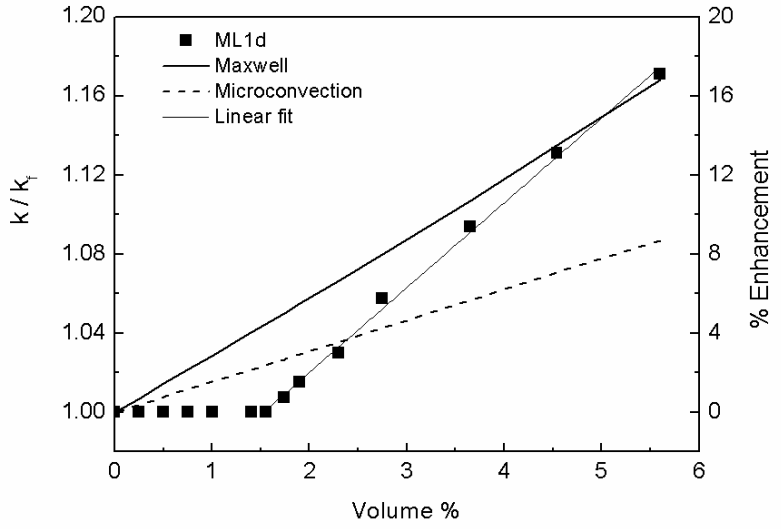

Figure 5.12. Variation of the relative thermal conductivity of ML1d with volume% (black squares), compared with theoretical models (dashed and thick solid line) and the experimental data fitted in the linear region (thin solid line).

Figure 5.12 shows variation of relative thermal conductivity of nanofluid (k/k_f, where k is the thermal conductivity of the nanofluid and k_f is the thermal conductivity of the solvent) of ML1d as a function of volume% of the Fe_3O_4 nanoparticles. No appreciable change in the thermal conductivity is observed below 1.6 volume% of Fe_3O_4 and above which almost linear increase in the thermal conductivity is observed up to the studied concentration of 5.6% of Fe_3O_4 (squares in Figure 5.12). Similar trend in the variation of the thermal conductivity with volume% has been reported for oleic acid coated magnetite nanoparticles (6.7 nm) dispersed in kerosene.[46] The experimental data points in the linear region are fitted by least-squares linear fit (thin solid line in the Figure 5.12), from which the slope is calculated as 0.043. This value is relatively larger than that obtained for decanoic acid and stearic acid coated samples discussed in Chapter 3 (Table 3.4).

Thermal conductivity of the stable dilute suspension of a solid in a liquid carrier can be explained by the classical Maxwell's model, described in section 1.4.1, equation 1.1 in chapter 1.[47] The experimental thermal conductivity ratio (k/k_f) matches with the Maxwell's model only at higher concentrations (>4 volume%) showing larger deviation at lower concentrations (thick solid line in Figure 5.12). In the Maxwell's model, the particles are

assumed to be motionless and the model does not consider the interaction between the particles. The experimental thermal conductivity is also compared with the Brownian motion induced microconvection model,[48] as described in section 1.4.2, equation 1.7 in chapter 1. The calculated relative thermal conductivity using the microconvection model by considering the interfacial resistance (R_b) as 2.16×10^{-8} m^2K/W and the constant $m=3.375$, as discussed in chapter 3, section 3.4.2, is shown in Figure 5.12 (dashed line). The Brownian motion induced microconvection model shows poor agreement with the experimental results at both higher and lower concentrations. Thus, microconvection cannot be the possible mechanism for the observed enhancement in the thermal conductivity.

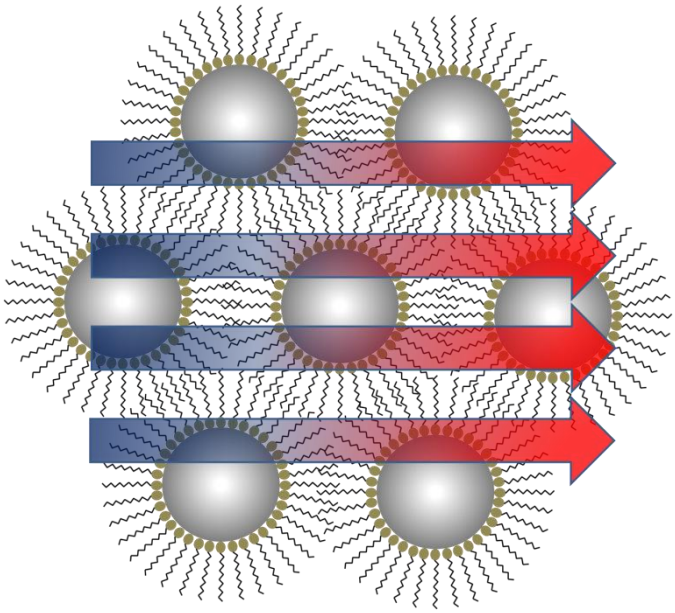

Figure 5.13. Schematic representation of heat transfer through the cluster formed by interdigitation of the surfactant molecules attached to neighbouring nanoparticles. The direction of the arrows indicate the heat flow direction, red color indicates hot end and blue indicates cold end.

In the case of superparamagnetic nanoparticles (<10 nm), the magnetic moment fluctuates randomly due to the thermal energy. The magnetic interaction between the nanoparticles is negligible for the fluctuating magnetic moments. Moreover, the surfactant stabilized magnetic nanoparticles are separated from one another which reduces the interparticle magnetic interactions between the particles in the fluid. In the case of smaller particles, the van der Waals interaction contributes more to the self-assembly of nanoparticles

than the magnetic interactions.[49, 50] At higher concentrations, the magnetic nanoparticles are closer to each other, and there can be increased van der Waals interaction between the surfactant coated particles. Due to the closer arrangement of the nanoparticles, the interdigitation of the fatty acid alkyl chain on the surface of the nanoparticles, with the surfactants in the nearby nanoparticles is possible, as shown in Figure 5.13.[51, 52] Even though the magnetic moments of the nanoparticles will be highly fluctuating at room temperature, the van der Waals interaction between the surfactant molecules could possibly form small clusters/aggregation-like self-assembly at higher concentrations, as shown in Figure 5.14.

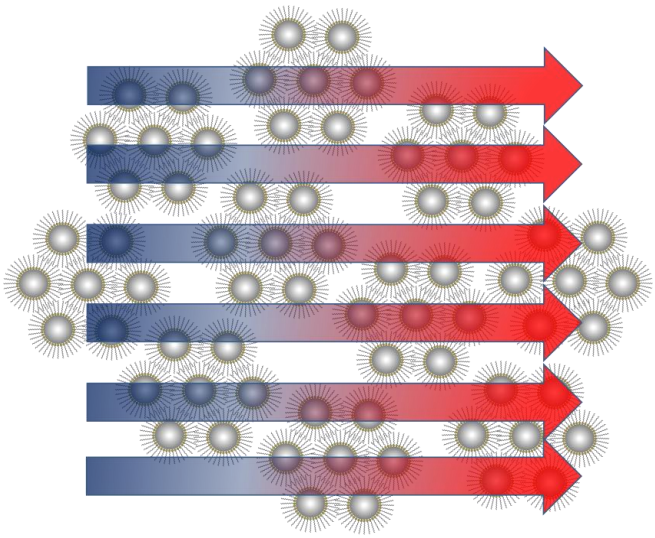

Figure 5.14. Schematic representation of the heat transfer through the clusters at higher concentration of the nanoparticles in a fluid. The arrows indicate the direction of heat flow.

Even in the absence of a magnetic field, there is a possibility for self-assembly of magnetic nanoparticles due to the small magnetic interaction induced by the magnetic nanoparticles.[49] The formation of the clusters/aggregates due to the van der Waals interaction in addition to the weak magnetic interaction could be the reason for observed enhancement in the thermal conductivity at higher concentration (>1.6 vol %). Philip *et al*[46] reported that the formation of small clusters (dimers and trimers) in the nanofluid containing oleic acid coated nanoparticles is responsible for the thermal conductivity enhancement at higher concentrations. The absence of any appreciable change in the thermal conductivity, at lower concentrations (<1.6 volume%), is likely to be due to the large separation between the particles (less van der Waals interaction as well as magnetic interaction) in the dilute dispersion and above a critical concentration, the particles come close together and effectively contribute to the thermal conductivity.

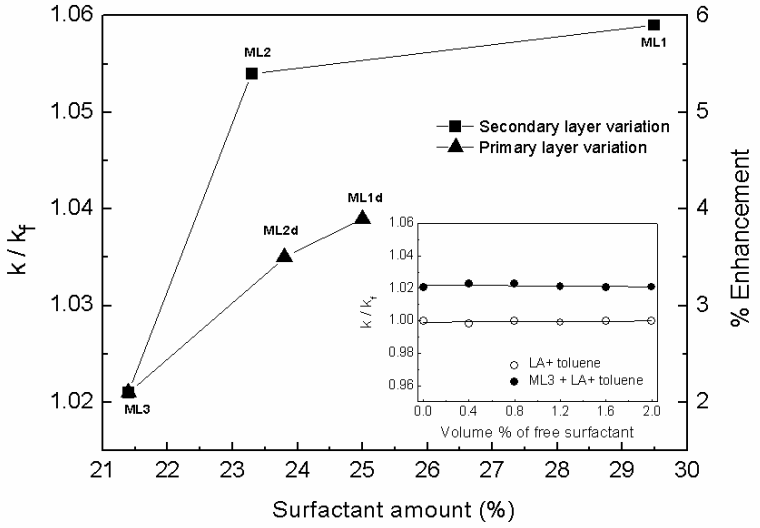

Figure 5.15. Variation of the relative thermal conductivity (filled squares and triangles) and as a function of the total amount of surfactant present on the nanoparticles surface. Inset shows the variation of relative thermal conductivity with the excess amount of surfactant added to the fluid sample ML3 (filled circles) and base fluid (open circles)

To study the effect of the amount of primary and secondary surfactants, thermal conductivity studies are made on nanofluids of ML1, ML2, ML3, ML2d, and ML1d, dispersed at 2.2 volume% in toluene. The experimental thermal conductivity ratio (k/k_f) for the different samples is plotted against the amount of total surfactant on the nanoparticles' surface (Figure 5.15). The observed percentage enhancements in the thermal conductivity of the nanofluid samples ML1, ML2, and ML3 over the base fluid (toluene) are 2.1%, 5.4%, and 5.9%, respectively (filled squares in Figure 5.15). For lower amount of the surfactant present, the enhancement in the thermal conductivity is relatively low. The amount of the primary surfactant being the same for all three samples, the enhancement in the thermal conductivity is mainly contributed by the secondary surfactant, where the thermal conductivity increases with increasing amount of the secondary surfactant. A non-linear increase of the enhanced thermal conductivity, with a saturation trend at higher amount of the surfactant, is observed. Figure 5.15 also compares the thermal conductivity enhancement of the dispersion ML3 with that of the samples (ML1d and ML2d) washed after a time delay of five minutes (filled triangles in Figure 5.15). The thermal conductivities of ML1d (3.9%) and ML2d (3.5%) with relatively larger amount of the surfactant are larger than that of ML3 (2.1%), as in the case of the first series. However, there is a large difference in the thermal conductivity enhancement

for the same samples washed immediately and after a delay. For example, the total amount of the surfactant is comparable for ML2 and ML2d, whereas there is a difference in the amounts of primary and secondary surfactants. The thermal conductivity enhancement is relatively lower for ML2d, compared to that of ML2. Similarly, for ML1d also, the thermal conductivity enhancement is relatively lower. The difference between the two sets of samples (washed immediately and after a delay of five minutes) is that the amount of the secondary surfactant is relatively lower for the latter fluids which are found to be more stable.

To verify that the observed enhancement in the thermal conductivity with increasing amount of the secondary surfactant is not due to larger amount of free surfactant present in the fluid, experiments are carried out by adding excess amount of the surfactant in the dispersion of ML3 having lower amount of the secondary surfactant. The results of the thermal conductivity measurements on the base fluid and the fluid containing ML3, after adding increasing amounts of excess free surfactant, are shown in the inset in Figure 5.15. There is no change in the thermal conductivity when excess free surfactant is present and thus, the results show that there is negligible effect on the thermal conductivity when excess free surfactant is present in the fluid, and that the enhanced thermal conductivity is due to the role or contribution of the secondary surfactant.

The large enhancement in the thermal conductivity for the fluids of ML1 and ML2 (among the first set of samples) than that of ML3 can be explained on the basis of the dispersing character of the samples. The more hydrophilic character for the samples ML1 and ML2 arises due to the large amount of the secondary surfactant and these samples showed poor dispersibility in the non-polar solvent (toluene). Due to the less amount of the secondary surfactant on the surface of the nanoparticle in ML3 showed better dispersion in the non-polar solvent due to the more hydrophobic nature of the surface of the nanoparticle. Thus, the well dispersed fluid of ML3 shows much less thermal conductivity enhancement than that for the relatively poorly dispersed fluids of ML1 and ML2. It has been reported that well dispersed stable nanofluids without any aggregation show less enhancement in the thermal conductivity than the fluids containing aggregated nanoparticles.[46,53] Due to the poor dispersion of the samples ML1 and ML2, the nanoparticles have less interaction with the solvent molecules and could form large aggregates and slow sedimentation of these aggregates are possible. The relatively larger enhancement in the thermal conductivity for these samples could be due to the heat transfer through the large aggregates. The close arrangement of the less dispersible solid nanoparticles might form highly conductive

percolation path like an aggregated solid structure.[54] The less dispersible and highly thermal conductive solid structures (7 W/mK)[55] with surfactants (0.16 W/mK)[56] in the base fluid (0.132 W/mK)[57] initially showed large enhancement in the thermal conductivity which reduced after sedimentation.

Even though the amount of the secondary surfactant is the same in the second set of samples (Table 5.3), whose fluids are stable, the dispersions of ML2d and ML1d show relatively larger enhancement in the thermal conductivity than that of ML3. The amount of the primary surfactant in these samples increases in the order ML3 < ML2d < ML1d, and the thermal conductivity also increases in the same order. The large amount of the primary surfactant on the surface of the nanoparticle makes the particles more wet, due to the larger surfactant-solvent interaction (more hydrophobicity). The increased wetting of the nanoparticles due to the more hydrophobic organic layer reduces the Kapitza resistance (interfacial thermal resistance), increasing the efficiency of heat transfer.[58] Moreover, formation of clusters at higher concentrations, for the sample with more primary surfactants (ML1d), is possible due to the larger hydrophobic interaction and interdigitation of the alkyl chain between the particles. This sort of small clusters in a stable nanofluid could increase the thermal conductivity of the nanofluid.

5.4.3. Thermal conductivity in a magnetic field

Thermal conductivity of the different fluids is measured in the presence of a magnetic field. Previous studies have shown that thermal conductivity of magnetic nanofluids can be enhanced by the application of an external magnetic field parallel to the temperature gradient.[59, 60] As shown in Figure 5.16, the thermal conductivity ratio increases at higher magnetic fields for all the fluid samples. However, the degree of enhancement is quantitatively different for the samples with different amounts of secondary surfactants on the surface. Fluids of ML1 and ML2 with relatively larger amount of the secondary surfactant (partially hydrophilic surface) do not show any enhancement in the thermal conductivity up to a field of 0.1 T and also show lesser enhancement in the thermal conductivity at higher fields, even though theses fluids (ML1 and ML2) showed larger thermal conductivity enhancement at zero field (Figure 5.16(a)). On the other hand, even though the dispersion of ML3 shows much less thermal conductivity enhancement at zero field, higher thermal conductivity is observed at relatively lower fields (~0.05 T). This difference in the effect of

the magnetic field on the thermal conductivity between the different fluids is clearly seen in the inset of Figure 5.16(a), where the thermal conductivity enhancement at zero field is normalized. The observed total enhancements from H = 0 to 0.16 T for the fluids ML1 and ML2 are 3.5% and 3.2% respectively, whereas at the same field, ML3 shows an enhancement of nearly 8.0%. Similarly, the highly dispersive samples (fluids of ML1d and ML2d) show enhancement at lower field (~0.05T) similar to sample ML3 (Figure 5.16(b)). The observed total enhancement at 0.16 T for the fluids ML3, ML2d and ML1d are 8.0%, 6.5% and 11.6%, respectively (Figure 5.16(b)).

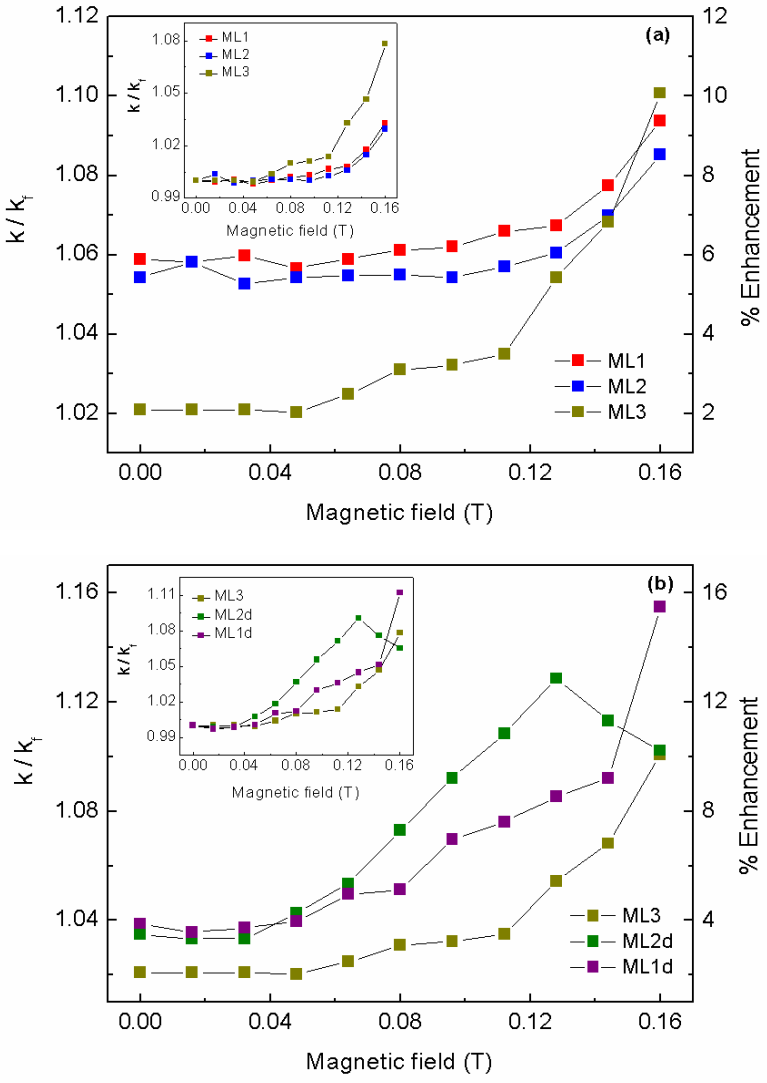

Figure 5.16. Variation of the thermal conductivity of lauric acid coated fluids with applied magnetic field. (a) samples containing different amounts of secondary surfactant (set 1) and (b) samples containing different amounts of primary surfactant (set 2). Insets show normalized relative thermal conductivity.

From a comparison of the enhancement of the thermal conductivity in the magnetic field, it is clear that nanoparticles with lower amounts of the secondary surfactant, which are more dispersible with hydrophobic nature of the surface (ML3, ML2d and ML1d) show relatively larger enhancement in the thermal conductivity in a magnetic field without any settling of the nanoparticles in the base fluid. The larger enhancement in the thermal conductivity for fluids with relatively less amount of the total surfactant (ML3 and ML2d) on the surface of the nanoparticles is due to the easy response of the magnetic nanoparticles in the presence of a magnetic field. The observed enhancement in the thermal conductivity by increasing the magnetic field is due to reversible aggregation of the magnetic nanoparticles in the direction of the magnetic field (parallel to the temperature gradient).[59, 61] In the absence of magnetic field, the magnetic dipoles are oriented randomly due to the large thermal energy (k_BT) over the dipole interaction energy ($U_d(ij)$) between the particles. By increasing the magnetic field, the magnetic dipoles in the magnetic nanoparticles start to orient in the direction of the magnetic field due to the increasing dipole interaction energy ($U_d(ij)$).[1] At higher magnetic fields, the magnetic dipole interaction energy ($U_d(ij)$) dominates over the thermal energy (k_BT) and forms reversible chain like aggregation which reduces the convection contribution to the thermal conductivity enhancement. The aspect ratio of the aggregated chain structures increases with increasing the strength of the applied magnetic field and heat energy is transferred through the aggregated chain of the nanoparticles.[62] In the case of ML2, despite the fact that the total surfactant amount is low (≈ML2d, see Table 5.3), less enhancement in the thermal conductivity is observed in the presence of a magnetic field. This is probably due to the presence of more secondary surfactant layer which reduces the dispersibility. Due to the low dispersibility (less compatibility of the surface with the solvent) of the nanoparticles, larger aggregates may form in the presence of the magnetic field, creating discontinuity in the chain like structure which leads to less enhancement in the thermal conductivity. This is also the probable reason for the reduced variation of the thermal conductivity with magnetic field for ML1 and ML2. In the case of ML1d, even though the total amount of surfactant is relatively larger, good response to the magnetic field is obtained, probably due to the less amount of the secondary surfactant layer which makes the particles highly dispersive (more hydrophobic and compatibility of the surface with solvent molecules) in the non-polar solvent.[41] Even though fluids of ML1 and ML2 showed sedimentation when kept aside for a week, no such effect was observed after applying a field on fresh fluids, even after repeated measurements. For example, as shown in Figure 5.17, the thermal conductivity

remains almost the same (within the error of the measurement) after repeated measurements on ML2.

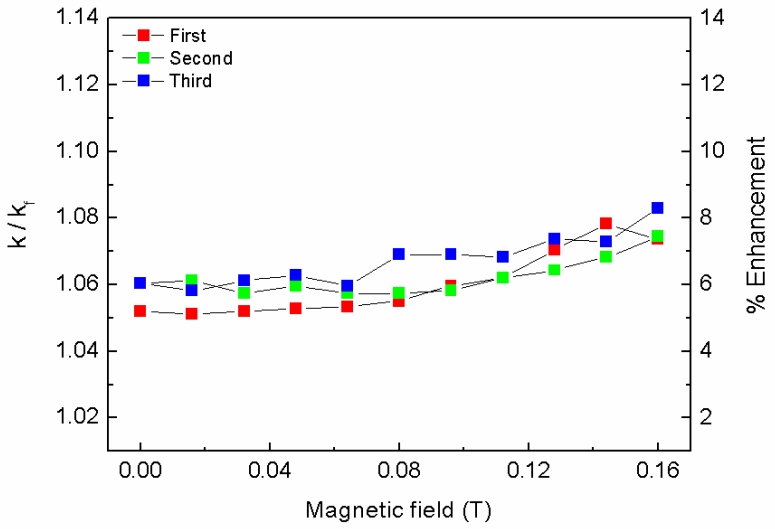

Figure 5.17. Repeated measurements of the thermal conductivity of the fluid of ML2 as a function of applied magnetic field.

The observed enhancement in the thermal conductivity in the presence of a magnetic field is less than that reported in the literature. For example, Philip *et al*[46] reported 125% enhancement in the thermal conductivity, in a magnetic field of 0.038 T, for 1.71 volume% of the 6.7 nm magnetite nanoparticles coated with oleic acid and dispersed in kerosene. Although the size of the magnetite nanoparticles used in the present study is comparable with the size reported in the literature, the observed large difference in the experimental thermal conductivity in the presence of a magnetic field could be due to various factors such as the difference in the particle size distribution, size and nature of the surfactant molecules (lauric vs oleic acid), the solvent used (toluene vs kerosene), the interaction between the surfactant and the solvent, the difference in the dispersibility of the coated nanoparticles and compatibility of the solvent with the primary/secondary surfactant on the surface of the nanoparticles, etc. More studies, using different surfactants and solvents, with controlled amount of the primary and secondary surfactants, are required to understand the difference between the results in the present study and the reported values.

5.4.4. Viscosity

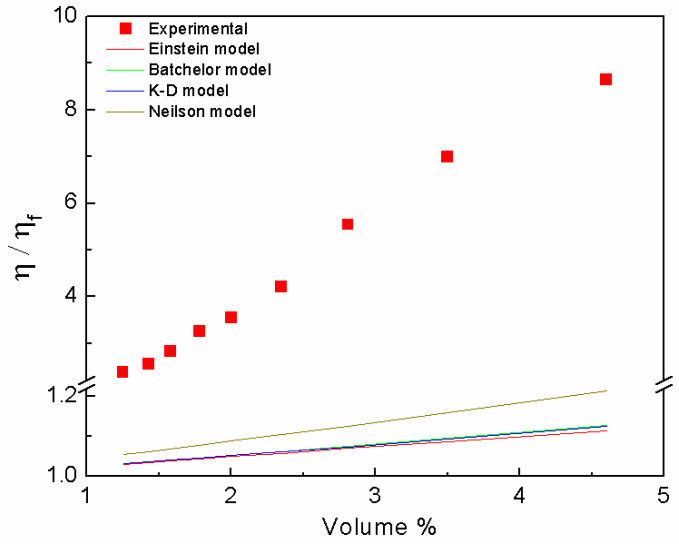

Figure 5.18. The variation of the relative viscosity with respect to the volume% of the particles (red squares) is compared with the theoretical models (solid lines)

Viscosity of the iron oxide nanoparticles of ML1d dispersed in toluene is measured as a function of the volume% of the particles to compare and correlate the changes in the thermal conductivity with viscosity. A corresponding increase in the viscosity of the dispersion is observed at higher concentrations, similar to the changes in the thermal conductivity, as shown in the Figure 5.18 (red squares). A similar increase in the viscosity with volume% is reported for Fe_3O_4 based nanofluids dispersed in aqueous[63] and non-aqueous[59] medium. The experimental viscosity is compared with the values calculated using different theoretical models as discussed in the chapter 3 (section 3.4.4). The calculated values of relative viscosity (η/η_f), using the theoretical models, show much lower enhancement compared to the experimental values (solid lines in the Figure 5.18). Thus, the increase in the viscosity of the nanofluid could be due to the contribution from various factors in addition to the volume% effect such as, increase in the hydrodynamic diameter due to the fatty acid surfactant, the cluster/aggregate formation due to the van der Waals interaction between the particles and between the surfactant molecules**,** interparticle magnetic interaction between the nanoparticles, and interdigitation of the surfactant alkyl chain with the surfactants in the neighboring particles at higher concentrations.[63] Since the particle size and hydrodynamic size do not vary with volume fraction, increase in the van der Waals and magnetic dipole

interactions with the volume% of the particles could form clusters/aggregation of nanoparticles in the fluid leading to a larger increase in the viscosity than that predicted by the theoretical models. In the same way, the small cluster/aggregate formation could be the reason for the enhancement in the thermal conductivity after the critical volume% (>1.6%) of the particles.[59]

The enhancement in the viscosity ratio for different fluids, plotted against the total amount of the surfactant present on the surface of nanoparticles, is shown in Figure 5.19 (open squares and open triangles). An increase in the viscosity with the increase in the amount of surfactant on the surface of the nanoparticles is observed. The enhancement in the viscosity, with increasing amount of the surfactant, can be attributed to the increase in the hydrodynamic size of the nanoparticles in the fluid. The increase in the hydrodynamic size reduces the Brownian motion of the nanoparticles in the fluid.[64] Also, the lower dispersibility of the nanoparticles increases the viscosity of the fluid. The fluids with less surfactant on surface of the nanoparticles (ML3, ML2d) show less enhancement in the viscosity and the fluids with more surfactant (ML1d, ML1) on the nanoparticles show relatively larger enhancement in the viscosity. However, the fluid of the particles having a relatively low amount of the surfactant ML2 (≈ML2d) shows large enhancement in the viscosity, probably due to the presence of more secondary surfactant molecules which make the particles less dispersible in the non-polar solvent. The less dispersible nature of the nanoparticles increases the viscosity of the fluid.

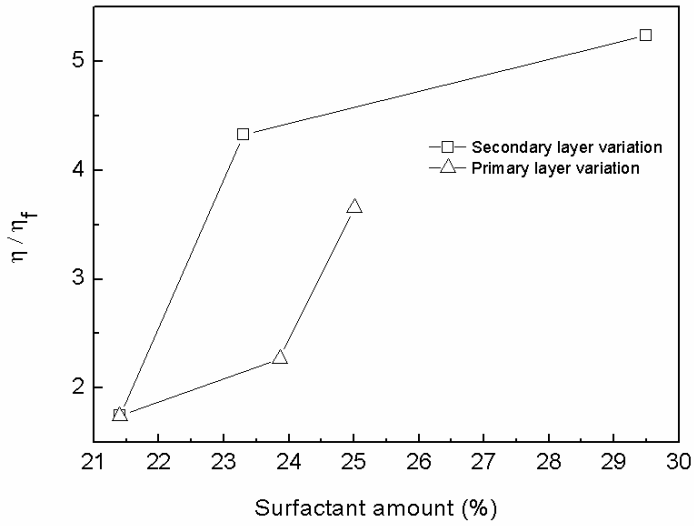

Figure 5.19. Variation of the relative viscosity with the surfactant amount for first set of samples (open squares) and second set of samples (open triangles)

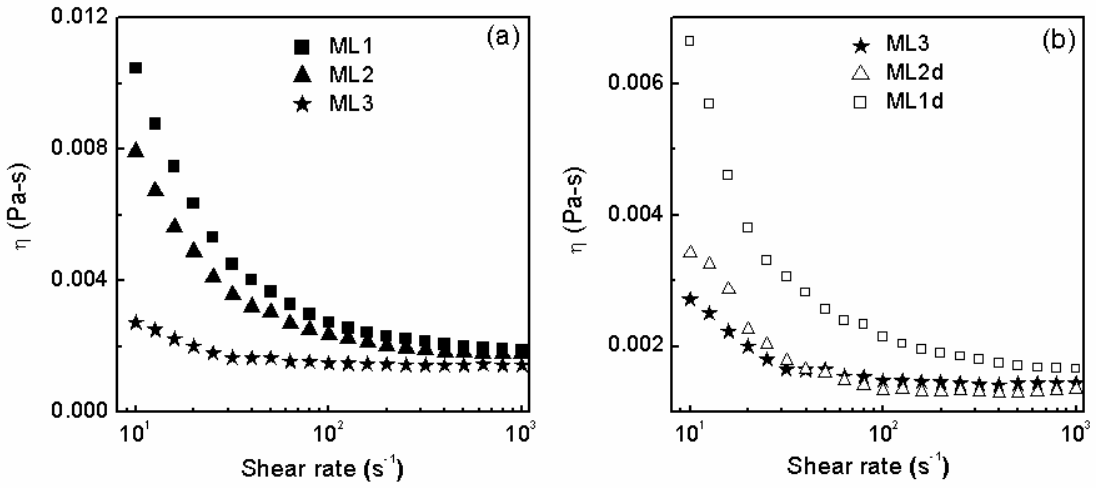

Figure 5.20. Variation of viscosity with shear rate for the two different sets of fluid samples, (a) set 1 and (b) set 2.

The shear viscosity of the different magnetic fluids as a function of shear rate is shown in Figure 5.20. The viscosity of all the fluids decreases with increasing shear rate indicating shear thinning behavior. Fluids with larger amounts of total surfactant on the nanoparticles' surface show higher viscosity at lower shear rate than the samples with less amount of surfactant. At higher shear rate, all the fluids show comparable viscosity. The samples with larger amount of the surfactant show shear thinning behavior up to 60 s^{-1} and after that the sample behave like a Newtonian fluid. The presence of the secondary surfactant layer on the surface makes the particles less dispersible in the non-polar solvent and therefore the fluids show higher viscosity at low shear rate. The samples with less secondary surfactant are highly dispersible and they show lower viscosity even at lower shear rate. This shows the Newtonian behavior of the fluid samples even at lower shear rate which require less pumping power and this will be useful for many applications.

5.5. Conclusions

Lauric acid coated magnetite nanoparticles with different amounts of surfactant on the surface of the particles are prepared by controlled washing of the as-synthesized nanoparticles containing excess surfactant. TGA studies indicated the presence of primary and secondary surfactant layers and the varying amount of the primary/secondary surfactant

after washing with acetone-hexane solvent mixture of different polarity. IR spectroscopy studies confirmed the presence of secondary surfactant layer along with the primary surfactant attached to the nanoparticle surfaces. Magnetic measurements confirmed the superparamagnetic nature of the particles and that the particles are effectively coated by the surfactant. Nanoparticles with less secondary surfactant showed stable dispersion in toluene compared to the samples having more secondary surfactant. Relatively larger enhancement in the thermal conductivity and viscosity is observed for the samples with higher amounts of the secondary surfactant. The larger enhancement in the thermal conductivity for less stable fluids is probably due to the heat transfer through the large aggregated nanostructures. The larger viscosity for the less stable fluids could be due to the increased hydrodynamic diameter and largely aggregated nanoparticles in the fluid.

The overall results suggested that the amount of the secondary surfactant as well as the compatibility between the nanoparticle surface (the free end group of the surfactant) and the solvent is very crucial in determining the stability which in turn affects the thermal conductivity of the studied nanofluids. It is found that the fluids with larger amounts of the secondary surfactant are relatively less stable whereas they showed larger enhanced thermal conductivity and viscosity. Moreover, these fluids show less response to applied magnetic fields due to the large amount of the non-magnetic layer on the nanoparticle surfaces, leading to less enhancement in the thermal conductivity in a magnetic field. The stable fluids showed relatively lower enhancement in the thermal conductivity as well as viscosity, due to the highly dispersive nature of the nanoparticles in the absence of the magnetic field, but these fluids showed large enhancement in the thermal conductivity due to the easy response to the magnetic field. Thus, the changes in the thermal conductivity and viscosity may be correlated with the dispersibility of the nanoparticles in the base fluid, apart from the amount of the surfactant, which is found to be different for the different samples. Thus, the considerable variation in the thermal conductivity ratio and dispersibility of the fluid samples with same volume% of particles must be due to the different surfactant structures on the surface of the nanoparticles.

References

1. Mendelev, V. S.; Ivanov, A. O. *Phys. Rev. E* **2004**, *70*, 051502.
2. Saterlie, M. S.; Sahin, H.; Kavlicoglu, B.; Liu, Y.; Graeve, O. A. *Chem. Mater.* **2012**, *24*, 3299-3306.
3. Murshed, S. M. S.; de Castro, C. A. N.; Lourenço, M. J. V. *J. Nanofluids* **2012**, 1, 175-179.
4. Vekas, L.; Bica, D.; Marinica, O. *Rom. Rep. Phys.* **2006**, *58*, 257-267.
5. Avdeev, M. V.; Bica, D.; Vékás, L.; Marinica, O.; Balasoiu, M.; Aksenov, V. L.; Rosta, L.; Garamus, V. M.; Schreyer, A. *J. Magn. Magn. Mater.* **2007**, *311*, 6-9.
6. Yee, C.; Kataby, G.; Ulman, A.; Prozorov, T.; White, H.; King, A.; Rafailovich, M.; Sokolov, J.; Gedanken, A. *Langmuir* **1999**, *15*, 7111-7115.
7. Lee, K. M.; Kim, S. G.; Kim, W. S.; Kim, S. S. *Korean J. Chem. Eng.* **2002**, *19*, 480-485.
8. Zhang, Y.; Kohler, N.; Zhang, M. *Biomaterials* **2002**, *23*, 1553-1561.
9. Schöpf, B.; Neuberger, T.; Schulze, K.; Petri, A.; Chastellain, M.; Hofmann, M.; Hofmann, H.; von Rechenberg, B. *J. Magn. Magn. Mater.* **2005**, *293*, 411-418.
10. Zhi, J.; Wang, Y.; Lu, Y.; Ma, J.; Luo, G. *React. Funct. Polym.* **2006**, *66*, 1552-1558.
11. Sahoo, Y.; Goodarzi, A.; Swihart, M. T.; Ohulchanskyy, T. Y.; Kaur, N.; Furlani, E. P.; Prasad, P. N. *J. Phys. Chem. B.* **2005**, *109*, 3879-3885.
12. Sreeja, V.; Jayaprabha, K. N.; Joy, P. A. *Appl. Nanosci.* **2015**, *5*, 435-441.
13. Sun, S.; Zeng, H. *J. Am. Chem. Soc.* **2002**, *124*, 8204-8205.
14. Park, J.; An, K.; Hwang, Y.; Park, J. G.; Noh, H. J.; Kim, J. Y.; Park, J. H.; Hwang, N. M.; Hyeon, T. *Nat. Mater.* **2004**, *3*, 891-895.
15. Zhang, L.; He, R.; Gu, H.-C. *Appl. Surf. Sci.* **2006**, *253*, 2611-2617.
16. Hajdú, A.; Illés, E.; Tombácz, E.; Borbáth, I. *Colloids Surf., A* **2009**, *347*, 104-108.
17. Tombácz, E.; Bica, D.; Hajdú, A.; Illés, E.; Majzik, A.; Vékás, L. *J. Phys.: Condens. Matter* **2008**, *20*, 204103.
18. Lee, D.; Kim, J.-W.; Kim, B. G. *J. Phys. Chem. B.* **2006**, *110*, 4323-4328.
19. Shen, L. F.; Laibinis, P. E.; Hatton, T. A. *Langmuir* **1999**, *15*, 447-453.
20. Prakash, A.; Zhu, H. G.; Jones, C. J.; Benoit, D. N.; Ellsworth, A. Z.; Bryant, E. L.; Colvin, V. L. *ACS Nano* **2009**, *3*, 2139-2146.
21. Shen, L. F.; Laibinis, P. E.; Hatton, T. A. *J. Magn. Magn. Mater.* **1999**, *194*, 37-44.

22. Wang, X. M.; Zhang, C. N.; Wang, X. L.; Gu, H. C. *Appl. Surf. Sci.* **2007**, *253*, 7516-7521.
23. Filippousi, M.; Angelakeris, M.; Katsikini, M.; Paloura, E.; Efthimiopoulos, I.; Wang, Y. J.; Zambouis, D.; Van Tendeloo, G. *J. Phys. Chem. C* **2014**, *118*, 16209-16217.
24. Guardia, P.; Batlle-Brugal, B.; Roca, A. G.; Iglesias, O.; Morales, M. P.; Serna, C. J.; Labarta, A.; Batlle, X. *J. Magn. Magn. Mater.* **2007**, *316*, E756-E759.
25. Felicia, L. J.; Johnson, J. C.; Philip, J. *J. Nanofluids* **2014**, *3*, 328-335.
26. Yuan, Y.; Rende, D.; Altan, C. L.; Bucak, S.; Ozisik, R.; Borca-Tasciuc, D. A. *Langmuir* **2012**, *28*, 13051-13059.
27. Younes, H.; Christensen, G.; Luan, X. N.; Hong, H. P.; Smith, P. *J. Appl. Phys.* **2012**, 111, 64308.
28. Fu, L.; Dravid, V. P.; Johnson, D. L. *Appl. Surf. Sci.* **2001**, *181*, 173-178.
29. Regmi, R.; Black, C.; Sudakar, C.; Keyes, P. H.; Naik, R.; Lawes, G.; Vaishnava, P.; Rablau, C.; Kahn, D.; Lavoie, M.; Garg, V. K.; Oliveira, A. C. *J. Appl. Phys.* **2009**, *106*, 113902.
30. Nowak, J.; Wiekhorst, F.; Trahms, L.; Odenbach, S. *J. Phys.: Condens. Matter* **2014**, 26, 176004.
31. Vekas, L.; Bica, D.; Gheorghe, D.; Potencz, I.; Rasa, M. *J. Magn. Magn. Mater.* **1999**, *201*, 159-162.
32. Patel, H. E.; Das, S. K.; Sundararajan, T.; Sreekumaran Nair, A.; George, B.; Pradeep, T. *Appl. Phys. Lett.* **2003**, *83*, 2931-2933.
33. Gnanaprakash, G.; Ayyappan, S.; Jayakumar, T.; Philip, J.; Raj, B. *Nanotechnology* **2006**, *17*, 5851-5857.
34. Sahoo, Y.; Pizem, H.; Fried, T.; Golodnitsky, D.; Burstein, L.; Sukenik, C. N.; Markovich, G. *Langmuir* **2001**, *17*, 7907-7911.
35. Muthukumaran, T.; Gnanaprakash, G.; Philip, J. *J. Nanofluids* **2012**, *1*, 85-92.
36. Zhao, S. Y.; Lee, D. K.; Kim, C. W.; Cha, R. G.; Kim, Y. H.; Kang, Y. S. *Bull. Korean Chem. Soc.* **2006**, *27*, 237-242.
37. Cullum, D. Introduction to Surfactant Analysis; Springer, 1994.
38. Waldron, R. D. Phys. Rev. **1955**, 99, 1727-1735
39. Gnanaprakash, G.; John, P.; Jayakumar, T.; Baldev, R. *J. Phys. Chem. B.* **2007**, *111*. 7978-7986
40. Ding, X.; Bao, L.; Jiang, J.; Gu, H. *RSC adv.* **2014**, *4*, 9314-9320.
41. Yang, K.; Peng, H.; Wen, Y.; Li, N. *Appl. Surf. Sci.* **2010**, *256*, 3093-3097.

42. Lenin, R.; Joy, P. A. *J. Nanofluids* **2015**, *4*, 310-317.
43. Jayaprabha, K. N.; Joy, P. A. *RSC adv*. **2015**, 5, 22117-22125.
44. Sreeja, V.; Joy, P. *Int. J. Nanotechnol.* **2011**, *8*, 907-915.
45. Zheng, R. K.; Gu, H. W.; Zhang, B.; Liu, H.; Zhang, X. X.; Ringer, S. P. *J. Magn. Magn. Mater.* **2009**, *321*, L21-L27.
46. Philip, J.; Shima, P.; Raj, B. *Nanotechnology* **2008**, 19, 305706.
47. Maxwell, J. C. A Treatise on Electricity and Magnetism. *Clarendon press* **1881**, *1*.
48. Prasher, R.; Bhattacharya, P.; Phelan, P. *Phys. Rev. Lett.* **2005**, *94*, 025901.
49. Wei, J.; Liqiu, W. *J. Appl. Phys.* **2010**, *108*, 114311.
50. Lalatonne, Y.; Richardi, J.; Pileni, M. P. *Nat. Mater.* **2004**, *3*, 121-125.
51. Sau, T. K.; Murphy, C. J. *Langmuir* **2005**, 21, 2923-2929.
52. Wang, J. C.; Neogi, P.; Forciniti, D. *J. Chem. Phys.* **2006**, 125, 194717.
53. Angayarkanni, S. A.; Philip, J. *J. Nanofluids* **2014**, 3, 17-25.
54. Prasher, R.; Phelan, P. E.; Bhattacharya, P. *Nano Lett.* **2006**, *6*, 1529-1534.
55. Eapen, J.; Rusconi, R.; Piazza, R.; Yip, S. *J. Heat Transfer* **2010**, *132*, 102402.
56. Cabeza, L. F.; Castell, A.; Barreneche, C.; De Gracia, A.; Fernández, A. *Renewable Sustainable Energy Rev.* **2011**, *15*, 1675-1695.
57. Kauffman, G. W.; Jurs, P. C. *J. Chem. Inf. Comput. Sci.* **2001**, *41*, 408-418.
58. Vladkov, M.; Barrat, J.-L. *Nano Lett.* **2006**, *6*, 1224-1228.
59. Philip, J.; Shima, P. D.; Raj, B. *Appl. Phys. Lett.* **2007**, *91*, 203108.
60. Krichler, M.; Odenbach, S. *J. Magn. Magn. Mater.* **2013**, 326, 85-90.
61. Shima, P. D.; John, P. *J. Phys. Chem. C* **2011**, *115*, 20097-20104.
62. Shima, P. D.; Philip, J.; Raj, B. *Appl. Phys. Lett.* **2009**, *94*, 223101.
63. Murshed, S. M. S.; Leong, K. C.; Yang, C. *Int. J. Therm. Sci.* **2008**, *47*, 560-568.
64. Fischer, B.; Huke, B.; Lücke, M.; Hempelmann, R. *J. Magn. Magn. Mater.* **2005**, *289*, 74-77.

Chapter 6

Effect of unsaturation and conformation of surfactant on the thermal conductivity of magnetite nanofluids

Abstract

Magnetic nanoparticles are coated with long-chain fatty acids containing the same number of carbon atoms but with differing degree of unsaturation in the alkyl chain (stearic acid $C_{18}H_{36}O_2$, oleic acid $C_{18}H_{34}O_2$, linoleic acid $C_{18}H_{32}O_2$ and linolenic acid $C_{18}H_{30}O_2$). The coated nanoparticles are dispersed in toluene for thermal conductivity and viscosity measurements. Viscosity studies on the fluids showed larger variation in the viscosity for saturated fatty acid coated fluid and less variation for unsaturated fatty acid coated fluids. The variation in the thermal conductivity and viscosity of the fluids with different surfactants is attributed to the conformation of the surfactant molecules. Due to the bend and hook structures of linoleic and linolenic acid, these fatty acids coated samples form less aggregation of particles in the fluid, whereas due to the straight and kink structures of the stearic and oleic acids on the coated samples, they form clusters/aggregated/self-assembled nanoparticles due to the large hydrophobic interaction between the alkyl chains. The aggregated nanoparticles in the corresponding nanofluids strongly influence the magnetic as well as thermophysical properties of the fluids. The aggregated nanoparticles in the nanofluids show increase in the thermal conductivity and viscosity, whereas the samples with highly dispersed and separated particles shows less enhancement in the thermal conductivity and viscosity.

6.1. Introduction

Fatty acids are the most widely used surfactants for stabilizing magnetite nanoparticles in aqueous as well as non-aqueous medium, and surfactants play an important role in stabilizing the nanoparticles from aggregation or clustering.[1-2] Monolayer fatty acid surfactant coated magnetic nanoparticles dispersed in non-polar solvents stabilize the nanoparticles through the long hydrophobic chain. The head group of the fatty acid is attached to the surface of the nanoparticles and the tail hydrocarbon chain is extended into the solvent. Steric stabilization due to the long hydrophobic chain reduces magnetic dipole-dipole interaction and van der Waals attraction between the magnetic nanoparticles by separating the particles away from each other. The surfactant coated magnetic nanoparticle form a stable magnetic fluid and the magnetic nanoparticles in the nanofluid could form reversible aggregation in the presence of a magnetic field, and the thermophysical properties can be tuned by the varying the magnetic field.[3] The directed assembly of magnetic dipoles of magnetic nanoparticles in the presence of an applied magnetic field has been found to be responsible for anisotropic thermal conductivity in magnetic fluids.[4]

Philip *et al*[5] observed large enhancement (300%) in the thermal conductivity over the base fluid by using oleic acid coated magnetite nanoparticles dispersed in kerosene in the presence of a small magnetic field (8.2 mT). The authors have attributed the observed large enhancement in the thermal conductivity to the formation of chain like arrangements (aggregation) of nanoparticles in the direction of the applied magnetic field and the heat energy transferred through the back bone of the chain. Altan *et al*[6] studied the thermal conductivity of decanoic (capric) acid coated magnetite nanoparticles dispersed in water and heptane. The authors observed linear enhancement in the thermal conductivity with magnetic field at low concentrations and at low magnetic fields. It has been argued that the enhancement in the thermal conductivity is not due to the nanoparticle chain formation because the used nanoparticle concentration is much lower for the chain formation. Therefore, it is concluded that the enhancement in the thermal conductivity is due to the thermomagnetic convection in the nanofluid in the presence of the magnetic field. In the former case, the magnetite nanoparticles are coated with unsaturated fatty acid (18 carbon oleic acid with kink at 9^{th} carbon atom) and in the latter case, the magnetite nanoparticles are coated with a saturated fatty acid (capric acid with 10 carbon straight chain). The observed conflicting reports on the changes in the thermal conductivity with magnetite nanoparticles

stabilized with two different surfactants suggests that probably the nature of surfactant at the interface could play an important role in the thermophysical properties of the magnetic nanofluids.

Unlike the directed assembly,[7] self-assembly of magnetic nanoparticles in a magnetic fluid is possible in the absence of an applied magnetic field, due to the internal forces between the nanoparticles.[8-9] In the case of self-assembly, the nanoparticles align in the direction of the local magnetic field created by the neighboring particles. The dipolar interaction energy ($U_d(ij)$) for thermally fluctuating magnetic moments cannot be negligible when the size of nanoparticle is larger, even with surface coating. But for smaller particles, the magnetic dipole-dipole interaction decreases due to the large thermal fluctuation of the magnetic moments and comparatively less than the van der Waals interaction. For smaller magnetic nanoparticles, the van der Waals interaction contributes more to the self assembly of nanoparticles in a fluid.[10, 11] In a highly concentrated magnetic fluid, the magnetic nanoparticles are close to each other, and the interparticle separation is less than twice the length of the surfactant molecule on the surface of the nanoparticles. The small separation of the magnetic nanoparticles causes interpenetration (interdigitation) of surfactant molecules attached to the neighboring particles, through hydrophobic interaction or van der Waals interaction between the surfactants.[12] In addition to the van der Waals attraction between the particles, the interpenetration of (interdigitation) surfactant molecules attached in the neighboring nanoparticles also causes the self-assembly.[13] The interdigitation of the long alkyl chain and the small magnetic interaction between the particles might form slightly aggregated/cluster (self-assembled) structures in the nanofluid. This slight aggregated structure strongly influences the magnetic and thermophysical properties of the magnetic fluid. The self-assembled surfactant coated magnetic nanoparticles show increase in the magnetic properties than the highly separated particles. Nakata *et al*[14] observed increase in the magnetization and blocking temperature of surfactant coated γ-Fe_2O_3 nanoparticles due to the aggregated and self-assembled nanoparticle chain than the separated particles. Jiang[11] reported that the nature of coating layer has effect on self assembly of nanoparticles in nanofluids and the self assembled structures strongly influence the thermal conductivity of nanofluids. From their studies they concluded that the surface of the nanoparticle is one of the important factors to be considered for thermal conductivity studies other than the nanoparticle and base fluids properties. The influence of interfacial related factors such as surfactants,

nature of surfactant, surfactant conformation and properties etc on thermal conductivity of nanofluids are still need to be studied.

In the present work four different fatty acid coated magnetite nanoparticles are prepared using different fatty acid surfactants with same chain length (18 carbons) and different degree of unsaturation in the carbon chain. The fatty acids, stearic, oleic, linoleic and linolenic acid containing number of unsaturation as 0, 1, 2, and 3 respectively, for surface coating on the magnetite nanoparticle, are used. The fatty acid coated nanoparticles are dispersed in toluene at different volume concentration and used for thermal conductivity and viscosity studies.

6.2. Materials and methods

6.2.1. Materials

Figure 6.1 shows structures of fatty acids used for the surface coating on the surface of the magnetite nanoparticles. Fatty acids used in the present study are all 18 carbon chain with different conformation. The conformation of the stearic (octadecanoic acid), oleic (cis-9-octadecenoic acid), linoleic (cis,cis-9,12-octadecadienoic acid), and linolenic acid (cis,cis,cis-9,12,15-octadecatrienoic acid) are straight, kink, bent and hook structures respectively.

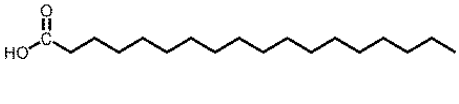

Stearic acid (C18:0)

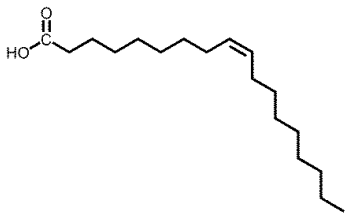

Oleic acid (C18:1(9))

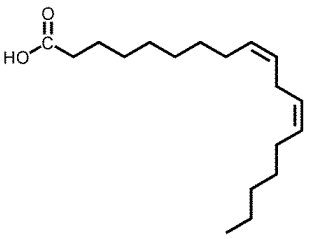

Linoleic acid (C18:2(9, 12))

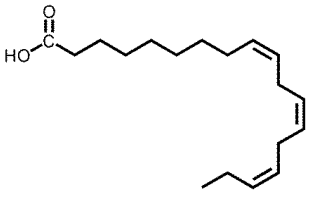

Linolenic acid (C18:3(9, 12, 15))

Figure 6.1: Structure of the different fatty acids used as surfactants[15, 16]

Figure 6.1 shows the structures of the fatty acids used as surfactants in the present study. The number of unsaturation increases from stearic acid to linolenic acid and the double bonds present in the fatty acid molecules are in *cis* configuration. Some of the physical properties of the fatty acids are given in Table 6.1.

Table 6.1. Physical properties of the fatty acids used as surfactants

S. No	Fatty acid	Formula	Melting point (K)[17]	Boiling point (K) (@1mmHg)[18]	Thermal conductivity (W/mK)
1	Stearic acid	$C_{18}H_{36}O_2$	343	500	0.173 (70°C)[20]
2	Oleic acid	$C_{18}H_{34}O_2$	286	496	0.18 (20°C)[21]
3	Linoleic acid	$C_{18}H_{32}O_2$	266	497	0.14 (25°C)[22]
4	Linolenic acid	$C_{18}H_{30}O_2$	263	498	~0.4 (5°C)[23]

6.2.2. Synthesis

Fatty acid coated magnetite nanoparticles are synthesized by the co-precipitation of iron chlorides ($FeCl_3.6H_2O$, $FeCl_2.4H_2O$) using ammonium hydroxide (NH_4OH) in presence of the corresponding fatty acid in the reaction medium. The synthesis procedure is similar to that discussed in the previous chapters. Fatty acid dissolved in acetone (stearic acid was dissolved in 2-propanol) was used for coating and remaining procedure is similar as discussed in section 2.2.2 in chapter 2. After the completion of the reaction, the black precipitate in the reaction medium (in water) was washed with acetone-hexane mixture to remove the excess surfactant on the surface of the nanoparticles (2-propanol-hexane mixture was used for washing the stearic acid coated nanoparticles). The dried powder samples are labelled as given in Table 6.2 and used for further studies.

Table 6.2. Fatty acid surfactants used for coating magnetite nanoparticles and the corresponding sample codes

S. No	Surfactant	Sample code
1	Stearic acid	MST
2	Oleic acid	MOL
3	Linoleic acid	MLE
4	Linolenic acid	MLN

The data for the stearic acid coated sample in the present study is the same as used in the chapter 3 and compared with other fatty acids.

6.3. Characterization of surfactant coated magnetite nanoparticles

6.3.1. Powder X-ray diffraction

Powder X-ray diffraction patterns of the dried powder samples show the formation of spinel phase, as shown in Figure 6.2, confirming the formation of magnetite. The calculated lattice parameter using the PCW software for the samples MST, MOL, MLE and MLN are 8.40Å, 8.38Å, 8.40Å, and 8.37Å respectively, and these values are closer to that of magnetite (8.40 Å), as reported in the literature (JCPDS: #19-0629). The average crystallite size of the synthesized samples is calculated using the Scherrer equation (equation 2.2 in chapter 2) from the width of the major peak corresponding to the (311) plane and is obtained as 7±1 nm for all samples.

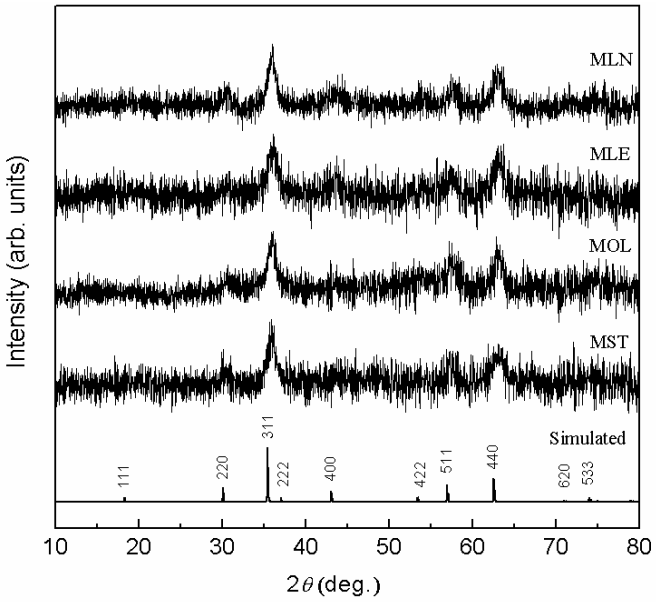

Figure 6.2. Powder XRD patterns of different fatty acid coated magnetite nanoparticles. The simulated pattern of Fe_3O_4 is shown at the bottom

6.3.2. Transmission electron microscopy

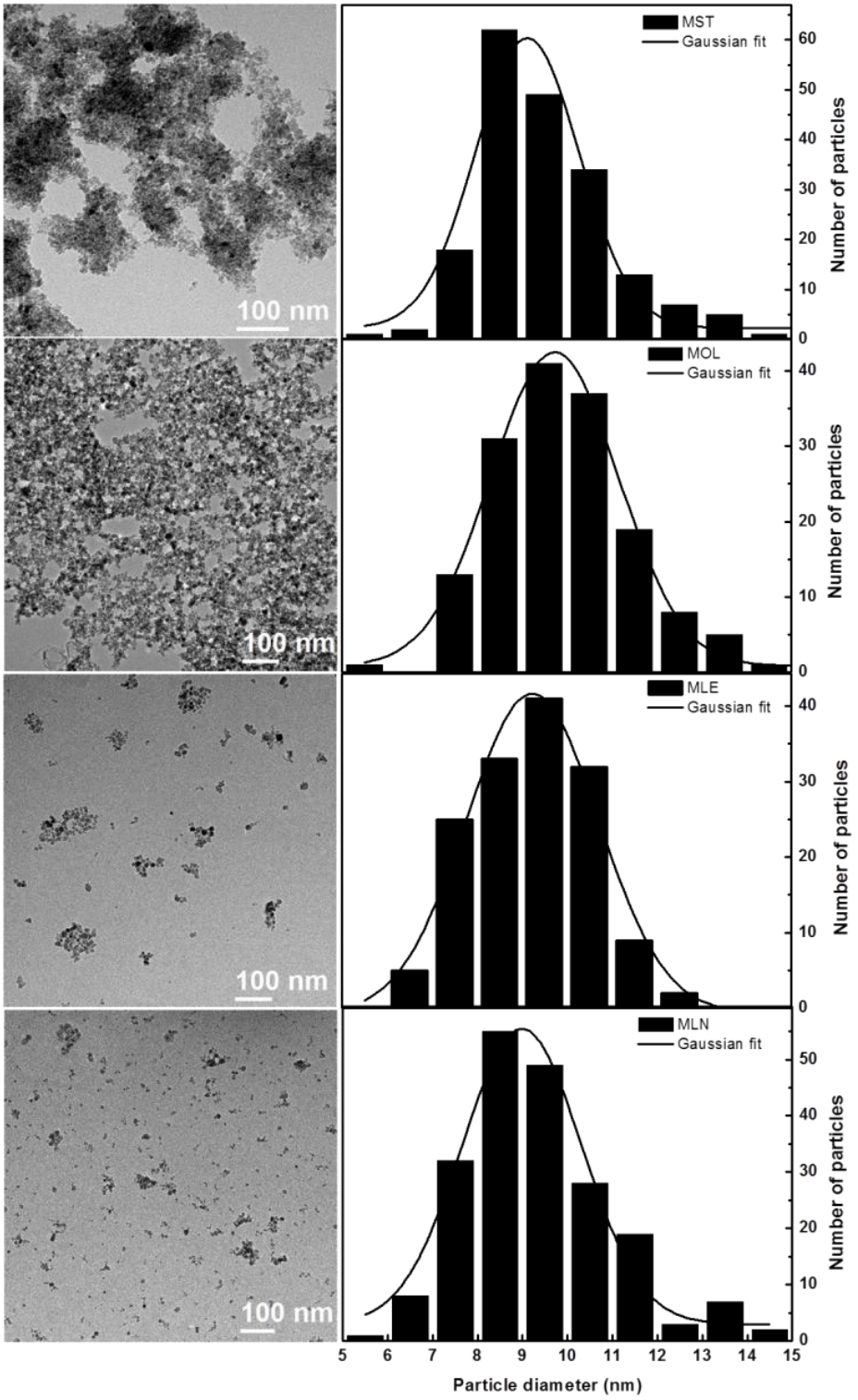

Figure 6.3. TEM images of the fatty acid coated samples and corresponding particle size distribution histogram

The TEM images and the corresponding particle size histograms of the different samples are shown in Figure 6.3. The average particle sizes obtained from the Gaussian fitted histograms are 9.1 nm, 9.7 nm, 9.2 nm and 8.9 nm for MST, MOL, MLE, and MLN, respectively. The size observed from the TEM image is slightly (~2 nm) larger than the crystallite size calculated from the XRD patterns. This could be due to the contribution from the amorphous layer present on the surface of the nanoparticles as well as fatty acid attached to the surface of the nanoparticles. For example, the chain length of stearic acid, oleic acid, linoleic acid and linolenic acid are reported as 2.42 nm, 1.75 nm, 1.2 nm and 1.2 nm respectively.[24-26] The size distribution calculated from the FWHM of the Gaussian fitted curve for all the fatty acid coated samples are shown in the Table 6.3, suggesting comparable particle size distribution. The stearic acid coated sample shows highly aggregated particles in the TEM image and the oleic acid coated sample shows slight aggregation (self-assembled) of the nanoparticles. However, the linoleic and linolenic acid coated samples show well separated particles with small clusters. In all cases, the individual particles are separated from each another due to the surface coating with the fatty acid molecules.

Table 6.3. Lattice parameter, particle sizes and distribution of the coated samples

S. No	Sample	Lattice parameter (Å)	Particle size (±0.5 nm)	Size distribution FWHM (nm)
1	MST	8.40	9.1	2.3
2	MOL	8.38	9.7	2.8
3	MLE	8.40	9.2	2.9
4	MLN	8.37	8.9	2.6

6.3.3. Thermogravimetric analysis

Thermogravimetric analysis of all the fatty acid coated samples shows almost similar weight loss profile (Figure 6.4). The TGA curves of the fatty acid coated samples show two weight losses below 500 °C in addition to the small weight loss below 200 °C which is likely to be due to the removal of moisture and/or free solvent molecules. The weight loss due to the solvent molecules is almost comparable (~3%) for all samples (Figure 6.4). The first weight loss below 300 °C corresponds to the decomposition of weakly bound fatty acid molecules

(hydrophobically attached) to the surface of the nanoparticles (secondary surfactant layer). The second major weight loss above 300 °C (below 500 °C) corresponds to removal of strongly bound fatty acid molecules (chemically bonded).[27] The TGA profile clearly shows that the fatty acid surfactants present on the magnetite nanoparticles is mainly monolayer (primary surfactant) with small amount of secondary layer of surfactant over the primary layer. The weight losses due to the total, primary and secondary surfactants are shown in Table 6.4. The total amount of the surfactant varies from 16 to 18% for the different fatty acid coated samples (shown in Table 6.4). The weight loss due to the secondary surfactant layer includes the solvent weight loss (3%) below 200 °C.

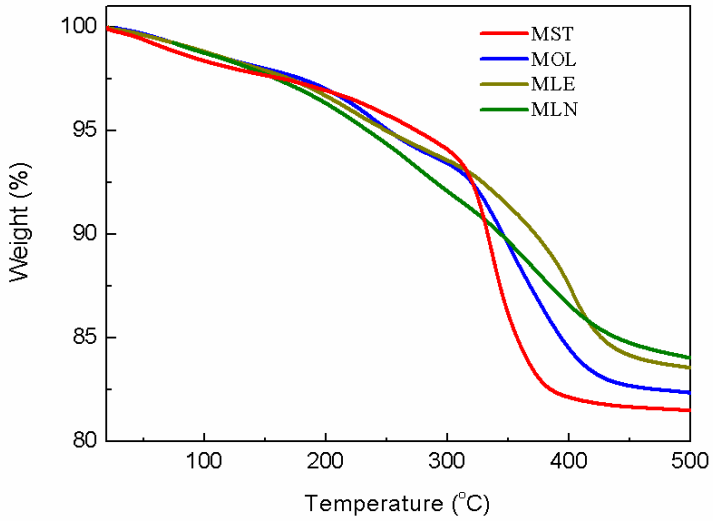

Figure 6.4. Thermogravimetric analysis curves of the fatty acid coated samples

Table 6.4. Amount of total, primary and secondary surfactants

Sample code	Total surfactant (±1%)	Primary surfactant (±1%)	Secondary surfactant (±1%)
MST	18	12	6
MOL	18	11	7
MLE	16	10	6
MLN	16	8	8

The total weight loss due to the coated fatty acid decreases with increasing the unsaturation in the carbon chain of the surfactant. Similarly, the weight loss due to primary surfactant decreases with increasing degree of unsaturation. This could be due to the different conformation of the carbon chain of the fatty acid molecules on the surface of the nanoparticles. The double bonds in the unsaturated fatty acids used in the current study are all in the *cis*-configuration. Stearic acid is a straight chain (all *trans* zig-zag) fatty acid. But in the case of oleic acid, the double bond at 9^{th} carbon makes a kink in the carbon chain. The kink in the surfactant makes less space available for the nearby surfactant molecule, which slightly reduces the number of molecules attached to the surface of the nanoparticle compared to the case of stearic acid coating. Linoleic and linolenic acids have bend and hook like structures with 2 and 3 double bonds in their carbon chain, respectively. Due to the bend and hook structures, the 18-carbon long alkyl chain bends towards the surface of the nanoparticles and makes less room for more surfactant to attach to the surface of the nanoparticles. Shahoo *et al*[28] observed less amount of dihexadecyl phosphate (DHDP) surfactant on magnetite nanoparticles compared to oleic acid, dodecyl phosphonic acid (DDP) and hexadecyl phosphonic acid (HDP) coated nanoparticles. This is due to the double chain surfactant DHDP occupying more area on the surface of the nanoparticles. Although the number of carbon atom is the same for all fatty acids used in the present study, the reduction in the total weight loss in the TGA curves with increasing the unsaturation in the surfactant molecules could be due to the different conformation of the surfactant chain on the surface of the nanoparticles.

6.3.4. Infrared spectroscopy

The infrared spectra of the coated powder samples are compared in Figure 6.5. The fatty acid coated samples show a strong band at 610 cm^{-1}, and this band corresponds to the Fe-O stretching vibration of Fe_3O_4.[29] The two bands at 2851 cm^{-1} and 2923 cm^{-1} in all the spectra correspond to the symmetric and asymmetric stretching vibrations of methylene ($-CH_2-$) groups in the fatty acid molecule. The weak band at 1710 cm^{-1} in all the samples corresponds to the carbonyl (-C=O) stretching vibration of free fatty acids. These free fatty acid molecules are probably due to the secondary layer present on the surface of the nanoparticles which are attached thorough weak hydrophobic interaction with the chemically bound primary layer of fatty acid molecules.

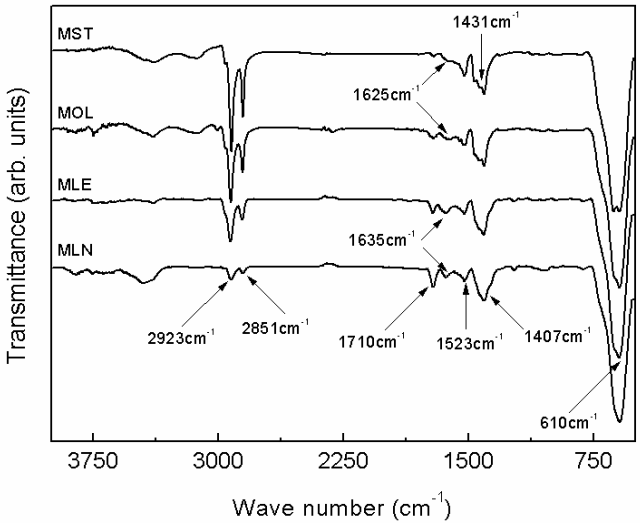

Figure 6.5. Infrared spectra of fatty coated samples

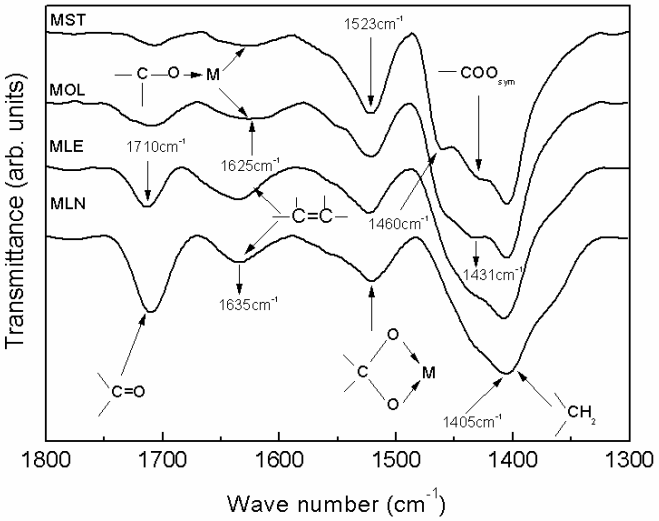

Figure 6.6. Close view of the IR spectra in the carboxylate region of the fatty acid coated samples

The bands observed in the region 1300 cm^{-1} to 1700 cm^{-1} correspond to the carboxylate ($-COO^-$) groups as shown in Figure 6.6. The strong band at 1431 cm^{-1} corresponds to the symmetric stretching vibration of the carboxylate ($-COO^-$) group. The bands at 1523 cm^{-1} and 1625 cm^{-1} (for MST and MOL) are due to the asymmetric stretching vibration of the carboxylate groups. In the Figure 6.6, the band at 1523 cm^{-1} corresponds to the chelating bidentate co-ordination of carboxylate group and the band at 1625 cm^{-1} corresponds to monodentate co-ordination of the carboxylate group to the iron atom on the surface of the nanoparticles, as discussed in the previous chapters (section 3.3.4, 4.3.4, 5.3.4). The intensity of the band at 1523 cm^{-1} is more than that of the band at 1625 cm^{-1} indicating that the chelating bidentate coordination is more predominant than the monodentate

coordination. The -C=C- stretching band of non-conjugated compounds is usually observed in the range 1660 cm^{-1} to 1640 cm^{-1}.[30] Thus, the band at 1635 cm^{-1} observed in the spectra of MLE and MLN could be due to the -C=C- stretching of the unconjugated double bond in the linoleic and linolenic acids. However, for oleic acid coated sample (MOL), this band is very weak (due to the single double bond) and merged with the monodentate co-ordination band at 1625 cm^{-1}. The bands at 1460cm^{-1} and 1405 cm^{-1} correspond to CH_2 deformation.

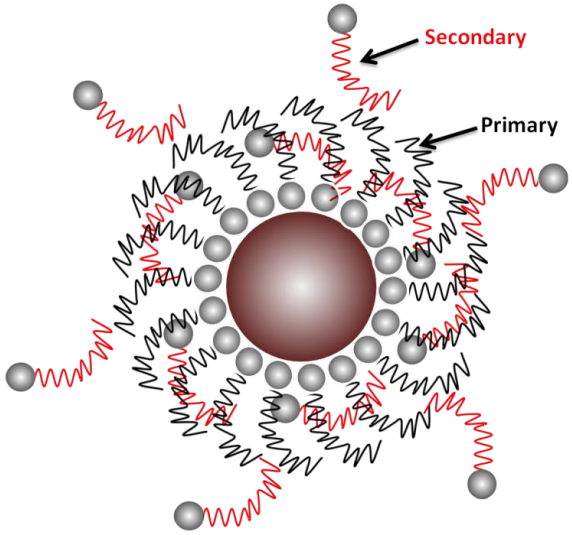

Figure 6.7. Schematic diagram showing the free surfactant molecules trapped within the primary and secondary surfactants attached to the surface of the nanoparticles.

The intensity of the band corresponding to the chelating bidentate (1523 cm^{-1}) coordination decreases with increasing the unsaturation in the fatty acid molecules attached on the surface of the nanoparticles and there is a corresponding increase in the intensity of the band due to carbonyl stretching vibration (1710 cm^{-1}). This is in accordance with the amount of primary and secondary surfactants, as obtained from TGA studies. This indicates that the free fatty acids (secondary surfactants) on the surface of the nanoparticles increase with increasing the degree of unsaturation in the surfactants. The possibility of interdigitation of the secondary surfactant molecules decreases from the sample MST to MLN due to the increasing bend conformation of the surfactant chain. However, the increase in the intensity of the band at 1710 cm^{-1} could be due to the trapped free surfactant molecules between the nanoparticle surfaces and the bend chain of the attached molecule as shown in Figure 6.7. The decreasing intensity of the band corresponding to the chelating bidentate coordination (1523 cm^{-1}) could be due to the different conformation of the fatty acid chain attached to the

nanoparticle surfaces. The bend and hook conformation of the fatty acids make less room for attaching more surfactants on the surface of the nanoparticles in the case of MLE and MLN when compared to the straight and kink conformation of fatty acids in the case of MST and MOL. In other words, packing of more number of stearic and oleic acid molecules with straight and kink conformation, respectively, is possible compared to the bend and hook conformation of linoleic and linolenic acids. The less intense band due to monodentate coordination at 1625 cm^{-1} in the spectra of MST and MOL becomes very weak in the case of MLE and MLN. The intensity of the band due to stretching vibration of the methylene groups (2851 cm^{-1} and 2923 cm^{-1} in Figure 6.6) decreases in the order MST>MOL>MLE>MLN due to the increased unsaturation (-CH=CH-) in the carbon chain from stearic acid to linolenic acid. The intensities of the bands due to symmetric (1431 cm^{-1}) and asymmetric stretching vibrations (1525 cm^{-1} and 1635 cm^{-1}) decrease with increasing the unsaturation in the carbon chain. This could be due to the decrease in the number of carboxylic acid molecules attached to the surface of the nanoparticle with increase in the degree of unsaturation in the carbon chain. TGA studies indicated slight decrease in the weight loss of samples coated with stearic acid to linolenic acid (Figure 6.4) indicating decrease in the number of fatty acid molecules attached to the nanoparticle surfaces.

6.3.5. Mode of attachment

From the IR studies, it can be concluded that the carboxylic group is attached to the surface of the nanoparticles and the hydrophobic alkyl chain is extended from the surface of the nanoparticles. The straight, kink, bend and hook conformation (orientation) of the fatty acids attached on the nanoparticles are schematically shown in Figure 6.8. Although all the fatty acids have the same number of carbon atoms in the carbon chain, the length of the fatty acid molecule is different for fatty acids with different degree of unsaturation in the carbon chain. The alkyl chain in the oleic, linoleic and linolenic acids form kink, bend and hook like conformation due to the 1, 2 and 3 *cis*-double bonds in the carbon chain, respectively. The length of the molecule decreases with increasing the unsaturation in the carbon chain. The length of the straight chain stearic acid is approximately 2.4 nm and is reduced with increasing the number of double bonds. The lengths of oleic, linoleic and linolenic acid molecules are 1.75 nm, 1.2 nm and 1.2 nm, respectively.[24-26] The bend structure of the carbon chain on the surface of the nanoparticles limits the number of surfactant molecules that can be attached on the surface of the nanoparticles.

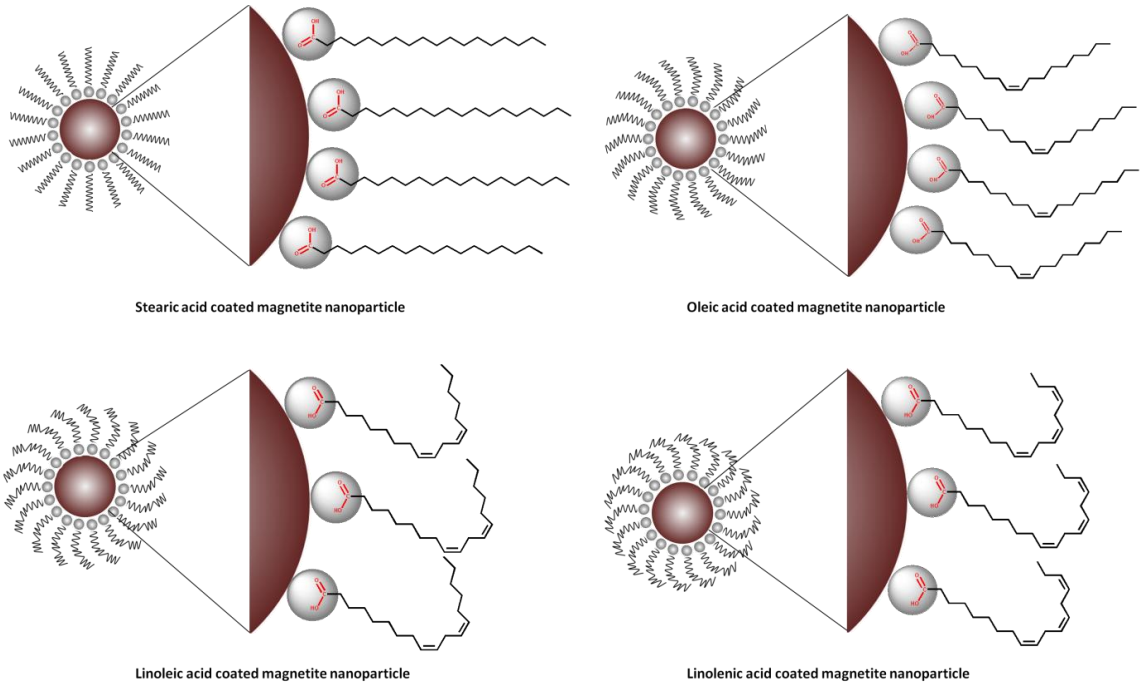

Figure 6.8. The conformation of the surfactant molecules on the surface of the coated nanoparticles

6.3.6. Magnetic measurements

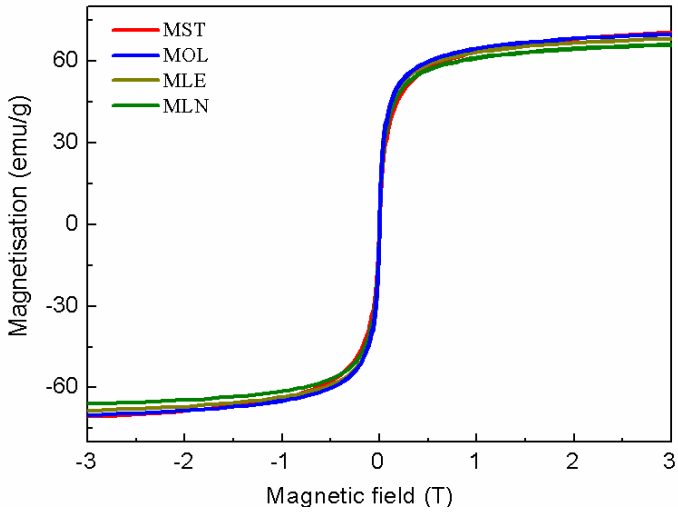

Figure 6.9. Room temperature magnetization curves of the fatty acid coated samples

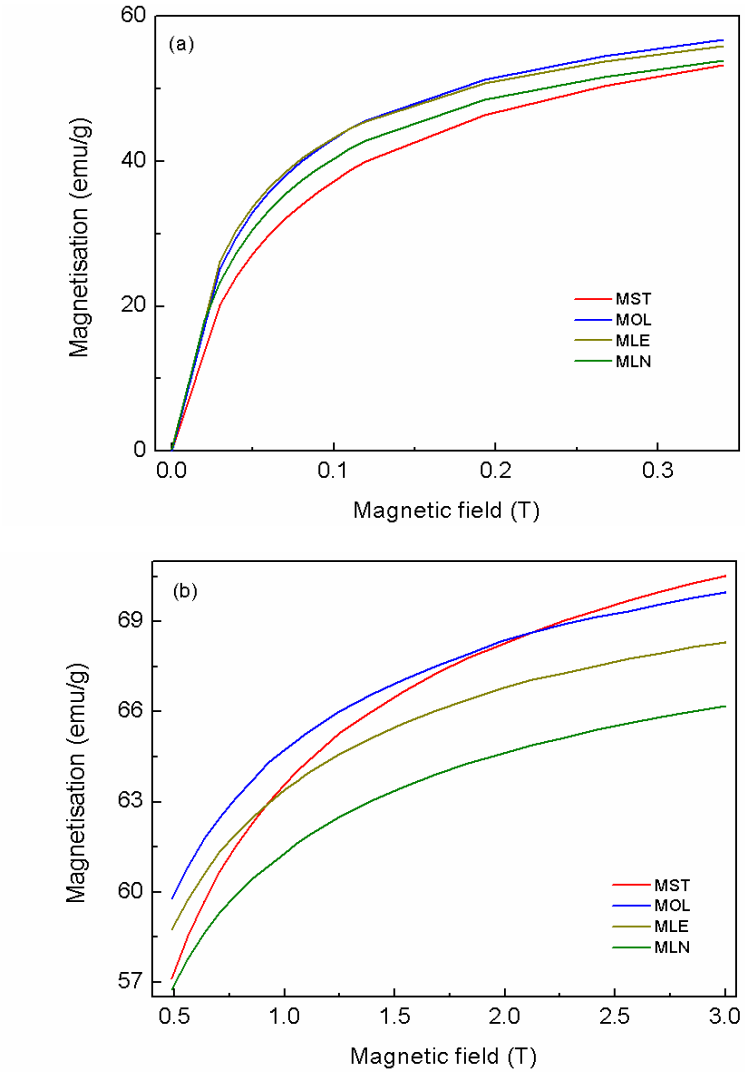

Figure 6.10. Zoomed initial magnetisation curves (a) at low and (b) high magnetic fields showing the different behaviour of the coated samples

Field dependant magnetization studies on the coated magnetite nanoparticles show formation of superparamagnetic nanoparticles with no remanence and coercivity at room temperature, as shown in Figure 6.9. Magnetization at the highest measured field of 3 T for the samples MST, MOL, MLE and MLN is 70.5 emu/g, 70.0 emu/g, 68.3 emu/g and 66.2 emu/g, respectively. The magnetization is reported as per gram of Fe_3O_4, based on the total weight loss from TGA studies. Even though the magnetization decreases slightly with increasing degree of unsaturation, the difference in the values of the magnetization is likely to be due to the small difference in the particle size distribution.

This is directly evidenced from the zoomed M-H curves at low and high fields, shown in Figure 6.10. For MST, the magnetization is lower at low fields and larger at higher fields whereas for MLN, the magnetization is relatively larger at low fields, compared to that of MST and much lower at high fields. The features observed in the magnetization curves are directly correlated with the particle size distributions shown in Figure 6.3, where MST has larger number of smaller particles compared to that of MLN and the average particle size of MLN is smaller than that of MST. The magnetization values of MOL and MLE are in between that of MST and MLN and again their magnetization behaviour as well as the particle size distribution correlates very well.

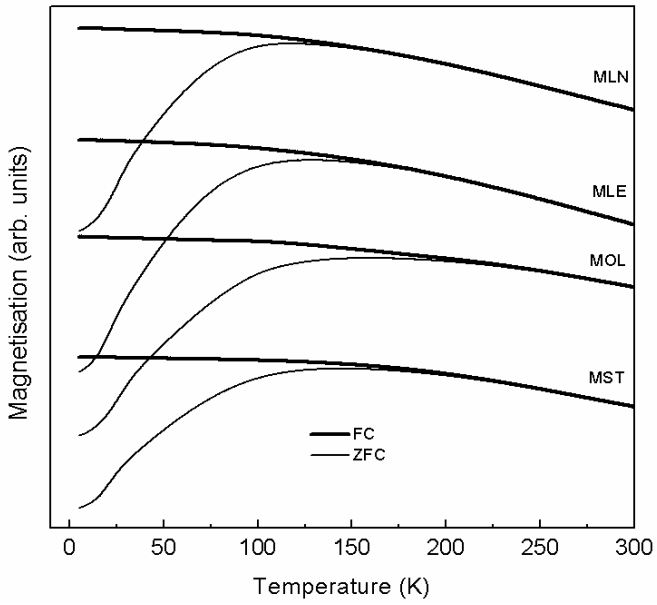

Figure 6.11. Field cooled and zero field cooled magnetization curves of the fatty acid coated samples

Temperature dependant magnetization studies are performed on the fatty acid coated powder samples and the results are shown in Figure 6.11. There are some minor differences in the temperature at which the maximum is observed in the ZFC curves, as shown in Figure 6.12(a). From the zero field cooled (ZFC) measurements, the superparamagnetic blocking temperatures, for MST, MOL, MLE and MLN are obtained as 145 K, 159 K, 128 K and 117 K respectively. The blocking temperature is known to depend on the average particle size and distribution, as well as the magnetic interaction between the particles.

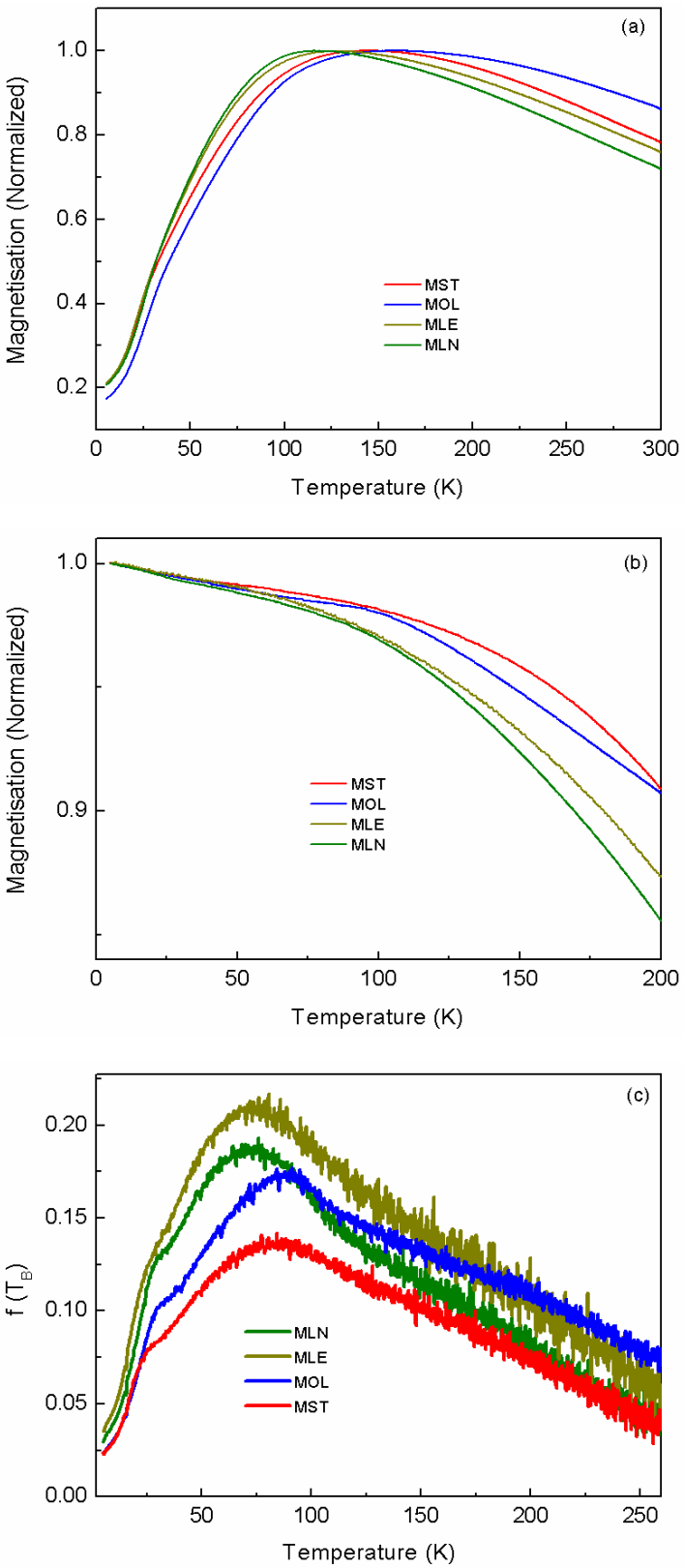

Figure 6.12. Normalized (a) ZFC and (b) FC curves, and (c) blocking temperature distribution calculated from the ZFC curves, for the fatty acid coated samples.

In the present case, the average particle sizes are obtained as 9.1, 9.7, 9.2 and 8.9 nm, respectively and the variation in the blocking temperature is in accordance with the average size. Minor differences in the size and distribution are reflected in the value of the blocking temperature, as observed in the case of the changes in the room temperature magnetization. The field cooled magnetization curves of all the fatty acid coated samples also show similar behaviour as shown in Figure 6.12(b). The distribution of the blocking temperature (T_B) of the particles is calculated from the zero field cooled (ZFC) curves using equation 2.4 in chapter 2. Figure 6.12(c) shows that the blocking temperature distribution is almost comparable for all the fatty acid coated samples, showing slight differences in the temperature at which the maximum is observed. The variation in the blocking temperature (T_B) for the different fatty acid coated samples could also be due to the magnetic anisotropy contribution from dipolar interparticle interactions, which depend on the separation between the nanoparticles.

The TEM images (Figure 6.3) showed that the stearic acid and oleic acid coated nanoparticles form aggregated and self-assembled nanoparticles whereas linoleic and linolenic acid coated nanoparticles are well separated with the formation of small clusters. The aggregated or self-assembled magnetic nanoparticles strongly influence the magnetic properties of the nanoparticles. The larger blocking temperature for the aggregated samples could be due to the increased anisotropy energy. Nakata *et al*[14] observed increase in the blocking temperature for aggregated and self-assembled nanoparticles than for well separated magnetic nanoparticles. The difference in the strength of the interparticle interactions between the nanoparticles is also obtained from the nature of the field cooled curves (FC). The normalized field cooled curves show slight differences in the magnetization behaviour as shown in Figure 6.12(b). The FC magnetization of the linoleic and linolenic acid coated samples (MLE and MLN) decreases much more than that of the stearic and oleic acid coated samples (MST and MOL) with increasing temperature. This indicates that the interparticle interaction is more in the case of MST and MOL compared to that in MLE and MLN.

6.4. Studies on nanofluids

6.4.1. Stability

The magnetic fluids prepared by dispersing the fatty acid coated magnetite nanoparticles at 2.2 volume% in toluene are shown in Figure 6.13 (a). The prepared fluid samples are found

to be stable for more than six months. The fluids are stable even in the presence of a strong applied magnetic field of 0.35 T. Figure 6.13(b) shows the response of the magnetic fluids in the presence of a magnetic field.

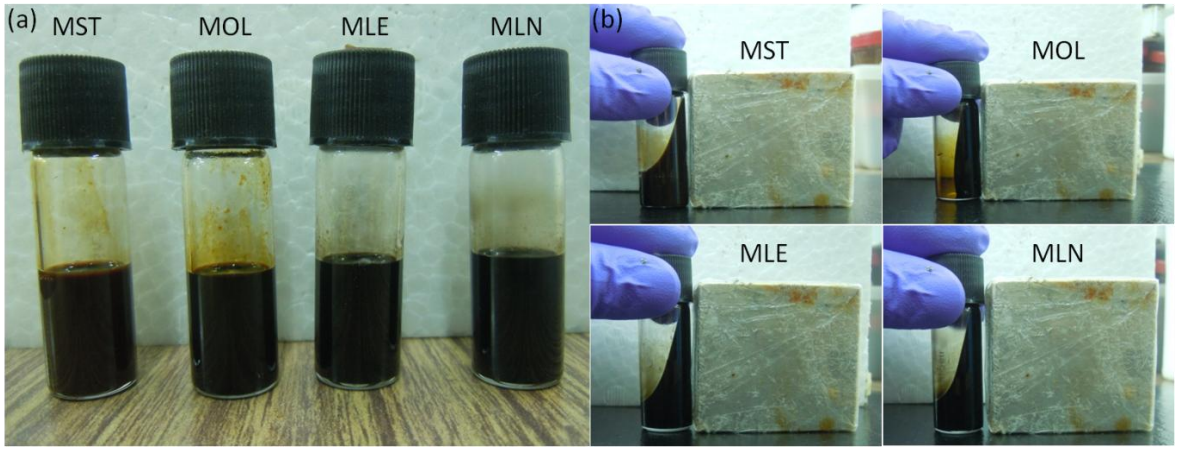

Figure 6.13. (a) Nanofluids prepared by dispersing the different fatty acid coated magnetite nanoparticles in toluene (b) nanofluids in the presence of an external magnetic field (0.35 T).

6.4.2. Magnetic measurements

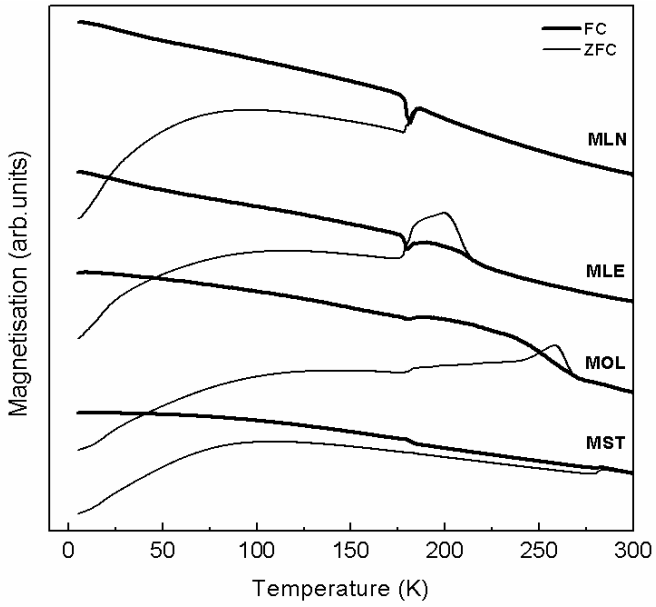

Figure 6.14. Temperature dependant magnetization of the different fatty acid coated magnetite fluids

In order to study and compare the magnetic behaviour, magnetic measurements have been carried out on the fluid samples. The fluid samples are prepared by dispersing the different fatty acid coated nanoparticles in toluene at 2.2 volume%. Zero field cooled (ZFC) and field cooled (FC) magnetization curves of the fluid samples are shown in Figure 6.14. The observed superparamagnetic blocking temperatures for the fluids of MST, MOL, MLE and MLN are 107 K, 143 K, 115 K and 95 K respectively. The blocking temperatures of the fluid samples are less than that of the corresponding solid samples. The reduction in the blocking temperature of the fluids when compared to that of solid samples is due the reduction in the interparticle interaction between the nanoparticles due to the solvent matrix. Vargas *et al*[31] observed higher blocking temperature and small bifurcation between the ZFC and FC curves for the solid magnetite nanoparticles, whereas a decrease in the blocking temperature and increase in bifurcation between the ZFC-FC curves are observed for the magnetite nanoparticles dispersed in liquid paraffin at different concentrations.

Table 6.5. Comparison of melting point of the fatty acids with the bifurcation temperature in the magnetization measurements

S. No	Sample code	Fatty acid melting point (K)	Bifurcation temperature (T_{irr}) (K)
1	MST	343	283
2	MOL	286	268
3	MLE	266	214
4	MLN	262	189
5	Toluene	178	-

The bifurcation temperature between the FC and ZFC curves in the temperature dependant magnetization measurements of the fluid samples is compared with the melting temperature of the corresponding fatty acids in Table 6.5. The melting point of the fatty acid decreases with increasing the unsaturation in the carbon chain due to the reduction in the hydrophobic interaction between the alkyl chains. The stearic acid molecules exist as solid at room temperature due the larger hydrophobic interaction between the alkyl chains forming dense packing. The other acids are liquids at room temperature due to the less dense packing of the alkyl chains due to the bend conformation and less hydrophobic interactions. The

bifurcation temperature decreases with decreasing the melting temperature of the fatty acid molecules. The bifurcation is likely to be due to the freezing of the fatty acid surfactant molecules attached to the surface of the nanoparticles. A small kink is observed in both the FC and ZFC magnetization curves at ~180 K which is at the melting point of toluene. The lower bifurcation temperature, compared to the melting point of the corresponding acid, is due to the smaller thickness of the coated layer of the acid molecules, as discussed in chapter 3 (section 3.4.1).

The number of carbons in the fatty acid chain is the same and the size and distribution of the magnetite nanoparticles as well as the amount of the surfactant coated on the surface of the nanoparticles are almost comparable for the all fatty acids coated samples. Therefore, the difference in the strength of the magnetic interactions between the magnetic nanoparticles could be mainly due to the nature of the surfactant molecules attached to the surface of the nanoparticles. Especially the structure and orientation of the surfactant molecules on the surface of the nanoparticle is different for different fatty acid coated samples due to their different conformation (as shown in Figure 6.8). The conformation of the surfactants on the nanoparticle surfaces strongly influences the interparticle interaction between the particles, eventually affecting the magnetic properties of the nanoparticles in the fluid. The continuous increase in the field cooled curve below the blocking temperature for the sample MLN in Figure 6.15 indicates the non-interacting behaviour of the nanoparticles. The saturating trend in the field cooled curve below the blocking temperature indicates highly interacting (aggregated) behaviour for MST. This is clearly seen from the normalized FC curves shown in inset in the Figure 6.15. The possible arrangements of the particles corresponding to the bifurcation in the ZFC-FC curves of the samples MLN and MST are shown in Figure 6.15.

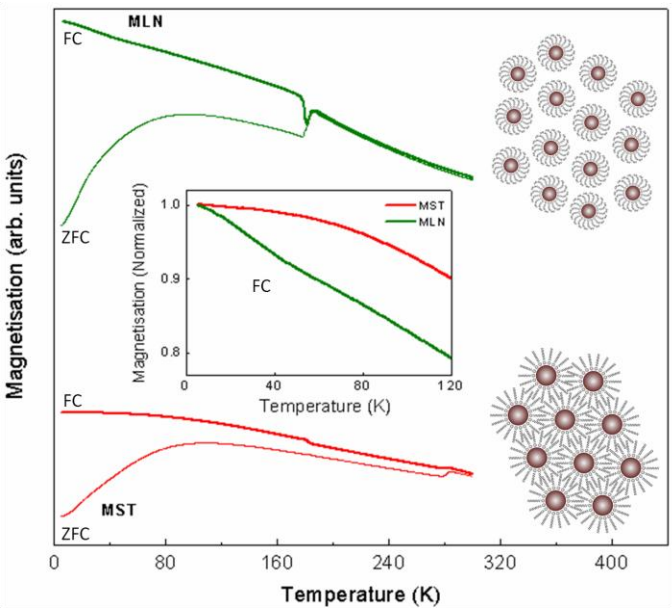

Figure 6.15. Temperature dependant magnetization curves of the stearic and linolenic acid coated fluids (left) and the possible arrangements of the nanoparticles in the corresponding fluid samples (right). Inset shows the normalized FC curves below the blocking temperature.

Since the size of the nanoparticles is comparable for all the samples, the magnetic interaction between the particles is also expected to be the same at a particular concentration of the nanofluid in toluene. At higher concentration of the magnetic fluid, the magnetic nanoparticles will be close to each other. If the separation between the particles is very low, then the interaction between the surfactants attached to the neighbouring particles, in addition to the magnetic interactions, also influences the arrangement of the particles. The interaction between the surfactants mainly depends on the orientation of the extended surfactant molecules in to base fluid (toluene) from the surface of the nanoparticles. Tadmor *et al*[32] studied the forces between oleic acid layers and forces between the stearic acid layers (on mica surface) using surface force balance (SFB) studies in hexadecane solvent in order to understand the stability and precipitation character of ferrofluids coated with oleic and stearic acid respectively. The authors observed collapse of the stearic acid tails on the surface (mica surface) due to the weak van der Waals attraction between the tethered C-18 tails and found that the kink in the C-9 carbon in oleic acid coated sample reduces this nematic interaction between the tethered chains.

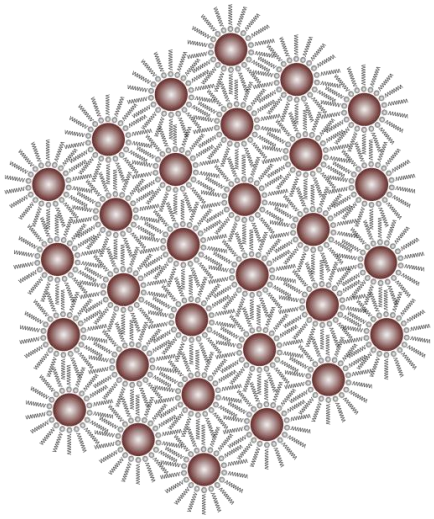

Stearic acid coated magnetite nanoparticle

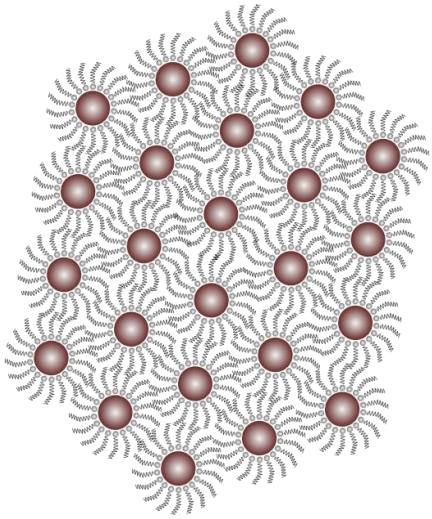

Oleic acid coated magnetite nanoparticle

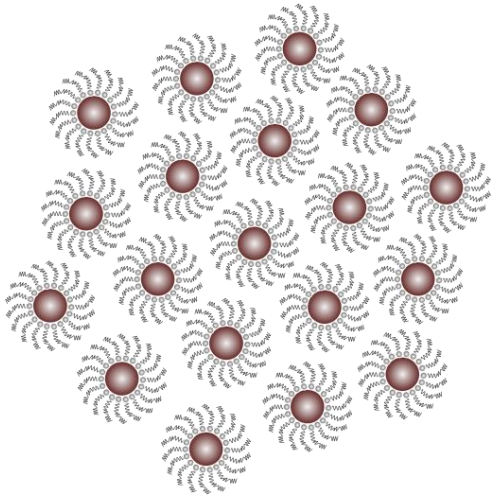

Linoleic acid coated magnetite nanoparticle

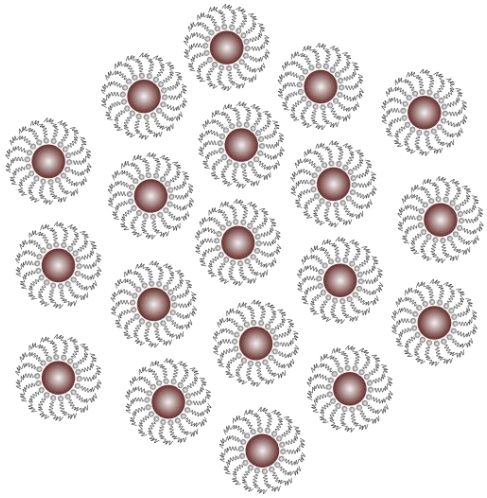

Linolenic acid coated magnetite nanoparticle

Figure 6.16. Schematic diagram showing the interaction between the different fatty acid coated particles in fluid through the surfactants.

In the present case, the spatial orientation of the surfactant molecules on the surface of the nanoparticles is straight chain, kink, bend and hook type of orientation for stearic, oleic, linoleic and linolenic acid coated magnetite nanoparticles, respectively (as shown in Figure 6.8). When the nanoparticles are close to each other (interparticle separation is less than twice the length of the surfactant), there is a possibility of interdigitation of the alkyl chain on the surface of one particle with the alkyl chain attached to the neighbouring particles. However, the spatial orientation of the surfactant molecules plays an important role in the

interdigitation of the surfactant molecules. In the present case, the straight alkyl chain of the stearic acid on the surface of the nanoparticles interpenetrates to the alkyl chains attached to the neighbouring particles when the particles are close to each other due to van der Waals interaction. In the case of oleic acid coated magnetite nanoparticles, the kink in the surfactant chain would reduce the interpenetration (interdigitation) of the surfactant molecules from the neighbouring particles. Shahoo *et al*[28] observed better dispersibility of oleic acid coated magnetite nanoparticles in the non-polar solvent, hexane, and this is ascribed to the reduced tendency to form secondary surfactants on the nanoparticles through interpenetration of the hydrophobic chain. The bend and hook structures of linoleic and linolenic acids make less availability of the tail end (hydrophobic chain end) on the surface of the nanoparticle. This less availability of the tail end completely reduces the possibility of interpenetration of surfactants with the neighbouring particles. As a result the stearic acid coated magnetite nanoparticles could form slightly aggregated structures, oleic acid coated particles could form the slightly assembled nanoparticles and linoleic and linolenic acid coated particles form completely separated particles as shown in Figure 6.16.

The above discussion is also in agreement with the observed TEM images of the fatty acid coated samples (Figure 6.3). The stearic and oleic acid coated magnetite nanoparticles showed slightly aggregated/self-assembled particles and linoleic and linolenic acid coated particles showed well separated particles. The temperature dependant magnetic measurements on the fluids also support the fact that the interparticle interaction between the magnetic nanoparticles is different for the different fatty acid coated samples (Figures 6.14 and 6.15). Stearic acid coated fluid shows less increase in the FC magnetization below T_B compared to that of linoleic acid coated fluid, indicating relatively larger interparticle interaction in the former case due to less separation between the particles.

6.4.3. Thermal conductivity

Magnetite nanofluids are prepared by dispersing the fatty acid coated magnetite nanoparticles in toluene at different concentrations. The thermal conductivity of these fluids as a function of the volume% of the particles is shown in Figure 6.17. The variation of thermal conductivity with the volume% follows a similar trend for all the fatty acid coated samples. The observed thermal conductivity of magnetite nanofluid is the same as that of the thermal

conductivity of the base fluid (toluene) up to a certain volume% of the particles. Up on further increasing the volume concentration, the thermal conductivity is increases over the base fluid. The concentration at which the thermal conductivity increases over that of the base fluid is the critical concentration for that fluid. After the critical concentration, the thermal conductivity increases almost linearly with concentration. Similar pattern of enhancement in the thermal conductivity with volume% of the particles has been observed for decanoic acid (chapter 3) as well as dodecanoic acid (chapter 5) coated magnetite nanofluids and also reported for oleic acid coated magnetite nanoparticles.[33]

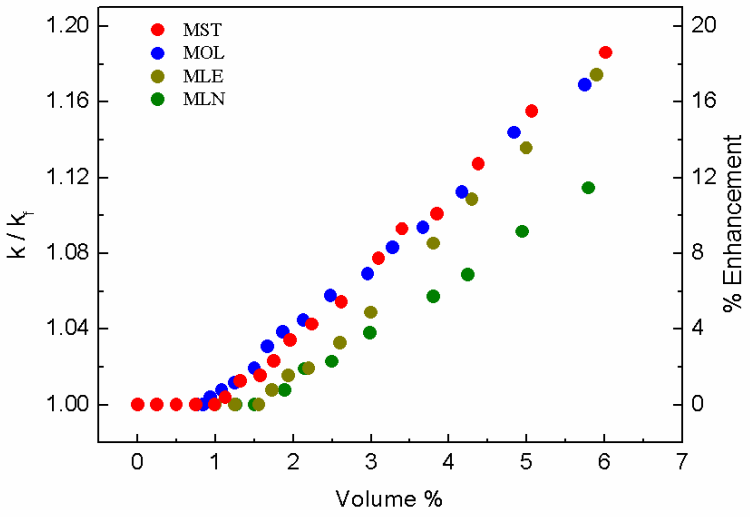

Figure 6.17. Variation of the relative thermal conductivity with volume% for the different fatty acid coated fluids

As discussed in the previous chapters, the absence of any enhancement in the thermal conductivity below the critical concentration could be due to the well separated particles (with no physical contact between the particles) and that the solvent matrix contributes more to the thermal conductivity of the nanofluid. At higher concentrations, the particles are close to each other and could form self-assembled/clustered/aggregated structures which make highly conductive path for heat transfer.[33] The highly conductive solid nanoparticles contribute more to the thermal conductivity of the nanofluids at higher concentrations. Although all the four fatty acid coated fluids show similar trend in the variation of the thermal conductivity with volume% of the particles, the critical concentration for the thermal conductivity enhancement is different for the different fatty acid coated samples (Figure

6.17). The critical concentration for the fluids of MST, MOL, MLE and MLN are 1.0, 0.8, 1.6 and 1.5 volume% respectively (shown in Table 6.6). The enhancement is observed at a lower critical concentration for the fluids with aggregation/self-assembly of the nanoparticles (MST, MOL) than the fluids with non-aggregated or well dispersed nanoparticles (MLE, MLN). The interpenetration or interdigitation of the alkyl chains on the surface of the nanoparticles makes highly conducting path through the aggregated or assembled nanoparticles. The Brownian velocity of the particles will be reduced due to the assembly of these nanoparticles and thus, the enhancement in the thermal conductivity may not be due to the Brownian motion of the particles. Due to the less possibility of interdigitation of the surfactant molecules on the surface of the nanoparticles in the case of the fluids of MLE and MLN, the particles remains well separated even though the particles are close to each other. The well separated particles require relatively higher concentration of the particles in the fluids for thermal conductivity enhancement. Philip *et al*[33] reported the critical concentration as 1.71 volume% for 6.7 nm Fe_3O_4 nanoparticles coated with oleic acid and dispersed in kerosene. Although the size of the nanoparticles used in the present study is comparable (9.7 nm) with the reported particle size, the observed difference in the critical concentration (0.8 volume%) for the thermal conductivity enhancement could be due to the relatively larger size of the particles, the difference in the base fluid, the compatibility of the solvent with the surface of the nanoparticles due to the possible difference in the amount of the primary and secondary surfactants.

The variation of the experimental thermal conductivity with volume% of the particles is compared with the Maxwell model and microconvection models in Figure 6.18. The suspension of non-interacting solid partilces in a liquid carrier can be explained based on the Maxwell's model (equation 1.1, chapter 1).[34] The experimental values are much lower than the Maxwell's predictions at lower concentrations and the values match with the Maxwell's model only at higher concentrations except for the fluid of the linolenic acid coated sample (MLN). At higher concentrations, the particles are very close to each other and forms self assembled clusters leading to larger enhancement in the thermal conductivity.

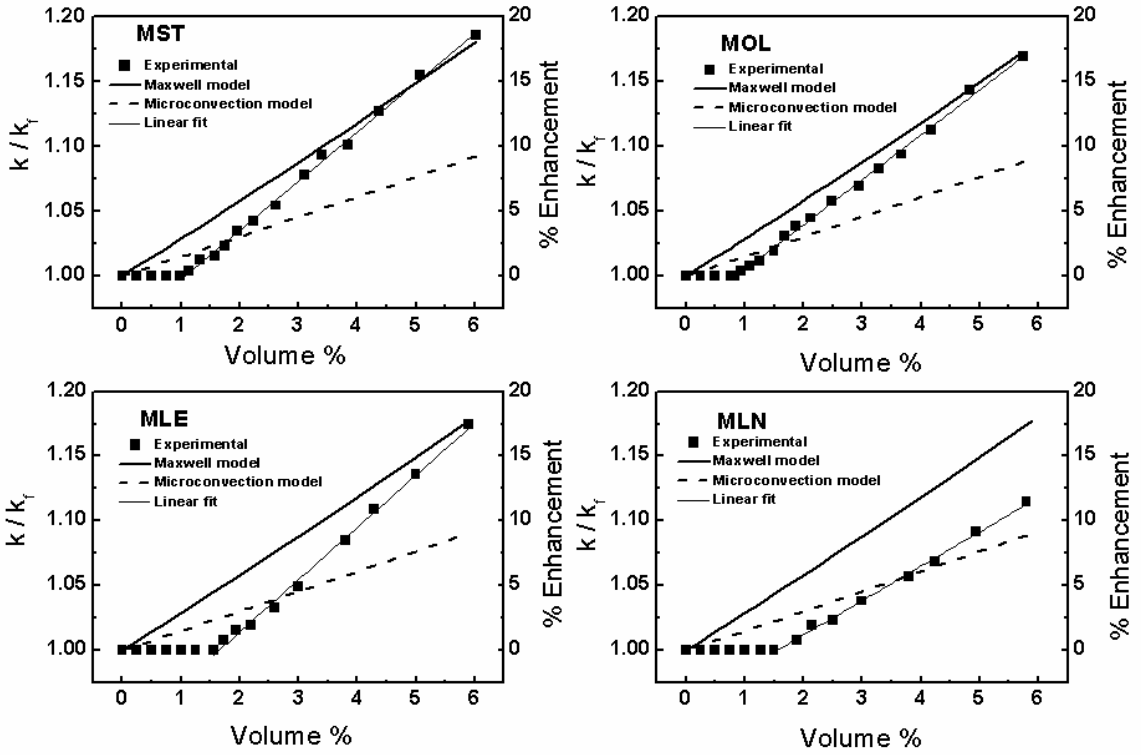

Figure 6.18. Variation of experimental thermal conductivity with the volume% of the particles (black squares) compared with the Maxwell (solid lines) and micro convection (dotted lines) models for different fatty acid coated samples. The thin solid lines are linear fit to the experimental data above the critical concentration.

Table 6.6. Comparison of the critical concentration and slope of the linear region in the variation of thermal conductivity for the different fatty acid coated fluids

S. No.	Sample code	Critical concentration (vol%)	Slope in the linear region
1	MST	1.0	0.038
2	MOL	0.8	0.035
3	MLE	1.6	0.040
4	MLN	1.5	0.026

The rate of increase of the thermal conductivity with respect to volume% above the critical concentration is claculated and the slope of the linear region (Figure 6.18) for the samples MST, MOL, MLE and MLN is calculated as 0.038, 0.035, 0.040 and 0.026, respectively. The slopes are almost comparable for the fluids of MST, MOL and MLE (Table 6.6). MLN shows much deviation from the Maxwell's model even at higher concentrations with a low slope of 0.026 in the linear region. The different rate of increase of thermal conductivity for the different samples could be due to the different surfactants and their orientation on the surface of the nanoparticles. The straight chain and kink in the chain for steatric acid (MST) and oleic acid (MOL) coated samples, respectively, could form clusters at lower concentration than the concentration at which the sample MLE forms clusters. This is due to the larger hydrophobic interaction and interdigitation of the fatty acid chain in the stearic and oleic acid coated samples. The reduced possibility of the interdigitation of surfactant molecules due to the bend conformation of linoleic acid coated nanoparticles requires much higher concentration for the nanoparticle cluster formation. In the case of MLN, the much less possibility for interdigitation of the surfactant molecules due to the hook structure of linolenic acid keeps the particles well separated even at higher concentrations due to which the thermal conductivity is much lower.

The experimental results are compared with the Brownian motion induced convection model proposed by Prashar *et al*[35] (equation 1.7, chapter 1) by considering the size of the average size of the nanoparticles as 9 nm in all the fluids, R_b as 2.6×10^{-8} m^2K/W and the constant '*m'* as 3.375 for toluene base fluid.[36] The calculated values from the equation 1.7 (dotted lines in Figure 6.18) deviate from the experimental results at higher concentrations for the fluids of MST, MOL, MLE. However, the Brownian motion induced convection model is closer to the experimental values for the fluid of MLN. The isolated nature of the particles due to lower interparticle and magnetic interactions between the particles increases the Brownian motion of the particles. The observed lower enhancement in the thermal conductivity through these well separated particles could be due to the contribution from the Brownian motion. In the case of MST, MOL and MLE, heat energy is transferred efficiently through the cluster/aggregation of the nanoparticles in the fluids leading to larger enhancement in the thermal conductivity. The mode of transfer of heat energy through aggregated and non-aggregated particles in the fluids is shown in Figure 6.19.

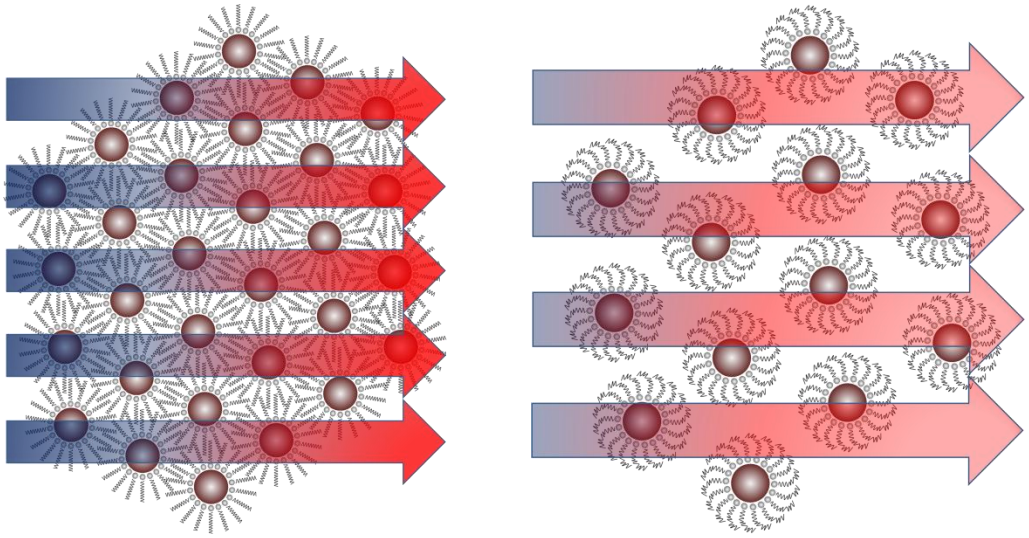

Aggregated nanoparticles *Well dispersed nanoparticles*

Figure 6.19. Schematic representation of heat transfer through the aggregated (left) and isolated (right) particles. The direction of arrow indicates the direction of the heat flow and the blue and red colours indicate the cold and hot end, respectively.

6.4.4. Thermal conductivity in a magnetic field

Thermal conductivity of fluids is measured by applying a magnetic field in the direction parallel to the temperature gradient. All the four fatty acid coated fluid samples show almost similar trend in the variation of thermal conductivity with magnetic field. Thermal conductivity increases initially, reaches maximum and then decreases with increasing the magnetic field. Fluids of MST and MOL show maximum enhancement in the thermal conductivity as ~40% at a magnetic field of 0.12. On the other hand the fluids of MLE and MLN show ~60% enhancement at 0.1 T (Figure 6.20). The large enhancement in the thermal conductivity at lower fields for the highly unsaturated fatty acid coated samples is due to the easy response of the individual magnetic nanoparticles to the magnetic field. At higher magnetic fields, there is a possibility of breakage of the conducting phase and forms discontinuity in the heat transfer path leading to less enhancement of thermal conductivity. The fluid samples with aggregation/clustering/assembly of magnetic nanoparticles show poor response to the magnetic field due to cooperative effect between the particles, especially at lower magnetic fields. In the case of aggregated nanoparticles in the fluid, higher field is required to overcome the cooperative effect and hydrophobic interaction between the particles.

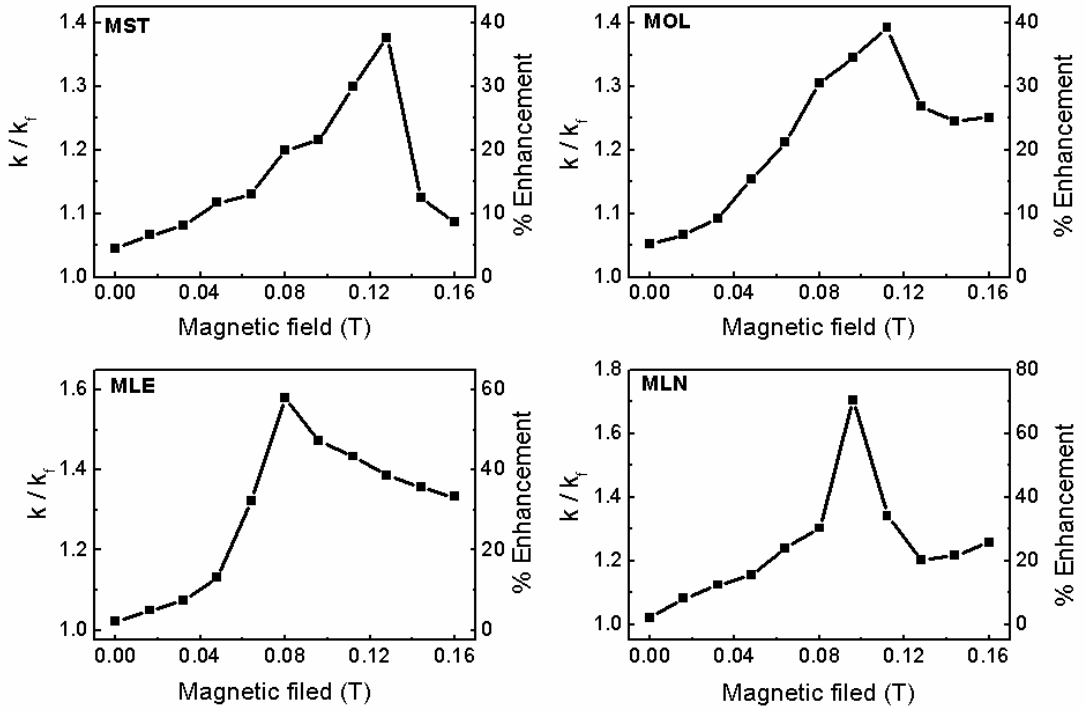

Figure 6.20. Variation of thermal conductivity with the applied magnetic field for the different fatty acid coated fluids.

6.4.5. Viscosity

The highly dispersive nature of the fatty acid coated magnetite fluids is verified from the viscosity measurements. Figure 6.21 shows variation of viscosity ratio with volume% of the nanoparticles for the saturated (MST) and unsaturated (MOL) fatty acid coated nanoparticles dispersed in toluene. Linear variation of viscosity with the volume% of the particles is observed for both saturated and unsaturated fatty acid coated fluids. However, large increase in the viscosity with volume% is observed for the saturated fatty acid coated fluid than for the unsaturated fatty acid coated fluid. Vekas *et al*[37] observed low viscosity for oleic acid (0.1 Pa-s) stabilized magnetite nanoparticles than the myristic acid (C-14 saturated) stabilized magnetite nanoparticles (0.7 Pa-s) dispersed in transformer oil. The difference in the viscosity observed for saturated and unsaturated molecule coated nanoparticles could also be due to the conformation of the coating layer on the surface of the nanoparticle. Surface force balance studies by Tadmor *et al*[32] on oleic acid layers and stearic acid layers on the mica surface in hexadecane medium showed that the solvent solvates the oleic acid molecule effectively than the stearic acid molecule. The kink in the oleic acid molecule leads to less nematic attraction

and the solvent solvate the molecule effectively. The stearic acid molecule is partially wetted by the solvent due to the high nematic attraction between the stearic acid molecules.

The difference in the magnitude of viscosity for the different nanofluids could be due to the difference in the dispersibility and compatibility of the surfactant molecules with the solvent. The better dispersion of the unsaturated fatty acid in the solvent (base fluid) reduces the viscosity of the nanofluids. The interdigitation of the surfactant molecules reduces with increasing the unsaturation in the surfactant attached on the surface of the nanoparticles. The less interdigitation of the surfactant molecules for the highly unsaturated surfactant coated nanoparticles in the fluid also reduces the viscosity of the nanofluid. The highly interdigitated stearic acid coated fluid sample shows larger increase in the viscosity with volume% which could be attributed to the highly aggregated structures. The viscosities calculated using different theoretical models (as explained in chapter 3, section 3.4.4) show much lower values than the experimental values (shown in the Figure 6.21). This could be due to the formation of the clusters or self assemblies or aggregation in the nanofluids at higher concentrations of the nanoparticles.

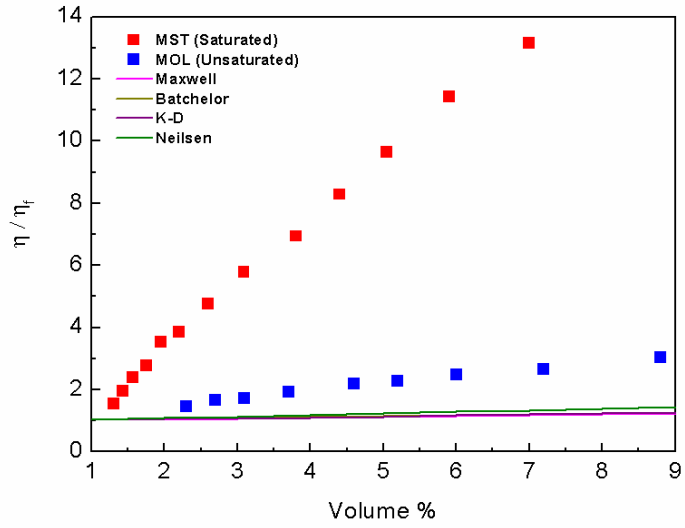

Figure 6.21. Comparison of the experimental viscosity of the saturated (red squares) and unsaturated fatty acid (blue squares) coated fluids with that calculated using different theoretical models (solid lines).

Viscosity of the fluids at 2.2 volume% is measured at different shear rates (10-10^3 s^{-1}). Viscosity with shear rate studies shows decrease in the viscosity with increasing shear rate (shear thinning behaviour) for all the fatty acid coated samples (Figure 6.22). The stearic and oleic acid coated samples (MST and MOL) show larger viscosity than the linoleic acid linolenic acid coated samples (MLE and MLN). At lower shear rate, fluids behaves as non-Newtonian fluids and at higher shear rate (> 25 s^{-1}), the fluid behaves like a Newtonian fluid. The observed shear stress is larger for the saturated fatty acid coated fluid, and decreases with increasing the unsaturation in the fatty acid surfactant on the surface of the nanoparticles.

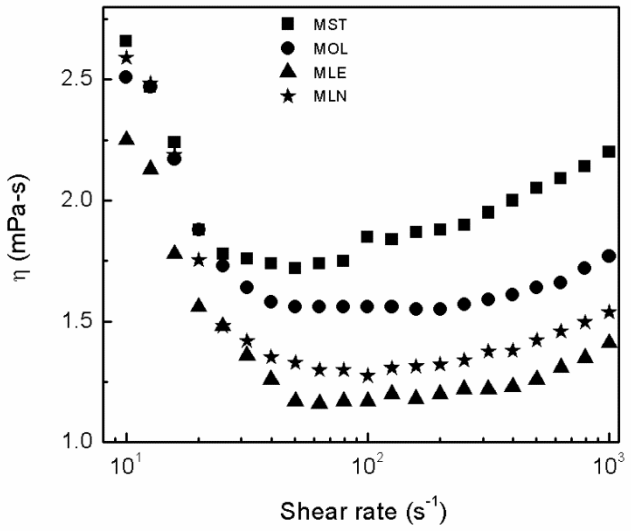

Figure 6.22. Variation of viscosity with shear rate for different fatty acid coated samples

6.5. Conclusions

Fatty acids with same number of carbon atoms but with different degree of unsaturation are used as surfactants to stabilize magnetite nanoparticles of comparable average size. The fatty acid coated magnetite nanoparticles are characterized using XRD, TEM, IR, TGA and magnetic studies. The average crystallite size calculated from the XRD is 7 nm, which is slightly lower than the average size obtained from the TEM images (9 nm). TEM images showed that saturated fatty acid coated sample forms highly aggregated particles and highly unsaturated fatty acid coated sample showed well separated particles. From IR studies the decrease in the intensity of the bands at 1523 cm^{-1} and 1625 cm^{-1} with increasing the degree of unsaturation in the surfactant indicate the decreasing amount of surfactant attached to the

surface of the nanoparticles. TGA studies showed slight decrease in the amount of surfactant attached on the surface of the nanoparticles with increasing unsaturation in the fatty acid surfactant. The decrease in the amount of surfactant with increasing unsaturation is due to the changes in the conformation of the surfactant molecules. The kink, bend and hook structures reduce the packing efficiency compared to the straight chain structure and reduces the number of surfactant molecules attached to the surface of the nanoparticles.

This different conformation of the fatty acid surfactant on the surface of the nanoparticles is found to influence the physical and thermophysical properties of the magnetic fluids. Temperature dependant magnetization studies of the fluid samples showed different interparticle interaction behaviour for different fatty acid coated samples. The interparticle interaction is found to be larger in the case of the saturated fatty acid coated fluid sample than for the unsaturated fatty acid coated samples. The interparticle interaction decreases with increasing the unsaturation in the fatty acid surfactant. This could be due to the interdigitation of the surfactant molecules on one nanoparticle with the surfactant molecules on the neighbouring particles leading to aggregation or clustering of the nanoparticles in the fluid. Thermal conductivity of the fluid with aggregated particles showed larger enhancement than for the fluids with non-aggregated particles, due to more heat energy transferred through the aggregates. Viscosity studies also confirmed the formation of aggregates or clustering of nanoparticles in the case of saturated fatty acid coated fluid, which showed large increase in the viscosity with the concentration of the particles in the fluid in comparison with the unsaturated fatty acid coated fluid samples.

References

1. Avdeev, M. V.; Bica, D.; Vekas, L.; Marinica, O.; Balasoiu, M.; Aksenov, V. L.; Rosta, L.; Garamus, V. M.; Schreyer, A. *J. Magn. Magn. Mater.* **2007**, *311*, 6-9.
2. Shen, L. F.; Laibinis, P. E.; Hatton, T. A. *Langmuir* **1999**, *15*, 447-453.
3. Shima, P. D.; Philip, J.; Raj, B. *Appl. Phys. Lett.* **2009**, *94*, 223101.
4. Reinecke, B. N.; Shan, J. W.; Suabedissen, K. K.; Cherkasova, A. S. *J. Appl. Phys.* **2008**, *104*, 023507.
5. Philip, J.; Shima, P. D.; Raj, B. *Appl. Phys. Lett.* **2007**, *91*, 203108.
6. Altan, C. L.; Elkatmis, A.; Yüksel, M.; Aslan, N.; Bucak, S. *J. Appl. Phys.* **2011**, *110*, 093917.
7. Grzelczak, M.; Vermant, J.; Furst, E. M.; Liz-Marzan, L. M. *ACS Nano* **2010**, *4*, 3591-605.
8. Min, Y.; Akbulut, M.; Kristiansen, K.; Golan, Y.; Israelachvili, J. *Nat. Mater.* **2008**, *7*, 527-538.
9. Butter, K.; Bomans, P. H.; Frederik, P. M.; Vroege, G. J.; Philipse, A. P. *Nat. Mater.* **2003**, *2*, 88-91.
10. Lalatonne, Y.; Richardi, J.; Pileni, M. P. *Nat. Mater.* **2004**, *3*, 121-125.
11. Jiang, W.; Wang, L. Q. *J. Appl. Phys.* **2010**, *108*, 114311.
12. Badia, A.; Singh, S.; Demers, L.; Cuccia, L.; Brown, G. R.; Lennox, R. B. *Chem. Eur. J.* **1996**, *2*, 359-363.
13. Jiang, J.; Chae, B.; Jeong, S. K.; Min, B. K.; Kim, S. H.; Piao, L.; Yoon, S. *J. Colloid Interface Sci.* **2013**, *394*, 639-642.
14. Nakata, K.; Hu, Y.; Uzun, O.; Bakr, O.; Stellacci, F. *Adv. Mater.* **2008**, *20*, 4294-4299.
15. Chauhan, A. K., A Textbook of Molecular Biotechnology; IK International Pvt Ltd, **2009**.
16. Craig, N.; Green, R.; Greider, C.; Cohen-Fix, O.; Storz, G.; Wolberger, C., Molecular Biology: Principles of Genome Function; OUP Oxford, **2014**.
17. Lide, D. R., *CRC Handbook of Chemistry and Physics*; CRC press, **2004**.
18. Cermak, S. C.; Kenar, J. A.; Evangelista, R. L., *Distillation of Natural Fatty Acids and Their Chemical Derivatives*; INTECH Open Access Publisher, **2012**.

19. Anneken, D. J.; Both, S.; Christoph, R.; Fieg, G.; Steinberner, U.; Westfechtel, A., Fatty Acids. *Ullmann's Encyclopedia of Industrial Chemistry* **2006**.
20. Vargaftik, N. B., *Handbook of Thermal Conductivity of Liquids and Gases*; CRC press, **1993**.
21. Mandelis, A.; Hess, P., *Life and Earth Sciences*; SPIE Press, **1997**; Vol. 3.
22. Yaws, C. L., Handbook of Thermal Conductivity, Volume 3:: Organic Compounds C8 to C28; Gulf Professional Publishing, 1995; Vol. 3.
23. Dadarlat, D.; Bicanic, D.; Gibkes, J.; Surducan, V.; Pasca, A. *J. Sci. Food Agric.* **1998**, *78*, 182-186.
24. Lane, C. A.; Burton, D. E.; Crabb, C. C. *J. Chem. Educ.* **1984**, *61*, 815.
25. Olsson, A.-M.; Sandberg, D. Modern Adhesion Theory Applied on Coating and Gluing of Wood.: Analysis of the Interaction between Wood and High Solid Linseed Oil Paint. **1996**.
26. Lee, D. K.; Kim, Y. H.; Kang, Y. S.; Stroeve, P. *J. Phys. Chem. B* **2005**, *109*, 14939-14944.
27. Zhao, S. Y.; Lee, D. K.; Kim, C. W.; Cha, R. G.; Kim, Y. H.; Kang, Y. S. *Bull. Korean Chem. Soc.* **2006**, *27*, 237-242.
28. Sahoo, Y.; Pizem, H.; Fried, T.; Golodnitsky, D.; Burstein, L.; Sukenik, C. N.; Markovich, G. *Langmuir* **2001**, *17*, 7907-7911.
29. Waldron, R. D. *Phys. Rev.* **1955**, *99*, 1727-1735.
30. Bronstein, L. M.; Huang, X. L.; Retrum, J.; Schmucker, A.; Pink, M.; Stein, B. D.; Dragnea, B. *Chem. Mater.* **2007**, *19*, 3624-3632.
31. Vargas, J. M.; Nunes, W. C.; Socolovsky, L. M.; Knobel, M.; Zanchet, D. *Phys. Rev. B.* **2005**, *72*, 184428.
32. Tadmor, R.; Rosensweig, R. E.; Frey, J.; Klein, J. *Langmuir* **2000**, *16*, 9117-9120.
33. Philip, J.; Shima, P. D.; Raj, B. *Nanotechnology* **2008**, *19*, 305706.
34. Maxwell, J. C. A Treatise on Electricity and Magnetism. *Clarendon press* **1881**, *1*.
35. Prasher, R.; Bhattacharya, P.; Phelan, P. E. *Phys. Rev. Lett.* **2005**, *94*, 025901.
36. Lenin, R.; Joy, P. *J. Nanofluids* **2015**, *4*, 310-317.
37. Vékás, L.; Bica, D.; Marinica, O. *Rom. Rep. Phys.* **2006**, *58*, 257.

Chapter 7

Effect of base fluid on the thermal conductivity of oleic acid coated magnetite nanofluids

Abstract

The effect of the base fluid (solvent) on the thermal conductivity enhancement of the magnetite nanofluids is studied. Oleic acid coated nanoparticles showed good dispersion in the base fluids toluene, xylene, mesitylene, kerosene, and methylcyclohexane, whereas the nanoparticles in the fluids octadecene and paraffin showed poor dispersion. Relatively larger enhancement in the thermal conductivity is observed for well dispersed nanoparticles compared to the poorly dispersed nanoparticles in the presence of a magnetic field. From the thermal conductivity studies at different concentrations of four different fluids, and nanoparticles dispersed at 2.2 volume% in seven different base fluids, the difference in the enhancement in the thermal conductivity is examined based on the thermophysical properties of the corresponding base fluids.

7.1. Introduction

The Brownian motion of the nanoparticles dispersed in nanofluids, aggregation/clustering of the nanoparticles, liquid layering at the interface of the nanoparticle and the nature of the base fluid are some of the important factors determining the thermal conductivity enhancement of nanofluids.[1-3] Nanoparticles dispersed in a fluid are always in Brownian motion, and the Brownian velocity of the particles depends on the size of the nanoparticles. A nanofluid containing smaller sized particles enhances the thermal conductivity due to the larger Brownian velocity than the fluid containing larger particles.[1] It is observed that the time scale for the Brownian motion is less than the time scale for thermal diffusion and the Brownian motion alone cannot be the mechanism for the thermal conductivity enhancement and the convection caused by the Brownian motion possibly increases the thermal conductivity of the nanofluids.[4-5] The dispersed nanoparticles in a fluid carry large amount of the surrounding solvent molecules along with them during the Brownian motion and the micro-scale interaction of the particles reduces the temperature gradient.[6]

The dynamic properties of the nanoparticles in a fluid are strongly influenced by the viscosity of the base fluid. For the nanoparticles dispersed in highly viscous base fluid, the particles experience more dragging force due to the surrounding solvent molecules, which reduces the Brownian velocity and eventually reducing the thermal conductivity of a nanofluid. Tsai *et al*[7] studied the effect of dynamic behavior of the nanoparticles on the thermal conductivity of a nanofluid by controlling the viscosity (η) of the base fluid by changing the ratio of diesel oil (η = 4.188 mPa-s) to polydimethylsiloxane (PDMS) (η = 5500 mPa-s), where the thermal conductivities of the base fluids are comparable, 0.14 W/mK for diesel oil and 0.15 W/mK for PDMS. From the results it was found that the highly viscous base fluid reduces the Brownian motion and the thermal conductivity matched with the Maxwell's prediction. Nara *et al*[8] investigated the effective thermal conductivity of alumina based nanofluids by using different base fluids of varying viscosities such as water (η = 0.934 mPa-s) and the anti-freezing liquids like ethylene glycol (η = 16.1 mPa-s) and propylene glycol (η = 41.1 mPa-s). The authors observed decrease in the thermal conductivity enhancement with increasing viscosity of the base fluid, where the water based fluid showed larger enhancement in the thermal conductivity than the fluids made from the anti-freezing liquids. It was claimed that the observed decrease in the enhancement of thermal conductivity

with increasing viscosity of the base fluid is due to the reduction in the Brownian motion of the nanoparticles in the fluids.

Kinetic theory based analysis of the heat transport in well-dispersed nanofluids showed that the Brownian motion induced hydrodynamic effect has only minor contribution on the thermal conductivity enhancement and the enhanced thermal conductivity could be well described by the effective medium theory.[9] Aggregation/clustering of the nanoparticles in nanofluids is a common phenomenon due to the van Waals interaction between the high surface energy nanoparticles. It was observed that aggregation/ clustering of the nanoparticles could form highly conductive heat transfer path in a fluid which influences the interaction between the particles leading to larger enhancement in the thermal conductivity.[10] The viscosity of the base fluid reduces the van der Waals interaction and reduces the aggregation of nanoparticles, eventually changing the heat transport properties. Hosseini *et al*[11] studied the effect of viscosity of the base fluid and the interaction between the nanoparticles on the thermal conductivity enhancement of β-SiC nanofluids. The authors observed larger enhancement in the thermal conductivity for mono ethylene glycol (MEG) based nanofluid than paraffin based nanofluid for all studied concentrations. From a correlation of the results with the viscosity of the base fluids, it is concluded that the larger thermal conductivity for MEG based nanofluid is due to the larger particle-particle interaction than in the highly viscous paraffin based nanofluid. The more viscous paraffin impedes the particle-particle interaction which leads to lesser enhancement in the thermal conductivity. Younes *et al*[12] observed slight aggregation of Fe_2O_3 nanoparticles in water and well separated particles in ethylene glycol based fluids through microscope images. The larger separation of the nanoparticles in ethylene glycol, even in the presence of a magnetic field, was attributed to the larger viscosity of the base fluid (η = 16 mPa-s).

The intrinsic thermal conductivity of the base fluids also plays an important role in the thermal conductivity enhancement of the nanofluids. A nanofluid with nanoparticles dispersed in a base fluid having high inherent thermal conductivity is expected to show larger thermal conductivity enhancement. However, previous studies showed that it is very difficult to get the expected enhanced thermal conductivity using base fluids with larger inherent thermal conductivity.[13-14] Xie *et al*[15] studied the enhancement in the thermal conductivity of α-Al_2O_3 nanoparticles dispersed in base fluids such as water (k = 0.614 W/mK), glycerol (k = 0.289 W/mK), ethylene glycol (k = 0.258 W/mK) and pump oil (k = 0.141 W/mK). Relatively larger enhancement in the thermal conductivity is obtained for nanoparticles

dispersed in the pump oil which has lower inherent thermal conductivity and the water based fluid showed lesser enhancement in the thermal conductivity where water has higher inherent thermal conductivity.

The interfacial layer at the nanoparticle-fluid interface is one of the important factors that influence the thermal conductivity of a nanofluid. The ordered liquid layer at the particle-fluid interface, interfacial thermal resistance, nature of the surface of the nanoparticles, the surfactant, compatibility of the solvent (base fluid) with the surfactant, solvation of the surfactants, etc are also important factors that contribute to the heat transport properties at the interface. The thermophysical properties of the base fluid at the interface also influence the heat transport at the interface in the nanofluid. Hosseini *et al*[11] found that the percentage enhancement in the thermal conductivity is more for the paraffin based β-SiC nanofluids than the MEG based nanofluids. The highly viscous paraffin based fluid could form larger thickness of the ordered liquid layer, compared to the MEG based fluid, at the particle-fluid interface which leads to larger enhancement in the thermal conductivity. Timofeeva *et al*[16] studied the thermal conductivity of SiC nanoparticles in ethylene glycol:water (50:50) mixture using particles of different sizes and compared the results with that of SiC dispersed in water. It was observed that the EG-H_2O based nanofluids show 4-5% larger enhancement in the thermal conductivity than the water based fluid for particles of all sizes. The authors suggested that the effect cannot be simply explained based on the lower thermal conductivity of the EG-H_2O base fluid and is likely to be related to the lower interfacial resistance of the EG-H_2O base fluid. Moreover, lesser enhancement in the viscosity was observed for the EG-H_2O based nanofluid than for the water based fluid. It was suggested that the behavior could be due to the structure and thickness of the diffuse layer around the surface of the nanoparticles which could be different for the different base fluids. Altan *et al*[17] studied the thermal conductivity of Fe_3O_4 nanofluids, synthesized by different methods (water born and oil born) and dispersed in different solvents (hexane, heptanes and light mineral oil). In all the cases, the water born particles showed larger enhancement in the thermal conductivity than the oil born particles. From the results, it was concluded that the enhancement in the thermal conductivity is not due to the inherent thermal conductivity of the base fluids. The compatibility of the base fluid with the surface of the particles and the solvation of the stabilizing layer with the solvent are ascribed to be playing the important role in the thermal conductivity enhancement. The stability of the nanofluid influences the heat transfer characteristics of the nanofluids and the stability mainly depends on the interaction between

the surface of the nanoparticles and the solvent molecules. Lopez *et al*[18] studied the interfacial free energy of interaction between the carrier molecules and the hydrocarbon chain, and the stability of the oleate coated magnetite nanoparticles was studied by dispersing the particles in different organic carriers with different dielectric constants. From the results, it was found that the less polar solvents form stable fluids than the more polar solvents.

Although there are some reports on the effect of the properties of the base fluids on the thermophysical properties of the corresponding nanofluids, no detailed studies are yet reported on the effect of the thermophysical properties of the base fluids on the interaction between the surface of the nanoparticles with the base fluid molecules and the compatibility of the surface with the solvent molecules on the thermal conductivity enhancement of the nanofluids. In the present study we have compared the thermal conductivity of oleic acid coated magnetite nanoparticles dispersed in various base fluids of comparable polarity (dielectric constant in the range 2.0-2.4) and thermal conductivity (from 0.11 to 0.14 W/mK) and the role of the different base fluids.

7.2. Synthesis and characterization

Oleic acid coated magnetite nanoparticles were synthesized by the co-precipitation of iron chlorides ($FeCl_3.6H_2O$ and $FeCl_2.4H_2O$) using ammonium hydroxide in the presence of oleic acid in the reaction medium, as discussed in section 2.2.2, chapter 2. The method of synthesis is similar to that reported in chapter 6. Details of the characterization of the oleic coated magnetite nanoparticles are described in chapter 6.

7.3. Thermophysical properties of base fluids

The thermophysical properties of the different base fluids used in the present study are compared in Table 7.1. The thermal conductivity values of the base fluids shown in the table are measured at 25 °C using the home made cell based on the transient hot wire method. The other thermophysical properties of the base fluids, at the same temperature, are taken from the literature.[19-21]

Table 7.1. Thermophysical properties of the base fluids.[19-21]

Base fluid	Thermal conductivity (W/mK)*	Viscosity (mPa-s)	Specific heat (J/gK)	Dielectric constant, ε	Density (kg/m^3)	Boling point (K)
Methylcyclohexane	0.109	0.679	1.88	2.1	769	374
Kerosene	0.114	1.64	2.01	2.0	780-840	423-448
Paraffin liquid (light)	0.125	26.15	2.13	2.0	820-880	553-623
Xylene	0.127	0.76	1.75	2.4	876	403
Toluene	0.129	0.56	1.70	2.38	865	383
Mesitylene	0.136	0.66	1.74	2.4	861	438
Octadecene	0.143	4.01	2.15	2.24	789	588

* Measured thermal conductivity at 25 °C. The base fluids are listed in the order of increasing thermal conductivity.

7.4. Preparation of nanofluids

Table 7.2 Base fluids and the sample codes of the corresponding nanofluids

Serial No.	Solvent (base fluid)	Nanofluid Sample code
1	Toluene	MTO
2	Xylene	MXY
3	Mesitylene	MME
4	Methylcyclohexane	MMC
5	Octadecene	MOD
6	Kerosene	MKR
7	Paraffin liquid (light)	MPL

Nanofluids are prepared by dispersing the dried oleic acid coated nanoparticles in different base fluids at different volume percentages. The nanoparticles are dispersed in the solvents toluene, xylene, mesitylene, methylcyclohexane, kerosene, octadecene and paraffin and the sample codes are mentioned in Table 7.2.

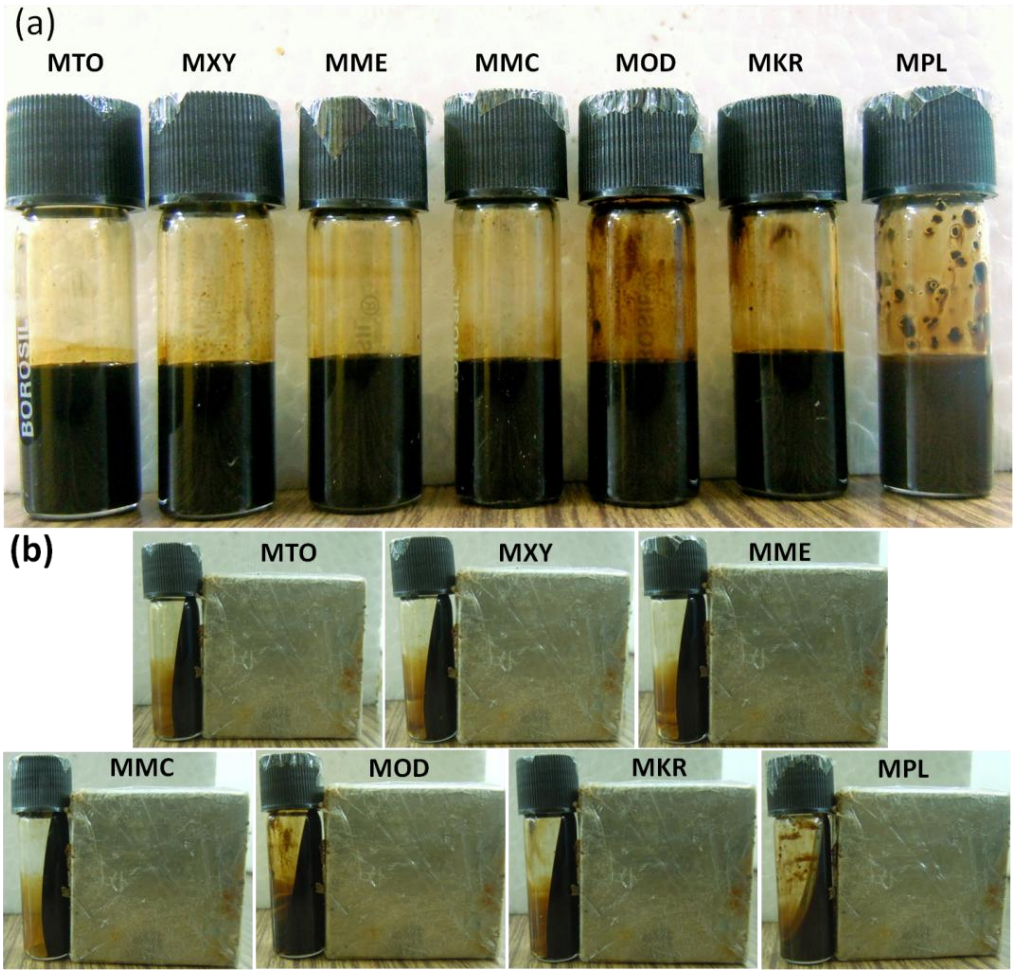

Figure 7.1. (a) Photographs of the nanofluids in different base fluids (MTO- Toluene, MXY- Xylene, MME- Mesitylene, MMC- Methylcyclohexane, MOD- Octadecene, MKR- Kerosene, MPL- Paraffin), and (b) fluid samples in the presence of an applied magnetic field

Figure 7.1 shows the images of the fluid samples by dispersing the dried powders in different base fluids at 2.2 volume%. From the images it can be clearly seen that the particles are less dispersed in octadecene (MOD) and paraffin (MPL). The images also show response of the fluids to an applied magnetic field using a laboratory magnet (0.35 T). The paraffin and octadecene based fluids show poor response to the magnetic field (more fluid at the base of the sample tubes) due to the higher viscosity of the corresponding base fluid. All other fluids show good response to the applied magnetic field (whole fluid is claimed in the sample tube wall near the magnet).

7.5. Magnetic measurements

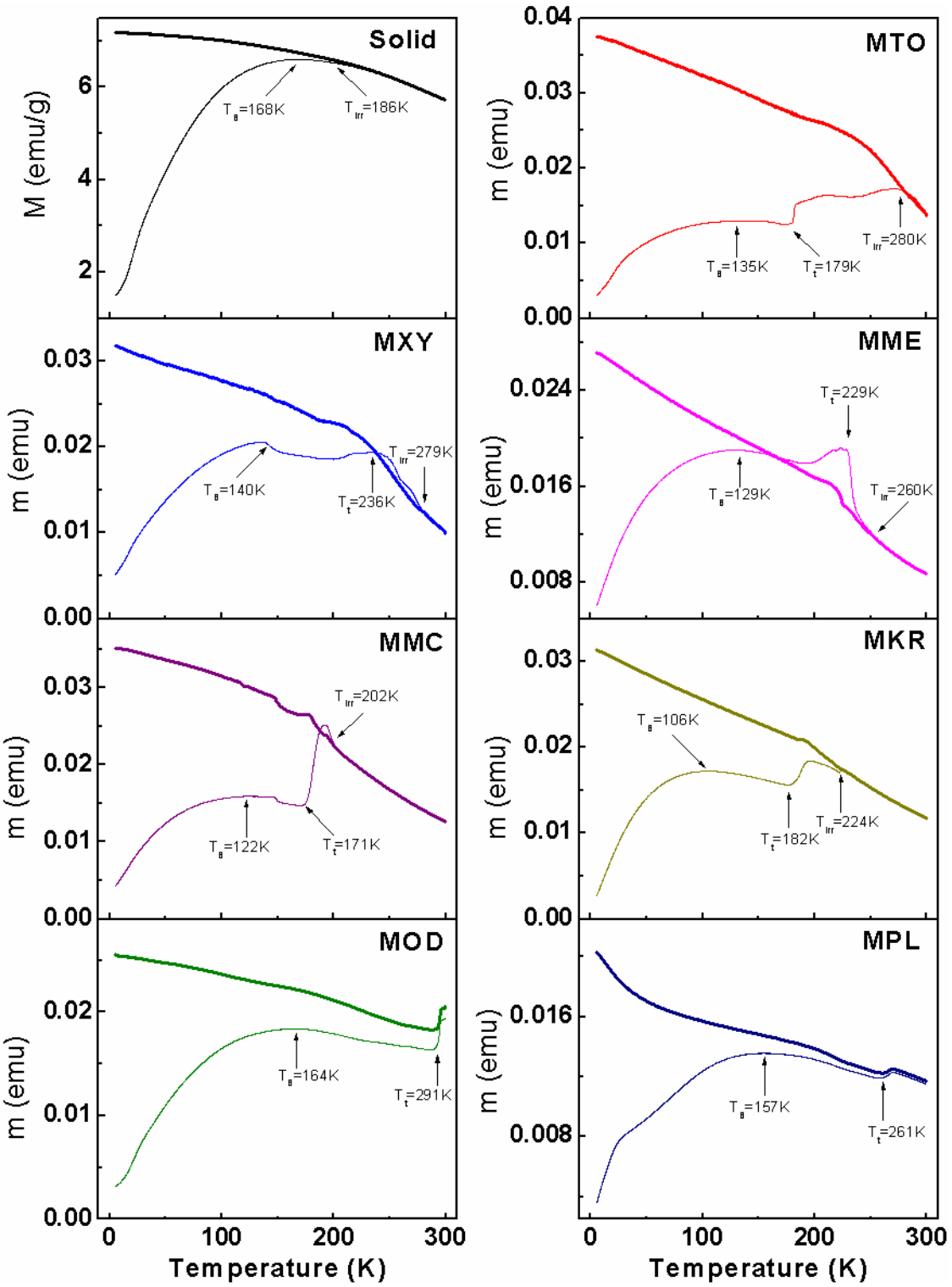

Figure 7.2. Zero field cooled (thin line) and field cooled (thick line) magnetization curves of the fluid samples dispersed in different base fluids are compared with that of the solid sample.

Table 7.3. Different characteristic temperatures obtained from the magnetic measurements of the nanofluids are compared with the melting point of the base fluids

Solvent (base fluid)	**Freezing point of solvent (K)**	**Blocking temperature, T_B (K)**	**Transition temperature, T_t (K)**	**Irreversible temperature, T_{irr} (K)**
Solid powder	-	168	-	186
Toluene	178	135	179	280
Xylene	239	140	236	279
Mesitylene	228	129	229	260
Methyl cyclohexane	147	122	171	202
Octadecene	289	164	291	>300
Kerosene	233	106	182	224
Paraffin liquid (light)	249	157	261	>300

Figure 7.2 shows the temperature dependant magnetization measurements of all the fluid samples and compared with that of the oleic acid coated solid sample. Fluid samples are prepared at the same concentration (2.2 volume% of Fe_3O_4) but show different magnetization behavior. For example, even though the same oleic acid coated powder sample is dispersed in different base fluids, the maximum in the ZFC magnetization curve (blocking temperature) is observed at different temperatures for the different fluids. The observed blocking temperatures (T_B) for the fluid samples are compared in the Table 7.3. The blocking temperature for all the fluid samples are less than the blocking temperature of the powder sample (168 K). The decrease in the blocking temperature for the fluid samples is due to the decreased interparticle interactions because of the larger interparticle separation when the particles are dispersed in the liquid matrix.[22] The larger separation between the particles reduces the anisotropy originating from interparticle dipolar interactions in the fluid thus requiring less thermal energy to overcome the anisotropy energy compared to that of the solid sample. Out of the seven fluid samples, the octadecene (MOD) and paraffin (MPL) based nanofluids show only a small decrease in the blocking temperature, 164 K and 157 K respectively, compared to that of the solid sample (168 K). The relatively smaller decrease in the blocking temperature is due to the lower dispersibility due to the highly viscous nature of the base fluids and therefore the particles remaining as agglomerates/clusters in the highly

viscous base fluids. Out of these, the more viscous base fluid, paraffin (η>20 mPa-s) is more effective to reduce the interparticle interaction probably because it reduces the dynamic behavior of the particles (reduced Brownian motion) compared to the octadecene (η=4.01 mPa-s) based fluid.

Nanoparticles dispersed in the base fluids toluene, xylene, mesitylene, methylcyclohexane and kerosene (MTO, MXY, MME, MMC and MKR) are found to form highly stable and well dispersed nanofluids and the blocking temperatures are much reduced (<140 K) than that for the octadecene (164 K) and paraffin (157 K) based fluids (shown in Table 7.3). Out of the different fluid samples, kerosene based fluid (MKR) shows the lowest blocking temperature (106 K). The relatively larger decrease in the blocking temperature for some of the fluids could be attributed to the better compatibility of the solvents with the surfactant molecules on the surface of the nanoparticles. The better interaction between the surfactant and the solvent at the particle-fluid interface allows the surfactant molecules to extent into the solvent matrix and separates the nanoparticles away from each other. The large separation of the nanoparticles due to the steric stabilization reduces the interparticle magnetic interaction effectively which in turn reduces the anisotropy energy.

A comparison of the dielectric constant and the blocking temperature shows a specific trend. The fluid in kerosene, with the lowest dielectric constant (ε=2.0), compared to other solvents, shows the lowest blocking temperature, even though the intrinsic viscosity of kerosene (1.64 mPa-s) is relatively larger compared to that of the other base fluids among the other well dispersed nanofluids (see Table 7.1). The better compatibility and viscous nature of kerosene separates the nanoparticles away from one another and reduces the magnetic interaction between the particles, resulting in the reduction in the anisotropy energy in turn reducing the blocking temperature (T_B). The same trend is also followed in the case of the nanofluids in octadecane and paraffin liquid. The dielectric constant of paraffin is lower than that of octadecane whereas the viscosity is larger and the fluid in paraffin shows relatively lower blocking temperature. From the above discussion, the observed variation of the blocking temperature can be attributed to the solvent-surfactant interaction or compatibility of the surface of the oleic acid coated nanoparticles with the solvent.

For the dried oleic acid coated nanoparticles, the temperature at which irreversibility is observed between the FC and ZFC magnetization curves (T_{irr} = 186 K) is just above the blocking temperature (168 K). As discussed in chapter 3, T_{irr} corresponds to the blocking

temperature of the largest sized particles and these particles are blocked so that magnetic hysteresis loop opens up below this temperature. However, for the nanofluids, T_{irr} is much larger than that of the powder sample, except for the methylcyclohexane based fluid. A comparison with the freezing points of the corresponding base fluids shows that T_{irr} of the particular fluid is closer to the freezing point of the solvent. As discussed in chapter 3 (section 3.4.1 and section 6.4.2), below the freezing points of the solvents, the solvent in which the oleic acid coated nanoparticles are dispersed freezes and thus the nanoparticles are dispersed in a solid matrix below this temperature. Brownian relaxation of the magnetization of the nanoparticles is no longer possible and hence the direction of the magnetic moment is frozen in random directions below the freezing point of the solvent. A comparison of the T_{irr} and the freezing point of the corresponding solvent shows that only for methyl cyclohexane based fluid, T_{irr} is comparable to that of the dry particles because the freezing point of the solvent is comparable to the T_{irr} of the dried particles. However, a small jump in the FC and ZFC magnetization curves of the fluid is observed at 146 K, at the freezing point of the solvent, due to the additional constraint to the relaxation of the particles due to the freezing of the solvent.

7.6. Thermal conductivity

The thermal conductivity of the different nanofluids is measured as a function of the volume% of the nanoparticles dispersed in the corresponding fluid, for the well dispersed stable fluids of MTO, MXY, MME and MKR. The relative enhancement in the thermal conductivity and % enhancement with the volume% of the particles are shown in Figure 7.3. No appreciable change in the thermal conductivity over that of the base fluid is observed up to a certain volume% for all the fluid samples. The thermal conductivity varies almost linearly with the volume% of the particles, above a certain critical concentration, which is found to depend on the solvent. The observed critical concentration is different for the different nanofluids, as shown in Figure 7.3(b), and the critical concentration for the fluid samples MKR, MTO, MXY, and MME are obtained as 0.4, 0.8, 1.1, and 1.1 volume%, respectively (shown in Table 7.4). The variation of the critical concentration for different base fluids may be attributed to the ease of formation of nanoparticle clusters in the fluid as well as the compatibility between the surfactant and the solvent or the dispersibility. Studies using different surfactants and the same solvent (chapter 3, section 3.4.2 and chapter 6, section 6.4.3) showed that the critical concentrations are different for different surfactants, confirming this argument.

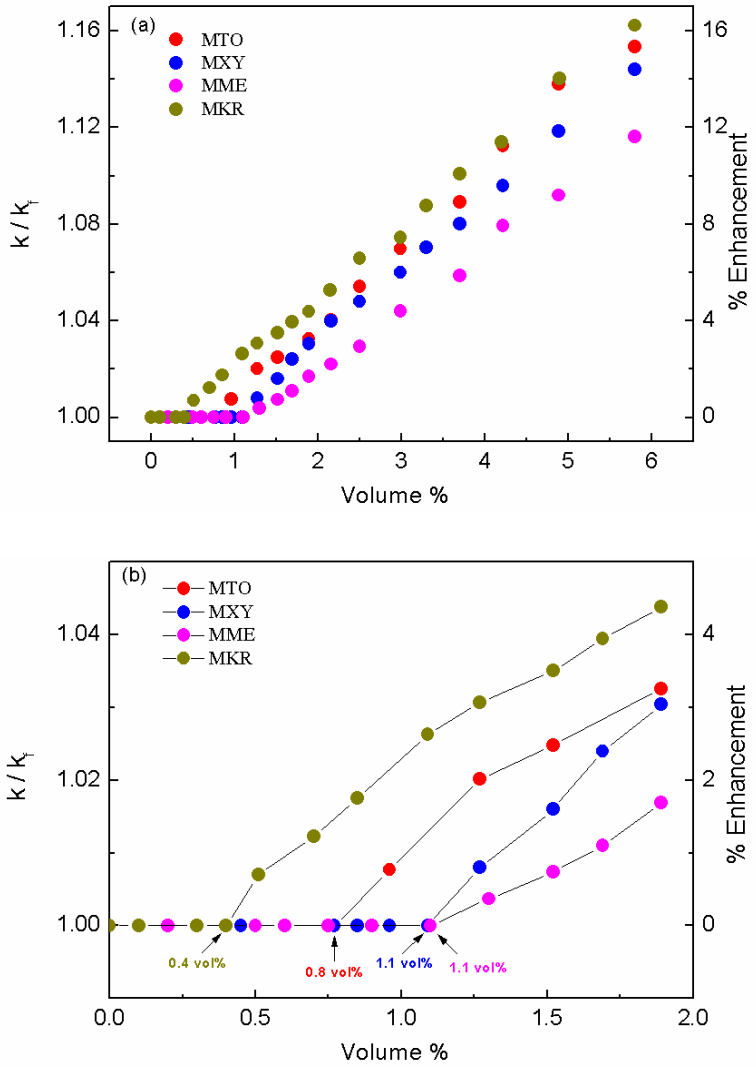

Figure 7.3. (a) Comparison of the variation of thermal conductivity with the volume% of nanoparticles for different fluid samples. (b) zoomed figure showing variation at lower concentration near the critical concentration.

In the present case, the critical concentration correlates well with dielectric constant of the base fluid. Out the four studied fluid samples for volume% variation of thermal conductivity, kerosene based fluid (MOK) shows the lowest critical concentration, and the critical concentration varies in the order MOK<MOT<MOX=MOM (0.4 < 0.8 <1.1=1.1), similar to the variation in the dielectric constant of the base fluid again in the order kerosene<toluene<xylene=mesitylene (2.0<2.38<2.4=2.4). Thus, the observed critical concentrations could be due to the compatibility of the solvent with the surface of the nanoparticles. Similar pattern of enhancement in thermal conductivity with the volume% of nanoparticles has been reported for 6.7 nm oleic acid coated Fe_3O_4 nanoparticles dispersed in kerosene and the reported critical concentration is 1.71 volume%.[23] In the present study, the

particle size of the Fe_3O_4 nanoparticles is comparable with that reported and hence the observed difference in critical concentration with that reported in the literature could be due the difference in the amount of surfactant (primary and secondary), the degree of wettability of the particle surfaces, interfacial resistance, etc, all of which are related to the compatibility between the surfactant and the base fluid.

The effective thermal conductivity (k) of the different nanofluids is calculated using the classical Maxwell model by considering the thermal conductivity of the solid and liquid, and volume% of the solid, as well as the microconvection model, as described in chapter 3. The calculated effective thermal conductivity is compared in Figure 7.4 (black solid line) with the experimental values. The experimental results of toluene (MTO) and kerosene (MKR) based nanofluids almost matches with the theoretical model, the xylene based (MXY) fluid shows slight deviation and mesitylene based fluid shows larger deviation from the Maxwell model. The deviation of the experimental results from the theoretical model for the xylene (MXY) and mesitylene (MME) based fluids is due to the less solvation of the surfactant on the surface of the nanoparticle in the solvents xylene and mesitylene. Due to the less solvation of the surfactant, nanoparticle clusters could not be formed even at higher concentrations due to the less van der Waals interaction between the surfactants. These samples require much higher concentration to achieve larger thermal conductivity in comparison with the toluene (MTO) and kerosene (MKR) based fluids. Still the observed thermal conductivity for these samples could be due to the Brownian motion of the dispersed particles in the fluid. Although the dispersed material is same for all four fluid samples, the observed difference in the variation of the thermal conductivity enhancement for different fluids could be due to the thermophysical and physicochemical properties of base fluids.

Table 7.4. The critical concentration for the thermal conductivity and the slope of the linear region for the studied different nanofluids

Solvent	Sample code	Critical concentration (volume%)	Slope in the linear region
Kerosene	MKR	0.4	0.030
Toluene	MTO	0.8	0.031
Xylene	MXY	1.1	0.030
Mesitylene	MME	1.1	0.025

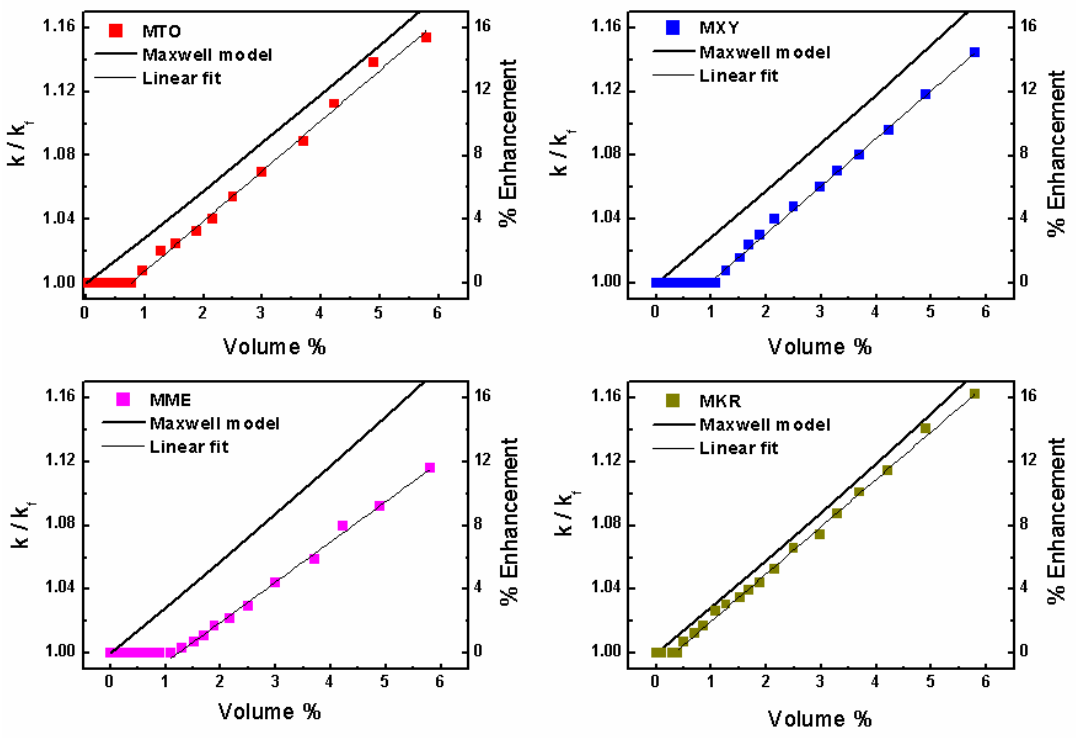

Figure 7.4. The calculated thermal conductivity using the Maxwell (thick solid lines) model compared with the experimental values (squares). The thin solid lines are linear fit to the experimental values above the critical concentration.

The linear part in the variation of thermal conductivity with volume% above the critical concentration is fitted by least-squares fit as shown in Figure 7.4 (thin solid lines). The slope of the linear fit (Table 7.4) indicates the rate of variation of relative thermal conductivity with volume% of the particles. The slopes are almost comparable for toluene, xylene and kerosene based fluids and relatively lower for the mesitylene based fluid. Mesitylene based fluid shows relatively smaller increase in the thermal conductivity, probably due to the poor compatibility of the solvent with the surface of the nanoparticles. It has been reported that the enhancement in the thermal conductivity of nanofluids is less for the base fluids having larger intrinsic thermal conductivity and larger enhancement for the base fluids having lower inherent thermal conductivity.[15, 13-14] Out of the four studied base fluids kerosene (0.114 W/mK) has the lowest intrinsic thermal conductivity and mesitylene (0.136 W/mK) has high the intrinsic thermal conductivity and this difference is reflected in the thermal conductivity of the respective nanofluids. However, the toluene based fluid shows larger enhancement in the thermal conductivity than the xylene based fluid even though the intrinsic thermal conductivity of toluene (0.129 W/mK) is larger than that of xylene (0.127

W/mK). This indicates that the larger intrinsic thermal conductivity of the base fluid is not always resposible for the larger enhancement in the thermal conductivity of nanofluids.

7.7. Viscosity

The relative viscosity of the nanofluids with respect to the base fluid as a function of the concentration of Fe_3O_4 nanoparticles (volume%) is shown in Figure 7.5. The relative viscosity varies almost linearly with the volume% of the nanoparticles for all the four nanofluids. Figure 7.6 shows a comparison of the variation of the relative viscosity for the different nanofluids with that calculated using the different models (using equations in Table 1.6). The experimental results are much larger than the values calculated using the theoretical models. The intrinsic viscosities of toluene, mesitylene, xylene and kerosene are 0.56, 0.66, 0.76 and 1.64 mPa-s, respectively (Table 7.1). The observed enhancement in the viscosity with increasing concentration of the nanoparticles shows relatively larger enhancement for the mesitylene based nanofluid and lowest enhancement for the kerosene based nanofluid. The enhancement in the viscosity is almost comparable for toluene and mesitylene based fluids. The variation is almost in the reverse order of the viscosity of the base fluid (toluene and mesitylene with comparable viscosities show the reverse trend). Thus, nanofluids in the base fluids with the lower intrinsic viscosity (toluene and mesitylene) show larger enhancement in the viscosity compared to the base fluid with higher viscosity (kerosene). Although the critical concentration for the enhancement in the thermal conductivity (due to formation of clusters) for kerosene based nanofluid is lower than that of toluene based fluid, the enhancement in the viscosity with concentration of the particles is much lower for the kerosene based fluid. This could be due to the intrinsic larger viscosity of kerosene, which is almost three times larger than the intrinsic viscosity of toluene. Thus, the addition of nanoparticles in the highly viscous base fluid (kerosene) has not affected the viscosity of the nanofluid effectively. The large enhancement in the viscosity of the mesitylene based fluid can be due to the formation of the clusters, but the observed thermal conductivity is much lower compared to other base fluids. This could be due to the less compatibility of the solvent (mesitylene) with the nanoparticle surfaces which increases the interfacial thermal resistance (Kapitza resistance) and reduces the thermal conductivity of nanofluids. From the above discussion it is clear that neither the intrinsic viscosity of the base fluids nor the viscosity of the nanofluid is the reason for the large enhancement in the thermal conductivity of the nanofluids.

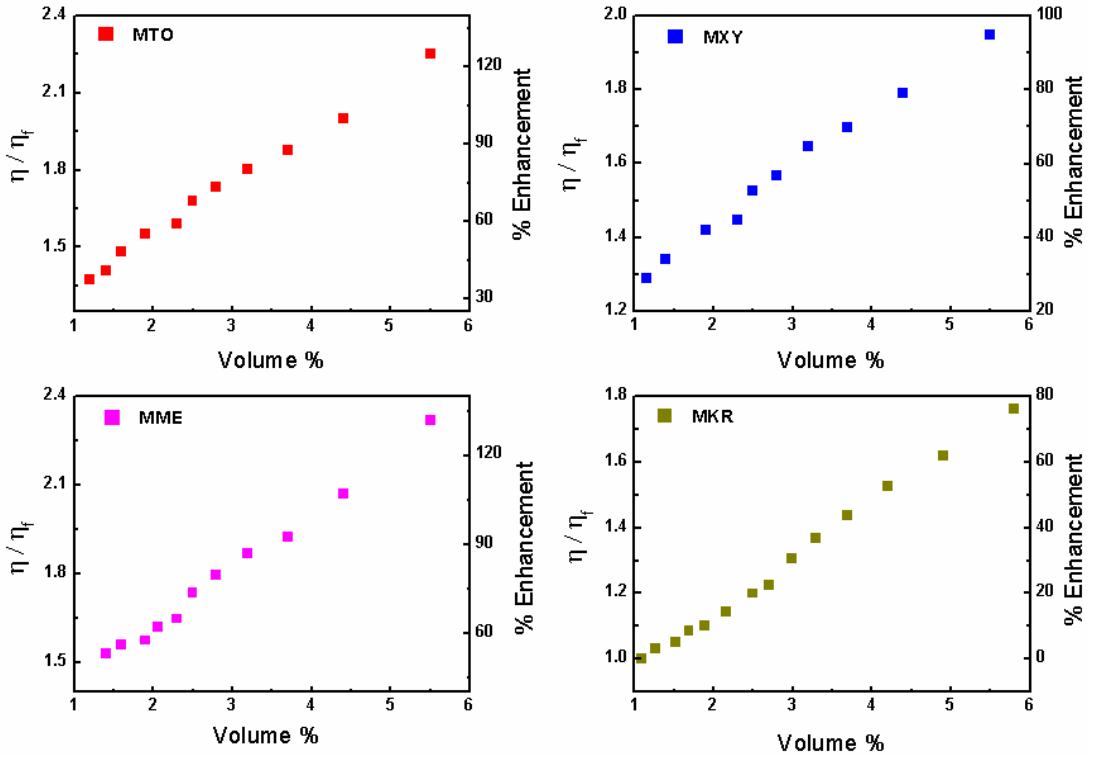

Figure 7.5. Variation of the relative viscosity of the fluids with the volume% of the nanoparticles

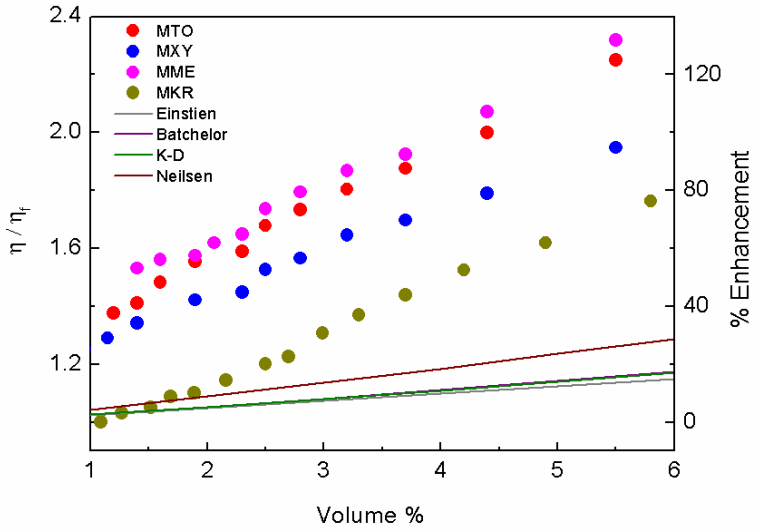

Figure 7.6. Comparison of the variation of viscosity with volume% of nanoparticles for different fluids (circles) with values calculated using theoretical models (solid lines)

7.8. Correlation of thermal conductivity with viscosity of nanofluids

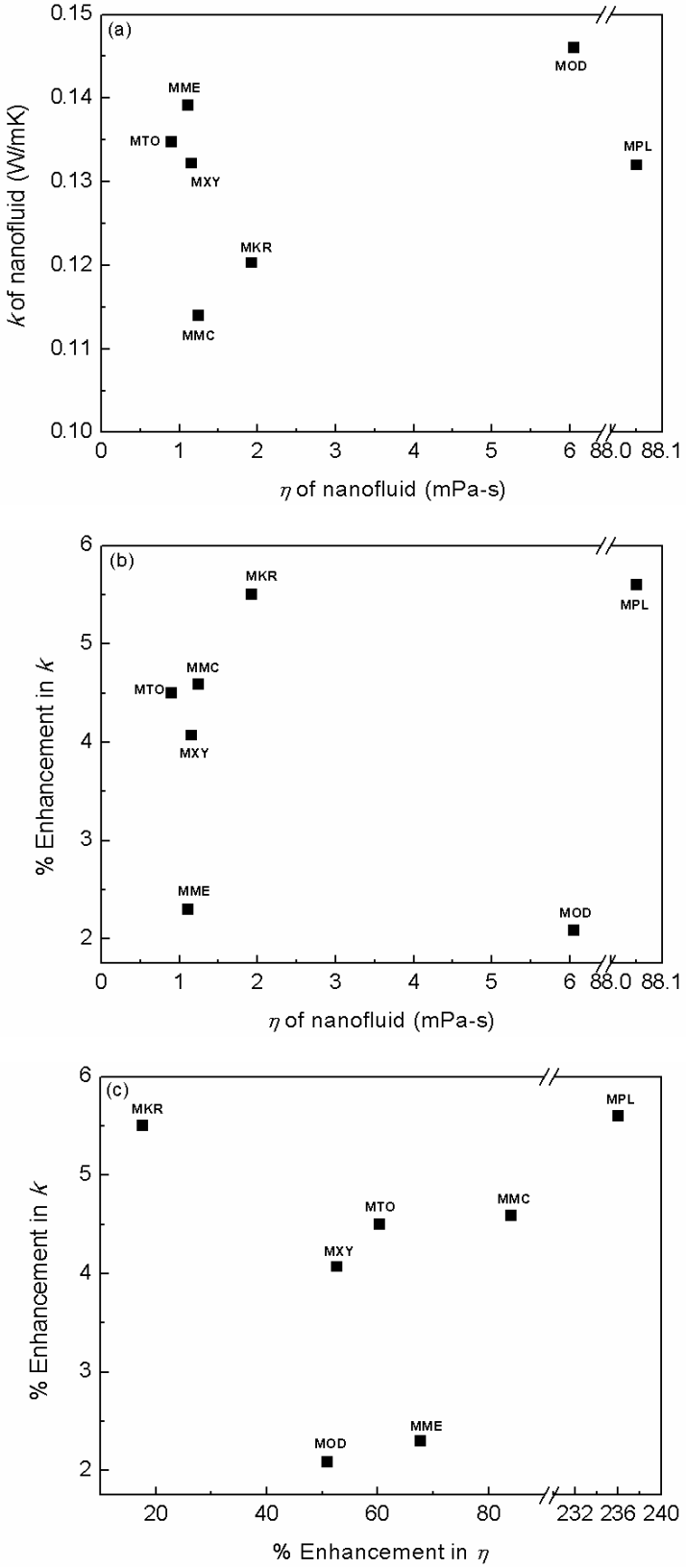

Figure 7.7. Variation of (a) absolute value of thermal conductivity and (b) percentage enhancement in the thermal conductivity with viscosity of nanofluids, and (c) percentage enhancement of thermal conductivity versus percentage enhancement in the viscosity for different nanofluids

In Figure 7.7(a), the thermal conductivity of the nanofluids at 2.2 volume% is plotted against the viscosity of the nanofluids at same volume% dispersed in different base fluids. The observed results show no correlation between the thermal conductivity of nanofluids with the viscosity of the nanofluids. Previous studies showed increase in the thermal conductivity with increasing viscosity.[24-27] The present results do not show any particular correlation between the thermal conductivity and viscosity of the nanofluids when the magnetite nanoparticles coated with the same surfactant is dispersed in different solvents.

The percentage enhancement in the thermal conductivity for different nanofluids is plotted against the viscosity of the nanofluids in Figure 7.7(b). The percentage enhancement increases with increasing the viscosity of the nanofluids, at lower viscosity range (<2 mPa-s). The enhancement in the thermal conductivity with increasing viscosity of the nanofluid could be due to the formation of more clusters in the nanofluids. The relatively low enhancement in the thermal conductivity of MOD could be due to the less dispersing nature and less compatibility of the solvent with the surface of the nanoparticles as well as the larger interfacial resistance at the particle-fluid interface. In the case of the fluid in paraffin, the nanoparticles are less dispersed forming larger aggregates (see Figure 7.1). The observed larger enhancement in the thermal conductivity of MPL compared to that of MOD could be due to the heat transfer through these larger aggregates.

Enhancement in the thermal conductivity is plotted against the enhancement in the viscosity of the nanofluids in Figure 7.7(c). Out of the studied fluids, only the kerosene based fluid shows less enhancement (~18%) in the viscosity over that of the base fluid. The paraffin based fluid shows larger enhancement in the viscosity (~236%) and the other nanofluid samples show moderate enhancement in the viscosity over the corresponding base fluids (50-90%). Moreover, the thermal conductivity enhancement is larger for the kerosene and paraffin based nanofluids compared to the other base fluids (fluids with lowest and highest enhancement in viscosity). The large enhancement in the thermal conductivity for the well dispersed kerosene based nanofluid could be due to the assembly or cluster formation even at lower concentrations (>0.4 volume%). Even though the cluster formation in the kerosene based fluid is more, the observed least enhancement in the viscosity (17%) could be due to the high dissolution or solvation of the surfactant molecules on the surface of the nanoparticles. The large enhancement in the viscosity for the paraffin based fluid is due to larger aggregates of the less dispersed nanoparticles and the other nanofluids are showing moderated enhancement in the viscosity due to the cluster formation. However, there is no

particular trend followed in the variation of the thermal conductivity enhancement with the viscosity enhancement for different nanofluids. The solvating ability of the solvent and the compatibility of the surface of the nanoparticles with the solvent are likely to play important roles in the enhancement of thermal conductivity as well as viscosity of the nanofluids.

7.9. Correlation between thermal conductivity of nanofluids and properties of base fluids

In order to get a clear picture on the factor(s) responsible for the difference in the enhancement in the thermal conductivity using different base fluids, the results are compared with some of the thermophysical properties of the base fluids. The properties of the different nanofluids using different base fluids at 2.2 volume% are compared.

7.9.1 Thermal conductivity of base fluid

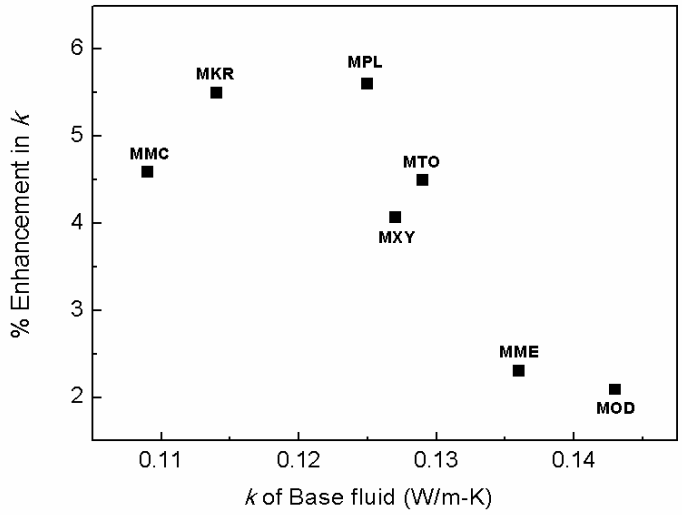

Figure 7.8. Enhancement in the thermal conductivity for different nanofluids (2.2 volume%) with the thermal conductivity of the base fluid

Figure 7.8 shows the percentage enhancement in the thermal conductivity against the intrinsic thermal conductivity of the base fluid. There is an overall decrease in the thermal conductivity of the nanofluid with increasing thermal conductivity of the base fluid, although

some deviations are observed. Nanofluids with the base fluid of larger intrinsic thermal conductivity shows lower enhancement and the base fluid with less intrinsic thermal conductivity shows larger enhancement in the thermal conductivity. Similar results are reported for α-Al_2O_3 nanoparticles dispersed in different base fluids showing larger enhancement in the thermal conductivity for the base fluid which has lower intrinsic thermal conductivity.[15] The observed deviation in the case of some base fluids could be attributed to the physicochemical properties such as solubility, dispersion or compatibility of the nanoparticle surfaces with the base fluid.

7.9.2 Viscosity of base fluid

In Figure 7.9, the percentage enhancement in the thermal conductivity is plotted against the intrinsic viscosity of the base fluid. No correlation is observed between the thermal conductivity enhancement of the nanofluid and viscosity of the base fluid. It has been reported that high viscosity of the base fluid reduces the Brownian motion of the nanoparticles in the fluid, which leads to reduction in the thermal conductivity.[7] Even for the less viscous base fluids, Brownian motion of the nanoparticles can be reduced by the internal organization of the particles inside the fluid and this could also lead to increase in the viscosity of the nanofluid. Increase in the thermal conductivity is also reported for the aggregated nanoparticles with reduced Brownian motion with different heat conduction mechanisms.[10] It is also reported that the nanoparticles in highly viscous fluids could form thick layer of molecules (liquid layer) at the fluid-particle interface compared to less viscous fluids, and this highly conducting interfacial layer could increase the thermal conductivity.[11] The present results are contradictory to the reported Brownian motion dependant thermal conductivity enhancement. The highly viscous paraffin based fluid (MPL) shows larger enhancement in the thermal conductivity than that of other low viscous fluids. Thus, the present results indicate that the thermal conductivity enhancement cannot be correlated to the viscosity of the base fluid alone and it also depends on various other factors such as the nature of the surface of the nanoparticles, dispersibility in the particular base fluid, wetting of the nanoparticle surfaces with the fluid molecules, interaction between the surfactants from the different nanoparticles, the compatibility of the surface of the nanoparticles with the fluid, etc.

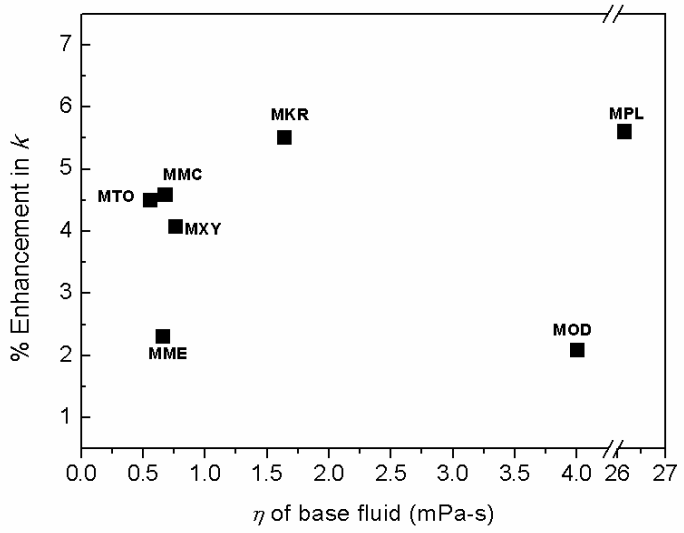

Figure 7.9. Enhancement in the thermal conductivity for different nanofluids with viscosity of the base fluid

7.9.3 Specific heat of base fluid

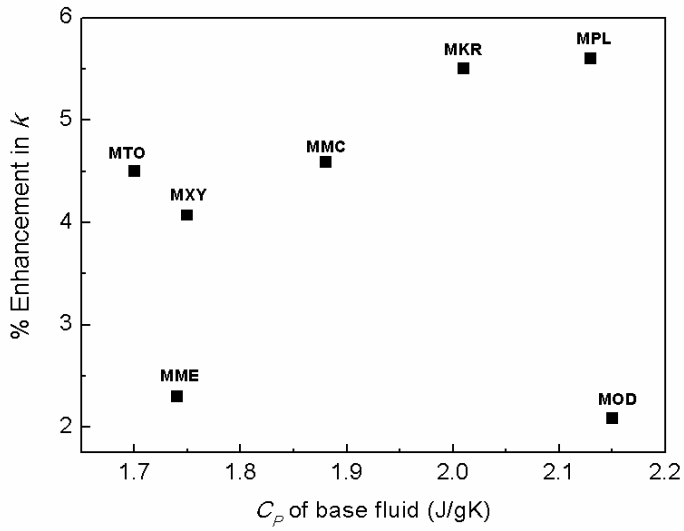

Figure 7.10. Enhancement in the thermal conductivity of different nanofluids with the specific heat of the base fluid

Figure 7.10 correlates the enhancement in the thermal conductivity with the specific heat of the different base fluids. The result shows a linear enhancement in the thermal conductivity with specific heat of the base fluid, except for MME and MOD. Even though the specific heat

of octadecene is larger, the lower enhancement in the thermal conductivity could be due to the less dispersibility and less wetting of the solvent with the surface of the nanoparticles. Similarly, the much lower enhancement in the thermal conductivity for the mesitylene based fluid could be due to the compatibility of mesitylene with the surface of the nanoparticles.

7.9.4 Dielectric constant of base fluid

Figure 7.11 shows the percentage enhancement in the thermal conductivity of different nanofluids against the dielectric constant of the base fluid. The results show that the base fluids with less dielectric constant give relatively larger enhancement in the thermal conductivity. The observed results can be directly correlated to the dispersibility of the oleic acid coated nanoparticles in different base fluids. The hydrophobic oleic acid coated nanoparticles show good dispersion in highly non-polar solvents than the polar solvents. When the polarity of the base fluid increases, the solvation of the hydrophobic chain with the solvent is decreased. It has been reported that oleic acid coated magnetite nanoparticles show good dispersion in the solvents with less dielectric constant or in less polar solvents.[18] Solvent with large dielectric constant shows less compatibility to the surface of the nanoparticle and strongly influences the heat transfer characteristics of the nanofluids. The deviation of the experimental results for octadecene based (MOD) fluid is probably due to less dispersibility of the nanoparticles in the base fluid.

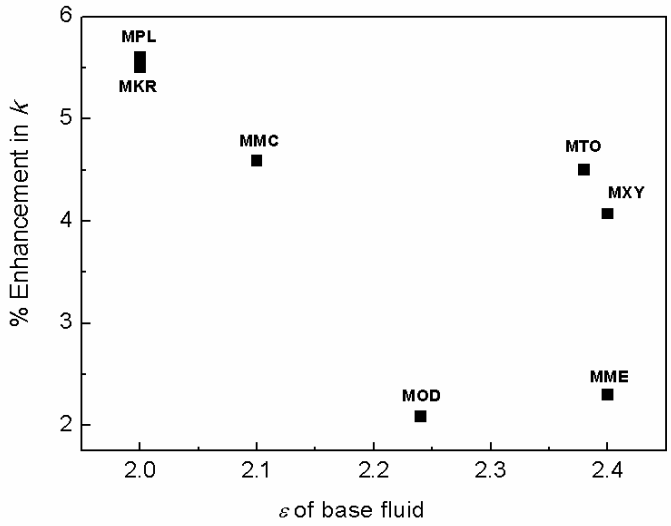

Figure 7.11. Enhancement in the thermal conductivity of different nanofluids with the dielectric constant of the base fluid

7.10. Role of solvent on thermal conductivity enhancement

From the above discussions, it is clear that no single property of the solvent is responsible for the enhancement in the thermal conductivity of the nanofluids. However, it can be concluded that less intrinsic thermal conductivity, large specific heat and low dielectric constant of the base fluid are the desirable factors for larger enhancement in thermal conductivity of the nanofluids. The viscosity of the base fluid appears to be not a contributing factor for thermal conductivity enhancement of the nanofluid. However, apart from the thermophysical properties of the base fluids, there are other factors which play important roles in the enhancement in the thermal conductivity of the nanofluids. Although the surfactant on the surface of the nanoparticles is the same for all fluid samples, the factors such as solvating ability of the solvent or compatibility of the solvent with the surfactant on the surface of the nanoparticle, liquid layering at the particle-fluid interface, interfacial thermal resistance at the particle-fluid interface are different for different base fluids. The present results may be limited to only oleic acid coated nanoparticles, and may vary with the surfactant, particle size, amounts of primary and secondary surfactants, etc.

7.11. Thermal conductivity in the presence of a magnetic field

The compatibility of the surface of the nanoparticles with the solvent and dispersion characteristics of the different nanofluids are reflected in the changes in the thermal conductivity in the presence of the magnetic field (Figure 7.12). Measurements are made on 2.2 volume% of oleic acid coated nanoparticles dispersed in different base fluids.

Figure 7.12(a) shows the enhancement in the thermal conductivity with applied magnetic field up to 1 T. The less dispersed samples MOD and MPL show very low enhancement in the thermal conductivity even at very high magnetic fields (1 T). The well dispersed nanofluids show larger enhancement with increasing the magnetic field showing a maximum at higher fields. Maximum thermal conductivity enhancement is observed for the fluids of MTO, MXY and MME at a field of ~0.55 T and the fluids of MKR and MMC show maximum enhancement at ~0.4 T. However, the enhancement in the thermal conductivity is different for different fluids and the observed maximum enhancements are 117%, 130%, 91%, 53%, 20%, 54%, and 10% for samples MTO, MXY, MME, MMC, MOD, MKR, MPL respectively. The lower enhancement in the thermal conductivity for MOD and MPL may be attributed to the large viscosity of the octadecene and paraffin based fluids.

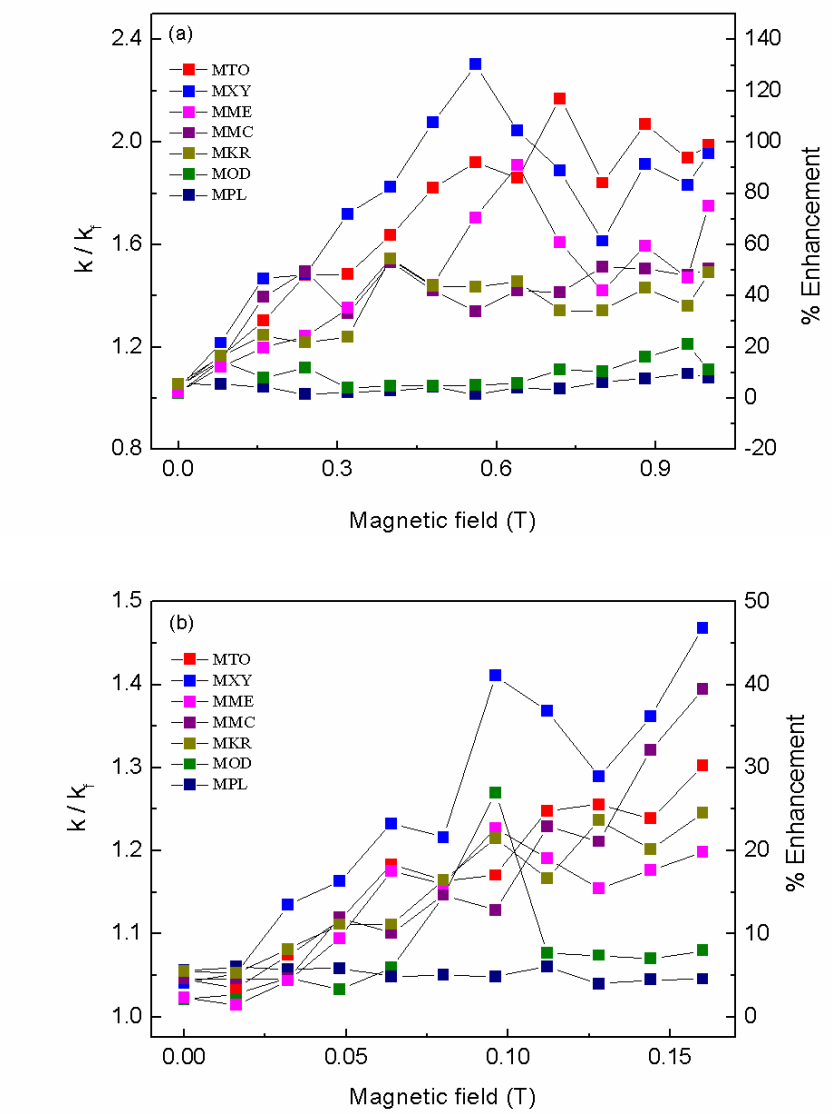

Figure 7.12. Enhancement in the thermal conductivity for different nanofluids (2.2 volume%) with applied magnetic field, (a) the variation in relative thermal conductivity under higher magnetic field (0 to 1 T) and (b) the variation at low field region (0 to 0.16 T)

Figure 7.12(b) shows the enhancement in thermal conductivity for various nanofluids at low magnetic fields (up to 0.16 T). The increase in the thermal conductivity may be attributed to the increase in the dipole-dipole interaction between the magnetic nanoparticles in presence of a magnetic field. The dipole-dipole interaction between the magnetic nanoparticles could form nanoparticle chains in the direction of the magnetic field and the aspect ratio of the chain increases with increasing the strength of the magnetic field. Heat energy is transferred through the back bone of the chain which leads to large enhancement in the thermal conductivity.[23, 28] The observed non-linearity in the experimental results could be due to stable nanofluids of highly dispersive nature of the nanoparticles.

The well dispersed fluids MTO, MXY, MME, MMC and MKR show relatively large enhancement in the thermal conductivity, whereas the less dispersed fluid MOD shows slight enhancement and MPL shows no appreciable enhancement in the thermal conductivity over the base fluid. The well dispersed fluids show enhancement even at very low magnetic fields (0.015T) and the enhancement increases with increasing the magnetic field. On the other hand, the less dispersed MOD fluid shows increase in the thermal conductivity only above 0.06T, and this could be due to the fact that the aggregation of the less dispersed nanoparticles requires more magnetic field to align the particles in the direction of the magnetic field due to the larger anisotropy of the aggregated particles in the fluid. The larger viscosity of the octadecene based fluid (4.01 mPa-s) restricts the dipolar interaction due to the reduced Brownian motion, and higher field energy is required to bring the particles closer to each other to form the chain aggregation. In the case of less dispersed fluid MPL, the larger viscosity of paraffin (>25 mPa-s) completely arrests the Brownian motion of the nanoparticles.

7.12. Conclusions

Thermal conductivity studies are performed on oleic acid coated magnetite nanoparticles dispersed in different base fluids (solvents). From magnetic measurements of fluid samples, it is observed that well dispersed fluids show larger reduction in the superparamagnetic blocking temperature and the poorly dispersed samples show less reduction compared to the solid nanoparticles. The difference in the blocking temperatures is correlated with the ability of the solvation of surfactant on the nanoparticle surfaces with the solvent, which changes the interparticle interactions.

Concentration dependant thermal conductivity variation is studied for four well dispersed fluids. Out of these, toluene and kerosene based fluids showed relatively larger enhancement even at lower concentrations compared to xylene and mesityelne based fluids The enhancement in the thermal conductivity at lower concentration could be due to the formation of clusters in the nanofluids. Interdigitation of the long chain surfactant from the different particles forms cluster of particles in the fluid. Mesitylene based fluid shows least enhancement in the thermal conductivity probably due to the less compatibility of the surface of the coated nanoparticles with the solvent molecules which increases the interfacial thermal resistance.

Comparison of the different thermophysical properties of the base fluids with the thermal conductivity enhancement showed that the thermal conductivity decreases with increasing the thermal conductivity and dielectric constant of the base fluid and increases with the viscosity and specific heat of the base fluid. However, the thermal conductivity enhancement could not be correlated with any particular property of the solvent. Thus, it is concluded that apart from the thermophysical properties of the base fluid, the compatibility of the solvent with the surface of the nanoparticles is crucial for the thermal conductivity enhancement since it affects the dispersion stability and interfacial resistance at the particle-fluid interface.

References

1. Chon, C. H.; Kihm, K. D.; Lee, S. P.; Choi, S. U. S. *Appl. Phys. Lett.* **2005**, *87*, 153107.
2. Prasher, R.; Evans, W.; Meakin, P.; Fish, J.; Phelan, P.; Keblinski, P. *Appl. Phys. Lett.* **2006**, *89*, 143119.
3. Yu, W.; Choi, S. U. S. *J. Nanopart. Res.* **2003**, *5*, 167-171.
4. Azizian, R.; Doroodchi, E.; Moghtaderi, B. *Ind. Eng. Chem. Res.* **2012**, *51*, 1782-1789.
5. Prasher, R.; Bhattacharya, P.; Phelan, P. E. *Phys. Rev. Lett.* **2005**, *94*, 025901.
6. Koo, J.; Kleinstreuer, C. *J. Nanopart. Res.* **2005**, *6*, 577-588.
7. Tsai, T. H.; Kuo, L. S.; Chen, P. H.; Yang, C. T. *Appl. Phys. Lett.* **2008**, *93*, 233121.
8. Nara, S.; Bhattacharya, P.; Vijayan, P.; Lai, W.; Rosenthal, W.; Phelan, P.; Prasher, R.; Song, D.; Wang, J. In *Experimental Determination of the Effect of Varying the Base Fluid on Static Thermal Conductivity of Nanofluids*, ASME 2005 International Mechanical Engineering Congress and Exposition, American Society of Mechanical Engineers: 2005; pp 755-758.
9. Evans, W.; Fish, J.; Keblinski, P. *Appl. Phys. Lett.* **2006**, *88*, 093116.
10. Prasher, R.; Phelan, P. E.; Bhattacharya, P. *Nano Lett.* **2006**, *6*, 1529-1534.
11. Hosseini, S. M.; Moghadassi, A. R.; Henneke, D.; Elkamel, A. *J. Therm. Anal. Calorim.* **2010**, *101*, 113-118.
12. Younes, H.; Christensen, G.; Luan, X.; Hong, H.; Smith, P. *J. Appl. Phys.* **2012**, *111*, 064308.
13. Lee, S.; Choi, S.-S.; Li, S.; Eastman, J. A. *J. Heat Transfer* **1999**, *121*, 280-289.
14. Hwang, Y. J.; Ahn, Y. C.; Shin, H. S.; Lee, C. G.; Kim, G. T.; Park, H. S.; Lee, J. K. *Curr. Appl Phys.* **2006**, *6*, 1068-1071.
15. Xie, H.; Wang, J.; Xi, T.; Liu, Y.; Ai, F. *J. Mater. Sci. Lett.* **2002**, *21*, 1469-1471.
16. Timofeeva, E. V.; Yu, W.; France, D. M.; Singh, D.; Routbort, J. L. *J. Appl. Phys.* **2011**, *109*, 014914.
17. Altan, C. L.; Bucak, S. *Nanotechnology* **2011**, *22*, 285713.
18. Lopez-Lopez, M. T.; Duran, J. D.; Delgado, A. V.; Gonzalez-Caballero, F. *J. Colloid Interface Sci.* **2005**, *291*, 144-151.
19. Lide, D. R. *Crc Handbook of Chemistry and Physics*; CRC press, 2004.
20. Dover, M. V.; Hensley, W. A. *Ind. Eng. Chem.* **1935**, *27*, 337-339.

21. Al-Kandary, J. A.; Al-Jimaz, A. S.; Abdul-Latif, A. H. M. *J. Chem. Eng. Data* **2006**, *51*, 2074-2082.
22. Vargas, J. M.; Nunes, W. C.; Socolovsky, L. M.; Knobel, M.; Zanchet, D. *Phys. Rev. B.* **2005**, *72*, 184428.
23. Philip, J.; Shima, P. D.; Raj, B. *Appl. Phys. Lett.* **2007**, *91*, 203108.
24. Silambarasan, M.; Manikandan, S.; Rajan, K. S. *Int. J. Heat Mass Transfer* **2012**, *55*, 7991-8002.
25. Indhuja, A.; Suganthi, K.; Manikandan, S.; Rajan, K. S. *J. Taiwan Inst. Chem. Eng.* **2013**, *44*, 474-479.
26. Prasher, R.; Song, D.; Wang, J.; Phelan, P. Appl. Phys. Lett. **2006**, *89*, 133108.
27. Murshed, S. M. S.; Leong, K. C.; Yang, C. *Int. J. Therm. Sci.* **2008**, *47*, 560-568.
28. Shima, P. D.; Philip, J.; Raj, B. *Appl. Phys. Lett.* **2009**, *94*, 223101.

Chapter 8

Conclusions and future perspectives

8.1 Conclusions

Nanofluids are considered to be future coolants due to their potential heat transfer characteristics compared to the conventional heat transfer fluids. Many experimental results on thermal conductivity of nanofluids showed anomalous enhancement beyond the effective medium approximation, even at very lower concentrations. Various theoretical predictions and mechanisms are proposed to account for the anomalous enhancement in the experimental thermal conductivity. Although numerous experimental and theoretical studies have been reported on the thermal conductivity of nanofluids, reproducibility of the results is one of the major issues. The lack of reproducibility in the experimental results could be due to the various factors, other than the basic factors such as thermal conductivity of the dispersed solid particle as well as the base fluid and volume fraction of the particles in the fluid. Factors such as particle size, particle morphology, surfactants, pH, temperature, viscosity of base fluid as well as the nanofluid etc, are additional factors which may strongly influence thermal conductivity of nanofluids. In addition to the above factors, the nanoscale effects such as Brownian motion of the nanoparticles in a fluid, aggregation/clustering of the nanoparticles and liquid layering at particle-fluid interface are other important that are proposed to account for the enhancement in the thermal conductivity of nanofluids. Also, the role of the surfactant which is used to stabilize the nanoparticles in a fluid is generally ignored. Dispersion and stability of a nanofluid are decided by the interaction and compatibility between the surfactant and the solvent molecules, and hence these contributions may play a crucial role in the thermal conductivity of the nanofluids. Due to the contribution of the above mentioned factors, individually or collectively, the system becomes more complex making it difficult to understand the exact cause for the enhancement in the thermal conductivity. Detailed studies on various factors are therefore required to understand the exact cause of the anomalous enhancement in the thermal conductivity of nanofluids.

In this thesis, we have analyzed surfactant related factors on the thermal conductivity of magnetite nanofluids which were not considered previously. Preparation of stable nanofluids is one of the major criteria to achieve reliable and reproducible results in the thermal conductivity of nanofluids. Surfactants play an important role in the dispersion and stability of nanofluids. Fatty acids are one of the important surfactants used to stabilize nanoparticles in polar as well as non-polar solvents. Fatty acid molecules attached to the surface of the nanoparticles separate the particles away from one another because of the long hydrocarbon chain. We have used fatty acids of two different chain lengths, short-chain

decanoic acid and long-chain stearic acid, as surfactants for surface coating on the surface of magnetite nanoparticles to understand the role of the chain length of the surfactant. The coated magnetite nanoparticles are prepared under identical conditions. The dispersion and stabilization characteristics of the surfactant coated magnetite nanoparticles dispersed in the non-polar solvent, toluene, are studied. XRD, TEM, and magnetic measurements showed that smaller particles with relatively narrower size distribution are stabilized when using decanoic acid as surfactant whereas larger particles are also stabilized when coated with stearic acid. TEM images of the decanoic acid coated sample showed well separated particles whereas stearic acid coated sample showed formation of clusters. Magnetic studies showed non-interacting nature of the decanoic acid coated particles whereas and the stearic acid coated magnetite nanoparticles showed evidence for weak inter-particle magnetic dipolar interactions. Thermal conductivity as a function of the volume fraction of the particles showed linear enhancement after a critical concentration, below which there is no enhancement in the thermal conductivity. The critical concentration for decanoic acid and stearic acid coated samples are obtained as 1.7 and 1.0 volume%, respectively. Larger enhancement in the thermal conductivity is obtained in the presence of a magnetic field for the decanoic acid coated fluid compared to the stearic acid coated fluid, due to the easy response of the short chain decanoic acid coated particles than the long chain stearic acid coated particles in the fluid. The chain length of the surfactant molecules as well as the thickness and amount of the surfactant layer on the surface of the nanoparticles could be responsible for the difference in the enhancement in the thermal conductivity in the two different magnetite fluids.

The size of the nanoparticles dispersed in a base fluid is one of the important factors to be considered for enhancement in the thermal conductivity of a nanofluid. However, most of the experimental and theoretical studies on particle size dependant thermal conductivity considered the average size of particles in a fluid, irrespective of the size distribution. The role of particle size distribution on thermal conductivity is studied by preparing different decanoic acid coated magnetite nanoparticles with comparable average particle size but with different size distribution. Particle size distribution is confirmed from TEM analysis and magnetic measurements. Thermal conductivity measurements on different fluids at the same volume fraction of the particles dispersed in toluene showed decrease in the thermal conductivity with increasing the average size of the particles. Fluids with particles of narrow size distribution showed relatively larger enhancement in the thermal conductivity and good

agreement with the microconvection model, compared to the fluids with wider particle size distribution. The larger deviation of the experimental results for wide particle size distribution is attributed to the reduced Brownian motion of the particles.

Although different coated samples in the particle size distribution studies were prepared under identical conditions, it was found that the amount of the surfactant (primary and secondary) are different on different coated powder samples which may also affect the particle-solvent interaction, thereby affecting the Brownian motion of the particles. The different amount of the surfactant present on the surface of the nanoparticles is likely to lead to different dispersion characteristics of the resulting fluid, and hence the thermal conductivity. The fatty acid coated nanoparticles were initially synthesized in aqueous medium, and need to be washed properly to get hydrophobic nanoparticles in order to disperse in a non-polar solvent. Excess surfactant present over the primary layer (free or secondary layer of surfactant) will affect the dispersibility of the nanoparticles in non-aqueous solvents. This issue has been studied by preparing dodecanoic acid (lauric acid) coated magnetite nanoparticles. Different amount of surfactants on the surface of the nanoparticles is managed by controlled washing of the as-synthesized nanoparticles. TGA and IR studies showed the presence of two groups of surfactants on the surface of the nanoparticles, primary surfactants which are directly attached to the surface of the nanoparticles through chemical bonding and secondary surfactants which are attached over the primary layer through weak van der Waals interaction. Magnetic studies showed decreasing interparticle magnetic interactions with increasing the amount of surfactants on the surface of the nanoparticles. Nanoparticles with smaller amount of the secondary surfactants showed good dispersion in toluene, forming a stable fluid. Nanoparticles with larger amounts of the secondary surfactant showed poor dispersion in toluene, forming less stable fluids. The less stable fluids showed relatively larger enhancement in the thermal conductivity and viscosity, whereas, the well dispersed stable fluids show comparatively less enhancements in the thermal conductivity and viscosity. The larger enhancement in the thermal conductivity for less stable fluids is ascribed to the heat transfer through larger aggregates in the fluid. Thermal conductivity in the presence of a magnetic field showed large enhancement in the thermal conductivity for the stable fluids due to the easy response of the magnetite nanoparticles to the magnetic field. Thus, the changes in the thermal conductivity and viscosity of the magnetite nanofluids could be correlated with the

dispersibility of the nanoparticles in the base fluid, apart from the amount of the surfactant, which is found to be different for the different samples.

The packing of surfactant molecules on the surface of nanoparticles depends on the structure or conformation of the fatty acid molecule. Apart from the amount of fatty acid surfactant, the nature of surfactant or the structural conformation of surfactant molecules on the surface of nanoparticle also affects the dispersibility of the coated particles in a fluid. To study the effect of the conformation of the surfactant molecules on the thermal conductivity of nanofluids, four different fatty acid molecules with the same number of carbon atoms with different degree of unsaturation in their carbon chain (stearic acid - $C_{17}H_{35}COOH$, oleic acid - $C_{17}H_{33}COOH$, linoleic acid - $C_{17}H_{31}COOH$, linolenic acid - $C_{17}H_{29}COOH$) are selected for coating on the surface of magnetite nanoparticles. TEM studies showed that the saturated fatty acid coated nanoparticles are highly aggregated and the unsaturated fatty acid coated particles remain well separated. IR and TGA studies showed slight decrease in the amount of the surfactant with increasing unsaturation in the surfactant molecule. This is ascribed to the changes in the conformation of the surfactant molecules, where the kink (oleic acid), bend (linoleic acid) and hook (linolenic acid) structures reduce the packing efficiency, compared to the straight chain (stearic acid) structure. Magnetic measurements of the corresponding fluids showed that the interparticle interaction is more for the saturated fatty acid coated nanoparticles than for the unsaturated fatty acid coated samples. The larger interparticle interaction for the saturated fatty acid coated sample could be due to the interdigitation of the surfactant molecules from one particle to the nearby particles at higher concentrations, which leads to aggregation or clustering of the nanoparticles in the fluid. The aggregated fluid samples showed relatively large enhancement in the thermal conductivity and viscosity, whereas, the fluid samples with non-aggregated nanoparticles showed less enhancement in the thermal conductivity and viscosity. The observed critical concentration for thermal conductivity enhancement is relatively smaller for the saturated fatty acid coated fluid compared to the fluids containing highly unsaturated fatty acid coated nanoparticles. The conformation of the surfactant molecules on the surface of the nanoparticles affects the dispersing ability of the nanoparticles which in turn affects the thermophysical properties of nanofluid.

The physical properties of solvents such as, thermal conductivity, viscosity, heat capacity, and dielectric constant are factors which are expected to influence the heat transfer characteristics of nanofluids. In this study, the effect of solvent on the thermal conductivity of

oleic acid coated magnetite nanoparticles is studied by dispersing the nanoparticles in different non-polar solvents. Nanoparticles dispersed in toluene, xylene, mesitylene, methylcyclohexane, and kerosene produced stable dispersion, whereas, the particles dispersed in octadecene and paraffin liquid (light) showed poor dispersion. From magnetic measurements of fluid samples, it is observed that well dispersed fluids show larger reduction in the superparamagnetic blocking temperature whereas the poorly dispersed fluids showed less reduction compared to that of the solid nanoparticles. The difference in the blocking temperatures is correlated with the reduced interparticle interactions due to the ability of the solvation of surfactant on the surface of the nanoparticles with the solvent. Concentration dependent thermal conductivity studies have been performed on four well dispersed fluids. Out of these, toluene and kerosene based fluids showed relatively larger enhancement even at lower concentrations compared to xylene and mesityelne based fluids The enhancement in the thermal conductivity at lower concentrations for the toluene and kerosene based fluids could be due to the formation of clusters in the nanofluids. Interdigitation of the long chain surfactant from the different particles forms cluster of particles in the fluid. Mesitylene based fluid showed least enhancement in the thermal conductivity probably due to the less compatibility of the surface of the coated nanoparticles with the solvent molecules which increases the interfacial thermal resistance. Comparison of the different thermophysical properties of the base fluids with the thermal conductivity enhancement showed that thermal conductivity decreases with increasing thermal conductivity and dielectric constant of the base fluid and increases with the viscosity and specific heat of the base fluid. However, the thermal conductivity enhancement could not be correlated with any one particular property of the solvent. Thus, it is concluded that apart from the thermophysical properties of the base fluid, the compatibility of the solvent with the surface of the nanoparticles is crucial for the thermal conductivity enhancement since it affects the dispersion stability and interfacial resistance at the particle-fluid interface.

From the studies on the thermal conductivity of magnetite nanoparticles coated with different fatty acid surfactants and dispersed in different solvents, it is clear that the solvent-surfactant interaction at the interface or compatibility of the solvent with the surfactant on the surface of the nanoparticle is an important factor determining the heat transfer characteristics of nanofluids. The thickness (length) of the surfactant molecule, amount of surfactant coated on the nanoparticles, nature of the attachment of surfactant (primary/secondary), chemistry of the surface of the surfactant coated nanoparticles, conformation of the surfactant molecules

on the surface of the nanoparticles, viscosity of the solvent, dielectric constant of the solvent are crucial factors which mainly decide the dispersibility of the nanoparticles in the particular solvent and compatibility of the nanoparticle surface with the solvent molecules. The present study suggests that these are some of the important factors to be considered while studying the thermal conductivity of nanofluids. Still more detailed studies are required on the interfacial properties at the particle-fluid interface to understand the exact cause of the enhancement of thermal conductivity of nanofluids.

8.2 Future perspectives

Some of the interfacial related problems which contribute to the thermal conductivity enhancement of nanofluids are discussed in this thesis. However, studies in this thesis are restricted to few surfactants and solvents. For example, thermal conductivity studies using different base fluids are restricted to oleic acid (mono unsaturated) coated magnetite nanoparticles of one particular size. Similarly, only toluene is used as the base fluid while studying the role of the surfactants. In order to get a clear picture about the compatibility of the solvent with surfactant on the surface of the nanoparticles, more studies need to be carried out different types of surfactants and solvents. Also, the present studies are limited to non-aqueous base fluids. Similar work can be extended to water based fluids to understand the issues related to compatibility, dispersibility and the role of particle-fluid interface to enhance the thermal conductivity of nanofluids, where the interfacial related effects are still complicated due to the surface charge, pH, etc. and these factors may affect the heat transfer characteristics of the nanofluids. Finally, all work reported in this thesis is done using spherical nanoparticles. Since thermal interactions occur at the surface of the nanostructures, studies using other morphologies may shed more light on the importance of various factors affecting the thermal conductivity of nanofluids.

List of publications

1. **Lenin, R.**; Joy, P. A. "Effect of Particle Size Distribution on the Thermal Conductivity of Decanoic Acid Stabilized Magnetite Nanofluids." *J. Nanofluids* **2015**, 4, 310-317.

2. **Lenin, R.**; Joy, P. A. "Role of Primary and Secondary Surfactant Layers on the Thermal Conductivity of Lauric Acid Coated Magnetite Nanofluids." *J. Phys. Chem. C* **2016**, 120, 11640-11651.

3. **Lenin, R.**; Joy, P. A. "Effect of Unsaturation and Conformation of Surfactant on the Thermal Conductivity of Magnetite Nanofluids," Manuscript submitted.

4. **Lenin, R.**; Joy, P. A. "Effect of base fluid on the thermal conductivity of oleic acid coated magnetite nanofluids," Manuscript under preparation.

5. **Lenin, R.**; Joy, P. A. "Effect of chain length of surfactant on the thermal conductivity of magnetite nanofluids," Manuscript under preparation.